

NORTHWESTERN UNIVERSITY

Micromechanical studies on chromosomes reveal interplay between chromatin, SMC complexes,  
protein networks and mitotic, meiotic, and centromeric stiffness

A DISSERTATION

SUBMITTED TO THE GRADUATE SCHOOL

IN PARTIAL FULFILLMENT OF THE REQUIREMENTS

for the degree

DOCTOR OF PHILOSOPHY

Field of Biological Sciences

By

Ronald Biggs

EVANSTON, ILLINOIS

December 2021

© Copyright by Ronald Biggs 2021

All Rights Reserved

## **Abstract**

Micromechanical studies on chromosomes reveal interplay between chromatin, SMC complexes, protein networks and mitotic, meiotic, and centromeric stiffness

Ronald Biggs

The purpose of my thesis research has been to understand the formation of mitotic chromosome structure by using chromosome micromanipulation. Folding mitotic chromosomes from their loose interphase form into their individualized, compacted form is required for easy handling of the chromosomes for cell division. This process is facilitated by several protein complexes, such as SMC complexes, topoisomerases, and barrier elements. It also coincides with structural changes to the underlying chromatin and activation of protein complexes that facilitate the chromosome division. My research has also delved into studying other forms of chromatin folding and division via micromanipulation. The four projects I have undertaken during my thesis research all use micromanipulation of chromosomes extracted from live cells using micropipettes to stretch the isolated chromosome. This has included the development of a new strategy of isolating the chromosomes from the cell. The first project is the study of protein depletion of condensin I, condensin II, both isoforms, cohesin, and Ki-67 using auxin-induced degradation to study the morphology and mechanics of mitotic chromosome bundles and isolated chromosomes. The next project observed how altering histone post-translational modifications and other controllers of chromatin state affect the stiffness of mitotic chromosomes to study the relationship between the underlying chromatin and the stiffness of the whole mitotic chromosome. The other project on mitotic chromosomes involved the study of the centromere's stretch in the chromosome in relation to other parts of the kinetochore. The other project studied meiotic chromosomes and the stiffness and structural relationship with the synaptonemal

complex. Our results show that there are several morphological effects from depleting protein complexes, but their rapid degradation does not weaken mitotic chromosomes. By contrast, the underlying chromatin was shown to affect mitotic chromosomes through control of heterochromatin, where increasing heterochromatin by histone post-translational modifications stiffened mitotic chromosomes but removing heterochromatin proteins weakened mitotic chromosomes. We demonstrated that the centromere was very stiff compared to the chromosome arms but was not affected by depleting members of the inner kinetochore. Finally, we demonstrated that meiotic I prophase chromosomes were structurally like mitotic chromosomes, but much stiffer. The increase in meiotic chromosome stiffness was not dependent on the presence of the central synaptonemal complex 1 protein. I conclude this thesis by presenting a synthesis of a theme for general findings of chromosomes and future projects, both related and unrelated to the projects described in this document.

## Acknowledgements

### **Prof. John Marko (Advisor)**

Prof. Alfonso Mondragón (Chair)

Prof. Sadie Wignall (Committee member)

Prof. Yuan He (Committee member)

Prof. Huanyu Qiao (Collaborator)

Prof. Aaron Straight (Collaborator)

Prof. Andrew Stephens (Experimental mentor)

Dr. Daniel Shams

Jessica Lenoir

Daniel Fernandez

Marko lab members

The teachers and advisors along the way

My parents

My other friends from the 2020-2021 pandemic

**List of Abbreviations**

AID	auxin-induced degron
CAP	condensin associated protein
CCAN	constitutively centromeric associated network
CENP	centromere protein
CTCF	CCCTC-binding factor
DMEM	Dulbecco's modified eagle medium
DNA	deoxyribonucleic acid
FBS	fetal bovine serum
IAA	indole-3-acetic acid
KMN (network)	KNL-1/Mis12 complex/ Ndc80 complex (network)
MNase	Micrococcal nuclease
PTM	post-translational modification
siRNA	small, interfering ribonucleic acid
SC	synaptonemal complex
SMC	structural maintenance of chromosome
SYCE	synaptonemal central element
SYCP	synaptonemal complex protein
TopoII	topoisomerase II
TSA	Trichostatin A
VPA	valproic acid

	7
Table of Contents	
Abstract.....	3
Acknowledgements.....	5
List of Abbreviations .....	6
List of Figures.....	12
Chapter 1. Introduction to micromanipulation, chromosome structure and organization.....	15
1.1 Preface and introduction - The cell cycle and the substages of mitosis .....	15
1.2 Chromosome isolation and mechanics .....	23
1.2.1 The physics involved in stretching chromosomes and mechanics .....	23
1.2.2 Newt experiments and basic mitotic structure using chromosome isolation .....	28
1.2.3 Study of human mitotic chromosomes and effects of protein complexes.....	33
1.2.4 How to perform chromosome isolations .....	39
1.3 Structural Maintenance of Chromosome (SMC) complexes and loop extrusion.....	43
1.3.1 The loop-extrusion hypothesis: purpose, theory, modeling, and evidence .....	43
1.3.2 The purpose of condensin and cohesin- the loop-extruding elements .....	50
1.3.3 Other cohesin roles in chromatin organization, function, and properties .....	57
1.3.4 Condensin - history, compaction, supercoiling, and removal .....	61
1.3.5 Other critical proteins in mitotic chromosome structure- TopoII and Ki-67 .....	71
1.4 Histone post-translational modifications (PTMs) and interactions .....	73
1.4.1 Histones, nucleosomes, modifiers, and chromatin background .....	73

1.4.2	Histone PTM interactions and interacting molecules.....	82
1.4.3	Mitotic chromosome structural changes and relation to histone PTMs .....	87
1.5	Meiotic chromosome division .....	94
1.5.1	Meiotic chromosome division, purpose, and background.....	94
1.5.2	Structural properties of meiotic prophase I chromosomes and components .....	102
1.6	Centromeric protein (CENP) complexes.....	108
1.6.1	How chromosomes divide - The physical machinery .....	108
1.6.2	Structure and behavior of the centromere and the CCAN.....	114
1.6.3	Centromere stretching and its stiffness .....	120
1.7	Introduction to the Chapters - questions asked and answered.....	124
Chapter 2. Rapid degradation of Structural Maintenance of Chromosome proteins using Auxin-Induced Degradation causes chromosomal morphological changes with no mechanical changes; Ki-67 degradation causes morphological changes and stiffens chromosomes.....		
2.1	Overview .....	127
2.2	Materials and Methods .....	133
2.3	Results .....	138
2.3.1	Fluorescence, localization, and removal of critical mitotic proteins.....	138
2.3.2	Protein localization and their effects on mitotic chromosome bundles.....	142
2.3.3	Mechanical stiffness of isolated mitotic chromosomes.....	143
2.3.4	Studying the dynamics and effects specific to SMC2 .....	146

	9
2.4	Conclusions, discussion, and future directions ..... 146
2.4.1	Results overview and recap ..... 150
2.4.2	The change in mitotic stiffness between lines, but not missing proteins ..... 151
2.4.3	Condensin studies based on fluorescence and dynamics ..... 153
2.4.4	Analyzing the degradations of non-condensin molecules ..... 155
2.4.5	Future directions of study ..... 157
Chapter 3. Heterochromatin components HP1 $\alpha$ and histone hypermethylation stiffen mitotic chromosomes and change their structure; hyperacetylation on mitotic chromosomes does not result in chromosomal mechanical changes..... 160	
3.1	Overview ..... 161
3.2	Methods ..... 170
3.3	Results ..... 173
3.3.1	HDACis increases H3K9ac in mitosis but have no change in stiffness ..... 173
3.3.2	Methylstat stiffens chromosomes and increases fixed cell histone methylation.. 177
3.3.3	Methylstat treatment does not change SMC2 levels ..... 180
3.3.4	HP1 $\alpha$ provides mechanical strength to mitotic chromosomes ..... 180
3.4	Conclusions, discussion, and future directions ..... 192
3.4.1	Histone PTM changes- original hypotheses and data analysis..... 192
3.4.2	Incorporating chromatin interactions into the model of mitotic chromosomes ... 193

3.4.3	Understanding the implications of increased methylation stiffening mitotic chromosomes and lack of effect from hyperacetylation.....	196
3.4.4	Analysis of HP1 $\alpha$ affects mitotic chromosome stiffness .....	197
3.4.5	Investigations into how chromatin could affect mitotic chromosome stiffness...	200
Chapter 4. Micromanipulation of prophase I chromosomes from mouse spermatocytes reveals high stiffness and gel-like chromatin organization.....		
		202
4.1	Overview .....	203
4.2	Materials and methods.....	208
4.3	Results .....	213
4.3.1	Properties of meiotic prophase compared to mitotic chromosomes.....	216
4.3.2	Nuclease treatments dissolve both chromosomes to a similar degree.....	216
4.3.3	Protease treatments weaken but do not fully dissolve both chromosomes .....	220
4.4	Conclusions, discussion, and future directions .....	222
4.4.1	Meiotic chromosomes in the context of mitotic chromosomes.....	222
4.4.2	Implications of meiotic chromosome digestion .....	222
4.4.3	Hypothetical purpose of high meiotic chromosome stiffness .....	223
4.4.4	Significance of the SYCP1 null mutant stiffness similarity to WT .....	226
4.4.5	Future experiments on meiotic chromosomes.....	227
Chapter 5. The innate high stiffness of the CENP-A labeled centromere is unaffected by the degradation of CENP-C and CENP-N by our detection methods .....		
		229

	11
5.1 Overview .....	230
5.2 Materials and Methods .....	235
5.3 Results .....	241
5.3.1 CENP-C/N is removed in auxin treatment with no CENP-A intensity effects .....	241
5.3.2 Short-term auxin treatments remove CENP-C/N with no stiffness effects .....	244
5.4 Conclusions, discussion, and future directions .....	248
Chapter 6. Conclusion – Achievements, findings, and future directions.....	254
6.1 Thesis proposal retrospective and achievements.....	255
6.2 Scientific findings and themes .....	257
6.3 Future directions from existing projects.....	259
6.3.1 SMC complex future directions .....	260
6.3.2 Histone PTM and chromatin state future directions.....	261
6.3.3 Meiotic chromosome and synaptonemal complex future directions.....	262
6.3.4 Centromere and CCAN future projects .....	263
6.4 Future directions - other projects.....	264
References.....	269
Appendix.....	292

## List of Figures

Figure 1.1. The cell cycle and mitotic substages. ....	21
Figure 1.2-1. Chromosome isolation and stretching procedure. ....	27
Figure 1.2-2. Structural experiments on mitotic chromosomes. ....	31
Figure 1.2-3. Micromechanical chromosome study with drug, enzyme, chemical perturbations, and other treatments. ....	37
Figure 1.3-1. Loop extrusion via SMC complexes. ....	47
Figure 1.3-2. Example images of SMC complexes. ....	55
Figure 1.3-3. Diagrams of SMC complex functions. ....	65
Figure 1.4-1. The structure of the nucleosome and placement of histone post-translational modifications. ....	81
Figure 1.4-2. Chromatin diagram and effects of histone post-translational modifications. ....	85
Figure 1.4-3. Mitotic chromosome structural changes and relation to histone PTMs. ....	89
Figure 1.4-4. Study of chromatin-dominated stiffness in the nucleus using micropipettes. ....	93
Figure 1.5-1. The substages of meiosis and the steps in meiotic prophase I. ....	99
Figure 1.5-2. Diagram of the synaptonemal complex, meiotic connections, and crossover. ....	105
Figure 1.6-1. Chromosome separation machinery diagram. ....	111
Figure 1.6-2. Diagram of the Constitutive Centromeric Associated Network (CCAN) in mitosis. .....	117
Figure 1.6-3. The centromere is enriched in elements that stiffen mitotic chromosomes. ....	122
Figure 2.1. Auxin treatment and single chromosome isolation. ....	135
Figure 2.2. The studied proteins localize to their correct locations and can be depleted with auxin treatment. ....	141

Figure 2.3. Analysis of SMC2 fluorescence over time and bundles lacking SMC2. ....	145
Figure 2.4. Study of isolated mitotic bundles and chromosome mechanics. ....	149
Figure 3.1. Experimental setup for chromosome micromanipulation, force measurement and image quantification. ....	166
Figure 3.2. Example capture of single chromosome. ....	167
Figure 3.3. Further fluorescent analysis of VPA and TSA treatments. ....	175
Figure 3.4. HDACis cause increased H3K9ac fluorescence in mitotic fixed cells and captured chromosomes, but have little effect on the stiffness of mitotic chromosomes. ....	179
Figure 3.5. Further fluorescent analysis of Methylstat treatments. ....	183
Figure 3.6. Methylstat (HDMi) treatment causes an increase in methylation for mitotic fixed cells and stiffens mitotic chromosomes. ....	184
Figure 3.8. HP1a is a mechanical component of the mitotic chromosome aiding proper segregation in mitosis. ....	191
Figure 3.9. HP1 $\alpha$ -AID-sfGFP displays cell and chromosome fluorescence and upon its degradation mitotic errors occur leading to higher curvature nuclei. ....	195
Figure 3.10. Model of mitotic chromosome and influence of histone PTMs. ....	199
Figure 4.1. Trypan cell viability assay. ....	206
Figure 4.2. Example images of wild-type (Sycp1 <sup>+/+</sup> ) meiotic cells before nuclei extraction. ..	207
Figure 4.3. Setup for micromanipulation experiments and chromosome isolation. ....	211
Figure 4.4. Example Force-Extension plots and corresponding calibration plots. ....	212
Figure 4.5. Additional physical measurements of mitotic and meiotic chromosomes. ....	215
Figure 4.6. SYCP1 is absent in Sycp1 knockout mutant spermatocytes. ....	217

Figure 4.7. Mitotic and meiotic chromosomes have a contiguous DNA connection, which is dissolved with 4bp restriction enzymes, but only weakens with 6bp restriction enzymes.....	219
Figure 4.8. Example MNase treatment of captured mitotic bundles and meiotic nuclei, both stretched between two pipettes. ....	221
Figure 4.9. Both meiotic and mitotic chromosomes are weakened, but do not dissolve when treated with Trypsin and Proteinase K.....	225
Figure 5.1. Auxin treatment, chromosome isolation, and force measurements.....	237
Figure 5.2. Examples and measurements of the centromeric fluorescent measurements.....	243
Figure 5.3. Quantification of the mechanics and fluorescence of isolated chromosomes.....	247

## Chapter 1.

### **Introduction to micromanipulation, chromosome structure and organization**

*This chapter contains in depth details about all the background of the subsequent chapters and research projects, which should give additional insight into the research field for the projects presented.*

## 1.1 Preface and introduction - The cell cycle and the substages of mitosis

This thesis will detail the findings from experimental projects investigating chromosome structure using micromanipulation to capture and analyze mitotic and meiotic chromosomes from living cells. Chapter 1 Section 2 details the background, history, and previous findings of this approach, while the Appendix describes its current implementation and specifics on the technique. This Chapter will also give background information into the four scientific topics as a primer to understand the findings of the four main projects and their relationship to mitotic chromosome structure in the following chapters. The four topics covered are Structural Maintenance of Chromosome (SMC) complexes (Section 1.3, Chapter 2), histone Post-Translational Modifications (PTMs) (Section 1.4, Chapter 3), meiotic chromosome structure and mechanics (Section 1.5, Chapter 4), and centromeric stiffness (Section 1.6, Chapter 5). A brief overview of DNA, chromatin, mitosis, and the cell cycle will be covered in this Section.

DNA is the information-carrying molecule and “genetic blueprint” of the cell. DNA is a polymer, with the monomers consisting of four nucleic acids, which act as the information storage of the cell. DNA typically forms a double-stranded (ds) helix, paired to its sister nucleic acid molecules. The ds helix can be imagined as a very fine thread at the macroscopic level. Inside the cell, DNA is typically not found in its naked state, but interacts with different structural proteins. In eukaryotic cells, such as humans, DNA is typically found wrapped around histone octamers as a first-level organizational step, but will also interact with transcription factors, DNA or RNA polymerases, SMC complexes, or other such proteins and complexes. These structures are present and interact with chromatin constantly, but chromatin structure also changes over the cell cycle.

Chromatin is the name given to the complex formed by the interaction of DNA and DNA-interacting elements. The DNA-interacting elements mainly consist of proteins with structural and organizational functions. Some of these DNA-interacting elements include histones, transcription factors, SMC complexes, topoisomerase II, and Ki-67 among many others. A continuous strand of chromatin is called a chromosome. The genome is the entire collection of a cell's DNA. A gene is a sequence of DNA that encodes for an amino acid sequence that will be translated into a protein. During the cell cycle the genome is duplicated in S-phase and separated in mitosis. The two chromatids that arose from the duplication are called sisters, which are paired together following duplication. In sexually reproducing organisms, a single chromosome is inherited from each of the two parents. The chromosomes that contain the same genes but differ in sequence (inherited from different parents), are called homologous chromosomes. A cell with two homologous chromosomes is called a diploid cell, whereas a cell with only one copy of each chromosome is called a haploid cell.

The cell cycle is a description of the morphological, structural, and functional changes to the cell and chromatin over time in preparation to divide into two daughter cells. G1 or gap 1 phase is the stage directly following the previous mitotic division in which the cell nucleus is reformed, and the cell accumulates energy and maintains its internal functions. G0 is a special stage of G1 in which the cell no longer progresses through the cell cycle, but is arrested at G1, either due to terminal differentiation (it maintains a highly specialized function through the rest of its life), or due to other factors such as limited nutrients. Following G1, the cell enters S or synthesis phase, where the whole genome is duplicated, and sister chromosomes are paired together. The G2 phase is another gap phase, where the cell grows to accommodate the additional chromatin from the S-phase genome duplication and the size needed to form two cells

after mitosis. G2 also involves performing cell maintenance, accumulating cellular energy, and proofreading the duplicated chromosome sequence. Following G2, the cell enters M phase, or mitosis, where the duplicated chromosomes are compacted, organized, paired, and are evenly divided into two cells. The two cells physically separate from one another, becoming two distinct identities then reenter G1. This is demonstrated in Fig. 1.1A.

Broadly speaking, the cell cycle can be divided into two chromatin states, interphase and mitosis, where interphase occurs during G1, S, and G2, *i.e.*, all non-mitotic stages. During interphase, chromatin adopts a relatively diffuse, open, globular shape contained in the nucleus. Interphase chromatin is relatively organized, compartmentalized, and linearly compacted compared to naked DNA (Fig. 1.1B) (Prakash & Fournier, 2018). The open state of chromatin in interphase allows it to be transcriptionally active, which allows for protein production, cellular maintenance, DNA synthesis, growth, and other activities. Interphase chromatin is also much more dynamic and varied, converting from a loose, transcriptionally accessible form, called euchromatin, to a compact, transcriptionally repressed form, called heterochromatin, or vice versa. The cell also typically possesses both chromatin states at the same time during interphase to control for transcriptional selection. During interphase, chromatin and the individual chromosomes are also much more entwined and entangled than in mitosis, compare Fig. 1.1B to Fig. 1.1C (Paulson, Hudson, Cisneros-Soberanis, & Earnshaw, 2021; Prakash & Fournier, 2018).

To maintain the information contained in the genome, cells must evenly distribute the chromosomes into the two daughter cells or face deviations from the original organism, which could be detrimental to their health. To effectively organize the genome into easily dividable, individualized chromosomes, it must compact the genome into very dense bundles of chromatin (Fig. 1.1C) (Paulson et al., 2021). Mitosis folds chromosomes into rod-like structures through

several complex mechanisms, which will be detailed later in the thesis. The chromatin in these rods is substantially less entangled than their interphase counterparts and have minimal interactions with the other chromosomes in the genome. The kinetochores act as “handles” on the chromosome, which are grabbed by opposing ends of the cell to pull the chromosomes apart. The kinetochores are built on top of the centromeric regions of chromosomes. The kinetochores are positioned opposite one another, which allows for the sisters to be divided evenly into the two daughter cells. Microtubules are also a key complex in mitosis, anchoring the pulling machinery at opposite ends of the cell, pushing the cells apart, and tethering to the kinetochores to separate the sister chromosome pairs. The microtubules that connect to the kinetochore are called the spindle microtubules. The separation of chromosomes is also subject to a stalling or “checkpoint” mechanism before both sides are ready for separation.

There are several substages in mitosis, during which there are notable cellular and chromosomal changes. In chronological order, the substages of mitosis are prophase, prometaphase, metaphase, anaphase, and telophase, which coincides with cytokinesis. In prophase, the initial compaction of mitotic chromosomes occurs, compacting the loose chromatin of interphase into the rod-shaped structures, similar to but longer and thinner than fully compact mitotic chromosomes. During prometaphase, a second stage of compaction starts as the nuclear envelope is broken down. During prometaphase the mitotic spindle microtubules start searching for the kinetochores from opposite ends of the cell. During metaphase, the microtubules attach to the kinetochore on all the chromosomes and begin pulling the chromosomes apart. The pulling force causes the chromosomes to align in the middle of the cell, termed the metaphase plate. Anaphase starts when cohesin, the protein complex responsible for sister chromatid cohesion (holding sister chromatids together), is cut. Cohesin cutting allows the sister chromosomes to

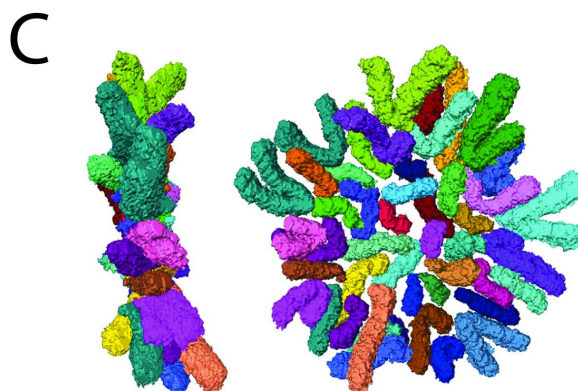
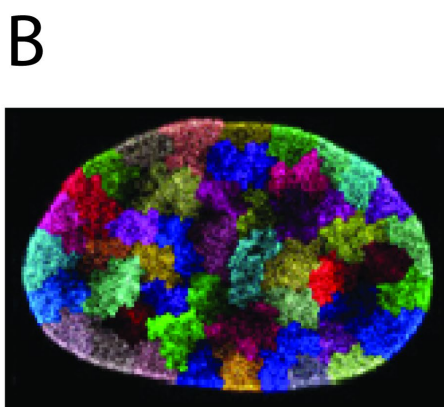
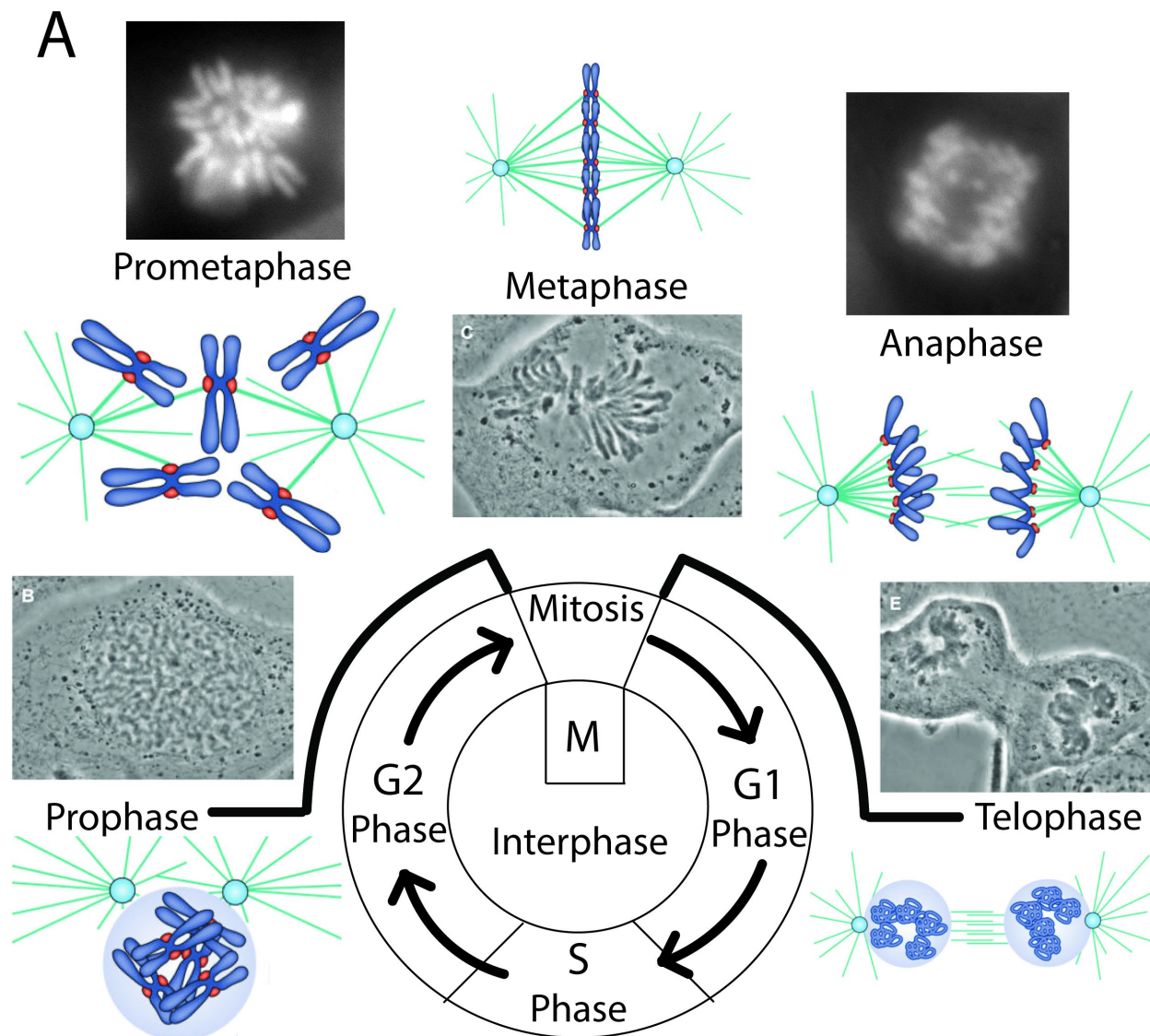


**Figure 1.1. The cell cycle and mitotic substages.**

(A) Diagram of the cell cycle and illustrations of meiotic substages. The middle diagram shows the four distinct stages of the cell cycle- Gap 1, Synthesis, Gap 2, and Mitosis. G1 and G2 are relatively longer cycles, while S phase is longer than the relatively short M phase. G1, S, and G2 constitute the interphase stage of the cell cycle, while M phase is the mitotic stage of the cell cycle. The morphological changes from G1 to G2 are relatively subtle, where the nucleus and cell membrane are enlarged to facilitate growth and chromosome duplication. The substages of mitosis are diagrammed surrounding the inner circle with images of real, non-diagrammed, examples nearby. In the diagrams, the DNA is marked in dark blue, the nucleus in light blue, the centromere/kinetochore in red, and microtubule-related items are marked in teal. Prophase, metaphase, and telophase are phase-contrast images of newt chromosomes undergoing mitotic division. Prometaphase and anaphase are fluorescent DNA-stained images of human cell culture cells undergoing mitotic division. In mitosis, the cell progresses from prophase, prometaphase, metaphase, anaphase, and ending in telophase. Prophase is the stage when the nucleus is still present, but the chromosomes start to compact into threads. In prometaphase, the nucleus is broken down, the chromosomes continue compacting, and the microtubules start attaching to the kinetochore. During metaphase, the microtubules have all attached to the centromere and the pulling forces of the microtubules cause the chromosomes to line up in the middle of the cell. In anaphase, sister chromatid cohesion is lost, and chromosomes start separating. In telophase, the nucleus starts reforming around the chromosomes and the nuclei are pushed apart via microtubules. In telophase, the cell also undergoes cytokinesis, where the cells are separated into individual entities. Prometaphase and anaphase images from personal data. Diagram images repurposed from (Verdaasdonk & Bloom, 2011). Phase-contrast images repurposed from (Marko, 2008). (B) A diagram of the cell during interphase. The different chromosomes are labeled in different colors. While the chromosomes are not individualized or in their compact, thread-like shape, they are still well organized. Image repurposed from (Prakash & Fournier, 2018). (C) Chromosomes labeled during metaphase. The thread-like, compact, and individualized structures of mitotic chromosomes are clearly shown with the different chromosomes depicted in varying colors. The image depicts chromosomes aligned at the metaphase plate in a side-view to the left and head-on view to the right. Image repurposed from (Paulson et al., 2021).

separate. In telophase chromosomes are pulled to either end of the cell, the chromosomes start to decompact, and the nucleus starts reforming around the chromosomes. Cytokinesis, which occurs during telophase, causes the cell membrane to pinch in on itself around the former metaphase plate until the cell has reconstructed the cell membrane, such that the two cells are physically isolated. The images of the mitotic substages can be seen in both a diagram and real images in Fig. 1.1A (Marko, 2008; Verdaasdonk & Bloom, 2011).

To cross a few technical hurdles, the mitotic chromosomes isolated in the current micromanipulation protocol occur during prometaphase, when the nuclear envelope has broken down, but when the mitotic spindle microtubules are not yet attached to the kinetochores. This allows us to easily access the chromosomes inside the cell without having any strong attachments that make isolation difficult. During this stage, the chromosomes can undergo further compaction as it progresses into metaphase, but still contains both condensin I and condensin II, the compacting SMC complexes in mitosis. In prometaphase cohesin, the SMC complex responsible for sister chromatid cohesion in mitosis, is present at the centromere, but is actively being removed from the chromosome arms. The prometaphase chromosome organizes chromatin, which contains histones, although the histones are modified in a mitotic-specific way. The centromere is present and contains the fully built kinetochore during prometaphase. Meiotic chromosomes in this thesis were isolated through the nuclear envelope during in prophase of meiosis I, where another meiotic specific structure, the SC, is constructed.

## 1.2 Chromosome isolation and mechanics

### 1.2.1 The physics involved in stretching chromosomes and mechanics

The main technique used in this thesis to study mitotic chromosomes is called single-chromosome micromanipulation. Micromanipulation involves the isolation of an object using micropipettes, which allows direct manipulation of the isolated object. Our technique uses the isolation of mitotic chromosomes directly from mitotic cells (Fig. 1.2-1). We can measure the physical and mechanical properties of mitotic chromosomes once isolated (Fig. 1.2-1A,B). The structure of an object will dictate its physical and mechanical properties, such as its behavior under tension, the point and type of mechanical failure at high forces, how varied regions of the object behave under tension, and other related features. Because of this relationship we can further our understanding of mitotic chromosome structure by measuring its mechanical properties (Fig. 1.2-2). We can also visualize the presence and number of important molecules on mitotic chromosomes to help us understand how they assist in its formation. Other experiments on isolated mitotic chromosomes utilize direct enzymatic and molecular treatments which allow us to gain insight into mitotic chromosome structure by relating the enzymatic target to the morphological changes of mitotic chromosomes (Fig. 1.2-3). Comparing mechanical properties of mitotic chromosomes from different cells (*e.g.*, containing mutated/engineered proteins), species, treatments, or chromatin-containing objects, we further our understanding of the structure of mitotic chromosomes through comparison of mechanics and structure.

Since our results involve understanding the physical properties of mitotic chromosomes, we will review some general terms and concepts involving the physics of material objects. Force applied to an object will cause it to deform in a characteristic manner. The deformation of the object will depend on the direction, speed, and type of the force applied to it. One of the simplest

relationships between force and deformation is that of force-extension through stretching. When an object is pulled while anchored, it will strain the object and anchor, cause it to stretch, and resist that stretch through a restoring force. If the anchor point is mobile, it can be used as a force readout. This can be seen in Fig. 1.2-1A,B. The relationship between the amount of force stretching the object ( $F$ ) (in units of force) and its stretch ( $\Delta L$ ) (in units of length) is called the spring constant ( $k$ ), calculated as  $k = F/\Delta L$ . Forces characteristic of mitotic chromosomes are 0.1-2.0 nN and length scales of 1-20  $\mu\text{m}$ . A force-extension graph can be seen in Fig. 1.2-1A, lower left panel. An elastic object is one that can return to its initial length with no structural changes after being stretched or compressed. An elastic object with a linear force-extension path is called Hookean. If the object is deformed by pulling, it is called plastic *i.e.*, has undergone plastic deformation. Hysteresis is when an object is brought back to its original shape, but through a substantially different force-extension path than the original. An object can also be called viscoelastic if it has properties of an elastic object, but also demonstrates properties of viscosity, such as stretching or returning to normal in a speed-dependent manner.

While the spring constant of an object is unique to every individual object, there are some measurements of physical properties that allow us to compare the stiffness between objects constructed from the same material. Longer elastic objects are easier to stretch a given distance than shorter objects. This relationship is linear, meaning stretching two objects made of the same material and thickness to double their initial length ( $L_0$ ), the length of the object under no stretching or compressive force, will require the same amount of force. This is known as the doubling force ( $F_{2L0}$ ) (in units of force), which can be measured by multiplying the spring constant of an object by its initial length. For objects that show nonlinear elasticity before doubling in length, one can extrapolate the initial linear behavior (*i.e.*, the slope of the linear

force-extension plot) to obtain the doubling force. To prevent damage to the chromosome, we typically pull the isolated chromosome 6  $\mu\text{m}$ , which stretches the chromosome 1-3  $\mu\text{m}$ . This initial stretch-deflection curve is used to generate a force-extension slope, which we use as the spring constant and multiply by the initial length to obtain the doubling force. Thicker objects of the same material are harder to stretch than thinner materials. This relationship is linearly proportional to its cross-sectional area ( $A$ ), *i.e.*, thickness (in units of area, or length-squared) if it has a uniform thickness. For example, if one uniformly thick object is twice as thick (having twice the cross-sectional area) as another object, it will require twice as much force to stretch the thicker object. The basic quantity expressing this feature is the Young's/elastic modulus ( $E$ ), which can be measured by dividing the length-doubling force of an object by its uniform cross-sectional area, if one remains in the linear elastic regime of deformation. Young's moduli can also be described as stress/strain, where stress is  $F/A$  and strain is  $\Delta L/L_0$ , by  $E=(L_0 F) / (A \Delta L)$

In our measurements, we idealize chromosomes as homogenous, uniformly thick cylinders to obtain their Young's moduli. The length and diameter are calculated from a documentation image of the isolated chromosome. The diameter of the chromosome is then used to calculate its cross-sectional area. In our stretch-deflection experiments, we use two pipettes, a stiff pulling pipette ( $p$ ), and an easily bendable, deflecting force pipette ( $f$ ). The chromosome ( $c$ ) stretch is calculated as the movement of the pulling pipette ( $\Delta x_p$ ) minus the deflection of the force pipette ( $\Delta x_f$ ). The force of the object at a specific time and stretch value is calculated as the deflection of the force pipette multiplied by the force pipette's spring constant ( $\Delta x_f k_f$ ). The spring constant of the chromosome ( $k_c$ ) is then calculated as the linear regression (slope) of a stretch vs. deflection graph. Put together,  $k_c = (\Delta x_f k_f) / (\Delta x_p - \Delta x_f)$ . Additional details on the measurements of chromosomal stiffness can be found in the Appendix.

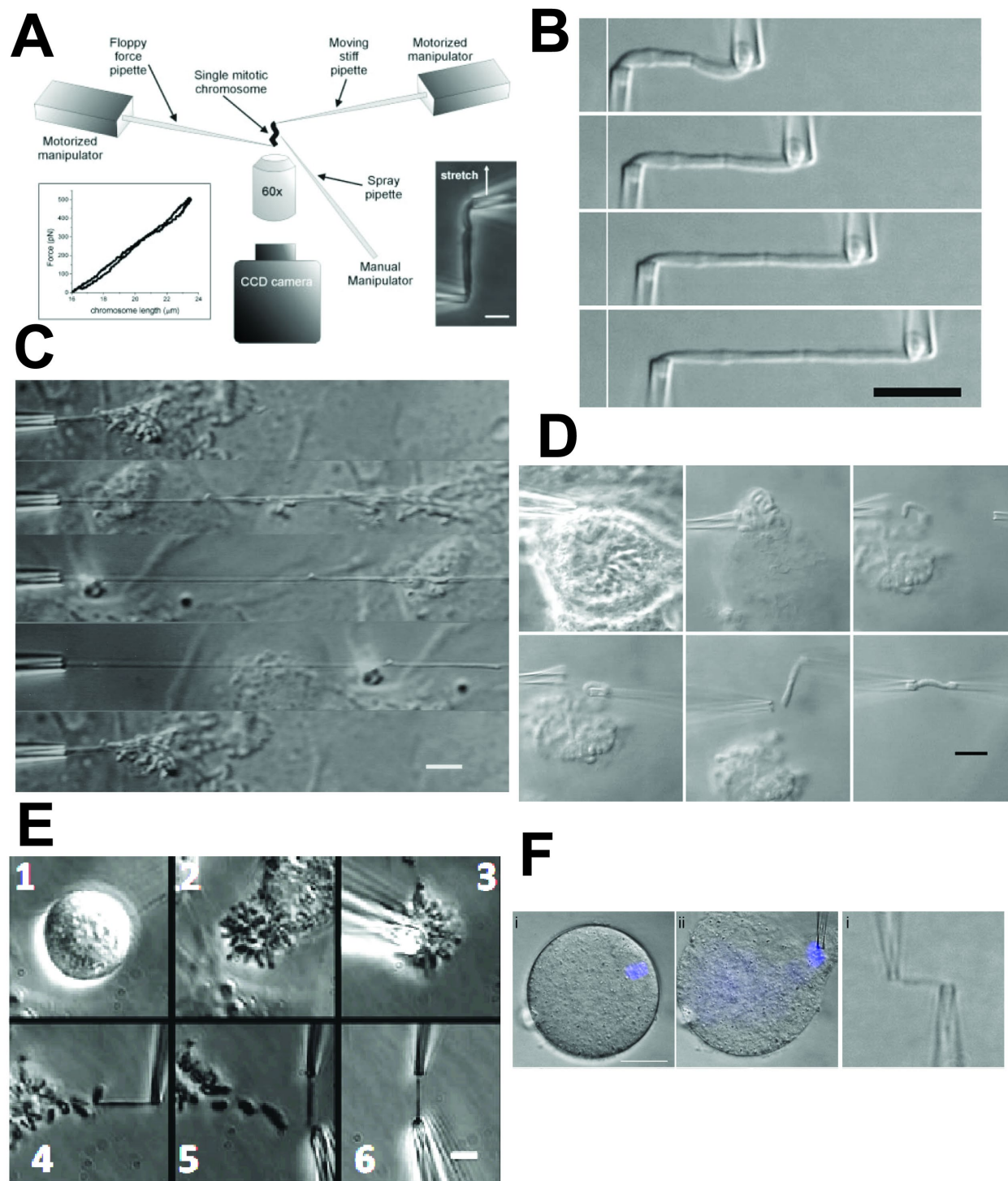


**Figure 1.2-1. Chromosome isolation and stretching procedure.**

(A) Microscope setup for isolating mitotic chromosomes via cellular lysis. Three pipettes were utilized to interact with the cells and chromosomes, then analyzed through a 60x objective and a CCD camera. Two pipettes were connected to motorized manipulators for precise control of the chromosomes. The stretch deflection can be seen on the sides as a diagram and a force-extension plot. Scale bar represents 5  $\mu\text{m}$ . Image repurposed from (Pope, Xiong, & Marko, 2006). (B) Images of a force-extension experiment. The stiff pipette is moved from the force pipette while the force pipette would deflect from its original position, stretching the chromosome via the pulling force. The tracking of the two pipettes would yield a curve like Fig. 1.2-1A. Scale bar represents 10  $\mu\text{m}$ . Image repurposed from (M. G. Poirier, Eroglu, & Marko, 2002). (C) Stretching mitotic chromosomes through liquid flow. Once a chromosome arm was aspirated into a pipette, the bundle could be removed from the cell, then liquid flow could be introduced into the chamber, which would stretch the chromosome. Stretching could also be repeated to determine when the chromosome was stretched in its elastic region, its plastic region, and to its snapping amount. Scale bar represents 10  $\mu\text{m}$ . Image repurposed from (Houchmandzadeh, Marko, Chatenay, & Libchaber, 1997). (D) Chromosome isolation from newt cells. The cell membrane is lysed with Triton-X in PBS, where the chromosomes begin drifting out of the cell. One arm is then aspirated into the force pipette, aspirated into the stiff pipette, then moved away from the cell to break the inter-chromosomal tethers. Scale bar represents 10  $\mu\text{m}$ . Image repurposed from (Marko, 2008). (E) Isolation of a chromosome from mammalian cell cultures. A mitotic cell would be identified, lysed, which would cause the chromosome bundle to fall out of the cell, where it would be aspirated into a pipette. Once stabilized in the pipette, one arm was grabbed, moved away from the bundle, then the other arm was aspirated into a stiff pipette. Scale bar represents 10  $\mu\text{m}$ . The chromosome bundle was then removed, and an isolated chromosome remained. Image repurposed from (R. J. Biggs, Liu, Peng, Marko, & Qiao, 2020). (F) Isolation of a meiotic chromosome from mouse oocyte cell arrested in metaphase II. A meiotic cell would be identified, isolated, and lysed, then a chromosome arm would be aspirated into a force pipette and the other side would be aspirated into an opposing stiff pipette. Object in blue stained for DNA. The meiotic arrested cells did not have normal inter-chromosomal tethers. Scale bar represents 25  $\mu\text{m}$ , the last image is zoomed in 5x. Image repurposed from (Hornick et al., 2015).

It should be noted that the approximation of a uniformly thick and homogenous cylinder is highly idealized, as the mitotic chromosome is constructed from a variety of molecules. These molecules are found at different densities along the chromosome, as seen by DNA staining and by densities of structural proteins. Mitotic chromosomes also contain specialized domains (such as the centromere and telomere), undergo structural changes over mitosis, and do not have a perfectly uniform circular cross-sectional area. While highly idealized, tracking the characteristic force and modulus of chromosomes in this way provides a simple and straightforward way to measure and compare the mechanics of chromosomes and other cellular objects.

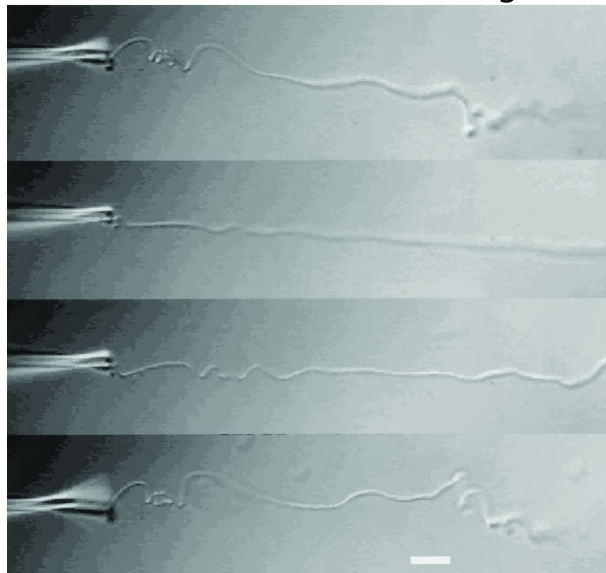
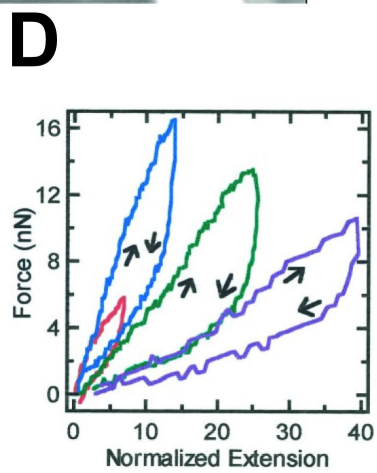
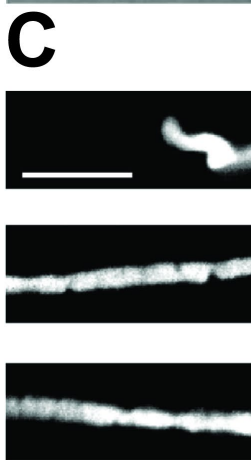
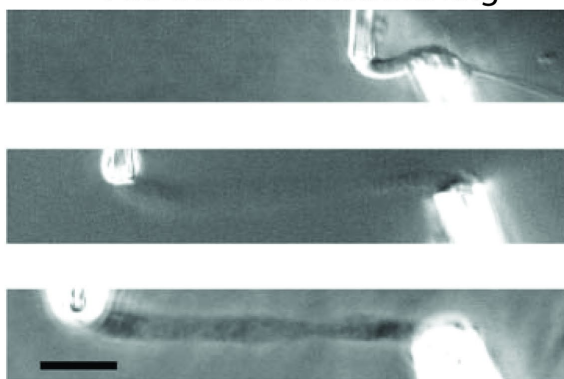
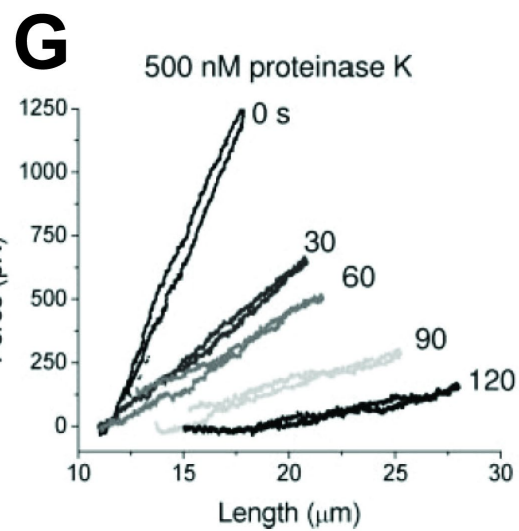
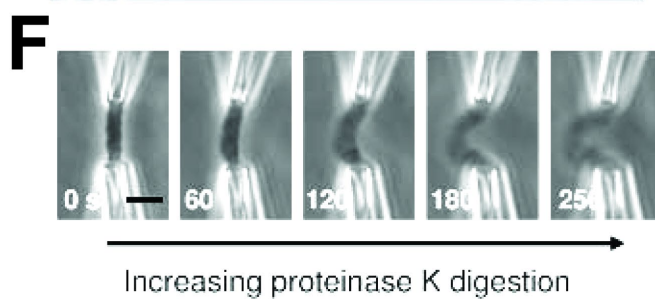
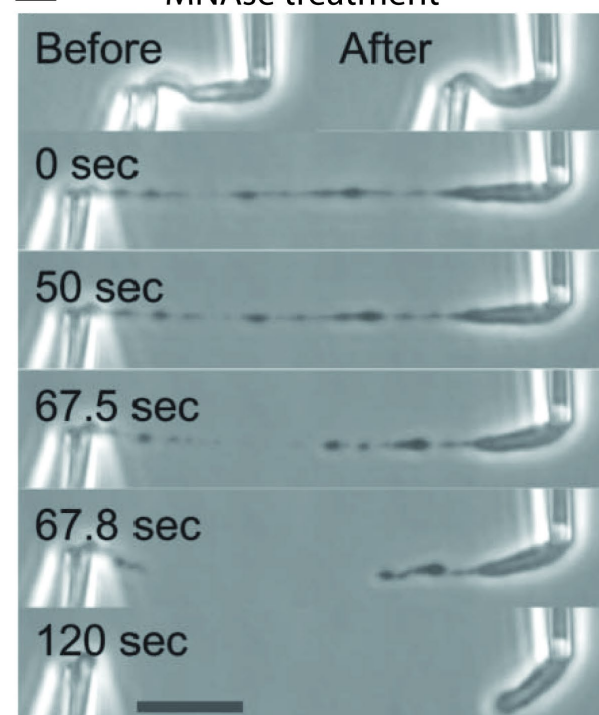
### **1.2.2 Newt experiments and basic mitotic structure using chromosome isolation**

A technical problem in isolating mitotic chromosomes for physical study is their small size. Interphase chromatin and individual chromosomes in interphase cannot be seen directly by light microscopy, but when the chromosomes are condensed in mitosis, they become dense, thick, and large enough to be seen by light microscopy. Observation under light microscopy is historically how cell division was first observed and studied. Another challenge is finding a way to manipulate mitotic chromosomes. Work performed on large, meiotic grasshopper spermatocyte cells demonstrated that glass micropipettes could be used to directly interact with meiotic chromosomes through the cell membrane (Nicklas, 1983; Nicklas & Koch, 1969). The direct interaction with the chromosome was used to study the drag on the chromosomes, the physical properties of cellular processes, and helped in the discovery of the spindle assembly checkpoint in meiosis and mitosis, as seen by the cells stalling chromosome separation when their chromosomes were grabbed.

Initial experiments of chromosome micromanipulation used cultured newt cells due to their large chromosome size, which made the chromosomes easier to isolate. These experiments

studied mitotic chromosome deformation under stress, rather than mitotic cellular processes. Mitotic chromosomes were initially studied by grabbing a single chromosome arm and watching the chromosome stretch using high-pressure flow to determine their physical properties (Houchmandzadeh et al., 1997) (Fig. 1.2-1C, 1.2-2A). This research showed that chromosomes remain elastic when stretched up to ten-fold their native length. Mitotic chromosomes stretched 10 to 100-fold their initial length underwent plastic deformation and nonhomogeneous stretching. Chromosomes would usually break after stretching more than 100-fold their initial length. Since the studied chromosomes remained elastic under large amounts of strain, these experiments suggested that mitotic chromosomes are a gel-like spring of chromatin and associated proteins. These experiments also demonstrated the physical resilience of mitotic chromosomes when subjected to comparatively high forces and strain.

Further experiments captured individual chromosomes between two pipettes to directly study their physical properties. These experiments showed that single mitotic chromosomes could be isolated by lysing a mitotic cell, aspirating both chromosome arms into opposing micropipettes, then moving the isolated chromosome away from the cell. Movement from the cell would break the attachments it had to the cell and other chromosomes (interchromosomal tethers) (Fig. 1.2-1D). Mitotic chromosomes' spring constants could be obtained once isolated by tracking the two pipettes over a stretch-deflection curve (Fig. 1.2-1A,B) (M. Poirier, Eroglu, Chatenay, & Marko, 2000; M. G. Poirier, Eroglu, et al., 2002; M. G. Poirier & Marko, 2002a). Stretching isolated mitotic chromosomes faster than 0.1 their native length per second ( $\sim 1 \mu\text{m}/\text{sec}$ ) caused them to undergo hysteresis and swell. The hysteresis and swelling showed that mitotic chromosomes display some viscoelastic properties (M. Poirier et al., 2000). This viscoelastic property again suggests that mitotic chromosomes are gels/form a discontinuous

**A** Flow-based overstretching**B** Pull-based overstretching**E** MNase treatment

**Figure 1.2-2. Structural experiments on mitotic chromosomes.**

(A) Effects of plastic overstretching of a newt chromosome using flow-based stretching. When the isolated chromosome was stretched over 10-fold its original length, it would return, but be very stringy and not fully recover its original thickness or length. Scale bar represents 10  $\mu\text{m}$ . Image repurposed from (Houchmandzadeh et al., 1997). (B) Pull-based overstretching of newt chromosomes when isolated between pipettes. The first image shows the chromosome before stretching while the other two were after overstretching. When the chromosome was stretched over 10-fold its original length then returned to its original position, it would expand and become much more translucent. In contrast to the flow-based overstretching, the pulling force was very slow, potentially allowing the crosslinking proteins and complexes to slowly disassociate from the chromosome. Scale bar represents 10  $\mu\text{m}$ . Images of (B-D) repurposed from (M. Poirier et al., 2000). (C) Fluorescent images staining for DNA from (B). Scale bar represents 10  $\mu\text{m}$ . (D) Stretch deflection after overstretching. The red curve represents the force-extension results after 7-fold its initial length, blue for 14-fold its initial length, green for 26-fold its original length, and purple for 40-fold its original length. From each step after stretching 14-fold its original length, the chromosome became weaker and underwent higher levels of hysteresis on their return curve to its native length. Scale bar represents 10  $\mu\text{m}$ . (E) Image of the gradual dissolution of the mitotic chromosome after DNA cutting. MNase treatment gradually caused the chromosome to thin until the connection between the pipettes were finally fully cleaved. Scale bar represents 10  $\mu\text{m}$ . The images in E-F repurposed from (Pope et al., 2006). (F) The morphological changes upon protein dissolving. The treatment with proteinase K through a spray pipette caused the chromosome to buckle and become more translucent. The numbers displayed are in seconds after treatment. Scale bar represents 5  $\mu\text{m}$ . (G) The force-extension of the chromosome after treatment with proteinase K. Each timestep between the treatment caused the chromosome to become progressively weaker but did not fully dissolve the chromosome.

spring structure. These experiments also showed that the chromosomes would undergo plastic deformation and hysteresis when stretched over fivefold their initial length (Fig. 1.2-2B-D).

Mitotic chromosome structure was also studied by observing chromosomes' reaction to nucleases and proteases, enzymes that degrade, cut, or otherwise destroy DNA and proteins, respectively. Chromosomes treated with MNase, which cut at every base pair of DNA, would slowly dissolve the chromosome in one area before it snapped and fully dissolved (Fig. 1.2-2E) (M. G. Poirier & Marko, 2002b). These chromosomes also dissolved with nucleases up to four base-pair sequence specificity. When treated with proteases, mitotic chromosomes would expand/swell along their long axis and start buckling outwards, curving to one side (Fig. 1.2-2F). The chromosomes would also become significantly weaker with protease treatment in a time/dose dependent manner (Fig. 1.2-2G) (M. G. Poirier & Marko, 2002b; Pope et al., 2006). This shows that the underlying connectivity (the molecule that holds the chromosome together and is attached to itself) of mitotic chromosomes is based in DNA, but proteins still provide substantial structural and mechanical support. The DNA-based connectivity of the chromosome suggests that there is no stable, proteinaceous core in mitotic chromosomes, as DNA degradation would leave behind a connected protein core if one were present.

To understand the mechanical role of electrostatics on mitotic chromosome structure, salts with different charges were sprayed onto isolated mitotic chromosomes. Ionic salts were used since they can interact with the negatively charged DNA molecules and affect the interactions of DNA with DNA-interacting proteins and complexes. Treatment with a monovalent (one charge per molecule) salt (NaCl) caused reversible decompaction, while treatment with a di- or trivalent (two-three charges per molecule) salts ( $\text{MgCl}_2$  and  $[\text{Co}(\text{NH}_3)_6]\text{Cl}_3$ ) caused the reversible compaction of the chromosome, with  $[\text{Co}(\text{NH}_3)_6]\text{Cl}_3$

shrinking the chromosome by one third its initial volume (M. G. Poirier, Monhait, & Marko, 2002). Prolonged exposure to these salts could cause permanent structural and mechanical changes. The electrostatic compaction occurs by displacing water and allowing DNA to form attractive interactions with the positively charged salt. These experiments demonstrate that approximately one third of the native chromosome's volume is occupied by water, as the DNA is free to condense around the positively charged salts.

### **1.2.3 Study of human mitotic chromosomes and effects of protein complexes**

The same approach of studying isolated mitotic chromosomes in newt cells was also performed on human chromosomes. An additional difficulty in isolating human mitotic chromosomes is that they are about half the length and width of newt mitotic chromosomes (Fig. 1.2-1E). Despite the size differences, these studies found many similar features between human and newt mitotic chromosomes (Sun, Kawamura, & Marko, 2011). For example, both dissolve when treated with nucleases (up to four base-pair sequence specificity), but only weaken with protease treatment. Both chromosomes also contain interchromosomal tethers, which need to be broken to isolate a single chromosome. Both chromosomes are also very resistant to damage and deformation by slow stretching. These experiments also demonstrated that while newt mitotic chromosomes have a much higher spring constant, when controlling for initial length and cross-sectional area, human chromosomes and newt chromosomes have a similar stiffness via Young's moduli measurements. This suggests that the underlying meshwork and structural makeup of newt and human chromosomes are similar.

Micromanipulation has also been used to probe the effects of reducing reagents on mitotic chromosomes to investigate how chemical treatments disrupt mitotic chromosome structure and mechanics. When mitotic chromosomes were treated with these reducing reagents,

*in-vitro* mitotic chromosomes from metaphase-arrested cells would gradually unfold from their compact shape while held in a reducing buffer over a few hours (Fig. 1.2-3A) (Eastland, Hornick, Kawamura, Nanavati, & Marko, 2016). These reducing reagents chemically reduced cysteines, which are important in crosslinking proteins together with a sulfur bridge (Kuga et al., 2007; Meikrantz, Suprynowicz, Halleck, & Schlegel, 1990). Spraying these reducing agents on *ex-vivo* extracted mitotic chromosomes from living, free-cycling human culture cells caused them to mechanically weaken (Fig. 1.2-3B). This further demonstrated the importance of chemical crosslinking to mitotic chromosome structure and gives insight into how cells could control mitotic compaction using chemical modification. The morphological effects and mechanical changes also revealed a relationship between morphology and mechanics.

To understand the interplay between chromatin entanglements and mitotic chromosome structure, newt mitotic chromosomes were treated with human topoisomerase II (TopoII) (Kawamura et al., 2010). TopoII is involved in removing entanglements from chromosomes to prevent DNA damage and the mitotic defects the entanglements can cause (Holm, Stearns, & Botstein, 1989). It performs this function by changing chromatin topology, which involves cutting and religating DNA (Berger, Gamblin, Harrison, & Wang, 1996). When active TopoII, which requires ATP, was sprayed onto newt mitotic chromosomes, the chromosomes became weaker (Fig. 1.2-3C). However, inactive TopoII, lacking ATP or chemically inhibited, did not change the stiffness of the chromosomes. This suggests that TopoII-sensitive DNA entanglements contribute to the stiffness of mitotic chromosomes and human TopoII does not interact with newt chromosomes in its inactive state. Spraying human TopoII onto human mitotic chromosomes stiffened the chromosomes, while active or inactive, the opposite results from newt mitotic chromosomes (Sun, 2014). This suggests that human TopoII can bind and hold

human chromatin together, *i.e.*, crosslinks chromatin. An interesting note is that TopoII has been known to have structural functions, as it has also been called structural complex 1 and can crosslink chromatin at different domains (Earnshaw, Halligan, Cooke, Heck, & Liu, 1985; Gasser, Laroche, Falquet, Boy de la Tour, & Laemmli, 1986; Lane, Gimenez-Abian, & Clarke, 2013).

Condensin depletion has also been used in conjunction with micromechanics to study mitotic chromosome structure. Condensin is vital for folding mitotic chromosomes into their rod-shaped structure and is thought to act as a “chromatin-crosslinker” (Hirano, Kobayashi, & Hirano, 1997; M. Sun, R. Biggs, J. Hornick, & J. F. Marko, 2018b; Takagi et al., 2018). In humans, it exists in two forms, condensin I and condensin II, which have different properties, such as interphase localization, stability on chromatin, and timing of interaction with chromosomes (Green et al., 2012; Ono et al., 2003). (More information regarding condensin and its role in mitotic chromosome formation can be found in Section 1.3). Using siRNA, which stops the production of proteins with a specified RNA sequence (Caplen & Mousses, 2003), human cells were gradually depleted of condensin I, condensin II, and both isoforms over several cell cycles (Sun, 2014; M. Sun et al., 2018b). Micromechanics were used to study how chromosome stiffness changed when lacking these major structural proteins. Condensin II depletion made the chromosomes much weaker, condensin I depletion made them moderately weaker, and the depletion of both weakened the chromosomes more than either isoform alone. Morphological changes to the genome lacking both forms of condensin can be seen in Fig. 1.2-3D, while mechanical changes to isolated chromosomes can be seen in Fig. 1.2-3E. The depletion of both also caused the chromosome bundles to lose their shape, becoming amorphous, expanding blobs of chromatin when held in buffer outside the cell (Fig. 1.2-3C).

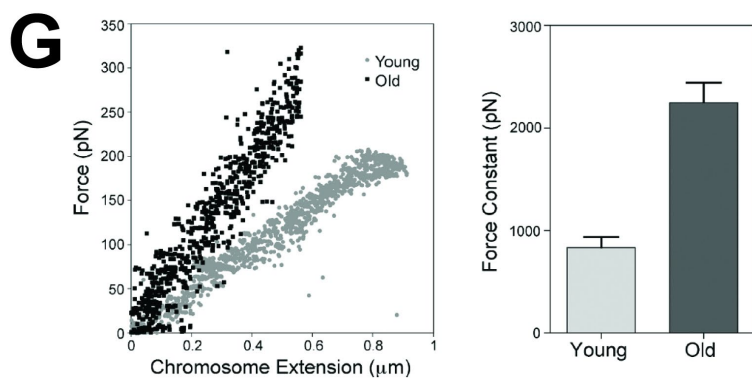
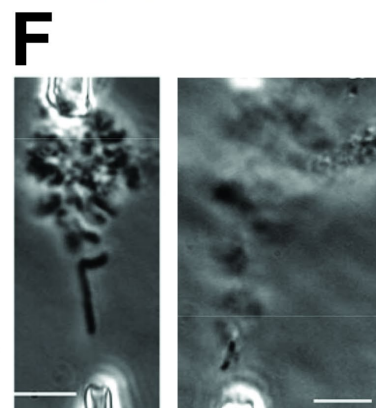
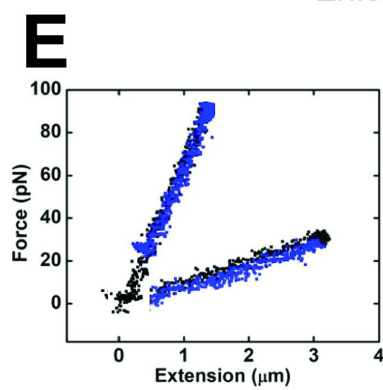
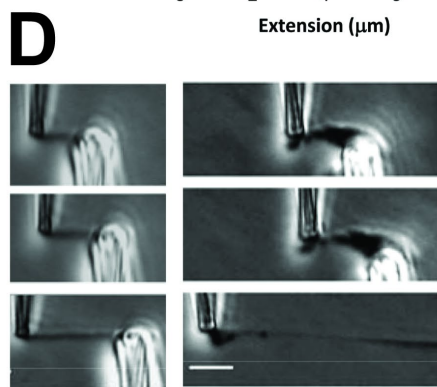
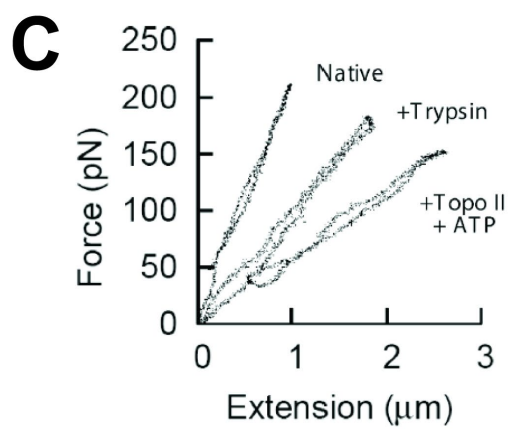
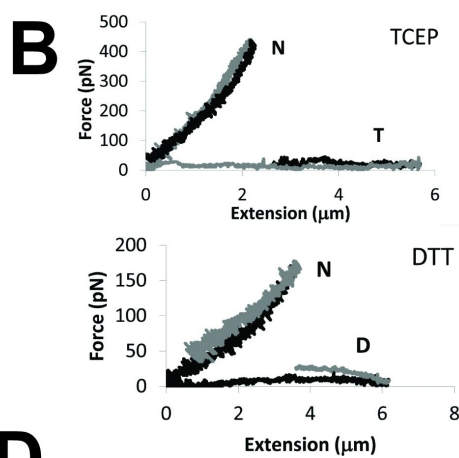
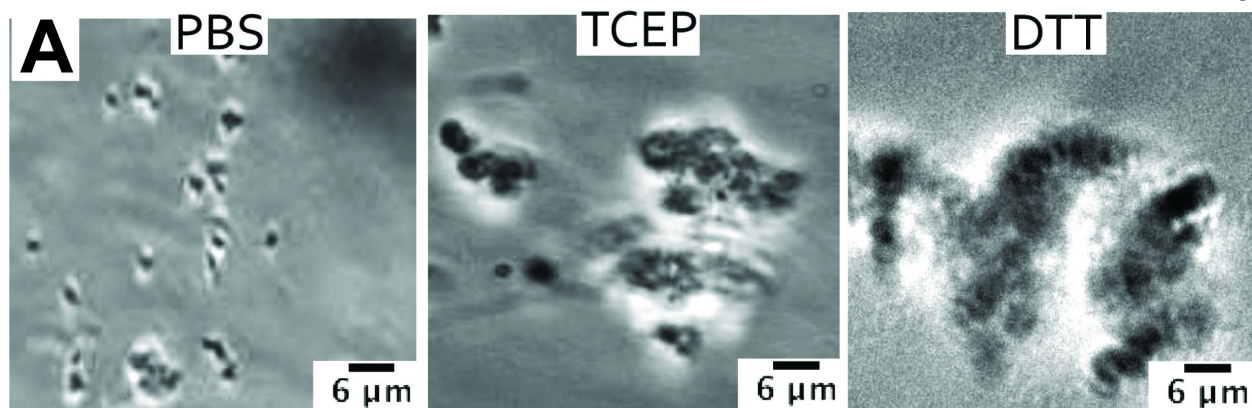


**Figure 1.2-3. Micromechanical chromosome study with drug, enzyme, chemical perturbations, and other treatments.**

(A) Morphological effects of treating chromosomes with reducing agents. When chromosomes were extracted from metaphase-arrested cells and stuck to a glass surface, the untreated (PBS) chromosomes were small, compact, and individualized. When the chromosomes were first treated with the reducing reagents TCEP and DTT, the chromosomes were much more diffuse and lacked a canonical structure of mitotic chromosomes from the loss of cysteine-based crosslinking. Scale bar represents 6  $\mu\text{m}$ . Images in Figures A and B repurposed from (Eastland et al., 2016). (B) Mechanical effects of treating chromosomes with reducing reagents. Reducing reagents sprayed onto chromosomes made them substantially weaker when the untreated chromosome (N traces) was sprayed with the reducing reagents, TCEP (T trace) and DTT (D trace). This weakening occurred through the removal of crosslinks in the chromosome. Chromosomes treated with either reagent had nearly no transduction of force along the chromosome, demonstrating the critical role of crosslinks in mitotic chromosome mechanics. (C) Effects of weakening mitotic chromosomes through removal of chromatin entanglements and protein digestion. This graph shows example traces of a newt chromosome, which had been lightly digested with the protease Trypsin, which caused the chromosome to weaken. This graph also compares the effect of active human TopoII sprayed onto the chromosome, which caused it to weaken through the removal of chromatin crosslinks. Image repurposed from (Kawamura et al., 2010). (D) Phase-contrast imaging of a stretched chromosome untreated (left) and with SMC2-siRNA-treated (right) cells. In untreated cells, the chromosome adopted its typical rod-shaped structure and would deform uniformly when stretched and remain elastic through stretching. When SMC2 was removed through siRNA treatment, the chromosome had patches of thin chromatin and would also be much thinner, *i.e.*, deform in a non-uniform manner when stretched. Scale bar represents 5  $\mu\text{m}$ . Panels D-F repurposed from (M. Sun et al., 2018b). (E) Example force-extension curve of chromosomes from untreated and SMC2-siRNA-treated cells. The top curve shows a representative trace of an untreated, elastic chromosome; the black line is the outgoing trace while the blue line is the return curve. The lower curve is the SMC2-depleted chromosome, which was still elastic, but much less stiff. (F) Morphology of a chromosome bundle with (left) and without (right) SMC2. The chromosome bundle from an untreated cell had individualized and obvious single chromosomes, while the SMC2-siRNA-treated had no obvious, thread-like chromosome remaining, leaving only diffuse strands of chromatin left in the bundle. The SMC2-depleted chromosome bundles also swelled over time in buffer. Scale bar represents 5  $\mu\text{m}$ . (G) Example force-extension trace and consolidated force constants from meiotic, metaphase II chromosomes from old and young mouse oocytes. Chromosomes from older mice were over two-fold stiffer than chromosomes from young mice, demonstrated in both the example trace and the bar graph. Image repurposed from (Hornick et al., 2015).

Metaphase arrest experiments of mitotic chromosomes were also used to demonstrate the role of condensin on mitotic chromosome structure. Treating cells with a high dose of nocodazole or colchicine causes the cells to arrest in metaphase (Florian & Mitchison, 2016). Metaphase arrest also caused the chromosome to become overloaded with condensin, which in turn caused the chromosome to become much stiffer (Sun, 2014; M. Sun et al., 2018b). Combining the condensin depletion data with the condensin overload data revealed a direct relationship between the fluorescent intensity (and thus amount) of condensin and mitotic chromosome stiffness. The direct (linear over a log vs log scale) relationship suggests that most of mitotic chromosome stiffness is facilitated by condensin. The overloading of condensin in metaphase arrest also suggests that condensin binding in mitosis is not halted in metaphase, but will continue until the chromosomes separate in anaphase, where condensin is removed from the chromosome after cell division. A consequence of the metaphase stall was the disappearance of the interchromosomal tethers. The removal of the interchromosomal tethers in condensin overloaded chromosomes also suggests condensin binding helps to disentangle mitotic chromosomes (Goloborodko, Imakaev, Marko, & Mirny, 2016; Martin et al., 2016; Nagasaka & Hirota, 2015).

Micromanipulation of metaphase II arrested chromosomes from mouse oocytes has also been used to study the effects of maternal age on chromosomal stiffness (Fig. 1.2-1D). Chromosomes extracted from older mouse oocytes were significantly stiffer than that of younger mice (Fig. 1.2-3D) (Hornick et al., 2015). This demonstrated that there are structural, disease-related changes that correlate to chromosomal defects (Duncan et al., 2012; Jones & Lane, 2013), which in turn correlate to mechanical changes, as age affects the health and function of meiotic

chromosomes and chromosome stiffness. This also demonstrated that the chromosomal isolation could be utilized to study meiotic chromosomes in addition to mitotic chromosomes.

#### **1.2.4 How to perform chromosome isolations**

There are many aspects of mitotic chromosome structure that can be explored by physically isolating them from mitotic cells. However, the process of chromosome isolation is complicated. Some challenges in isolating a mitotic chromosome involve removing the cellular membrane, as it acts as a barrier to the mitotic chromosomes, delicately breaking the entanglements of the interchromosomal tethers without damaging the target chromosome, anchoring the chromosome between two pipettes, and performing the experiments at the force/length scale of mitotic chromosomes. Details of the challenges and how they are overcome are described in the following section, but in short, a mitotic prometaphase cell is found, lysed with a detergent-containing pipette, the genome stabilized by a third pipette, each arm of the chromosome is aspirated into opposing micropipettes, then the chromosome is separated from the rest of the bundle, snapping the interchromosomal tethers.

The first step in chromosome isolation is to open a hole in the cell membrane, called cell lysis, with the use of detergents, like Triton-X. During prophase, the nuclear envelope remains as an additional and more stable barrier to mitotic chromosomes. However, during prometaphase, which follows prophase, the nuclear envelope is deconstructed called nuclear envelope breakdown (NEBD). This deconstruction allows free access to the chromosomes once the cell membrane is removed. During metaphase, which follows prometaphase, the chromosomes are attached to the mitotic spindle microtubules at the kinetochore, which are not easily separated from the chromosomes. Thus, prometaphase cells are specifically targeted and identified for performing mitotic chromosome isolation.

To anchor the chromosome for isolation, one needs to make micron-scaled pipettes. These pipettes must also contain a micron-scaled opening to aspirate the chromosome arms. Chromosome arms can be aspirated into the pipette when connected to a vacuum source and will anchor at the tip of the pipette by electrostatic glass-to-DNA interactions. This opening must be balanced to allow enough of a vacuum to aspirate only the tips of the chromosome arms without aspirating the entire chromosome, which is difficult at the small chromosomal length/force scale. While difficult, chromosome isolation is possible with the use of high contrast and magnification microscopes, micropipette manipulators for the greater control/stability needed, and access to a variety of pipette sizes, including very small and very sensitive (easily deflected by forces in the few hundred piconewton range) pipettes, available by varying the micropipette puller settings and cutting methods. Pipette openings can be made small enough to interact with the cell, chromosome bundles, and chromosomes, which allows us to study the physical properties of mitotic chromosomes.

Prometaphase chromosomes also contain interchromosomal tethers, which must be removed for chromosome isolation and several methods have been developed to address this challenge. One method of isolation involves anchoring each arm of a mitotic chromosome with a pair of pipettes (one for each arm) after cell lysis and moving the pipettes away from the cell. The movement away from the cell breaks the interchromosomal tethers, leaving an isolated chromosome remaining between the pipettes (cell removal method) (Fig. 1.2-1D). This can also be done by moving the whole genome bundle out of the cell, stabilizing it with a pipette, then repeating the process above (one pipette anchoring each arm), removing the bundle-aspirated pipette from the chromosome instead of moving the chromosome pipettes away (bundle removal method) (Fig. 1.2-1E). A final method of isolation involves removing the bundle from the cell,

stabilizing it with a wider pipette in the stiff-pipette position, grabbing a chromosome arm with a force pipette, then aspirating the rest of the bundle into the stabilizing stiff pipette, leaving only one chromosome between the force and stiff pipettes (bundle-hold method). In rare cases or in specific treatments, chromosomes can be found lacking their interchromosomal tethers and merely need each arm aspirated into micropipettes, although the chromosome will usually be much more unstable and drift quickly around the well (free capture method) (Fig. 1.2-1F).

Once isolated, mitotic chromosomes can be analyzed in several ways to study their physical properties, the properties of molecules associated with the mitotic chromosomes, and how their molecules affect the physical properties. A simple force-extension experiment of an isolated chromosome can be performed by tracking the chromosome-anchoring pipettes during a stretching experiment (Fig. 1.2-1B). The stiff pipette pulls away from the force pipette, causing the chromosome to stretch. The stretching then causes the weaker pipette to deflect, which can act as a force readout. Analysis of the pipette tracking can then be used to derive the physical properties of the isolated chromosome, described in Section 1.2.1 (detailed in the Appendix).

Enzymes directly sprayed onto isolated chromosomes can cause changes in chromosomal structure. This can manifest in both qualitative, morphological changes or can manifest in mechanical changes, obtained by repeating the force-extension protocol. By comparing the physical properties of the chromosome before and after treatment, we gain an understanding in how the target of the treatment affects the overall mitotic chromosome structure. Molecules can be visualized through endogenous fluorescent proteins in engineered cell lines or through fluorescent antibodies that attach to their specified target. The location of these molecules, their intensity (correlated to the amount of protein present), and co-localization with other molecules is informative to their function in the mitotic chromosome.

Since this technique involves isolation from live cultured cells, they can be treated to study how the drug affects mitotic chromosome structure. Example treatments include drugs that affect the mitotic cycle, DNA chemistry, structural proteins, or DNA-interacting enzymes. The mitotic chromosome from those treated cells may show a structural and mechanical change in their properties. The mechanical changes would thus demonstrate a link between the affected system, molecule, or enzymatic target and the structure of mitotic chromosomes. Two cell treatments used with mitotic chromosome isolation are small interfering RNA (siRNA) and Auxin-Induced Degradation (AID) systems. Both these techniques remove target proteins, which are used to study the protein's role in mitotic chromosome structure. siRNA causes the cell to destroy the RNA transcript that encodes for the protein, slowly depleting the protein pool in the cell over time/cell cycles (Caplen & Mousses, 2003). AID involves engineering a cell to express a protein that has an AID sequence and a protein complex that can ubiquitinate the AID target (TIR1). When the small molecule, auxin, or its synthetic analogue, indole-3-acetic acid (IAA) is added to the engineered cell, the AID-tagged protein is polyubiquitinated and subsequently degraded (Prozillo et al., 2020). These techniques can be used in conjunction with chromosome isolation to study mitotic chromosome structure and its relationship with the target proteins.

This thesis utilizes the micromanipulation of mitotic chromosomes to understand the effects of rapid SMC complex degradation on mitotic chromosome mechanics (Chapter 2); the effect of histone PTM alterations and histone PTM readers on mechanics (Chapter 3); the physics and structure of meiotic chromosomes (Chapter 4); and the stiffness of the centromere (Chapter 5). Additional ideas for experimental projects are included in the conclusion section (Chapter 6) including both experimental projects inspired by questions raised from work in this thesis and projects from ideas accrued during this thesis. The Appendix also covers the methods

described here in additional detail so that one can learn the chromosome isolation procedure, experimental setup, data analysis, and the currently used experimental devices.

### **1.3 Structural Maintenance of Chromosome (SMC) complexes and loop extrusion**

#### **1.3.1 The loop-extrusion hypothesis: purpose, theory, modeling, and evidence**

The exact structure of the mitotic chromosome remains unknown, but there are several hypotheses that seek to explain its structure. We will describe the overall bottlebrush structure of mitotic chromosomes, their hypothesized construction via loop extrusion, how loop extrusion explains mitotic chromosome structure, and how the loop-extruding enzymes, condensin and cohesin, function within mitotic chromosomes to form their bottlebrush-like structure. Before continuing, we will describe the findings of some important early experiments in the study of structural maintenance of chromosome (SMC) complexes. Early investigations into SMC complexes demonstrated their importance to mitotic chromosome structure. Cohesin defects in yeast showed that its inactivation by a temperature sensitive mutant caused the yeast to no longer divide or enter anaphase (Strunnikov, Larionov, & Koshland, 1993). The mutations would also eventually kill the yeast cells. The yeast cells would also not enter mitosis in nocodazole-arrest treatments. Other papers focused on cohesin's sister SMC complex, condensin. These early papers revealed that condensin defects caused an increase in chromosome compaction defects, which led to cell death and mitotic arrests (Hirano & Mitchison, 1994; Strunnikov, Hogan, & Koshland, 1995). These papers also showed that condensin defects caused chromosomes to not fold properly and the chromosomes formed anaphase bridges. The predicted structure of these proteins during their early study also predicted their coiled-coil formation, although the whole complexes' shapes were unknown. Other chromatin structure work hypothesized that loops of chromatin could affect its organization for transcription in interphase (Riggs, 1990). Early

reviews eventually also hypothesized that the SMC complexes could extrude chromatin loops to compact the genome during mitosis to form the bottlebrush-like rod structure (Nasmyth, 2001).

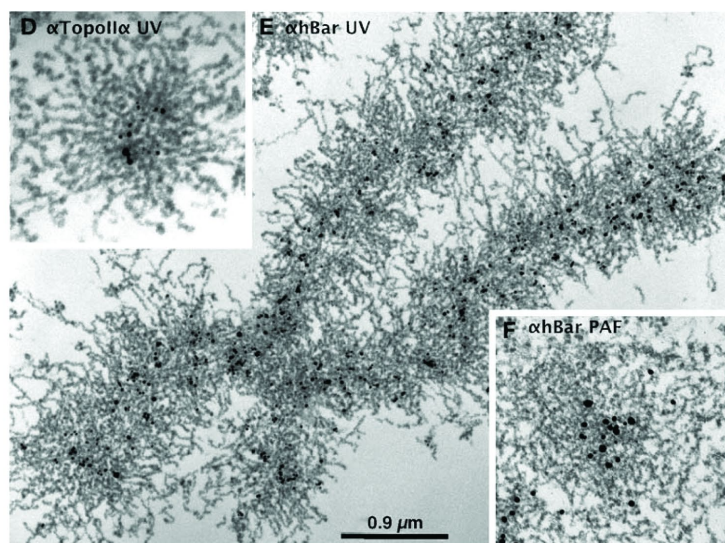
The bottlebrush-structure hypothesis depicts the mitotic chromosome as resembling a brush used for cleaning bottles or a pipe cleaner. This model envisions the mitotic chromosome as containing a semi-flexible structural core with smaller fibers emerging from the core (Marko & Siggia, 1997). This hypothesis was partly inspired from early electron microscopy experiments analyzing histone-free mitotic chromosomes (Paulson & Laemmli, 1977). These experiments displayed a dense, protein-rich structure in the middle of the mitotic chromosome and loose, random patterns of DNA loops emerging from the protein core. The structural core was formed from the central chromatin-organizing proteins, whereas the fibers were formed from the chromatin loops, which formed the bottlebrush-like structure. The mitotic chromosome was hypothesized to appear as the typical rod-shaped structure under less-detailed magnification. Further experiments were also used to analyze the location of structural proteins along the mitotic chromosome (Fig. 1.3-1A) (Maeshima, Eltsov, & Laemmli, 2005).

Some questions that arose from these experiments was how the core is formed, when it forms, and how it interacts with chromatin. The loop-extrusion hypothesis was created to address these questions (Alipour & Marko, 2012; Brahmachari & Marko, 2019; Davidson & Peters, 2021; Goloborodko et al., 2016). In this hypothesis, the protein core is not fully constructed before interacting with the chromatin but is a consequence of ring-like proteins binding and extruding stable loops of chromatin. With enough of these proteins the diffuse, globular structure of the interphase chromosome could fold into the typical rod-shaped structure of mitotic chromosomes, given enough rings and consistent loop sizes (Fig. 1.3-1B). The loop-extruding proteins would coalesce in the middle of the mitotic chromosome due to their loop extrusion

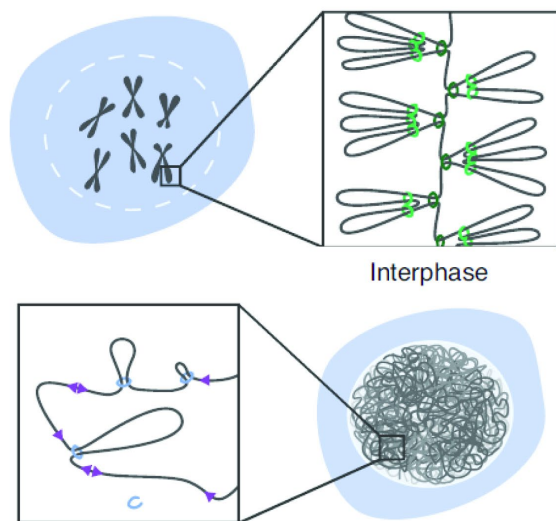
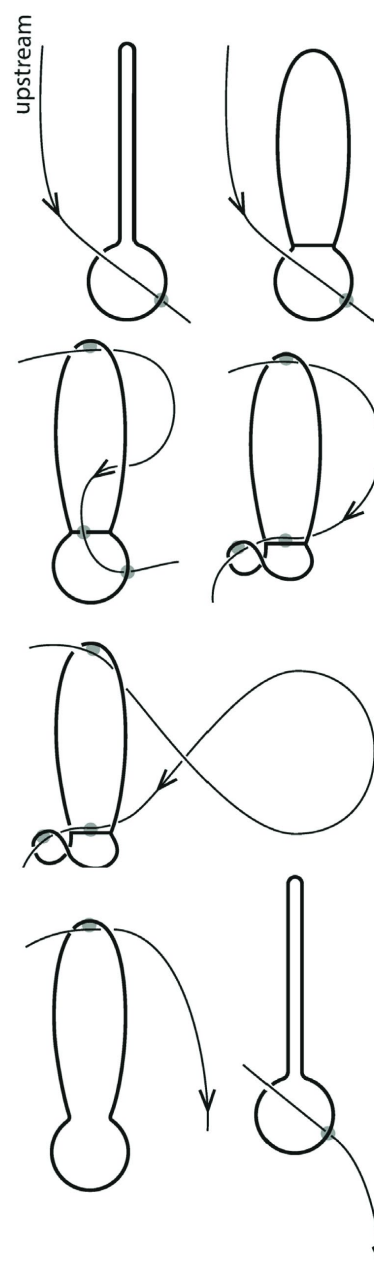
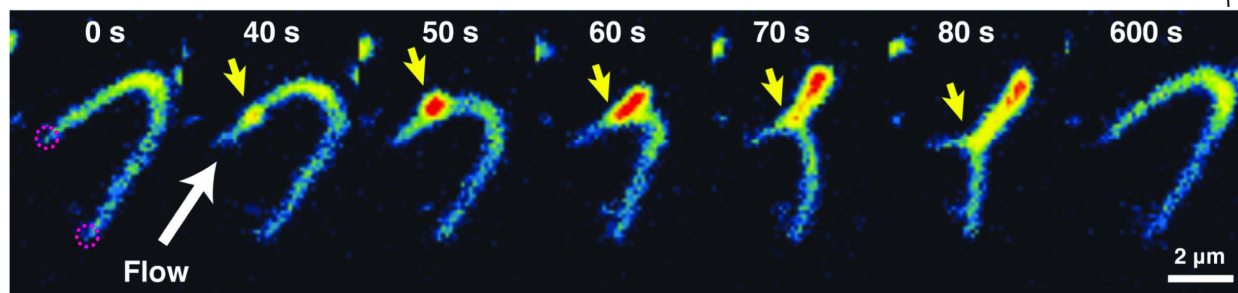
function and appear as the dense protein core. The extruded loops of chromatin from the extrusion process would appear as the chromatin fibers emanating from the proteinaceous core. Questions regarding the protein core, such as if the inner proteins form a contiguous core (Beseda et al., 2020), the loading and anchoring of the loop-extruding enzymes, if the loops are extruded in a one or two sided manner (Banigan, van den Berg, Brandao, Marko, & Mirny, 2020), and other questions remain avenues of active exploration.

Despite the remaining questions, the loop-extrusion hypothesis has become the most utilized model to describe mitotic chromosome structure and formation. This is in part due to the discovery and study of SMC complexes, which are described as the ring-like effector molecules of loop extrusion. Research into SMC complexes includes modeling how they extrude loops of chromatin assists in mitotic chromosome formation. One model demonstrates that the chromatin fiber loops in mitotic chromosomes could repel other chromatin loops to facilitate chromosome individualization (Bohn & Heermann, 2010, 2011). Other modeling research demonstrates how condensin's loop-extrusion capabilities could optimize chromatin loop size for removing entanglements (Brahmachari & Marko, 2018, 2019). This would occur by biasing the function of topoisomerase II (TopoII) towards removing chromatin entanglements rather than introducing entanglements, as TopoII does not intrinsically favor removal of entanglements over their formation (Holm et al., 1989).

Modeling experiments have also been used to relate SMC complex structural changes to their loop-extrusion functions (Fig. 1.3-1C) (Marko, De Los Rios, Barducci, & Gruber, 2019). Since SMC complexes have well-defined structures and domains, modeling their structural changes from one state to another helps us envision how they could repeatedly extrude chromatin loops. These experiments could also help relate their structural changes and enzymatic dynamics

**A**

Mitosis

**B****C****D**

### Figure 1.3-1. Loop extrusion via SMC complexes.

(A) Electron microscopy image of a mitotic chromosome with gold-labeled hBarren (CAP-H). Dark circles in the center of the chromosome mark condensin I location via metal infused complexes. The circles were found in the dense middle of the chromosome, spatially close to each other. From these dots emanated lines of chromatin, which are likely loops of chromatin anchored at the condensin molecule location. This showed the full chromosome folded via loop-extruding condensin with the two chromatid arms individualized and connected at the centromere. The view down the axis also demonstrates the location of condensin (lower left image) in the center of the long axis with the enrichment of TopoII in the middle (upper right image). Scale bar represents 0.9  $\mu\text{m}$ . Upper left and lower right images zoomed in 2-fold. (Maeshima et al., 2005). (B) Example of how SMC complexes extrude loops and organize chromatin in interphase and mitosis. In interphase, cohesin (blue ring) extrudes loops to organize chromosomes (grey), but not into the highly ordered structure of mitosis. Cohesin will stop extruding loops in interphase once barred from further movement by CTCF (purple triangles) sites on the chromosome. In mitosis, condensin II (dark blue ring) will form large loops until interacting with a nearby condensin complex and no more chromatin can be extruded. Condensin I (teal ring) will form additional, smaller loops on the condensin II-facilitated loops of chromatin, folding the chromosome into their dense, compact, and individualized mitotic form. Image repurposed from (Sedeno Cacciatore & Rowland, 2019). (C) SMC complex movements that allow the complex to translocate along chromatin. Once anchored onto a strand of chromatin (thin lines), the SMC complex (thick lines) can open its ring to allow chromatin to pass as well as bias the movement of the SMC complex in a specific direction. The SMC complex can then undertake a form in which the chromatin can pass through the ring fully. The ring can then close, pushing the chromatin further from its original loading position. If another part of the SMC complex remains attached to the original loading location on the chromosome, the SMC complex will extrude a loop of chromatin instead of merely translocating along the chromosome strand. Image repurposed from (Marko et al., 2019). (D) Biochemical evidence for condensin-based loop extrusion. A string of chromatin (visualized in fluorescence as a heat map, blue is less dense than yellow, which is less dense than red) was anchored at both ends to a glass surface, where the chromatin was visualized. After flowing in condensin, a molecule randomly bound to the tethered chromatin and started extruding a loop. This loop first appeared as an increase in chromatin density, but as the loop expanded in size, the directionality of the loop became more apparent under liquid flow. After some time, the condensin molecule disassociated from the chromatin, returning the tethered chromatin to its original state. In these experiments, condensin only pulled in chromatin from one side of its binding spot, leaving the other side the same size as when it originally bound. This shows evidence of one-sided loop extrusion. Scale bar represents 2  $\mu\text{m}$ . Image repurposed from (Ganji et al., 2018).

to their loop-extruding functions. Most systems modeling loop extrusion are constructed with an anchor point on the SMC complex, which extrudes loops by use of its translocase activity facilitated by their coiled-coil domains dynamically opening and closing (Banigan & Mirny, 2020; Brahmachari & Marko, 2018; Marko et al., 2019). The anchor point of DNA in these complexes remains unknown, but they may anchor DNA in their kleisin ring, between their heat repeat proteins, or inside their tripartite ring (Kschonsak et al., 2017; B. G. Lee et al., 2020; Piazza et al., 2014) (see Section 1.3.2 for descriptions of these domains). A critical step in loop extrusion is the ability for the enzyme to translocate along the string-like chromatin. One such modeling experiment demonstrated that SMC complexes could translocate across DNA by opening its ring, altering its structure while biasing DNA to exit outside the hole, then closing the ring once again (Fig. 1.3-1C) (Marko et al., 2019). Once a SMC complex binds DNA while translocating across DNA, it extrudes a loop away from its binding site. How and where SMC complexes bind DNA are studied using computer-modeling simulations to understand how SMC complex dynamics could extrude loops (Banigan et al., 2020; Goloborodko et al., 2016; Matityahu & Onn, 2021).

Modeling has also been used to determine the structure of chromatin after SMC-facilitated loops. Loop extrusion has been hypothesized to organize chromosomes in both interphase (topology/transcriptional control) and mitosis (compaction/individualization) (Fig. 1.3-1B) (Riggs, 1990; Sedeno Cacciatore & Rowland, 2019). Biochemical experiments on SMC complexes demonstrated they can extrude one-sided loops by binding and anchoring DNA then pulling chromatin into an extruded loop (Fig. 1.3-1D) (Ganji et al., 2018). However, modeling suggests that this method would not sufficiently compact a mitotic chromosome as it would leave chromatin gaps and thus requires two-sided loop extrusion (Banigan et al., 2020). SMC

complexes could switch the side it extrudes the loop or form a structure that allows two-sided loop extrusion. The handcuff model hypothesis involves SMC complexes dimerizing to form a paired structure that could extrude a loop on each side of each molecule (Barrington, Finn, & Hadjur, 2017; Brackley et al., 2018; N. Zhang et al., 2008). Another model suggests that the SMC complexes may interact with each other to form a multimeric, rosette-like structure (Badrinarayanan, Reyes-Lamothe, Uphoff, Leake, & Sherratt, 2012; Barysz et al., 2015).

There are some aspects of mitotic chromosome structure that loop-extrusion does not explicitly describe. One such aspect is the nature of the protein core in mitotic chromosomes. In the early electron microscopy experiment, it appeared that the mitotic chromosome formed a contiguous protein core (Paulson & Laemmli, 1977). However, isolated mitotic chromosomes treated with nucleases dissolved without leaving a connected protein structure behind (M. G. Poirier & Marko, 2002b; Sun et al., 2011). This suggests there is no stable, spatially close protein core at the middle of mitotic chromosomes but forms a more gel-like structure. The SMC complexes could utilize loop extrusion, chromatin crosslinking, and self-interaction to compact the chromosome without forming a stable, fully connected protein core. This gel-like structure is both challenged and supported by modeling research investigating the potential twist of the protein core in mitotic chromosomes (Almagro, Rivelino, Hirano, Houchmandzadeh, & Dimitrov, 2004; Gibcus et al., 2018; Poonperm et al., 2015; Yusuf, Kaneyoshi, Fukui, & Robinson, 2019). Ongoing modeling research into structural features of SMC complexes includes their ability to crosslink chromatin, self-interact, self-oligomerize, and if multimeric forms are required for mitotic chromosome formation. Modeling SMC complexes and their dynamics also attempts to address their behaviors regarding impediments on chromatin, such as

histones or transcription factors (Costantino, Hsieh, Lamothe, Darzacq, & Koshland, 2020; Davidson & Peters, 2021; Gibcus et al., 2018).

### **1.3.2 The purpose of condensin and cohesin- the loop-extruding elements**

Condensin and cohesin are two ring-shaped complexes that use loop extrusion and chromatin entrapment to transform interphase chromatin into mitotic chromosomes. Condensin and cohesin are part of the SMC complex family, which also includes the yet unnamed SMC5/6 complex involved in DNA repair (Aragon, 2018; Palecek, 2018). SMC complexes are a vital part of chromatin organization, present in nearly all forms of life (Hirano, 2016). All SMC complexes are thought to be capable of loop extrusion, although not all their activities relate to loop extrusion (Fig. 1.3-1D, Fig. 1.3-2A-C) (Davidson et al., 2019; Ganji et al., 2018; Lawrimore & Bloom, 2019; Palecek, 2018). Experiments on condensin have demonstrated its role in compacting and individualizing mitotic chromosomes (Kimura, Cuvier, & Hirano, 2001; Ono et al., 2003; M. Sun et al., 2018b; Takagi et al., 2018) (Fig. 1.2-3F) (Hirano, 2016). Mitotic chromosome individualization describes how mitotic chromosomes are organized such that they function as an individual object, *i.e.*, disentangled from other chromosomes. Condensin's actions have been shown to be important for both individualization on its own and through its interaction with other enzymes (Hartl, Sweeney, Knepler, & Bosco, 2008; Hirano, 2004; Howard-Till & Loidl, 2018). Sister chromatid cohesion is the act of keeping each of the chromatid pairs in the chromosome attached to each other until cell division and proper chromosome alignment (Fig. 1.3-2A). Sister chromatid cohesion is maintained until all chromosomes are aligned properly such that each daughter cell inherits only one copy of each chromosome (Diaz-Martinez & Clarke, 2009; Meadows & Millar, 2015). Experiments on cohesin have demonstrated its

importance in sister chromatid cohesion (Boavida, Santos, Mahtab, & Pisani, 2021; Henrikus & Costa, 2021; Klein et al., 1999).

Despite being responsible for different features of mitotic chromosome structure, condensin and cohesin share a remarkably similar structure. The basic structure of an SMC complex is comprised of a pair of rod-shaped SMC proteins, connected to each other at one end and connected to a bridging element, called a kleisin, at the other end (Davidson & Peters, 2021; Murayama, 2018; Palecek & Gruber, 2015) (Fig. 1.3-2A-C). SMC proteins adopt a rod-like shape by bending back on themselves around half their linear length and coiling around the initial section, forming a flexible coiled-coil rod (Fig. 1.3-2A-C). When two SMC proteins interact in the SMC complex, they interact at the halfway point when they bend back on themselves to form the hinge domain of the complex (Anderson, Losada, Erickson, & Hirano, 2002). The two SMC arms can contain two copies of the same protein or two different proteins, although they typically form a non-symmetrical ring even if they are formed from the same proteins (Hirano, 2016; Upton & Sherratt, 2013). Opposite the hinge are the ATPase-containing heads of the SMC arms, which interact with the kleisin unit to form a basic, complete SMC complex (Davidson & Peters, 2021; Hirano, 2016). The interactions of the core SMC complex create a flexible, ring-like structure that can interact with DNA. The dynamic opening and closing of the ring can be used to organize DNA. Additional regulatory proteins, called HEAT repeat proteins, associate with the kleisin, allowing for regulatory control of the SMC complex's function (Palecek & Gruber, 2015) (Fig. 1.3-2B) (Palecek, 2018).

Human cohesin arms are formed by the interaction of SMC1 and SMC3, which interact with Rad-21 as the kleisin unit (Losada, Hirano, & Hirano, 1998; Losada, Yokochi, Kobayashi, & Hirano, 2000; Toth et al., 1999). Stag/SA1 or Stag/SA2 are the Rad-21-associated HEAT

repeat regulatory proteins and are typically mutually exclusive. The entire human cohesin complex contains SMC1/SMC3/Rad-21/SA1 or SA2. There are also meiotic specific forms of cohesin that utilize different SMCs, kleisin, and regulatory proteins, covered in more detail in Section 1.5. Humans have two isoforms of condensin, termed condensin I or condensin II (Gerlich, Hirota, Koch, Peters, & Ellenberg, 2006; Hirano et al., 1997; Losada et al., 1998; Ono et al., 2003). Both condensin isoforms' arms are formed from SMC2 and SMC4. Condensin I's kleisin is the Condensin-Associating Protein (CAP)-H, which associates with both CAP-D2 and CAP-G as regulatory proteins. Condensin II's kleisin is CAP-H2, which associates with CAP-D3 and CAP-G2 as the regulatory proteins. The depiction of human SMC complexes can be seen in Fig. 1.3-2B (Palecek, 2018).

Condensin I and condensin II display different behavior in the cell. Condensin I is cytoplasmic during interphase while condensin II is nuclear (Gerlich et al., 2006; Green et al., 2012; Walther et al., 2018). Consequently, condensin II is constantly interacting with chromatin in interphase. Condensin II is also the first isoform used in mitotic chromosome compaction, since condensin I can only interact with the mitotic chromosome after NEBD in prometaphase. Condensin I is more dynamic on mitotic chromosomes, while condensin II is more stable on mitotic chromosomes. There is about four-six times more condensin I than condensin II on metaphase chromosome (Walther et al., 2018). Condensin I is found relatively proximal on mitotic chromosomes, while condensin II is comparatively axial. Condensin I removal results in longer, thinner mitotic chromosomes, while removal of condensin II results in shorter, fatter mitotic chromosomes (Green et al., 2012; Shintomi & Hirano, 2011).

The different features of the two condensin isoforms are thought to be functionally important. It is hypothesized that since condensin II binds first, more stably, and more centrally

on mitotic chromosomes, it is important for the initial compaction of mitotic chromosomes (Fig. 1.3-3D). These initial loops are thought to be larger, but more stable and serve as a backbone for further compaction. Condensin I properties suggest bind to the large, condensin-II-based chromatin loops to form more, but smaller, dynamic loops (Fig. 1.3-3E). These smaller, more frequent loops are thought to further compact the chromatin into its final, fully compacted mitotic state (Fig. 1.3-3F) (Hirano, 2016). When condensin II is removed from mitotic chromosomes, the only remaining chromatin-compacting loops are formed from the shorter, more frequent loops of condensin I, which results in a longer, thinner, and kinked mitotic chromosome (Ono et al., 2003; Shintomi & Hirano, 2011). When condensin I is removed from mitotic chromosomes, the only remaining chromatin-compacting loops are the stable, larger condensin II-based loops, which result in the shorter, fatter mitotic chromosome (Elbatsh et al., 2019; Green et al., 2012; Walther et al., 2018).

The loop-extrusion capabilities of SMC complexes have been long hypothesized, due to their ring-shaped structures and importance in chromosome structure (Fig. 1.3-2D) (Nasmyth, 2001). Recent biochemical *in vitro* experiments have demonstrated experimental evidence of their loop-extrusion capabilities by observing their interactions with tethered purified DNA (Fig. 1.3-1D) (Ganji et al., 2018). One technique used a one-sided DNA tether, forming long, horizontal strings or a “curtain” of DNA, hanging down from its tether point. When purified condensin was added to the experimental chamber, the DNA formed into bright dots and condensin translocated along the DNA (Cutts & Vannini, 2020; Kim, Shi, Zhang, Finkelstein, & Yu, 2019). The other condensin experiment utilized strands of DNA tethered to two points with enough excess length that DNA compaction could be observed (Ganji et al., 2018; Golfier, Quail, Kimura, & Brugués, 2020). Once again, a bright dot of DNA was observed after addition

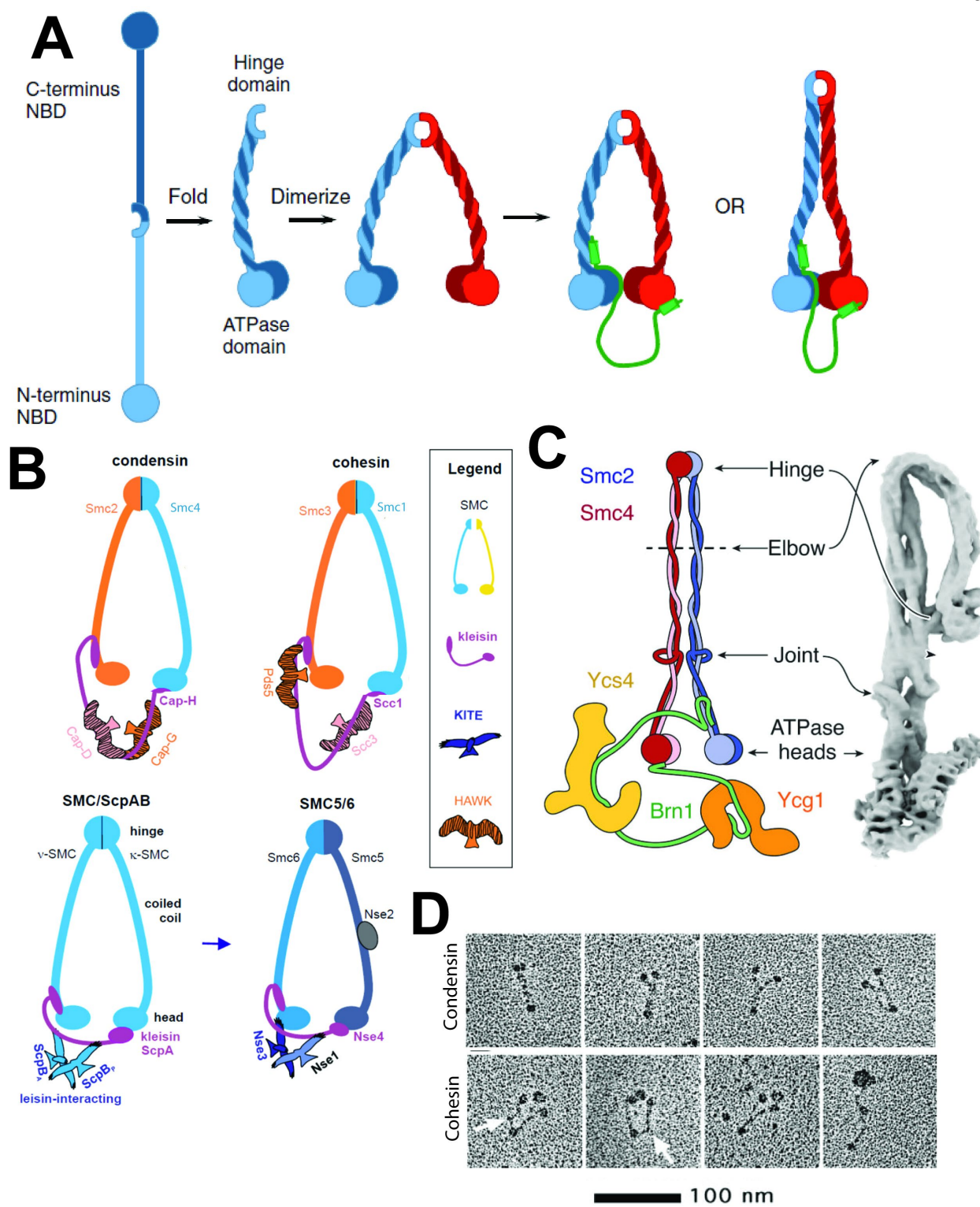


**Figure 1.3-2. Example images of SMC complexes.**

(A) SMC protein folding into a functional complex. The SMC protein (blue) will form a coiled-coil structure, where the C-terminus will interact with the N-terminus together to form the ATPase domain, while the opposite end in the middle will form the hinge domain. Two of these SMC proteins (blue and red) will attach at the hinge domain and form a tight angle. The two ATPase domains of the SMC proteins are connected by a kleisin protein (green) to form the basic complex. The final folding of the complex can adopt a more ring-like shape or triangle-like shape. Image repurposed from (Barrington et al., 2017). (B) Diagram of different SMC complexes and their components. SMC proteins are illustrated as straight arms (blue, yellow, and orange), which connect to each other and to the kleisin units. Kleisin proteins (purple) are depicted as horizontal, curved lines that interact with the SMC ATPase heads and the regulatory units KITEs (dark blue) (Kleisin Interacting winged-helix Tandem Elements) and HAWKs (orange) (Heat proteins Associated With Kleisins). KITEs and HAWKs are depicted as broad, bird-like shapes that associate with the kleisins. Condensin is formed from SMC2/4, CAP-H or H2, CAP-G or G2, and CAP-D2 or D3. Cohesin is formed from SMC1/3, Rad-21, and SA-1 or 2. The bacterial SMC complex SMC/ScpAB and human SMC5/6 complexes are also diagrammed to demonstrate the similarity of SMC complexes. Image repurposed from (Palecek, 2018). (C) Yeast condensin diagram with electron-microscopy-based reconstruction. The typical diagram of SMC complexes (colored schematic) displays a straight pair of coiled-coil proteins forming the SMC core of SMC complexes, but in this image, the filaments bend back on one another at the elbow and the hinge reconnects with the stiff beam of the SMC protein pair. Additional structural features, such as the SMC protein joints, their heads, and the structure of the kleisin and accessory proteins can be seen in the diagram with the corresponding reconstruction (grey object). The kleisin itself appears as connected discs, which connect to the rod-like structure of the SMC arms. Image repurposed from (B. G. Lee et al., 2020). (D) Electron microscopy images of the typical forms of condensin (top) and cohesin (bottom). Condensin had a much greater probability of forming an I- or V-like shape, suggesting it spends minimal time in an O-like shape. Cohesin was typically found either in a circle-like shape or with the SMC arms separated, suggesting that it forms circles for sister chromosome cohesion. Scale bar represents 0.1  $\mu\text{m}$ . Image repurposed from (Anderson et al., 2002).

of purified condensin. After this dot was found, a directional liquid flow was created in the chamber and caused the DNA dot to unfurl into a dense string along the flow direction. This demonstrated that the compacted DNA dot was in the form of a loop. The loop of DNA would grow until a certain loop size was reached while condensin remained attached to the DNA. The growth rate and maximum size of the DNA loop was used to obtain force generation and stall force of condensin in loop extrusion. Both the dot formation and loop growth depended on ATP, which active condensin utilizes. The loop extrusion cohesin experiments also used “curtains” of DNA. Once cohesin was added to the chamber, it compacted the DNA in the curtains and translocated along the DNA strands. The compaction and translocation of cohesin along the DNA demonstrated its DNA loop-extrusion capabilities.

Despite their structural similarities and loop-extruding capabilities, condensin and cohesin have different roles in mitotic chromosome structure. Investigations into the typical mitotic structures of condensin and cohesin were performed to see if structural differences could explain their respective mitotic functions. Electron microscopy demonstrated that cohesin tends to form a more open and circle-like structure, while condensin tended to adopt a straight, rod-like shape or a triangle-like shape (Fig. 1.3-2D) (Anderson et al., 2002). While the exact function of these shapes remains unknown, it is hypothesized that cohesin adopts the open, ring-shaped structure to facilitate sister chromatid cohesion by holding the two sister chromatids together (Boavida et al., 2021; Murayama, 2018; N. Zhang et al., 2008). Condensin is thought to adopt the rod and triangle-like structure due to its involvement in active chromatin compaction via loop extrusion. This is thought to occur by binding to chromatin, opening the SMC ring, and pushing chromatin through the SMC ring by zipping up and closing its ring-like opening (Fig. 1.3-1C) (Marko et al., 2019). Experiments on yeast condensin have revealed that the straight, entwined

arms of the SMC core contain a kink that folds back on itself (Fig. 1.3-2C). This fold is termed the elbow (B. G. Lee et al., 2020). Its function has been hypothesized to assist in the regulation of the enzymatic activity and chromatin capture.

### **1.3.3 Other cohesin roles in chromatin organization, function, and properties**

Despite having loop-extruding properties, the mitotic function of cohesin is chromatin entrapment and sister chromatid cohesion (Fig. 1.3-3A-C). Premature cleavage of the cohesin ring resulted in premature sister chromatid separation and demonstrated its role in sister chromatid cohesion (Pauli et al., 2008; Sonoda et al., 2001; Uhlmann, Wernic, Poupart, Koonin, & Nasmyth, 2000). Defects in sister chromatid cohesion resulted in inheritance defects when chromatids separated too early (Nasmyth, 2002; Remeseiro et al., 2012). The premature separation of mitotic chromatids led to an uneven distribution of the genome into the two daughter cells, which resulted in genomic instability, aneuploidy, and death. Cohesin can topologically entrap mini chromosomes, important for sister chromatid cohesion as it requires topologically entrapping multiple strands of chromatin (Makrantonis & Marston, 2018; Srinivasan, Fumasoni, Petela, Murray, & Nasmyth, 2020). The DNA-cohesin structure separated when either the DNA or cohesin ring was cleaved but did not disassociate when treated with denaturing levels of salt. This demonstrated that cohesin ring's structure can be deformed and molecules separated via non-covalent bonding, but still topologically entraps the DNA. Cohesin, which is enriched in the centromere, also assists in orienting the sister chromatids' kinetochores away from each other so the mitotic spindle can biorient (Stephens et al., 2013; D. Stevens, Gassmann, Oegema, & Desai, 2011). Bi-orientation of the kinetochore assists in even, accurate distribution of the chromosomes into their respective daughter cells. Additional information on the centromere and kinetochore is covered in Section 1.6.

Anaphase onset requires that the sister chromatids are free to separate into each daughter cell which requires cohesin removal to stop sister chromatid cohesion. Mitotic cohesin must adopt a careful balancing act of stably binding to sister chromatids to prevent premature sister chromatid separation, but not so stably that sister chromatid pairs cannot freely separate into their respective cells when cohesin is cleaved during anaphase. Defects in anaphase separation were likewise observed in cells containing non-cleavable cohesin mutants (Hauf, Waizenegger, & Peters, 2001; Kumada et al., 2006). The lack of anaphase separation resulted in metaphase arrest, DNA damage, and long anaphase bridges. The cohesin ring must also open for chromatin entrapment, but also remain closed once bound to the sister chromatids. Cohesin mutants that possessed a ring fused together could no longer topologically entrap minichromosomes which demonstrated the cohesin ring must be opened for chromatin entrapment and sister chromatid cohesion (Srinivasan et al., 2018).

Cohesin is associated with chromosomes throughout the cell cycle, but its function in sister chromatid cohesion begins in S-phase, when the chromosomes are duplicated (Boavida et al., 2021; Srinivasan et al., 2020). While cohesin can rebind to mitotic chromatin after S-phase, it is insufficient for proper sister chromatid cohesion (Lyons & Morgan, 2011; Peters & Nishiyama, 2012; Uhlmann & Nasmyth, 1998). This demonstrates that cohesin must be loaded onto chromosomes during S-phase for its mitotic function. Cohesin is thought to topologically entrap sister chromatids by binding to chromatin while it is being duplicated. It is unknown how sister chromatid cohesion uses cohesin. Some hypotheses include one cohesin ring engulfing two chromatin strands, two cohesin rings each binding a strand of chromatin non-covalently bound to each other, or two cohesin rings topologically entrapped in one another (Barrington et al., 2017; Brackley et al., 2018; N. Zhang et al., 2008) (Fig. 1.3-3A). Cohesin on the chromosome arms is

removed in prophase (Peters & Nishiyama, 2012). This occurs by opening the cohesin ring, similar to its interphase dynamics (Onn, Heidinger-Pauli, Guacci, Unal, & Koshland, 2008). WAPL, a protein associated with cohesin and responsible for opening cohesin's ring during interphase, has been implicated in opening cohesin's ring during mitosis as WAPL associates with cohesin on the chromosome arms during mitosis (Bloom, 2017; Kueng et al., 2006). Centromeric cohesin is resistant to WAPL-induced ring opening in mitosis (Boavida et al., 2021; Henrikus & Costa, 2021), which is only removed once SMC3 is cleaved in anaphase. This cleavage only occurs once the anaphase-promoting complex is active (Batty & Gerlich, 2019; Meadows & Millar, 2015). Activation of the anaphase-promoting complex occurs once spindle microtubules attach to all kinetochores, mitotic chromosomes are aligned at the metaphase plate, and the spindle assembly checkpoint (SAC) has been satisfied. Further information of the SAC is covered in Section 1.6.

The dominant role of interphase cohesin appears to be chromatin loop extrusion, stabilization, and organization, instead of sister chromatid cohesion and chromatin entrapment. Chromosome conformation capture (3C) or its variants like Hi-C are used to investigate cohesin's role in creating and maintaining loops of chromatin (Srinivasan et al., 2018) (Fig. 1.3-3B,C) (Davidson & Peters, 2021; Rao et al., 2017; Sedeno Cacciatore & Rowland, 2019). Hi-C involves sequencing DNA and observing which sequences are spatially close together via coincident sequencing reads (Goel & Hansen, 2020). An increase in DNA-DNA spatial interactions can be observed by an increase in coincident reads. These reads are strongest at DNA sequences that are very close in the linear DNA sequence, called the diagonal. However, there are also areas that contain greater interactions more than closer regions, called corners (Davidson & Peters, 2021). The presence of corners suggests the chromatin spatially folds back

on itself, in a loop-like manner (Costantino et al., 2020). The diagonal-to-corner region can also see an increase of interactions, which are called sides. The presence of sides suggests one spatial point of DNA has a higher likelihood of interacting with all the sequence between the two points. This can occur if a DNA sequence is anchored to one point and is moving towards another stop point, which has been claimed to demonstrate loop extrusion.

CTCF is a protein that associates with cohesin and is thought to prevent cohesin from moving further along chromatin, acting as a stopping point (Alpsoy, Sood, & Dykhuizen, 2021). Using Hi-C on interphase cells, corners can be seen where CTCF is located, and sides occur between CTCF-bound sequences. These experiments suggest that cohesin pseudo-topologically associates with chromatin and extrudes that chromatin until it hits a CTCF boundary (Eagen, 2018; Kim et al., 2019). The cohesin stopped at the CTCF boundaries stabilizes the DNA contacts, forming the corner dot on the contact map. Cohesin depletion results in the loss of these corner dots while cohesin stability defects cause these dots to weaken and fade (Wutz et al., 2017). It is thought that these loops are created and maintained so cohesin can assist in compaction, organization, and transcriptional control of the genome (Alpsoy et al., 2021; Beseda et al., 2020; Boavida et al., 2021). The control of chromatin topology is thought to affect the transcriptional makeup of the cell, although this is still debated.

Transcriptional defects and regulation occur when cohesin is perturbed in interphase cells. This is used as evidence relating its loop-extrusion properties to its ability in controlling DNA transcription (Alpsoy et al., 2021; Beseda et al., 2020; Boavida et al., 2021). Genetic depletion of WAPL results in increased stability of cohesin on interphase chromatin, since WAPL causes cohesin to open its ring-like structure (Kueng et al., 2006). The opening of the cohesin ring causes it to disassociate with chromatin. WAPL depletion then causes the

chromosomes to fold into compact shapes, which are termed vermicelli (Tedeschi et al., 2013). Vermicelli are chromatid-like structures, although they do not fully mimic mitotic chromosome compaction. Altering cohesin stability by depletion of SCC1 siRNA rescued the vermicelli phenotype in WAPL depleted cells by returning the chromosome back its natural, decondensed state. WAPL depletion also results in mitotic defects, such as an increase in anaphase bridges and bi-nucleated cells at the end of mitosis (meaning the chromatids did not properly separate as distinct identities). The increase in mitotic defect arises from the inability for chromosomes to properly separate during anaphase.

Since cohesin has two distinct modes of operation between loop extrusion in interphase and sister chromatid cohesion in mitosis, there must exist some mechanism to change its activity. The acetylation of cohesin by ESCO1 and ESCO2 affect cohesin's stability on chromosomes and its sister chromatid cohesion strength differently (Tedeschi et al., 2013). Cohesin stability is related to the WAPL-assisted cohesin ring opening, which is inhibited by the acetylation of SMC3 by ESCO1 and ESCO2. ESCO2 is hypothesized to be the controlling factor in sister chromatid cohesion for the cohesin complex, since it follows a cell cycle pattern, is necessary for sister chromatid cohesion, and does not preferentially associate with CTCF like ESCO1.

#### **1.3.4 Condensin - history, compaction, supercoiling, and removal**

Condensin is the SMC complex typically associated with mitotic chromosome compaction through loop extrusion (Batty & Gerlich, 2019; Davidson & Peters, 2021; Marko, 2008). Eukaryotic Condensin was identified as a five-part complex through purification in *Xenopus* extract (Hirano et al., 1997). Antibody-targeting based depletion of condensin caused mitotic chromosomes to become puffy, entangled, brittle, and globular, *i.e.*, lost its rod-shape structure. These condensin-depleted chromosomes could no longer individualize or form their

typical X-shaped structure, as expected of chromosomes that were not compact and had no underlying organization. Condensin is also required for chromosome segregation, as its depletion results in non-individualized, inseparable chromosomes (Gerlich et al., 2006).

Condensin dynamics are another area of experimental interest. Early FRAP experiments on condensin I resulted in rapid recovery of fluorescence on mitotic chromosomes after photobleaching (Gerlich et al., 2006). This demonstrated condensin I's dynamic nature on mitotic chromosomes. FRAP experiments on condensin II during mitosis after NEBD did not recover much of its fluorescence after photobleaching. Condensin II rapidly recovered about half its fluorescence intensity during prophase and rapidly recovered its fluorescence during interphase. These experiments were one of the first to demonstrate the different properties between the two condensin isoforms during mitosis. These experiments also showed that condensin II's dynamics are influenced by the cell cycle. Depletion of SMC2, which affects both condensin isoforms, caused a high amount of cell lethality and led to very little mitotic chromosomal compaction and organization (Green et al., 2012; Ono et al., 2003). Depletion of condensin I by targeting CAP-H had a small amount of lethality and still compacted mitotic chromosomes but led to short, fat chromosomes. Depletion of condensin II by targeting CAP-D3 resulted in a higher level of lethality than condensin I depletion, but less than SMC2 depletion. The condensin II-depleted chromosomes also still compacted their chromosomes, but formed longer, thinner, kinked, and twisted mitotic chromosomes.

Condensin contains two ATPase sites where the SMC2-SMC4 heads interact in their closed-form state (Anderson et al., 2002; Barysz et al., 2015). Studying and comparing perturbations to the different ATPase sites using engineered cell lines resulted in different mitotic defects as studied by live cell chromosomal morphology and interactions with purified

DNA (Elbatsh et al., 2019). These experiments created viable (non-lethal) ATPase mutants, which was useful since most condensin defects result in cell lethality. Perturbation of the first ATPase site (Smc2 L1048V) caused the chromosomes in the cell to become fuzzy and decompact. The purified condensin with the site 1 defect compacted DNA and extruded loops slower than purified wild type condensin while showing no changes to its stability on mitotic chromatin. Perturbation to the second ATPase site (Smc4 L1323V) caused the chromosomes in the cell to become hypercompact, short, and fat, like condensin II depletion.

The purified condensin with the site 2 defect compacted DNA faster than wild type while showing no changes to its stability on mitotic chromatin or rate of loop extrusion. Condensin I depletion rescued the chromosomal shape defects from the site 2 condensin mutation, although still contained mitotic defects, like segregation errors and anaphase bridges. The differences in the ATPase mutations suggested the ATPase sites may affect the processivity of condensin-extruded loops. The processivity control may also be under functional control. Condensin's alternate ATPase functions may also assist in the final formation of mitotic chromosomes. This research also revealed knowledge gaps about condensins' function, which can be explored by functional analysis of its enzymatic domains.

Rapid super resolution imaging of condensin I and condensin II was used to further study their functional differences with better time resolution (Green et al., 2012). Condensin II was again shown to be very stable on mitotic chromosomes while condensin I was shown to be very dynamic (Walther et al., 2018). Condensin II was also located more axially than condensin I, which was located more distally on mitotic chromosomes. This research found a 4 to 6:1 ratio of condensin I to condensin II depending on the substage of mitosis. Condensin I bound in two waves: one wave that bound at the beginning of nuclear envelope breakdown in prometaphase,

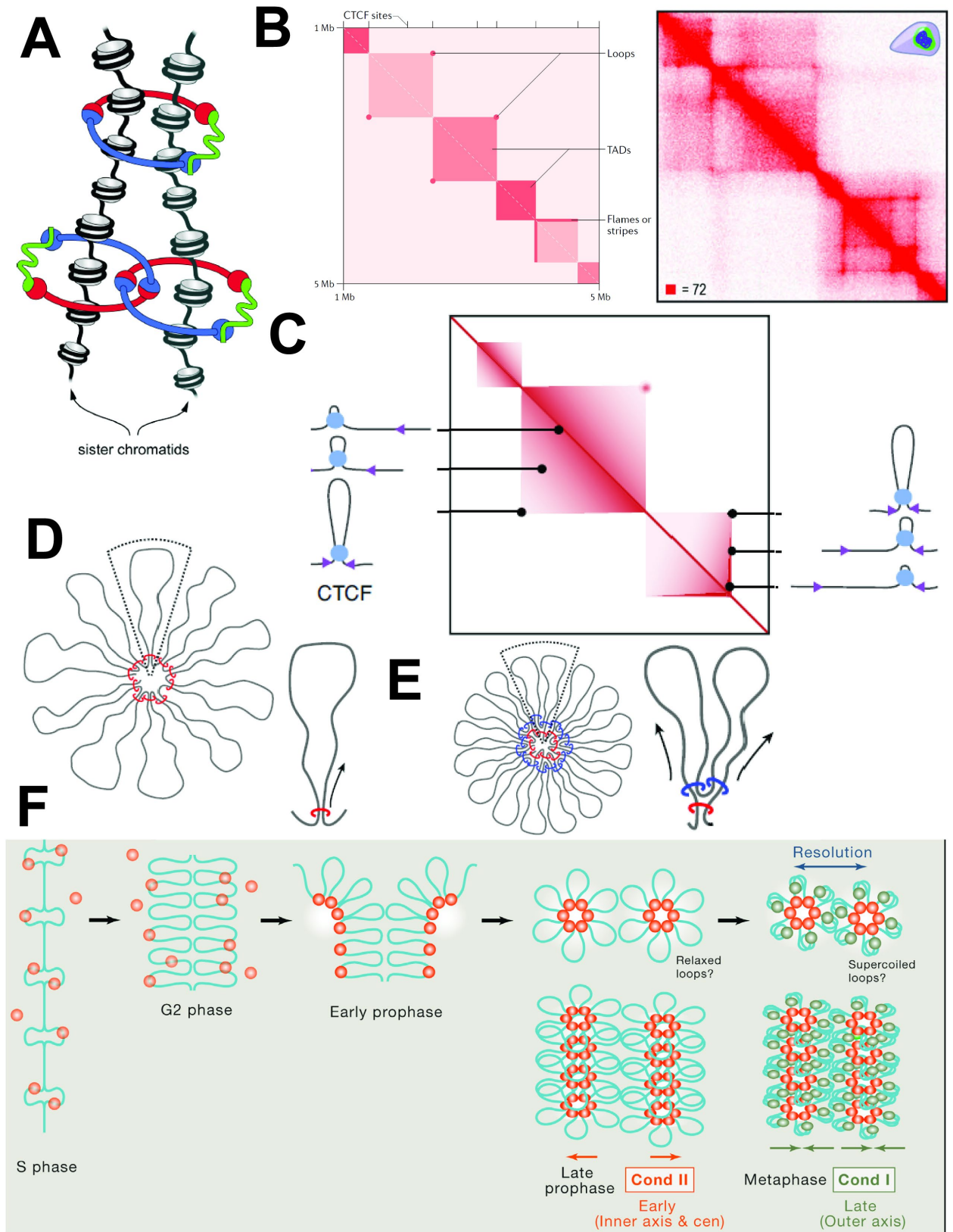


### Figure 1.3-3. Diagrams of SMC complex functions.

(A) Sister chromatid cohesion by cohesin binding in a single-complex configuration (top) and handcuff-model configuration (bottom). Cohesin (in red, blue, and green for the SMC arms and kleisin, respectively) entraps chromatin (DNA in black, histones in grey), holding the strands topologically entwined with each other. The single-complex configuration engulfs both strands of chromatin, while the handcuff model uses two molecules of cohesin topologically entwined with each other and their respective chromatin strands. Image repurposed from (Haering & Jessberger, 2012). (B, C) Hi-C data demonstrating loop formation in interphase and diagrams of how cohesin creates the Hi-C pattern observed. (C, left) The heat maps depicted show the contact frequency of an interphase chromosome with the base pair on the x and y axes. The most frequent interactions occur along the diagonal, where linearly close regions will be more likely to interact with one another. Off the diagonal, there are areas where there is an increase in interactions, due to a loop of chromatin pinned down at one location via cohesin holding. At these points, chromatin is much less likely to interact with other regions positioned close together. (C, right) Regions in this close-interacting domain are called topological associating domains. Stripes are instances where the edge of a loop has increased interactions with an underlying area. This occurs when cohesin has reached one CTCF domain and cannot pass, meaning the pinned area interacts along that edge more than any deeper area. (D) The formation of these domains is diagrammed in the bottom portion of the Figure. Images in C and D repurposed from (Davidson & Peters, 2021; Rao et al., 2017; Sedeno Cacciatore & Rowland, 2019). (D, E) Simplified diagram of how condensins fold mitotic chromosomes. (D) Condensin II (red) binds to chromatin (grey) and extrudes the chromatin into large loops. Eventually the condensin II complexes will pack together at the center axis of the chromosome, potentially interacting with one another and forming rosettes. (E) Condensin I (blue) will form additional, but smaller loops on the chromosome to further compact the chromosome and make it denser. Images in Figures D and E repurposed from (Batty & Gerlich, 2019). (F) Time course of condensin binding and function of condensin on mitotic chromosomes. Condensin II (orange) can bind to chromosomes (blue) at S-phase and remain during G<sub>2</sub>, potentially crosslinking some regions of the chromosome. Upon entry to prophase, condensin II will start forming loops of chromatin, beginning the process of chromosome compaction and chromosome organization. Late in prophase, condensin II may start interacting with other condensin II complexes and form rosettes of chromosomes, which makes the entire structure adopt its rod-like shape. Upon nuclear envelope breakdown into metaphase, condensin I (green) will bind to chromatin on the outer chromosome loops into denser structures, which may assist in chromosome resolution/individualization and disentanglement. Image repurposed from (Hirano, 2016).

and a second wave that bound during anaphase. The second wave of condensin I binding suggested additional complexity of condensin I dynamics and function. CAP-H or H2 was shown to be the limiting factor of condensin binding to mitotic chromosomes for their respective isoform. This research recapitulated the loop-extrusion model of compaction by condensin due to verifying previous condensin I and condensin II findings, which the authors diagrammed.

Condensin can form multimers, which may be functionally relevant in the loop-extrusion hypothesis. The SMC head of one condensin complex can interact with another condensin complex SMC head, which may assist in multimer formation (Badrinarayanan et al., 2012; Barysz et al., 2015; Matoba, Yamazoe, Mayanagi, Morikawa, & Hiraga, 2005). Experiments on purified bacterial condensins revealed stoichiometries that suggest a kleisin unit is being shared between multiple condensins. Elutions of purified yeast condensin also contain peaks that correspond to condensin multimers (Keenholtz et al., 2017). In DNA-based magnetic bead experiments, the multimer was better in ATP-based compaction of DNA, compacted DNA under a greater amount of force, and compacted DNA faster than the monomer. These experiments suggested a functional difference between the monomeric and multimeric form of condensin. Models of mitotic chromosome formation have hypothesized the use of condensin multimers (Green et al., 2012). Several condensin complexes interact to form rosettes of condensin in these models. Chromatin would then form loops off the dense condensin rosettes. Some models further state a continuous rosette formation throughout the entire chromosome to form the contiguous protein core seen in electron microscopy experiments (Paulson & Laemmli, 1977) (Fig. 1.3-1A) (Maeshima et al., 2005). The contiguous core would give rise to a central helical coil, seen in other images of mitotic chromosomes (Beseda et al., 2020). However, mitotic chromosomes

treated with DNases left behind no protein core, suggesting there is not a stable, contiguous protein core (M. G. Poirier & Marko, 2002b; Sun et al., 2011).

Condensin loading onto mitotic chromosomes is also not fully known and remains an area of active study. In the previous magnetic tweezers experiments condensin compacted DNA without the use of ATP under physiological salt conditions (Keenholtz et al., 2017). This suggested condensin may physically bind chromosomes without its enzymatic function. However, other experiments suggested condensin may require ATP to bind chromatin in addition to condensin's loop-extruding, enzymatic functions (Burmam et al., 2017; Gruber & Errington, 2009). Bacteria contain DNA-specific condensin binding sites, but it remains unknown if human condensin also functions this way or binds randomly to mitotic chromatin (Gruber & Errington, 2009). Nucleosome eviction can assist in condensin loading, suggesting that the histone-free regions of the chromosome may be preferred for condensin loading (Toselli-Mollereau et al., 2016). Nucleosome-free sites include areas of the genome undergoing active transcription or duplication, which may assist in condensin II binding, as it is nuclear during S-phase (Schwabish & Struhl, 2004). While cohesin has dedicated loading complexes, dedicated loading complexes for condensin have not been found. Condensin may not topologically entrap chromatin in its ring, like cohesin, but forms pseudo-topological entrapments and extrudes loops out of its ring (Srinivasan et al., 2018).

Folded chromosomes have been constructed *in-vitro* by taking cell-free chromatin from *Xenopus* extract and adding purified proteins (Shintomi et al., 2017; Shintomi, Takahashi, & Hirano, 2015). Depending on the proteins added back into solution, the chromosome will adopt different shapes, suggesting different roles for the different proteins not present in the extract. Without any additional proteins, the initial sperm chromatids appeared as a small, snake-shaped

bundles. When complete *Xenopus* extract was added to the sperm nuclei, they folded into bundles of dense threads. The bundle formed an amorphous cloud of chromatin with condensin removal. The chromosome swelled into a larger S-shape, but not into dense threads with condensin alone. This suggested that condensin alone is not responsible for the condensed, thread-like structure of mitotic chromosomes. This research demonstrated that only 6 purified components- core histones, condensin I, TopoII and three histone chaperones (nucleoplasmin, Nap1, and FACT) were needed to transform the initial sperm chromatid into its final state of condensed threads. The addition of these six components phenocopied the addition of complete *Xenopus* extract. This data suggested that mitotic chromosome formation, structure, and compaction utilizes histones, histone remodelers, chromatin topoisomerases, and condensin.

Rapid depletion of SMC2 using auxin-induced degradation (AID) tags caused the chromosome to become greatly entangled (Takagi et al., 2018). The complete lack of chromosome structure only occurred when both Ki-67 (see section 1.3.5 for additional information) and SMC2 were degraded. This again demonstrated that while condensin is important for compaction, other proteins are required for proper mitotic chromosome formation and can support structure. When TEV was activated in cells with a TEV-sensitive-cleavage-site condensin containing condensed meiotic chromosomes, the meiotic chromosome would swell (Houlard et al., 2015). The swelling demonstrated condensin must be able to form a closed, ring-like structure to properly function. It also showed that while condensin I depletion resulted in a shortened chromosome phenotype, condensin II depletion was lethal and led to very long chromosomes with long anaphase tails. This long-tail phenotype resulted in further chromosome defects. Together these experiments demonstrate the importance of condensin and its closed,

ring-shaped form in compacting mitotic chromosomes into their dense, loop-based structure like cohesin required for chromatin compaction.

Condensin is important for maintaining the physical and mechanical stiffness of mitotic chromosomes (M. Sun et al., 2018b). siRNA against CAP-G, CAP-G2, and SMC2 depleted condensin I, condensin II, and both isoforms, respectively, from the cell. Following condensin depletion, single chromosomes were isolated and stretched to find their mechanical stiffness (see Section 1.2 and the Appendix for more information). SMC2 depletion caused the mitotic bundle to lose all its shape, like the experiments found inside the cell with AID-based degradation (Takagi et al., 2018). The bundle would also swell when held in buffer outside the cell. SMC2 depletion also caused the chromosome to lose nearly all its stiffness, CAP-G depletion showed a small reduction in stiffness, while CAP-G2 depletion caused an intermediate reduction in stiffness. Condensin II, which forms the center, stable core of mitotic chromosome was shown to contribute more to chromosomal stiffness of mitotic chromosomes, but both condensin isoforms were shown to be important and have a mechanical impact on mitotic chromosomes.

SMC complexes have been shown to be mechanically important in maintaining stiffness of the centromere. In yeast, the centromere to centromere distance and variation of distance was used to determine mitotic centromeric stiffness (Stephens et al., 2013). Both condensin and cohesin are enriched at the centromere in yeast and humans. The enrichment is presumed to be important for protecting the chromosomes from the higher forces applied to the kinetochore and centromere by the spindle microtubules, which can be as high as 700 pN (in grasshopper cells) (Nicklas, 1983). Depletion of condensin or cohesin increased the value and variation of the mitotic centromere-to-centromere distance. This suggested a relationship between mitotic

chromatin stiffness and SMC complexes. This supported the hypothesis that the centromeric enrichment of condensin and cohesin is important for mechanical stability.

Condensin II is purported to possess loop-extrusion capabilities in the interphase nucleus, although its function remains unclear. Condensin II's localization in the nucleus may merely be useful for the initial binding of condensin to mitotic chromosomes in prophase. Condensin has been shown to bind chromosomes as soon as S-phase, which may assist in individualizing mitotic chromatids (Ono, Yamashita, & Hirano, 2013). Condensin II, like cohesin may also play a role in organizing the chromatin into loops during interphase for spatial control and transcriptional regulation (Hocquet et al., 2018; Hoencamp et al., 2021). However, it should be kept in mind that condensin is dynamic in interphase, which can be compared to its mitotic stability and cohesin's interphase stability (Costantino et al., 2020; Green et al., 2012; Walther et al., 2018). Condensin II modifications and its activity on mitotic chromosomes may also be related, like the changes cohesin undergoes between mitosis and interphase.

The localization of TopoII and condensin binding in mitosis are related (Cuvier & Hirano, 2003). Condensin defects lead to entanglement issues, which are normally resolved by TopoII binding and activity, suggesting a relationship between the two complexes (Hartl et al., 2008). Condensin binding causes positive supercoiling of DNA, which preferentially attracts TopoII. TopoII preferentially binds positive supercoils, which may be how TopoII is recruited to condensin-enriched areas and resolves entanglements (Baxter et al., 2011; Kimura & Hirano, 1997). Compaction of mitotic chromosomes could also make the entanglements more pronounced and easily accessible, resulting in chromatin disentanglement by TopoII.

### **1.3.5 Other critical proteins in mitotic chromosome structure- TopoII and Ki-67**

Topoisomerase II (TopoII) and Ki-67 are two additional, non-SMC-complex proteins important in the formation of mitotic chromosomes. Type II topoisomerases are protein complexes change the topology, or connectedness of a target DNA molecule/polymer (Hanke, Ziraldo, & Levene, 2021). TopoII binds two strands of DNA, cuts one of the DNA strands while holding the other, structurally changes so that the cut strand is put on the opposite side of the held strand (relative to its starting position), then religates the cut strand. Catenated DNA rings were separated when incubated with active TopoII, which demonstrated its topology-changing capabilities (Goto & Wang, 1982; L. F. Liu, Liu, & Alberts, 1980). Free DNA rings were catenated together (topologically linked) when incubated with active TopoII. The middle of a very long strand of chromatin can be approximated as a circle. Sister and other chromosomes can act like to two rings of DNA, where TopoII can catenate unlinked chromosomes (increasing entanglements) or decatenate unlinked DNA (decreasing entanglements). DNA damage occurs when there are still entanglements present during anaphase. The DNA damage occurs by physically breaking the entangled DNA from the force generated by the spindle poles. The improperly broken DNA can introduce genetic errors by the DNA damage. TopoII inhibition causes cells to accumulate DNA damage and die or accumulate other cellular disfunctions that are too toxic for the cell proliferation (Gulliya et al., 1994; Negri, Bernardi, Donzelli, & Scovassi, 1995). Indeed, a popular anti-cancer therapeutic drug inhibits TopoII activity. Since cancer cells rapidly divide, damage to their DNA in mitosis is greater than slower replicating cells, causing the cancer cells to die quicker. The increased DNA damage via replication is how anti-cancer TopoII-inhibitor therapeutics function.

TopoII has weakens and stiffens mitotic chromosomes depending on the context (Kawamura et al., 2010; Sun, 2014; Sun et al., 2011). Mitotic newt chromosomes were slightly weakened when sprayed with active human TopoII and ATP (Kawamura et al., 2010). Inactive TopoII lacking ATP or chemically inhibited did not affect mitotic newt chromosome stiffness. This suggested that naturally occurring chromatin entanglements stiffen mitotic chromosomes, as their removal weakens mitotic chromosomes. However, TopoII treatment on human mitotic chromosomes stiffened them, whether it was active or inactive in a dose-dependent manner (Sun, 2014). This suggested complicated behavior of TopoII and its interactions with chromatin.

The stiffening phenotype suggested that TopoII may structurally influence mitotic chromosomes by binding and crosslinking mitotic chromatin. Indeed, an early name for TopoII was scaffold protein 1 (SC1) when its other enzymatic functions were unknown. This naming convention suggested evidence for TopoII to structurally influence and stiffen mitotic chromosomes. TopoII can bind chromatin in two places, meaning it can act as an effective chromatin crosslinker (Lane et al., 2013). Active crosslinking creates a stronger gel meshwork for the mitotic chromosome by introducing more anchor points for the underlying fibers. The binding function of TopoII was compared to its enzymatic function and found that its binding function did not require its enzymatic function. It was also discovered that there are two different TopoII chromatin-binding sites, one to DNA and another to histones, which was also influenced by histone PTMs. By binding and crosslinking chromatin, TopoII could influence their center-chromosome localization.

A final protein important for the formation of mitotic chromosomes is Ki-67. Ki-67 is used a cell proliferation marker and localizes to mitotic chromosome (Gerdes, Schwab, Lemke, & Stein, 1983). Ki-67 is often used in cancer studies due to its relationship to cell proliferation

(and cancer cells rapid proliferation). It localized to the perichromosome (outer surface of the chromosome) during mitosis which makes it a good tool for identifying mitotic cells and chromosomes (Endl & Gerdes, 2000; Gerdes, 1990). Ki-67 functions as a surfactant barrier around the chromatids. This barrier prevents entanglements between chromosomes, important for chromatid individualization (Cuylen et al., 2016). Ki-67 is also highly dynamic on mitotic chromosomes to create said barrier. Without Ki-67, mitotic chromosomes lose their individualization, in a separate pathway to condensin, but still maintain some of their core structure and do not form into chromatin blobs (Takagi et al., 2018). Ki-67 also functions in heterochromatin and cell cycle control, which will not be discussed further (Sobecki et al., 2016).

## **1.4 Histone post-translational modifications (PTMs) and interactions**

### **1.4.1 Histones, nucleosomes, modifiers, and chromatin background**

The basic unit of the genome is double stranded (ds) DNA, which can be imagined as a very fine thread. dsDNA is typically not found in the cell as naked DNA but is organized by DNA-interacting proteins. In eukaryotes, such as humans, cells organize their DNA by wrapping it around bead-like structures called histones. Functional histones typically form an eight-part structure, called a histone octamer, formed from two copies of each of the core histone proteins (Alabert, Jasencakova, & Groth, 2017; Doenecke, 2014; V. Morales et al., 2001). The four core histone proteins are H2A, H2B, H3, and H4. Two copies of histone H3 and H4 each will form a tetramer  $(H3-H4)_2$ . Two dimers of H2A and H2B will interact with the  $(H3-H4)_2$  tetramer to form the octamer, which adopts a flat, disk-like structure (Fig. 1.4-1A) (V. Morales et al., 2001). The dsDNA fiber is wound around the circumference of the histone octamer about 1.7 times (about 146 base pairs) (Fig. 1.4-1B) (Prieto & Maeshima, 2019). DNA wrapped around the

histone octamer gives rise to the “beads on a string” model of chromatin, with the DNA imagined as a string and the histone octamer imagined as a bead (Bell, Tiwari, Thoma, & Schubeler, 2011; Marko & Siggia, 1997; Marsden & Laemmli, 1979). The histone octamer and the DNA wrapped around it is called a nucleosome, which is the base unit of chromatin. Another histone protein, histone H1, can link octamers together for organization and compaction. The addition of histone H1 was thought to link nucleosomes together to adopt the “30 nm fiber” (Alabert et al., 2017; Bell et al., 2011; Marko, 2008). However, other structural studies on cellular chromatin suggest the 30 nm fiber does not occur consistently in live cells (Joti et al., 2012; Maeshima, Imai, Hikima, & Joti, 2014).

Each of the histones in the octamer contain histone “tails”, which are relatively unstructured regions of the histone. Tails extrude from the “bead” part of the octamer (Doenecke, 2014; V. Morales et al., 2001; F. Wang & Higgins, 2013; L. Wang, Xu, Khawar, Liu, & Li, 2017). The extrusion of the tails from the octamer makes them easily accessible for post-translational modifications (PTMs), which are utilized to alter chromatin structure. Some histone PTMs occur in the core of the octamer, not the tails. Reading conventions for histone PTMs can be seen in Fig. 1.4-1C (Prakash & Fournier, 2018). Some common modifications of histones include phosphorylation, ubiquitination, deamination, acetylation, and methylation (Doenecke, 2014; Kouzarides, 2007; F. Wang & Higgins, 2013) (Fig. 1.4-1D) (Rodriguez-Paredes & Esteller, 2011). These marks are attached to the histones by histone “writers”, removed by histone “erasers”, and cause histone “readers” to attach to the marks and thus affect chromatin structure (Doenecke, 2014; Villasenor & Baubec, 2021; F. Wang & Higgins, 2013). Since there are many types and locations for these modifications, it has been proposed that the different combination of marks could lead to different chromatin states more than the marks themselves,

called the histone hypothesis code (Jenuwein & Allis, 2001; L. Wang et al., 2017). All these marks can modify chromatin structure, but we will focus on acetylation and methylation as they are two of the most common marks related to chromatin state changes. Phosphorylation will be covered in a later section due to its relevance in mitosis. Methylation (me) and acetylation (ac) typically occur on lysines (K), where these two marks are mutually exclusive. Lysines can be methylated up to three times, termed mono-, di-, and tri-methylation (me<sup>1</sup>, me<sup>2</sup>, me<sup>3</sup>). Some common histone lysines that are acetylated or methylated to change chromatin state are H3K4, H3K9, H3K27, H2B-K120, H4K5, H4K8, and H4K20.

Histone marks are commonly used in the cell to create loose, spread-out, diffuse, and accessible chromatin, called euchromatin (Alabert et al., 2017; Doenecke, 2014; Villasenor & Baubec, 2021; Yandim, Natisvili, & Festenstein, 2013) (Fig. 1.4-3D) (Prakash & Fournier, 2018). Histone marks can also cause nucleosomes to cluster together, which creates dense, inaccessible, transcriptionally repressed, and compact chromatin, called heterochromatin. Heterochromatin can also be broken down into two subcategories, constitutive and facultative heterochromatin. Constitutive heterochromatin is chromatin that is constantly in its dense, heterochromatic form and is usually be found in repetitive, gene-poor regions of the genome (Saksouk, Simboeck, & Dejardin, 2015). Some specialized domains of the genome, such as the pericentromere and the telomere are also constitutively heterochromatic (Casale, Cappucci, & Piacentini, 2021; Janssen, Colmenares, & Karpen, 2018; Lawrimore & Bloom, 2019). Facultative heterochromatin is chromatin that switches between its heterochromatic state and euchromatic state depending on histone PTMs. Facultative heterochromatin may be used as a transcriptional control mechanism.

A common lysine that is modified to control and differentiate the two chromatin states is H3K9 (Alabert et al., 2017; Kouzarides, 2007; L. Wang et al., 2017). Acetylation of H3K9 (H3K9ac) is associated with euchromatin, more transcriptionally active regions of the genome, and less DNA-dense regions of the interphase nucleus. Trimethylation of H3K9 (H3K9me<sup>3</sup>) is associated with constitutive heterochromatin, denser nucleosome packing, less transcriptionally active regions of the genome and repetitive regions of the genome, and DNA dense regions of the interphase nucleus. Since these two marks are mutually exclusive, they are some of the most common and studied marks used to distinguish euchromatin from heterochromatin. Another commonly modified lysine is H3K27. H3K27me<sup>3</sup> is associated with facultative heterochromatin, while H3K27ac, is associated with active promoters. The two marks are mutually exclusive, meaning H3K27ac blocks the methylation of H3K27 and prevents heterochromatic formation, while H3K27me<sup>3</sup> blocks the acetylation of H3K27 and euchromatic formation. The role of these marks, their changes to chromatin structure, and relation to transcriptional accessibility can be found in Fig. 1.4-2 (Rodriguez-Paredes & Esteller, 2011; Yandim et al., 2013).

Some methyl marks are associated with transcriptional activity, such as H3K4me<sup>1</sup>, found at primed enhancers, or H3K4me<sup>3</sup>, found at transcriptionally active promoters (Alabert et al., 2017; Jenuwein & Allis, 2001; Zaidi et al., 2018). Methyl marks are also associated with different chromatin states depending on the amount of methylation, such as H4K20me<sup>1</sup>, associated with transcriptional activation and condensin II binding, H4K20me<sup>2</sup>, associated with the cell cycle and DNA damage response, or H4K20me<sup>3</sup>, associated with transcriptional repression (van Nuland & Gozani, 2016). DNA itself can also be methylated to form heterochromatin but will not be discussed further (Casale et al., 2021; Janssen et al., 2018; Villasenor & Baubec, 2021).

It is unknown if histone methylation and acetylation on their own affect nucleosome clustering and chromatin structure or if it is controlled mainly through histone readers. The histone chemical modifications could affect nucleosome packing by altering the electrostatic interactions between the PTMs, DNA, and other nucleosomes (Fenley, Anandakrishnan, Kidane, & Onufriev, 2018). Lysine has an innate positive charge, which is attracted to the negatively charged DNA wrapped around the histone. Acetyl groups are negatively charged, which neutralizes the positive charge on the lysine, making the histone less likely to associate with DNA and less likely to interact with neighboring nucleosomes. Methylation is non-polar. Trimethylated lysines could attract one another via non-polar interactions. While investigating this hypothesis, cryogenic electron microscopy (cryo-EM) was used to study the shape and orientation of nucleosome dimers (Bilokapic, Strauss, & Halic, 2018). Nucleosome dimers would usually align in a disk-to-disk or a rim-to-disk pattern but could also adopt a rim-to-rim form. In all these formations, histone tails could physically interact with neighboring nucleosomes and histone tails. If histone tails and their chemical modifications interact with neighboring nucleosomes, then it is possible that the electrostatic differences favor compaction or dispersion through the modification alone.

Histone acetylation is controlled by histone acetyl transferases (HATs) and histone deacetylases (HDACs) (Alabert et al., 2017; Kouzarides, 2007; L. Wang et al., 2017). Chromatin state is thought to affect transcriptional control by altering the ease that transcription factors bind to DNA at the target gene. Acetylation of histones is also thought to facilitate histone eviction from DNA (Fenley et al., 2018). There are also histone readers that can bind to nucleosomes to affect the way chromatin is dispersed or compacted, which will be discussed in a later section. There are inhibitors that can affect the activity of HATs and HDACs which in turn affect histone

acetylation. By inhibiting HATs or HDACs, the levels of acetylation are reduced or increased. Two common HDAC inhibitors are valproic acid (VPA) and Trichostatin A (TSA) (De Souza & Chatterji, 2015; Gottlicher, 2004). TSA functions as an inhibitor of many different types of HDAC classes, while VPA is more selective in inhibiting class I type HDACs, including enhancing proteasomal degradation of HDAC2 (Huynh, Everts, & Ampornaramveth, 2017; Shetty, Pai, Deaver, Satyamoorthy, & Babitha, 2021). Some normal mitotic functions are also altered in TSA treatment, such as inducing premature sister chromosome separation. VPA has been used in other contexts as a mood stabilizer, anti-cancer therapeutic, and other such therapeutics. Both have HDAC inhibiting properties, useful to create higher H3K9ac levels (De Souza & Chatterji, 2015; Gottlicher, 2004; Marchion, Bicaku, Daud, Sullivan, & Munster, 2005).

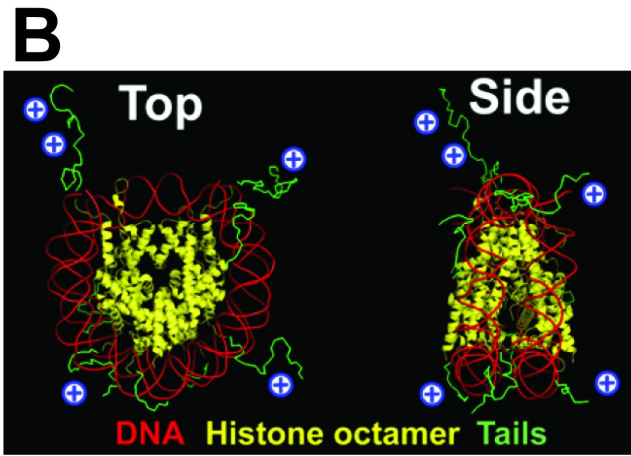
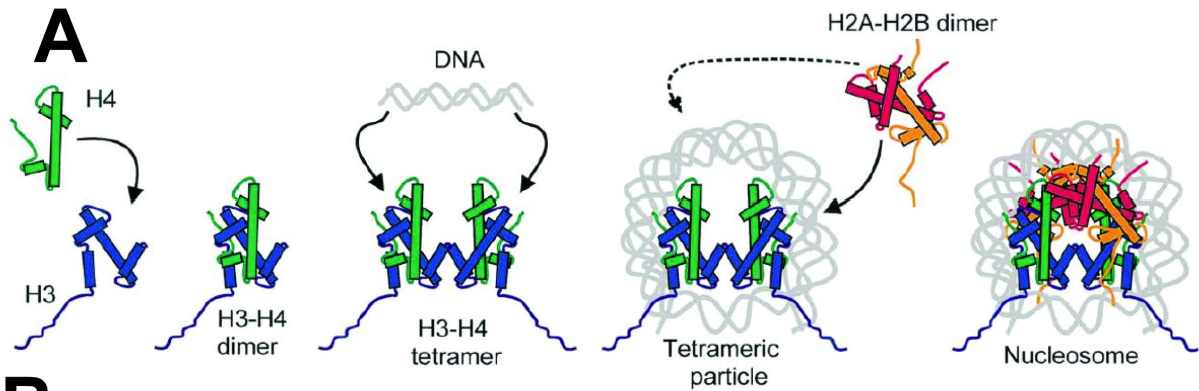
Histone methylation is controlled by histone methyltransferases (HMTs) and histone demethylases (HDMs) (Alabert et al., 2017; Kouzarides, 2007; L. Wang et al., 2017). There are inhibitors that can affect the activity of HMTs and HDMs, which in turn affect histone methylation. By inhibiting HMTs or HDMs, the levels of methylation are reduced or increased. Histone demethylases and demethylation are less understood than their deacetylase counterparts, since it was previously thought that histone methylation was a stable PTM in the cell (Bannister, Schneider, & Kouzarides, 2002). However, research into the cell and drug testing showed that a drug called methylstat could inhibit Jumonji C-containing histone/lysine demethylases. This inhibition led to an increase in methyl histone marks associated with heterochromatin (Luo et al., 2011).

These drugs have been used to investigate how chromatin state affects nuclear stiffness (Stephens, Banigan, Adam, Goldman, & Marko, 2017; Stephens et al., 2018; Strom et al., 2021). Nuclear mechanical stiffness has been analyzed in a similar manner as single chromosome

studies, where nuclei were isolated between two micropipettes, then manipulated/stretched to obtain force-extension curves (Fig. 1.4-4A) (Stephens et al., 2017). Nuclear stiffness has two distinct regimes, where under a 3  $\mu\text{m}$  stretch, its stiffness was dominated by chromatin. Over a 3  $\mu\text{m}$  stretch, the lamin network of the nucleus dominates nuclear stiffness. This was observed by a dramatic weakening of the short-range stretch when the DNA was dissolved or otherwise cut by restriction enzymes, but still resulted in a relatively normal force extension when stretched more than 3  $\mu\text{m}$  (Stephens et al., 2017). Perturbations to the lamin network resulted in a decrease in the larger force-response regime but did not affect nuclear stiffness below a 3- $\mu\text{m}$  stretch.

Histone-PTM-modifying drugs changed the force response of the nucleus in the chromatin-dominated regime (stretched under 3  $\mu\text{m}$ ) but did not affect the stiffness of the lamin-dominated regime (stretched more than 3  $\mu\text{m}$ ). This work was accompanied with a model of the nucleus that depicted chromatin as a soft, flexible polymer constrained by a stiffer, lamin-based shell (Banigan, Stephens, & Marko, 2017). VPA or TSA treatment caused nuclei to become hyperacetylated and weaker in the chromatin-dominated regime. DZNep, a HMT inhibitor, treatment caused nuclei to become weaker and less methylated at heterochromatin marks in the chromatin-dominated force regime (Stephens et al., 2018). These experiments demonstrated that increasing polymer euchromatin or decreasing heterochromatin affected nuclear stiffness in the chromatin-dominated regime. Increasing heterochromatin through treatment with the HDM inhibitor, methylstat, increased nuclear stiffness in the chromatin-dominated regime, an opposite effect of the DZNep treatment. These experiments demonstrated that structural changes to the underlying chromatin affected the mechanical properties of the nucleus.

Nuclear stiffness correlates with nuclear deformities and defects (Stephens et al., 2018; Strom et al., 2021). A nucleus with more euchromatin or a weaker lamin structure has an



**C** amino acid residue      type of modification

**H3K27me3**

histone 3      position of the amino acid from the N terminal

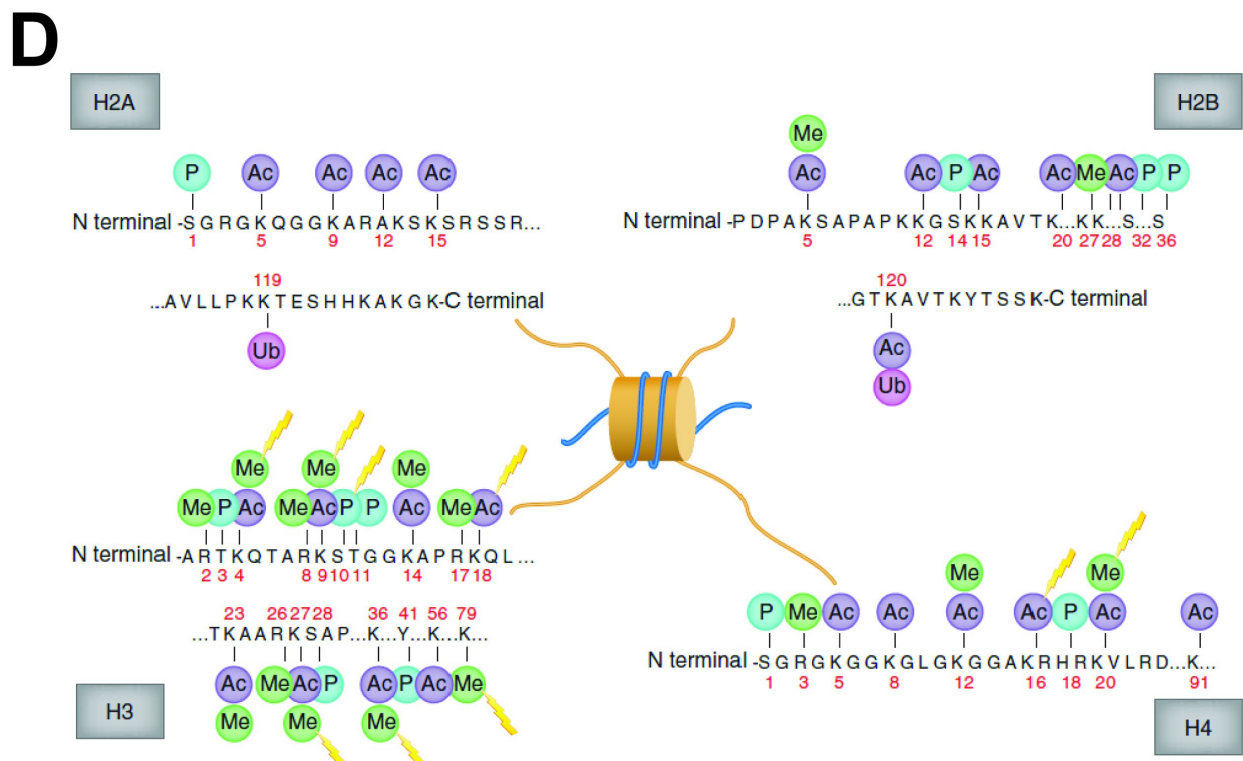


**Figure 1.4-1. The structure of the nucleosome and placement of histone post-translational modifications.**

(A) Schematic of histone nucleosome assembly. Histone H4 (green) will dimerize with histone H3 (blue) to form the H3-H4 dimer. Two H3-H4 dimers will interact with each other to form the  $(\text{H3-H4})_2$  tetramer, which then recruits DNA (grey). Histone H2A (orange) will dimerize independently with H2B (red). Two H2A-H2B dimers will interact with the  $(\text{H3-H4})_2$  tetramer to form the histone octamer, thus creating the functional nucleosome. Image repurposed from (V. Morales et al., 2001). (B) Nucleosome structure top and side view. DNA (red) in its double-stranded form will wrap around the histone octamer (yellow) with the positively charged histone tails (green) protruding from the nucleosome structure. In a top-down view, the histone appears as a circle with the DNA wrapping around it less than two times. In a side view, the DNA wraps around the histone like a string around a wedge. In total, this shows the disc-like structure of the nucleosome. The interactions between the DNA, the histone octamer, and the histone tails are facilitated by grooves in the DNA and octamer as well as electrostatic interactions from the negatively charged DNA molecules and the positively charged histones and histone tails. Image repurposed from (Prieto & Maeshima, 2019). (C) Methodology of how histone modifications are designated and labeled. The histone on which the mark occurs is first, labeled in orange. The amino acid residue follows, labeled in red. The position of the target amino acid (canonically from the N-terminus of the protein) is next. The last portion of the modification label is the specific mark (labeled in blue). Image repurposed from (Prakash & Fournier, 2018). (D) Histone tails and their modifications. There are regions of histone tails that can be chemically, post-translationally modified. Several common marks include methylation (green), acetylation (purple), phosphorylation (blue), and ubiquitination (pink). Histones H3 and H4 have accessible tails at the N-terminus, while histones H2A and H2B have modifiable tails at the N- and C-terminus with the intervening sequences forming their respective parts of the histone core. These marks may interact with the electrostatics of the surrounding DNA and other histones but may also recruit molecules that alter the spacing of nearby histones. The core histones in the octamer and their tails are depicted in orange with the DNA looping around it in blue in the center of the Figure. Marks commonly associated with various cancers highlighted in yellow. Image repurposed from (Rodriguez-Paredes & Esteller, 2011).

increased likelihood of rupturing and forming blebs. A rupture is a hole in the nucleus, causing some of the nuclear content can leak out of the cell, which can also cause DNA damage (Pfeifer et al., 2018; Stephens et al., 2019; Xia et al., 2018; Xie, Walker, & Irianto, 2020). A bleb is an abnormal nuclear structure/morphology that protrudes from the main nuclear body, correlated with ruptures. Strengthening the lamina or increasing the amount of heterochromatin in the cell grants the nucleus resistance to rupture and bleb formation. When bleb-prone nuclei were treated with drugs to increase heterochromatin or decrease euchromatin, they had a reduction in blebbing, like wild-type rates of blebbing. This demonstrated a relationship between the outer shell and the inner chromatin of the nuclei. The blebbing phenotype was also associated with diseases such as cancer; cancer cells tend to bleb more often than normal cells (Butin-Israeli, Adam, Goldman, & Goldman, 2012). This demonstrated that physical phenotypes, mechanical stiffness, and diseases are related.

#### **1.4.2 Histone PTM interactions and interacting molecules**

Histone “readers” attach to histones, histone PTMs, and affect chromatin’s ability to condense or expand (Bell et al., 2011; Kadauke & Blobel, 2013; F. Wang & Higgins, 2013). Since acetylated histones are associated with transcriptionally active regions of the genome, the readers of acetylated histones are associated with chromatin-remodeling enzymes. These remodeling enzymes can evict histones from the DNA to increase its transcriptional accessibility (Alabert et al., 2017; Bell et al., 2011; Maeshima, Ide, & Babokhov, 2019). Since DNA transcription requires nucleosome-free DNA, the transcription machinery itself can assist in nucleosome eviction. Nucleosome eviction makes chromatin looser and weaker than when wrapped around histones.

Some notable heterochromatic histone readers include the heterochromatic proteins (HP) and polycomb repressive complexes, which are associated with repressive methyl marks (Eissenberg & Elgin, 2000). HP1 $\alpha$  is a protein of particular interest that is associated with constitutive heterochromatin that attaches to H3K9me<sup>2,3</sup> and DNA (James & Elgin, 1986; Singh et al., 1991). HP1 $\alpha$  can dimerize and crosslink chromatin by attaching to two nearby strands of heterochromatic chromatin but is also very dynamic on mitotic chromatin (Canzio et al., 2011; Cheutin et al., 2003; Machida et al., 2018; Strom et al., 2021). HP1 $\alpha$  is required for heterochromatin formation and is important in sustaining heterochromatin (Bannister et al., 2002; Krouwels et al., 2005). It has been hypothesized that HP1 $\alpha$  can phase separate in the cell, and it specifically causes heterochromatin to adopt a liquid-liquid phase separation state from euchromatin (Larson et al., 2017; Strom et al., 2017). This hypothesis states that HP1 $\alpha$ 's self-interaction and interaction with other items in heterochromatin causes heterochromatin and euchromatin to separate like two immiscible fluids, such as oil and water. Since HP1 $\alpha$  and heterochromatin generally tends to self-associate, it has been thought that it will create a barrier and exclude euchromatin.

The original hypothesis for the phase-separation hypothesis came from experiments on biochemically isolated and purified HP1 $\alpha$  (Larson et al., 2017). When HP1 $\alpha$  was saturated in an aqueous solution, it formed droplets that continued to grow when it encountered other HP1 $\alpha$  droplets. Additional experiments demonstrated that heterochromatin demixed from the aqueous phase, grew in clusters, and had semi-rapid exchange with fluorescent HP1 $\alpha$  inside the cell. These experiments suggested that HP1 $\alpha$  could phase separate in a cellular environment (Larson et al., 2017). In opposition to phase separation, there is still some debate if the phase-separation model behaves more like compaction.

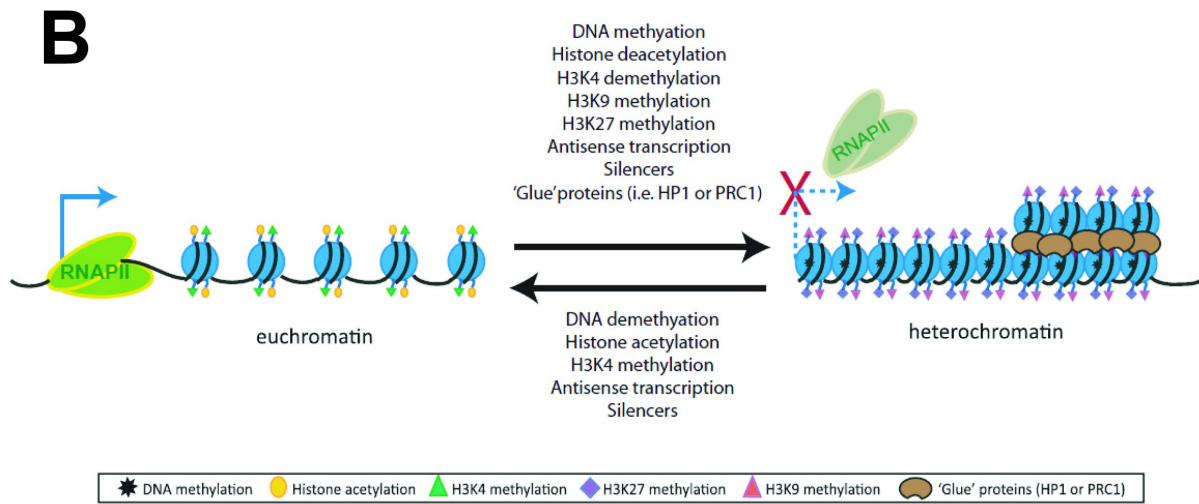
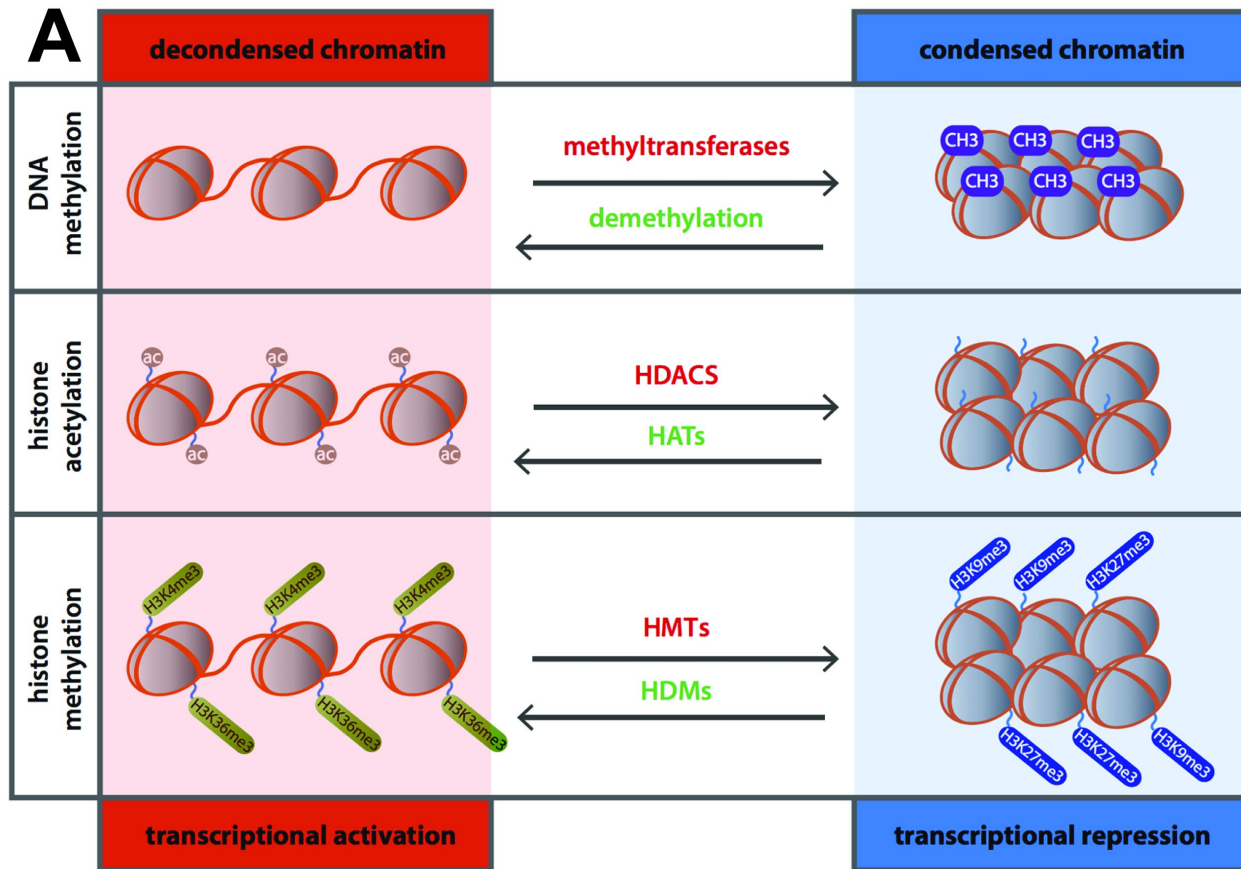


**Figure 1.4-2. Chromatin diagram and effects of histone post-translational modifications.**

(A) Structural changes from histone acetylation and methylation. DNA demethylation (top), histone acetylation (middle), and histone H3K4me<sup>3</sup> (bottom) are all associated with open, diffuse, and transcriptionally active euchromatin (left). DNA methylation (top), histone deacetylation (middle), and histone H3K9me<sup>3</sup> (bottom) (as well as H3K27me<sup>3</sup>, not depicted) are all associated with compact, inaccessible, and transcriptionally silent heterochromatin (right). The movement from euchromatin to heterochromatin can be facilitated by DNA methyltransferases, histone deacetylases, and several histone methyltransferases. The reverse movement from heterochromatin to euchromatin can be facilitated by DNA demethylases, histone acetyl transferases, and several histone demethylases. Image repurposed from (Duygu, Poels, & da Costa Martins, 2013). (B) Transcriptional and structural changes from histone acetylation and methylation and associated proteins. When chromatin is open and has transcriptionally active marks, RNA polymerase can be recruited to chromatin, making it transcriptionally active. When chromatin is closed, there is no space for RNA polymerase to bind and therefore does not create RNA for creating genes. In addition to the marks discussed in (A), this Figure also depicts how HP1 proteins or polycomb proteins can bind to methyl marks to further compact chromatin. Image repurposed from (Yandim et al., 2013).

Hi-C experiments demonstrated heterochromatin associated with itself and excludes euchromatin, which formed its own domain (Belaghzal et al., 2021). This was seen as distant interactions within chromatin types increasing in coincident reads while excluding reads from opposite chromatin states. The separation of euchromatin and heterochromatin is called compartmentalization, where A compartments denote the open euchromatin phase and B compartment denote the dense, rarely transcribed heterochromatin phase (Fig. 1.4-3) (Zhao, Rivera-Mulia, & Gilbert, 2017). This occurs due to the self-association of heterochromatin and exclusion of euchromatin. Since genes are contiguous with heterochromatic regions, some regions must be outside of the dense region, then return to the dense region when the next heterochromatic section appears (Fig. 1.4-3E) (Prakash & Fournier, 2018).

Experiments on nuclei have also been used to investigate HP1 $\alpha$ 's role in nuclear stiffness and morphology. A GFP-AID-HP1 $\alpha$  strain was created to study its impact on transcription and stiffness in the nucleus (Strom et al., 2021). The HP1 $\alpha$  protein had normal localization that would be degraded rapidly when the cells were treated with auxin. This degradation had minimal effect on transcription. The degradation also caused the nucleus to weaken in a similar manner to DZNep and VPA treatment. The weakened nucleus also increased the likelihood of nuclear blebbing, like previous experiments on stiffness. Both phenotypes of degraded HP1 $\alpha$  degradation could be rescued with the additional treatment with methylstat, as the nuclei returned to the untreated level of stiffness and rate of nuclear blebbing. This demonstrated an interesting link between the relationship between of HP1 $\alpha$  and H3K9me<sup>2,3</sup>. It was hypothesized that methylstat treatment caused an increase in nuclear stiffness by increasing H3K9me<sup>2,3</sup> levels, which recruited more HP1 $\alpha$ -based crosslinking and heterochromatin formation. However, since methylstat treatment increased nuclear stiffness in the absence of HP1 $\alpha$ , it suggested that there are at least

two routes where heterochromatin formation influences nuclear stiffness. There may be some level of intrinsic chemical modification of heterochromatic marks that facilitates the formation of heterochromatin, although there could also be more effects and histone PTM readers causing these effects apart from HP1 $\alpha$ .

Another finding of this study relates nuclear shape changes to HP1 $\alpha$ 's dimerization function. When a wildtype rescue HP1 $\alpha$  protein was expressed in cells with the degraded HP1 $\alpha$ , it rescued nuclear shape phenotypes, like abnormal shape of the nucleus and curvature (Strom et al., 2021). However, expressing a rescue construct that was unable to dimerize showed abnormal nuclear shape and curvature near identical to completely losing HP1 $\alpha$ . An additional finding of this study modeled HP1 $\alpha$ 's effect on chromatin through chromatin crosslinking. The model suggested HP1 $\alpha$ 's stiffening phenotype occurs through its ability to self-associate and crosslink chromatin. These experiments suggested that heterochromatic effects of HP1 $\alpha$  are due to its ability to crosslink chromatin and form larger blocks of chromatin that stiffens the nucleus.

### **1.4.3 Mitotic chromosome structural changes and relation to histone PTMs**

During mitosis, the chromatin landscape dramatically changes from its interphase state of loose chromatin fibers into its mitotic state of dense, individualized, compact, and thread-like structure. While this macroscopic transition is greatly facilitated by condensin, cohesin, topoisomerases and other such proteins, the underlying chromatin, nucleosome structure, and nucleosome-interacting molecules also undergo a noticeable change. One of the purposes and consequences of the chromatin changes during mitosis is the halting of most transcription (Janssen et al., 2018; Kadauke & Blobel, 2013). Instead of transcribing genes, the cell focuses on packaging and compacting the genome. The levels of H3K9ac on histones are also reduced in mitosis, which may be involved with the reduction in transcriptional activity and allow

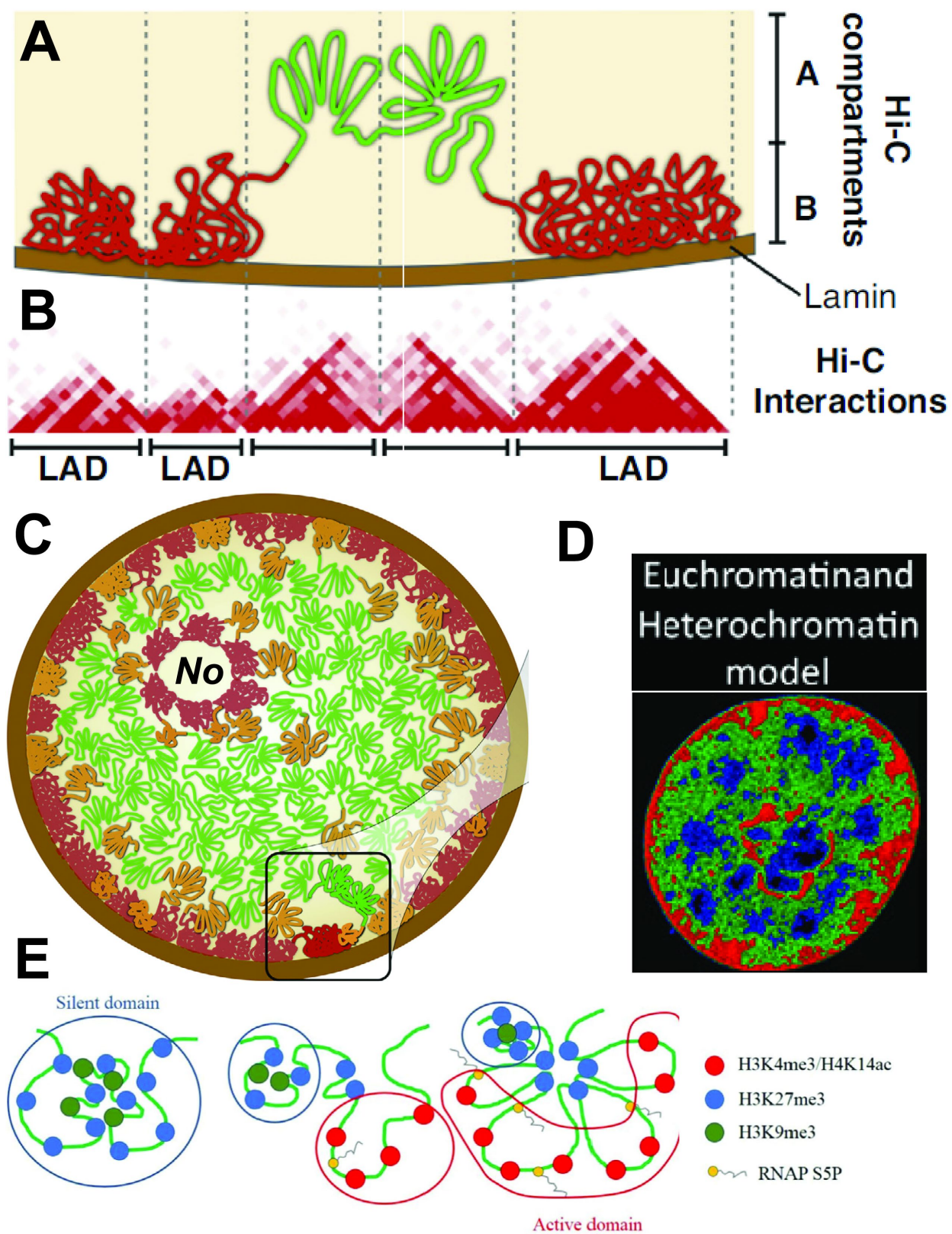


**Figure 1.4-3. Mitotic chromosome structural changes and relation to histone PTMs.**

(A) Heterochromatin and euchromatin will form different associated networks called compartments in Hi-C maps. The repressive heterochromatin (red) will attach to the lamins to further its transcriptional repression in the B compartments, making them more likely to associate with other regions of heterochromatin. The open and active euchromatin will associate with transcriptional machinery, making it less likely to associate with the repressive heterochromatin and form the A compartments. Images from Figures (A-C) repurposed from (Zhao et al., 2017). (B) Hi-C interaction map based on compartmentalization. The physical spacing from compartments diagrammed in (A) will form different Lamin-Associating domains (LADs), which are facilitated by the histone PTM and transcriptional state of the chromatin (eu or hetero-chromatin). This distinction between domains contrasts with topological associated domains (TADs), whose interactions are facilitated by SMC complexes and loop formations. (C) The cell diagrammed with respect to chromatin compartments. Repressive marks (red) will associate with the lamina of the cell and become transcriptionally repressed. The nucleolus (no) will also associate with the repressed heterochromatin. Transcriptionally active chromatin (green) will mix with a larger volume of the cell, due to its diffuse, accessible state. Some portions of the genome can switch between transcriptionally accessible and repressive chromatin, which will form an intermediate domain in their respective compartments (orange). (D) Eu- and hetero-chromatin depicted in a cell with pseudo coloring of an actual cell depicting chromatin density. Repressive marks form the outer, lamin-associated phase of heterochromatin, while the more transcriptionally active euchromatin can be found throughout the cell in green. Domains which can switch or are repressed outside of the lamin-associated domains are depicted in blue. Images from Figures (D) and (E) repurposed from (Prakash & Fournier, 2018). Cell diagram of different chromatin states. (E) Cartoon schematic of different chromatin states alter the behavior of chromatin strands. The constitutive heterochromatin mark, H3K9me<sup>3</sup> compacts deep and dense into inaccessible chromatin folds, while the facultative heterochromatin mark, H3K27me<sup>3</sup> associates at the boarder of transcriptionally active and diffuse H3K4me<sup>3</sup>, H4K14ac, and H3K9ac marks, which are open and spread out in a diffuse pattern, ready for transcriptional machinery to bind and create RNA for transcribing genes.

nucleosomes to pack against the electrostatic spreading of acetylation (Park et al., 2011). While interphase chromatin can be broadly split between two distinct states, euchromatin and heterochromatin, mitotic chromosomes appear more uniformly compact. However, when mitotic chromosomes are stained, banding patterns can be visualized along the chromosome length demonstrating there is still some variation in density (Bayani & Squire, 2004; Dolan, 2011).

A hallmark and well-studied change at the nucleosome level during mitosis is known as the phospho-methyl switch (Fischle et al., 2005; Sales-Gil & Vagnarelli, 2020). This switch describes the interplay between histone phosphorylation and the removal of several heterochromatic readers of methylated histones. One example is the phosphorylation of H3T3 (H3T3ph), which may interfere with binding promoting complexes that bind to H3K4me<sup>1</sup> (Varier et al., 2010). H3S10ph causes HP1 $\alpha$  eviction from the adjacent H3K9me<sup>2,3</sup>. While HP1 $\alpha$  is removed from the chromosome arms, it is maintained around the centromere (discussed further in Section 1.6). H3S28ph also removes the polycomb repressive complex that associates with H3K27me<sup>3</sup>. Several proteins removed by the phospho-methyl switch are associated with dense, heterochromatin marks in interphase, but strangely, the purpose of mitotic compaction is to create a similarly dense chromatin structure. The phospho-methyl switch could be used so chromatin compaction in mitosis is organized through the actions of SMC complexes, like condensin and cohesin, rather than through globular compaction or liquid-liquid phase separation of the typical heterochromatic-associated changes.

The different chromatin states found between interphase and mitosis can be understood by studying the role of histone PTM changes in their compaction. One experiment compared the likelihood and ability for purified histones from mitotic and interphase cells to compact DNA (Zhiteneva et al., 2017). Mitotic histones had a greater likelihood of compacting DNA.

Compaction was compared by mixing the purified histones with DNA and imaged. This research showed more, and denser dots of DNA formed with mitotic histones than with interphase histones. Mitotic histones showed increased histone phosphorylation and decreased acetylation compared to interphase histones by mass spectrometry. They were unable to show a change in methylation between the two populations. While not a conclusive mechanism for driving mitotic chromatin compaction, as there are still many other ongoing compaction mechanisms during mitosis, the innate changes to the histone PTMs may cause greater DNA condensation in mitosis merely by the histone PTM changes in mitosis.

Bookmarking genes and maintaining the cell's transcriptional state after mitosis is another nucleosome-related mitotic function. Bookmarking is the act of preserving the histone PTMs or using mitotic-specific histone PTMs to maintain the cellular identity or transcriptional state of a cell through mitosis (Doenecke, 2014; Kadauke & Blobel, 2013; F. Wang & Higgins, 2013). This preservation in identity and transcriptional state facilitates the continuation of a specific environment for the cell. The process of bookmarking starts during the synthesis phase of the cell cycle, where histones are removed from chromatin for DNA polymerase accessibility. The old histones in the cell are reincorporated into one of the duplicated chromatids, while new histones are deposited into the other chromatid, which is still nearby (Alabert et al., 2015; Escobar, Loyola, & Reinberg, 2021; Stewart-Morgan, Petryk, & Groth, 2020). The new histones are post-translationally modified to replicate the chromatin landscape for both chromatids leaving cell identity identical in both daughters. Other forms of bookmarking involve DNA methylation, use of specific histone variants, or incorporation of other histone modifications. These forms of bookmarking are utilized right before mitosis to reestablish heterochromatin formation or rapid reactivation of highly transcribed and vital genes.

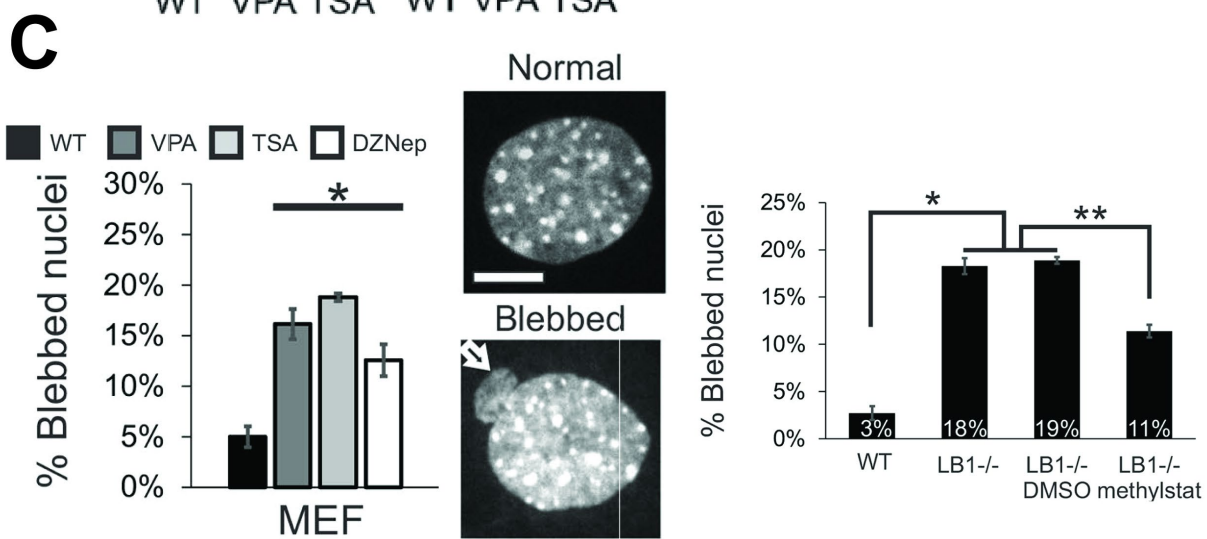
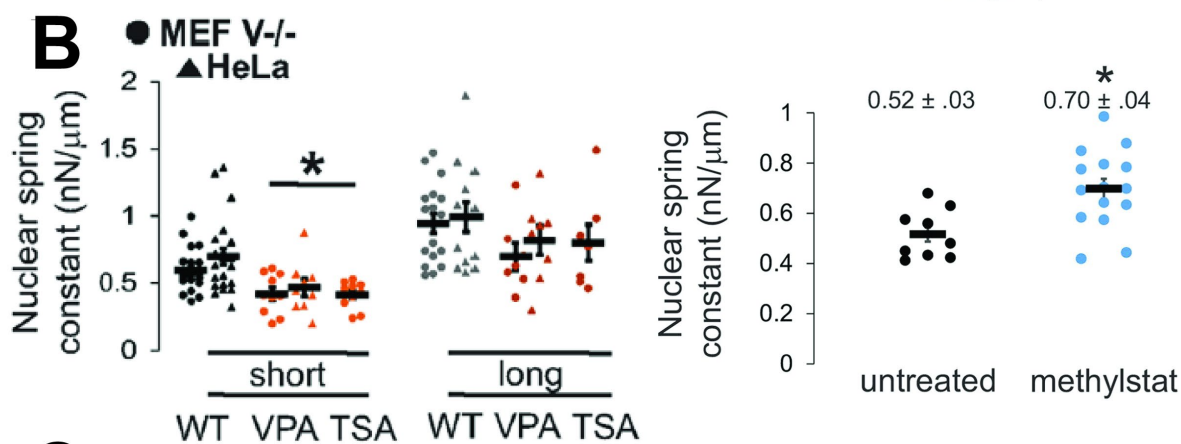
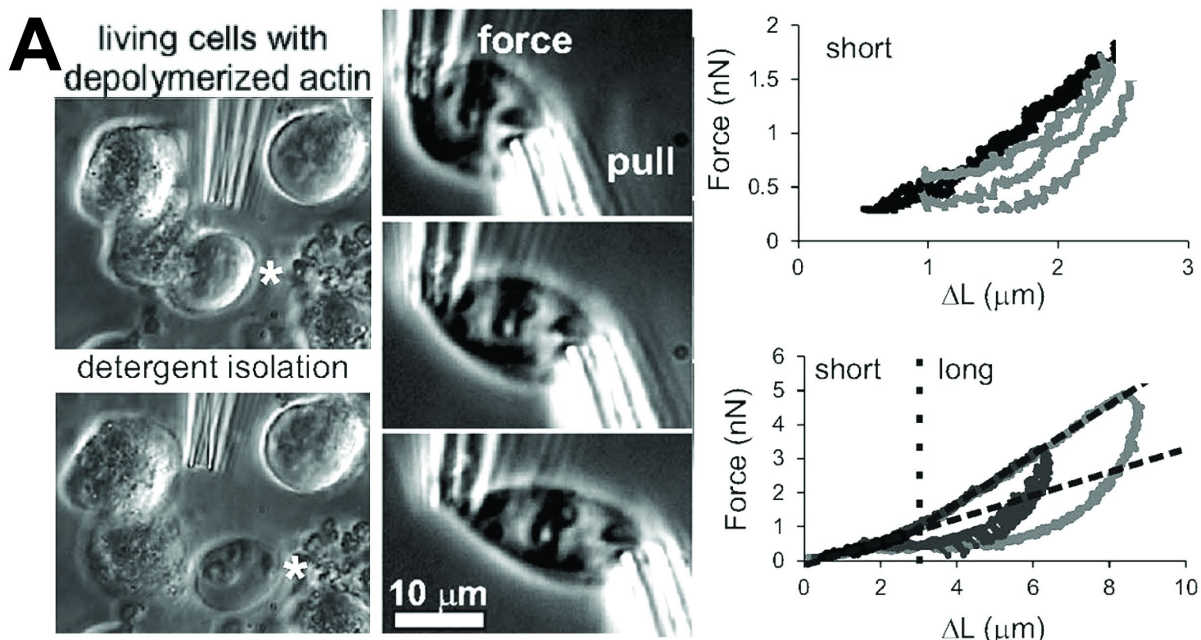


**Figure 1.4-4. Study of chromatin-dominated stiffness in the nucleus using micropipettes.**

Measuring isolated nuclei stiffness using micropipettes, like mitotic chromosomes. Live interphase cells can be sprayed with a Triton-containing PBS solution to destabilize the cell membrane and extract an interphase nucleus. Once outside the cell, two pipettes, one stiff for pulling on the nucleus and the other a weak, force-measuring pipette to deflect and convey the force unit per stretch unit are used to study nuclear stiffness. Nuclei have two force regimes: short, chromatin-based stiffness and long, shell/lamina-based stiffness. Nuclei typically show viscoelastic hysteresis when stretching. The isolation procedure is documented to the left, while the stretch-deflection is presented in the middle. An example trace of both the long- and short-range extension is shown to the right. Scale bar represents 10  $\mu\text{m}$ . Image repurposed from (Stephens et al., 2017). (B) The chromatin-dominated, short regime of nuclear stiffness can be altered by changes to histone PTMs. Hyperacetylation of histones causes a drop in the beginning of nuclear stretching (orange) compared to untreated cells (black), shown on the left, but does not affect the increase in stiffness at longer-ranged pulls, shown in the center. By contrast, hypermethylation by methylstat treatment (blue) causes an increase in nuclear stiffness, while increasing heterochromatin shown on the right. Image repurposed from (Stephens et al., 2017) and (Stephens et al., 2018). (C) Nuclear stiffness has an inverse correlation with nuclear stability. Hyperacetylation or hypomethylation of histones weakens nuclear stiffness, while increasing the likelihood of chromosomes to bleb, where a part of the nuclear envelope bursts from the normal shell. Reversing this trend, an increase in nuclear stiffness, associated with an increase in histone methylation, causes bleb-prone nuclei to resist blebbing. The effects of histone PTM-modifying drugs are quantified on the left, while lamin B1 knockdown and hypermethylation recovery is quantified on the right. An example image of blebbing is shown in the middle panel. Scale bar represents 5  $\mu\text{m}$ . Image repurposed from (Stephens et al., 2018).

Detrimental effects can arise from their perturbations to normal histone PTM changes. Some experiments were done to study the rise in mitotic defects in mitotic cells treated with HDAC inhibitors (Burgess et al., 2004; F. E. Stevens, Beamish, Warrener, & Gabrielli, 2008; Warrener et al., 2003). TSA treatment caused a variety of mitotic defects such as metaphase misalignment, anaphase bridges, and aneuploidy. The inhibition of the HDACs may also cause defects independent from their role on H3K9ac specifically (Warrener, Chia, Warren, Brooks, & Gabrielli, 2010). Other experiments utilizing the degradation of HP1 $\alpha$  through auxin treatment or other methods of removing HP1 $\alpha$  also resulted in similar mitotic defects when HP1 $\alpha$  was not present, specifically metaphase misalignment and ana/telophase bridges (Strom et al., 2021). Most mitotic HP1 $\alpha$  localizes to the centromere and may function as a stabilizing force for the division machinery of the chromatids, which may affect proper chromosome segregation. The defects of HP1 $\alpha$  therefore may relate to its role in stabilizing the centromere.

## **1.5 Meiotic chromosome division**

### **1.5.1 Meiotic chromosome division, purpose, and background**

Many organisms, including humans and mice, will typically have two sets of similar, but non-identical chromosomes. These chromosomes are called homologous chromatids, with one inherited from each parent. Cells that have two copies of homologous chromosomes (one from each parent) are called diploid cells. When cells duplicate their chromosomes, they create two identical copies of their chromosomes, called sister chromatids. During mitosis two genetic copies of the mother cell are created by separating the sister chromatids evenly into two daughter cells. Meiosis, by contrast, pairs the homologous chromosomes together during meiotic prophase I following their replication during meiotic prophase I (Hassold & Hunt, 2001; Ivanovska & Orr-

Weaver, 2006; Kleckner et al., 2004). Following their recombination, the chromosomes undergo two rounds of chromosomal division separating homologous and sister chromatids from one another. This yields four haploid cells, where each cell contains only one copy of each chromosome. This general scheme can be seen in Fig. 1.5-1A (Gray & Cohen, 2016).

Meiosis creates genetic diversity instead of perfect chromosomal duplication as found in mitosis. Genetic diversity allows for exploration of the genetic landscape contained within each of the two parent genomes. This exploration results in genetic variation, which leads to selection of favorable traits over time through natural selection and evolution (Lescqque, Glemin, Lartillot, Mouchiroud, & Duret, 2014; Liow, Van Valen, & Stenseth, 2011). Homologous recombination in meiosis furthers the exploration of diversity by allowing each donated chromosome to be different from a perfect copy from either of the parent's chromosomes. This diversity is achieved by swapping genetic material with its homologue in a process called crossover (Cobb & Handel, 1998; Zickler & Kleckner, 1999). Sexual reproduction combines one chromosome from each of the compatible parents' haploid cells to form a genetically distinct individual, different from both parents. This reproduction scheme results in increased genetic diversity. Sexual reproduction occurs when two compatible organisms donate one copy of their chromosomes in their haploid cells to create a new diploid organism.

The first meiotic division, termed meiosis I, has many different substages which compacts, organizes, and alters the chromosomes' structure. Following the pre-meiotic S-phase the cell enters meiotic prophase I which also has several distinct substages and associated chromatin changes. The first substage of meiotic prophase I is leptotene, where chromosomes start condensing and compacting (Ivanovska & Orr-Weaver, 2006; Kleckner et al., 2004; Zickler & Kleckner, 1999). Leptotene chromosomes are compacted primarily using a modified and

meiosis-specific form of cohesin rather than condensin (Gray & Cohen, 2016; Mirkovic & Oliveira, 2017; Rong, Matsuda, Hiraoka, & Lee, 2016). The backbone of the meiotic prophase I chromosome formed from meiotic-specific cohesin, called the cohesin core (Kouznetsova, Benavente, Pastink, & Hoog, 2011; Rong et al., 2016). The duplicated sister chromatids are also bound with their homologues in meiotic prophase I. These chromosomes bundled together are called tetrads, since there are four total chromosomes in the bundle. During this phase, the chromosomes also undergo preprogramed dsDNA breaks through a specialized topoisomerase II enzyme, called Spo11 (Gray & Cohen, 2016; Keeney, 2008; Keeney, Giroux, & Kleckner, 1997). The DNA breaks are swapped with sections on their homologue, repaired, and lead to homologous recombination, discussed later. Following leptotene is zygotene. In zygotene, homologous regions of each chromosome find and attach to each other. The binding of each homologous region pairs the homologous chromosomes together where the Spo11 breaks were formed. This binding allows homologues to be separated with their sisters, which are separated from each other in meiosis II, ensuring even distributions in the final haploid cells (Ivanovska & Orr-Weaver, 2006; Kleckner et al., 2004; Kouznetsova et al., 2011). The homologous regions of the paired chromosomes will swap with each other at random crossover points, which were formed by the dsDNA breaks during leptotene. Following crossover, the double stranded breaks are repaired on the new chromosomes during the following phases of meiotic prophase I (Keeney, 2008).

The synaptonemal complex (SC) (discussed in depth in the next section) starts forming between the paired homologous chromosomes in zygotene. Through pachytene the SC attaches to the central element and performs a zipper-like action to bind the homologous chromosomes together (Enguita-Marruedo et al., 2018; Gao & Colaiacovo, 2018). After pachytene, diplotene

occurs, where parts of the synaptonemal complex are removed and only remain at specific points, called chiasmata (Pattabiraman, Roelens, Woglar, & Villeneuve, 2017; S. Wang, Zickler, Kleckner, & Zhang, 2015). The chiasmata remain when moving into the next stage of meiosis prophase I, diakinesis. The chromatids also become progressively more individualized as each of the chromatids in the tetrad are compacted and organized. At this stage, each chromatid in the tetrad can be individually seen. Meiotic prophase I can last for weeks at a time or longer in which the nuclear envelope remains present (Bennett, 1977). The construction of the Synaptonemal Complex over meiotic prophase I can be seen in Fig. 1.5-1B (Bolcun-Filas & Schimenti, 2012).

The first metaphase occurs after diakinesis which is when some species arrest meiotic development (J. Lee, 2017; Sen & Caiazza, 2013). Meiotic metaphase I, minus the common arrests, proceeds like the mitotic chromosome pathway and undergoes a following meiotic anaphase, telophase, and cytokinesis. During meiosis I, when homologous chromosomes are separated, the sister chromosomes need to be continually paired for the following cell division. The method of selective chromosome separation depends on the specialized way homologous chromosomes are attached to one another, using meiotic-specific complexes (Garcia-Cruz et al., 2010; J. Lee, 2017; J. Lee & Hirano, 2011). The daughter cells from the first meiotic cell division may be processed in a different manner depending on the specific species and meiotic program (discussed later). The second round of division occurs like the mitotic program, where sister chromatids are separated; however, it must undergo this process by reactivating the cell and chromosome division machinery without going through the full process of chromosomal duplication, which we will not cover (Wassmann, 2013). The second round of chromosome division in meiosis II can also undergo metaphase arrest depending on the cell's programming,

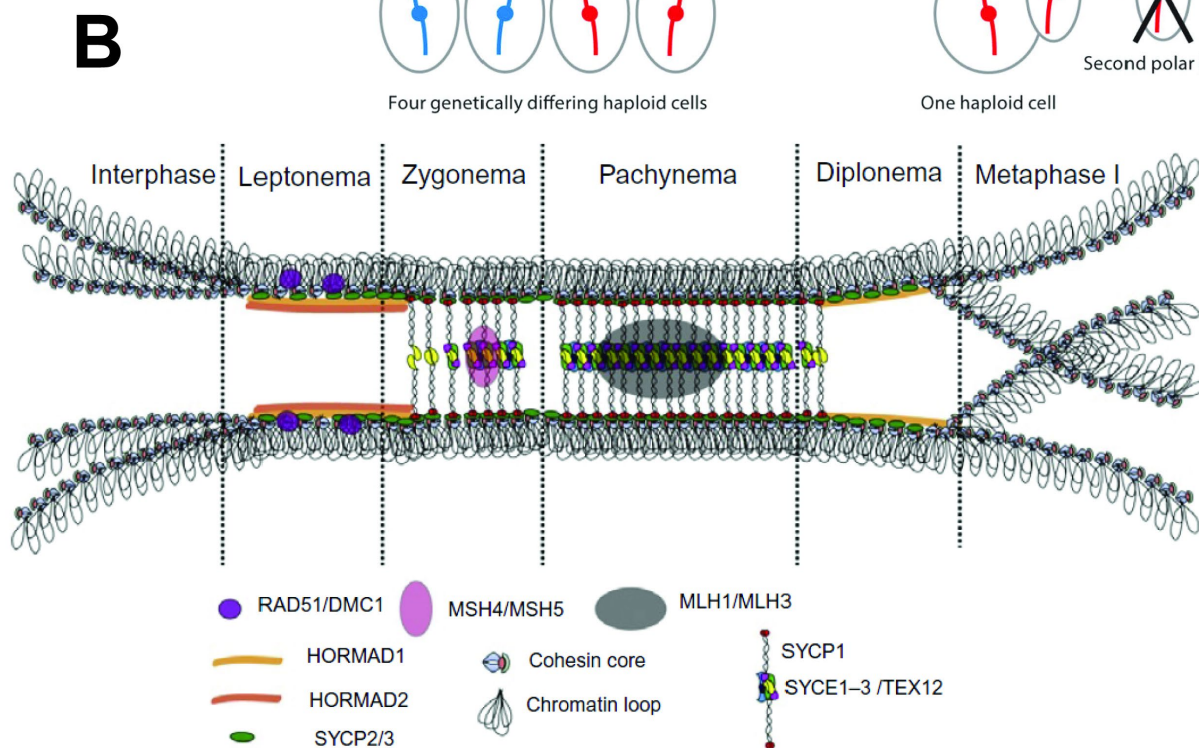
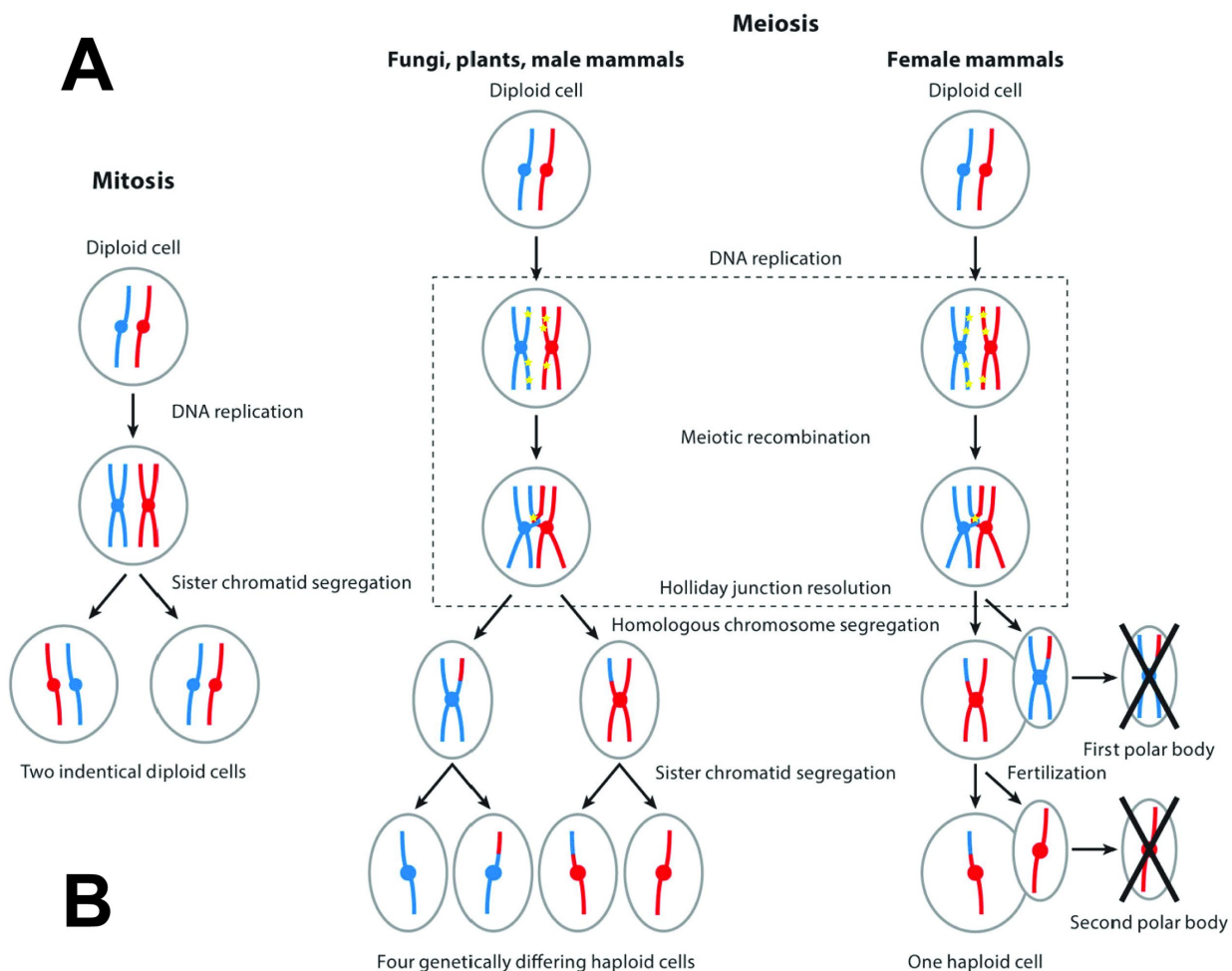


**Figure 1.5-1. The substages of meiosis and the steps in meiotic prophase I.**

(A) Depiction of the differences between mitosis and meiosis. Both systems of chromosome separation and cell division (mitosis and meiosis) start by duplicating the DNA. During this phase, sister chromosomes (same color) are paired together. In mitosis, the sister chromosomes are separated from one another in a single round of cell/chromosome division. In mitosis, the homologous chromosomes do not interact. In both forms of meiosis, the chromosomes undergo directed dsDNA breakages (yellow), which are then repaired in a specific fashion that allows meiotic recombination of homologous chromosomes. These repaired homologous chromosomes will remain paired together and undergo homologous chromosome separation in meiosis I, followed by sister chromosome separation in meiosis II. Male meiosis in mammals will yield 4 small, viable, haploid cells. Female mammalian meiosis will create two non-viable cells called polar bodies and one viable haploid cell, which is substantially larger than their male counterparts. Image repurposed from (Gray & Cohen, 2016). (B) Diagram of the Synaptonemal complex (SC) during meiotic prophase I. During meiotic prophase I, the SC (via SYCP2/3 (green)) will associate with the cohesin core (blue/pink diamond). The cohesin core is responsible for forming meiotic chromosomes into condensed loops of chromatin (grey loops). As leptotene continues, the axial elements (SYCP2/3) will continue recruiting other proteins (orange and red bars) as well as proteins involved in fixing the double-strand DNA breaks, which facilitate homologous recombination (Rad-51). During the following sub-phase of meiosis prophase I, zygotene, the SC becomes bridged by SYCP1 (red dot and coil) and is stabilized by the central element proteins SYCE1-3/TEX12 (green, yellow, purple dots). The SYCP2/3 complex is renamed at this stage to the lateral elements. During pachytene, the SC increases its association with itself, forming a zipper-like activity to bind the SC together until the entire chromosome is paired. During diplotene, parts of the SC are removed, remaining only at the chiasmata, where crossover occurred previous in meiotic prophase I. Upon entry into metaphase I, the homologous chromosomes are separated from one another, and remaining elements of the SC are dissolved. Image repurposed from (Bolcun-Filas & Schimenti, 2012).

such as during mammalian ovulation (Bolcun-Filas & Schimenti, 2012).

Since meiotic cell division has a direct link to sexual reproduction, one of the differences between meiotic programs comes down to the program of cell division between the sexes. One of the biggest differences in meiotic programming between male and female meiosis is the cell size of the final cell after the two rounds of division (Gray & Cohen, 2016). In most mammals, the male meiotic programming leads to four very small and viable cells with very compact DNA. The female meiotic programming by contrast leads to a very large, single viable cell, of which the two small, inviable cells will be formed into polar bodies (Gray & Cohen, 2016) (Fig. 1.5-1A). An additional outcome of the unviability of these cells is the formation and prevalence of “selfish” genes and genetic elements (Plohl, Luchetti, Mestrovic, & Mantovani, 2008). Selfish genes possess elements that will bias themselves to be selected into the viable cell, which can be detrimental to the final cell. Since mammalian females are born with all the haploid cells through their life, they will arrest for years at a time in metaphase I and arrest in metaphase II post ovulation. Male meiotic programming undergoes rapid development and renewal by comparison (Escalier, 2002). Male meiotic cells will arrest for proofreading purposes, but defects displaying a strong-arrest phenotypes can cause sterility or other fertility issues (R. S. Wang, Yeh, Tzeng, & Chang, 2009). Spermatogenesis is the process where the male reproductive organs produce mature sperm. Spermatogenesis is an integral part in understanding fertility, since it is the process that produces viable meiotic cells for males (de Kretser, Loveland, Meinhardt, Simorangkir, & Wreford, 1998; Hess & Renato de Franca, 2008; Neto, Bach, Najari, Li, & Goldstein, 2016). In mice, the meiotic cells undergo development through the seminiferous tubules, which loop around the outside of the testis then steadily move deeper into the tissue (Hess & Renato de Franca, 2008). During this process, the cells undergo meiosis I for

approximately two weeks, spending most of their time in pachytene, close to the outside of the surface. Going further into the tissue, further developments occur as they proceed through the subsequent stages of meiosis. Following the final meiotic division, cells undergo further morphological changes by growing tails, storing energy, compacting their chromosomes into the small cell of the spermatids to allow them to move quickly. The developed spermatids and mature sperm cells, possessing tails, can be easily differentiated from the very large meiotic I cells.

One of the important functions of studying meiotic chromosomes is an investigation into fertility. A concern of this exploration into fertility comes from an observation that as women age, there is a decrease in fertile viability in the cells, which correlates to an increase in aneuploidy (Chiang, Duncan, Schindler, Schultz, & Lampson, 2010; Jones & Lane, 2013). One experiment sought to determine if there was a physical difference between chromosomes derived from young and old meiotic II arrested female mice, underpinning the fertility defects (Hornick et al., 2015). It is possible to isolate and study meiotic chromosomes like mitotic chromosomes. The meiotic II arrested chromosomes from the young mice were substantially stiffer (doubling force of 830 pN) than the previously studied untreated human mitotic chromosomes (doubling force of 300pN) (M. Sun et al., 2018b). This finding supports the hypothesis that arresting cells in metaphase causes a general stiffening phenotype in chromosomes. When comparing meiotic II chromosomes from young mice to ones from older mice, the older chromosomes were over two-fold stiffer, with a doubling force of 2250 pN. This increase in stiffness was correlated with a reduction in meiotic II cells per animal and an increase in aneuploidy, suggesting that studies in physical properties can be correlated with observed macroscopic phenotypes (Hornick et al., 2015).

### 1.5.2 Structural properties of meiotic prophase I chromosomes and components

The meiotic specific form of cohesin uses SMC1b or SMC1a with SMC3, where the mitotic program only uses SMC1a (Bolcun-Filas & Schimenti, 2012; Eijpe, Offenber, Jessberger, Revenkova, & Heyting, 2003; Garcia-Cruz et al., 2010). The meiotic program will also utilize specialized kleisin units REC8 (most used in meiosis) and RAD21L in addition to RAD21, which is the only kleisin unit used in mitotic division. The meiotic-specific form of cohesin will also use STAG3 as the accessory unit to cohesin, where the mitotic program will use either SA1 or SA2. (SMC complexes reviewed in Section 1.3).

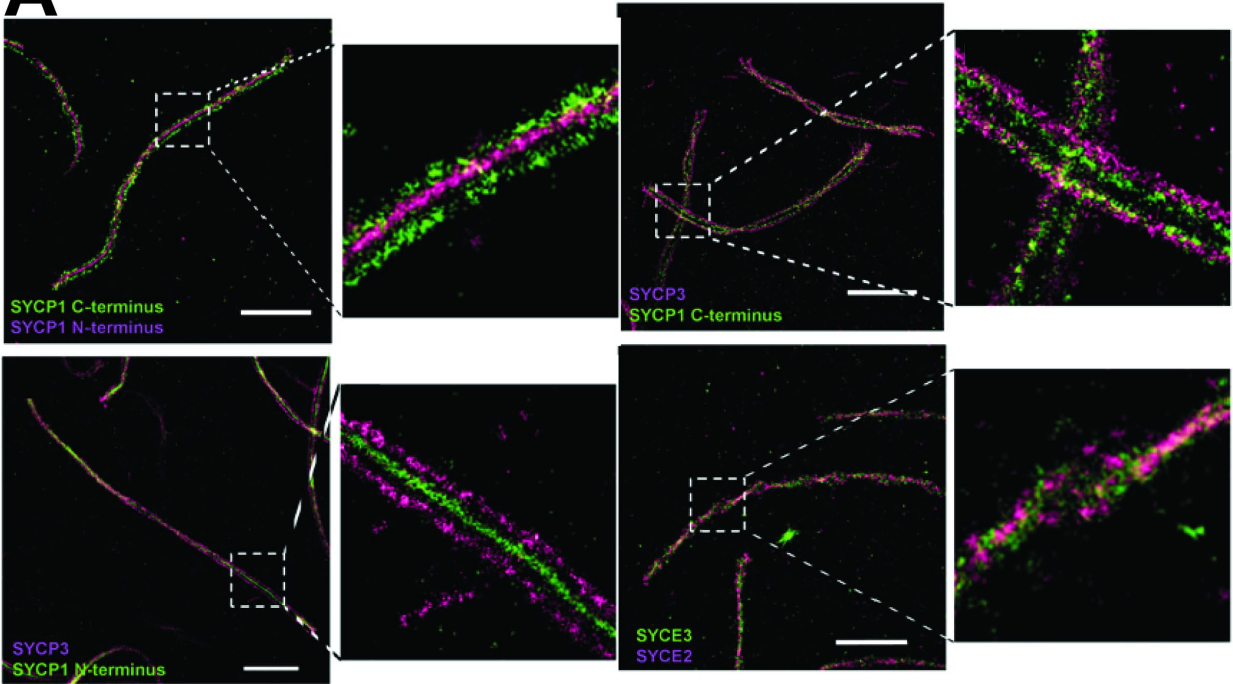
Meiotic prophase I chromosomes are initially folded and organized using the meiotic-specific cohesin variants, which form the cohesin core (Bolcun-Filas & Schimenti, 2012; Fraune, Schramm, Alsheimer, & Benavente, 2012; Rong et al., 2016). During meiotic anaphase I, REC8 is cleaved, freeing both the sister chromatid arms and the homologous chromosomes from each other (Brooker & Berkowitz, 2014; Buonomo et al., 2000; Garcia-Cruz et al., 2010). Only the centromeric cohesin holding sister chromatids remain, keeping the sisters paired while separating the homologues. This remaining attachment is not fully understood but is in part achieved by the presence of shugoshin and the subsequent recruitment of protein phosphatase 2A at the centromere (Brooker & Berkowitz, 2014; Garcia-Cruz et al., 2010).

An additional structure called the synaptonemal complex (SC) is formed systematically on the cohesin core (Bolcun-Filas & Schimenti, 2012; Garcia-Cruz et al., 2010). The SC links and binds homologous chromosomes together throughout meiosis I (Enguita-Marruedo et al., 2018; Rog, Kohler, & Dernburg, 2017). The SC also assists in several critical meiotic functions. The first step in the formation of the SC is the formation of the axial elements, formed by the interactions between the SYnaptonemal Complex Protein (SYCP2 and 3) and the cohesin core.

SYCP2 and 3 are codependent on each other for the formation of the axial elements (Yang et al., 2006; Yuan et al., 2000). Both directly interact with the cohesin core and are responsible for its maintenance in meiosis I, but not its initial formation (Kouznetsova, Novak, Jessberger, & Hoog, 2005). SYCP2 and 3 begin to fuse with each other to form a rigid core along the sister chromosomes through prophase I. The fusing of SYCP2 and 3 creates the axial core structure. After the axial core has materialized, SYCP1 forms a structure called the central element by attaching to each of the axial elements through its tail. During this time the axial element is renamed the lateral element, as it is lateral to the central SYCP1 complex element. SYCP1 performs a zipper-like action (synapse) to the SC by interacting with SYCP2/3 at its tail, dimerizing at its head domain, and recruiting other central elements at the center of the SC, such as SSynaptonemal Central Elements (SYCE) 1, 2, and 3 (Enguita-Marruedo et al., 2018; Fraune et al., 2012; Schucker, Holm, Franke, Sauer, & Benavente, 2015). Through the complete formation and synapsis of the SC, the homologous chromosomes and their sisters become physically paired together. The interplay of SYCP1's N and C terminus with SYCP3 (which also localizes with SYCP2) can be seen in Fig. 1.5-2A in addition to the central elements along the central axis (Schucker et al., 2015). Fig. 1.5-2B demonstrates the order of formation and interconnectedness between the different elements of the SC (Fraune et al., 2012).

The ordered construction of the SC from SYCP1, 2, 3 and the inner SYCE 1, 2, and 3 proteins creates a highly organized, periodic, and rigid structure. The SC has structural similarity between different forms of eukaryotic life, from yeast, worms, mice, and humans. Due to the rigidity and highly ordered structure of the SC, it was assumed that the SC was a static, crosslinking object, locked into place and bound to the cohesin core and central elements. This view is challenged since chromosomes morphologically change over mitosis and SC elements

**A**



**B**

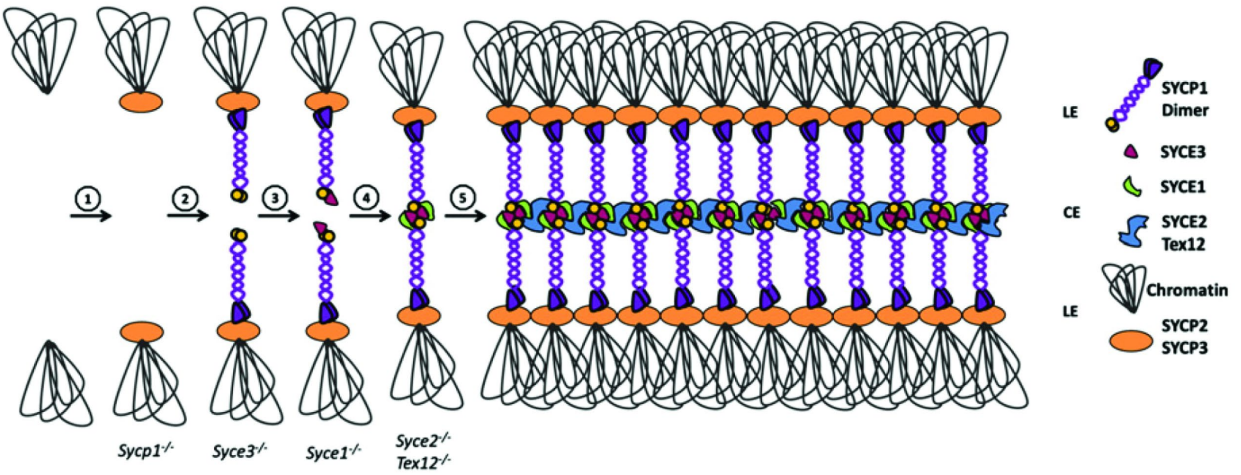


**Figure 1.5-2. Diagram of the synaptonemal complex, meiotic connections, and crossover.**

(A) High resolution imaging of Synaptonemal Complex (SC) proteins (SYCP). The N-terminus of SYCP1 and its C-terminus were labeled in two different colors and imaged under a high-resolution imaging protocol (STORM). With the increase in imaging fidelity, it became clear that the N-terminus and the C-terminus of SYCP1 occupied two distinct domains in the SC. It was also very apparent from these images that both termini of SYCP1 were constructed in a highly organized and structured pattern. Using high resolution microscopy, the N-terminus of SYCP1 was shown to always be central, opposite SYCP3, but the C-terminus was found to be on either side of the central axis and associated spatially close to SYCP3. Other elements of the central element (SYCE3 and 2) were also shown to be very spatially close and connected. Scale bar represents 2  $\mu\text{m}$ . Image repurposed from (Schucker et al., 2015). (B) Synaptonemal complex assembly in a stepwise manner. Meiotic specific cohesin will bind to the duplicated meiotic chromosomes and extrude loops for compaction, like mitotic condensins. Upon formation of this, SYCP2/3 is required to form the lateral elements; SCs lacking this protein will not continue forming the SC. Next, SYCP1 binds to SYCP2/3 to create a space for linking the two axial elements of the SC. Without SYCP1, this extension is not formed. SYCE3, then SYCE1 bind sequentially, and lacking either does not allow the SC to continue forming or bridge SYCP1 normally. SYCE2 and Tex12 then bind the central elements and crosslink with one another to zip-up the SC and form the synapsed SC, without which the SC would not fully form and synapse. Image repurposed from (Fraune et al., 2012).

can continue assembling off a complete SC through mitosis (Henzel et al., 2011; Page & Hawley, 2004; Voelkel-Meiman, Moustafa, Lefrancois, Villeneuve, & MacQueen, 2012).

Further experiments demonstrated the liquid-crystal-like properties of the SC (Rog et al., 2017). In these experiments, SYP-2, a component in the central element, involved in meiotic recombination, would freely float in the cytoplasm when Htp-3, a component of the lateral element, was removed from the cell. However, the floating SYP-2 object was highly organized and would aggregate with other floating particles. Further evidence of the SC's dynamic nature was observed when gonads (containing meiotic cells/chromosomes) of wild-type worms were treated with hydrophobic and electrostatic-disrupting chemicals. This treatment caused the SC to disassociate from the chromosomes but reformed when the liquid was diluted out of the system. This paper also demonstrated that the SC helps facilitate crossover points by stabilizing elements of the SC after crossover formation. This stabilization was also hypothesized to be related to the high stiffness of meiotic chromosomes associated with the beam-film model of crossover interference, discussed later.

Crossover is the event where one chromosome arm is exchanged with its paired homologue. This process is a requisite event for proper segregation during meiosis (Kleckner et al., 2004; Zickler & Kleckner, 1999). During leptotene, Spo11 induces specialized double stranded DNA breaks, which will then recruit specialized repair proteins (Keeney, 2008). The recruitment of the repair proteins form repair nodules, which are regions enriched with repair proteins that interact with one another (Bolcun-Filas & Schimenti, 2012; Fraune et al., 2012). Some of the repair nodules cross over the central element and swap with its homologous nodule, then repair and religate to the homologous chromosome. Crossover is completed when the repair nodules are integrated into the homologous chromosome section. There is conflicting evidence

that the SC is required for normal crossover formation, but the SC is responsible for holding the homologous chromosomes spatially close, which may facilitate crossover formation (Bisig et al., 2012; Kouznetsova et al., 2011; Page & Hawley, 2004; Qiao et al., 2012).

The obligate crossover and crossover interference are two important features of mitotic crossover formation. The obligate crossover refers to the requisite crossover per homologue pair, while crossover interference refers to the inhibition of existing of new, nearby crossovers by inhibiting existing crossovers (Gray & Cohen, 2016; Zickler & Kleckner, 1999). Crossover interference is resilient even when there is an increase in crossover precursors. There are several hypotheses as to how crossover interference is accomplished. Some hypotheses include the formation of chemical spreading of the signal from crossover points. Other hypotheses include the spreading of a physical pressure that extends from crossover points. A prevalent physical model of crossover interference is called the beam-and-film model, which depicts the meiotic chromosome as a stiff beam, covered by a thin film (Kleckner et al., 2004; L. Zhang, Liang, Hutchinson, & Kleckner, 2014; Zickler & Kleckner, 1999). The hypothesis states that fluctuations of the underlying meiotic chromatin generate stress within the beam. These fluctuations will create a higher likelihood of breaking through the film, making the obligate crossover more likely. The breakthrough of the crossover also creates a relief from the fluctuations' stress, inhibiting additional breakthroughs in the surrounding area. The ability of the chromosome to relay the physical stiffness to the other areas of the chromosome would require a very stiff core. This stiffness and stress relief could be further facilitated by inhibiting dynamic elements of the SC upon crossover insertion (Rog et al., 2017).

## 1.6 Centromeric protein (CENP) complexes

### 1.6.1 How chromosomes divide - The physical machinery

Chromosome division involves the interactions between many complex networks and superstructures. Several key networks and proteins in chromosome division are the microtubules (MTs), which bind to and pull on the chromosomes; the centrosomes, which organize the MTs; the kinetochore (KT), which facilitates the connection between the chromosomes and MTs; the chromosome passenger complex (CPC), which controls the steps in chromosome division and the spindle assembly checkpoint (SAC); and the centromere, which is where the KT is constructed and integrated into the chromosome (Carmena, Wheelock, Funabiki, & Earnshaw, 2012; Kixmoeller, Allu, & Black, 2020).

Microtubules (MTs) are structures formed from a repeat of  $\alpha$ - and  $\beta$ -tubulin in a corkscrew pattern, which folds itself into a higher-ordered, tube-like structure (Goodson & Jonasson, 2018; McIntosh, 2016). The pattern of the  $\alpha$ - and  $\beta$ -tubulin subunits are also very consistent, allowing MTs to have directionality in their assembly process (Goodson & Jonasson, 2018). MTs that are anchored to their organizing and nucleating center are called the minus (–) end, while their growing ends are called the plus (+) end. MTs also have rigid trunks and flexible tips that rapidly assemble and disassemble during mitosis. MTs' flexible tip and their rapid, dynamic growth in mitosis allow them to efficiently search the cell for different anchor points. In general, there are three types of mitotic MTs depending on their location and anchor points (Goodson & Jonasson, 2018; McIntosh, 2016; Petry, 2016). MTs that attach to the nearby cell membrane are called aster MTs, which help anchor the centrosomes (the MT-organizing center) and prevent centrosome movement when they pull on the chromosomes. MTs that connect to the KT are called KT or spindle microtubules, which pull on the chromosomes through the KT by

depolymerizing on the DAM1 ring. MTs that interact with the opposite spindle's MTs are called polar MTs, which helps the centrosomes/chromosome spindle orient properly by pushing against one another. This is facilitated in part by the opposite directionality of the + ends of the polar MTs since they both grow from opposite sides of the cell (Conduit, Wainman, & Raff, 2015; Goodson & Jonasson, 2018; McIntosh, 2016; Petry, 2016). The forces generated by polar MTs are also assisted by motor proteins. An overall diagram of the MTs, centrosomes, and KT attachments are diagramed in Fig. 1.6-1A (Petry, 2016).

The centrosomes organize MTs and act as their anchor point, where all – end MTs group (Conduit et al., 2015). The centrosomes form from by a pair of centrioles, which also recruit a dense web of MT-organizing proteins called the pericentriolar matrix (Petry, 2016). At the beginning of the cell cycle, just after cell division, only one pair of centrioles is present. The centriole pair is duplicated during the G1 to S phase transition when DNA is also being duplicated (Conduit et al., 2015; Petry, 2016). During mitosis, the centriole pairs will then orient themselves to different sides of the cell to form the two opposite spindles, sides, and poles of the dividing cell. This orientation and movement to opposite sides of the cell is facilitated and stabilized in part by the polar MTs. We will not discuss the additional complexity of the centrosome in detail.

The kinetochore (KT) is a large, complicated, interdependent structure formed from many subnetworks, complexes, and proteins (Hara & Fukagawa, 2017; Musacchio & Desai, 2017; Nagpal & Fukagawa, 2016; Perpelescu & Fukagawa, 2011). The KT is the force transducer between the spindle MTs and the chromosomes, which pull away from its duplicated sister at anaphase onset. The KT can be conceptually split between the outer KT and inner KT. The inner KT, also known as the Constitutively Centromeric Associated Network (CCAN), is

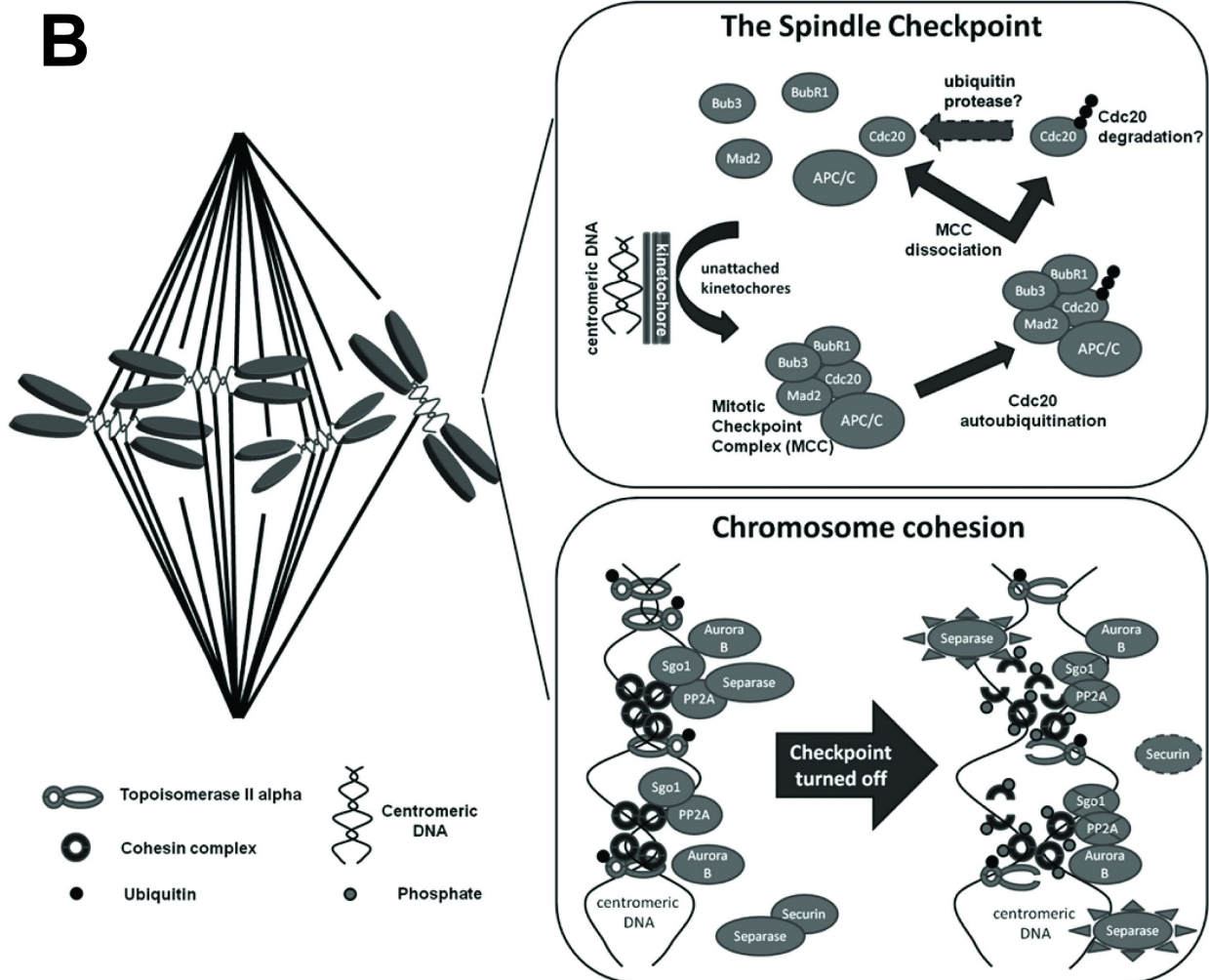
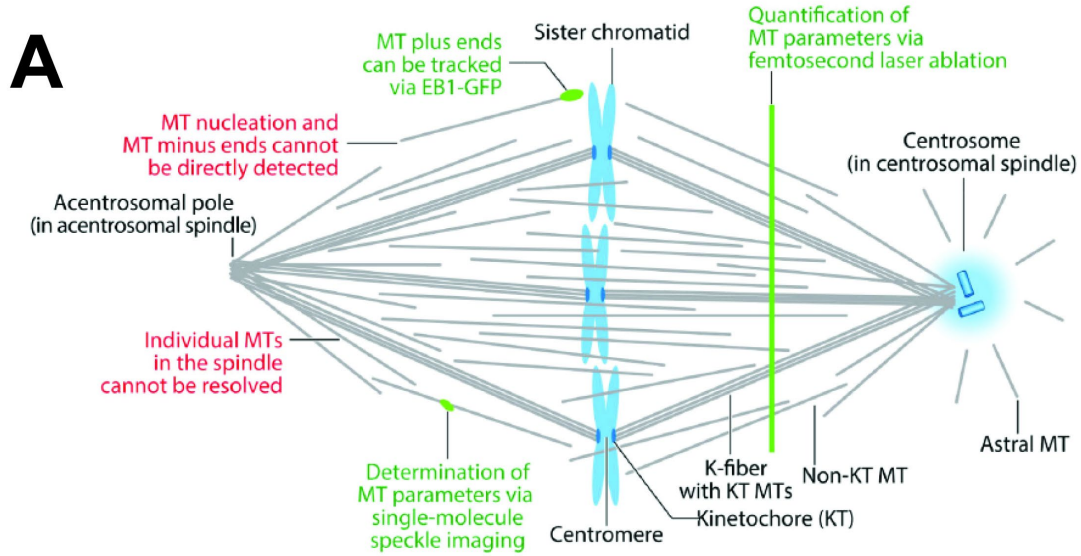


**Figure 1.6-1. Chromosome separation machinery diagram.**

(A) Interplay of chromosomes and microtubules. In mitosis, the centrosome (blue rods and haze) will extrude fibers of microtubules (grey). These microtubules will then interact with the cell membrane and become astral microtubules, interact with the chromosomes' kinetochores (dark blue dots) (K-fibers/KT MTs), or interact with the opposing spindle's microtubules, recruit motor proteins, and drive cell separation (not explicitly labeled). Figure also contains notes on how microtubule studies are performed. Image repurposed from (Petry, 2016). (B) Diagram of the spindle assembly checkpoint. Chromosome unattached at the kinetochore by microtubules will undergo a complex pathway to inhibit the cleavage of cohesin, protecting the sisters from premature separation. This holding pattern depends on several back-and-forth phosphorylations and dephosphorylations, which are only overcome once all chromosomes are attached and undergo tension. Upon proper tension, the anaphase-promoting complex ubiquitinates the centromeric cohesin, causing its degradation, which in turn allows chromosomal separation and anaphase onset. Image repurposed from (Diaz-Martinez & Clarke, 2009).

consistently associated with the centromere over the cell cycle, described later. The outer KT, also known as the KMN network directly interacts and associates with spindle MTs. The KMN network is composed of the Knl1 complex, the Mis12 complex, and the Ndc80 complex.

The Mis12 complex attaches to the CCAN during mitosis and acts as an anchor for the other members of the KMN network by forming a long, thin, comma-like structure (McAinsh & Meraldi, 2011; Nagpal & Fukagawa, 2016; Perpelescu & Fukagawa, 2011). The Mis12 complex is composed of MIS12, NNF1, DSN1, and NSL1 in humans. The Knl1 complex interacts with several proteins but is structurally composed of only the KNL1 protein. It is important for coordinating SAC functionality with KT proteins, can help attach the Ndc80 complex to the Mis12 complex in some species, and governs some aspects of spindle microtubules to the kinetochore, although this role is mostly associated with SAC functionality. The Ndc80 complex consists of the proteins NDC80, NUF2, SPC25, and SPC24. The Ndc80 complex is the predominant interactor between the spindle MTs and the kinetochore. It is also the target of the SAC, strengthening or weakening its interactions to the spindle MTs depending on if the kinetochores are properly attached to the spindles. The Ndc80 complex can also stabilize and dimerize the Dam1 ring on spindle MTs (Carmena et al., 2012; Musacchio & Desai, 2017). The interaction between the Dam1 ring and MTs is hypothesized to generate the force required for chromosome separation and spindle tension. While this is an oversimplification of the KMN network, we will continue our overview of the chromosomal separation machinery.

To evenly separate the duplicated sister chromosomes in mitosis to the different poles of the mitotic cell, the cell must ensure that each spindle captures one and only one of each sister chromosome to preserve genetic integrity. The Spindle Assembly Checkpoint (SAC) is a mitotic function that involves stalling anaphase onset until all the chromosomes' KTs are properly

attached to their respective spindles (Carmena et al., 2012; Musacchio & Desai, 2017). The SAC is governed by the chromosome passenger complex, which is located in between the sister chromatids' centromeres and is composed of Aurora B, INCENP, Borealin, and Survivin (Nagpal & Fukagawa, 2016). For simplicity, we will focus on the action of Aurora B in describing the mechanism of the SAC. When MTs are unattached, they tend to rapidly depolymerize, then repolymerize to search the cell for stable attachments. Aurora B's kinase activity destabilizes MT-KT attachments. This destabilization allows chromosomes to reorient themselves so both sister kinetochores can be captured by the opposite centrosomes if not properly positioned. Once all the chromosomes are properly bioriented and attached to their respective spindle poles, Aurora B can no longer interact with the MTs (Cairo & Lacefield, 2020). The depolymerizing force of the MTs start balancing the forces on each chromosome pair and each chromosome in the pair, and line up at the metaphase plate. Centromeric cohesin is then cleaved and allows the sister chromosomes to separate. The separation of sister chromosomes is the onset of anaphase. These steps and interplay with centromeric cohesin are depicted in Fig. 1.6-1B (Diaz-Martinez & Clarke, 2009).

There are two hypothesized pathways that the SAC functions: one by MT occupation at the KT and the other through tension sensing (Cairo & Lacefield, 2020; Musacchio & Desai, 2017; Nagpal & Fukagawa, 2016). When MTs have properly attached to KTs, it stabilizes the connection, although if Aurora B is active and close to the outer KT, Aurora B will destabilize the MT-KT interaction, acting as a timer to achieve bi-orientation. Once a chromosome pair has both of its KTs occupied to opposing sides, Aurora B becomes unable to interact with the spindle MTs, leading to a stable MT-KT interaction. There is debate if the bioriented spindle and the force generated in the spindle tug-of-war directly inhibits Aurora B activity through a tension

sensing mechanism in the CPC or if the pulling force of the spindles physically separates Aurora B from the KT-MT site and cannot physically reach the proteins to phosphorylate them (Cairo & Lacefield, 2020; Krenn & Musacchio, 2015; Musacchio & Desai, 2017). In either case, the MT-KT interactions demonstrate an important function of forces in the coordination and timing of chromosome separation and mitosis in general.

### **1.6.2 Structure and behavior of the centromere and the CCAN**

The Constitutively Centromeric Associated Network (CCAN) is the inner part of the kinetochore, which directly interacts with the centromere over the cell cycle (Hara & Fukagawa, 2017; McAinsh & Meraldi, 2011; Musacchio & Desai, 2017; Nagpal & Fukagawa, 2016; Perpelescu & Fukagawa, 2011). The CCAN bridges the centromere with the outer kinetochore in mitosis (Fig. 1.6-2A,D) (McAinsh & Meraldi, 2011; Musacchio & Desai, 2017). In humans the centromere localizes to a repetitive sequence of DNA on different chromosomes (regional centromeres), while other organisms have centromeres that localize to a single DNA sequence per chromosome (point centromeres), or all along the chromosome at specific DNA sequences (holocentromeric) (Musacchio & Desai, 2017). Human centromeres vary along the length of the chromosome depending on the specific chromosome (*i.e.*, chromosome number). Some centromeres localize close to the telomere (telocentric), while others localize near the center of the chromosome (metacentric) (Musacchio & Desai, 2017). Perturbations to the centromere cause chromosomal segregation defects such as chromosome misalignment, aneuploidy, chromosome breakage, anaphase bridges (which can lead to DNA damage), and chromosome rearrangements. All these defects are associated with and can facilitate the onset of some cancers (Carmena et al., 2012; Morrison & Thakur, 2021; Perpelescu & Fukagawa, 2011; van der Waal, Hengeveld, van der Horst, & Lens, 2012).

Both the CCAN and the histone variant that demarcates the centromere are called CENTromere Proteins or CENPs. CENP-A is a histone H3 variant that marks the centromere by localizing to the repetitive centromeric DNA sequence (Musacchio & Desai, 2017; Nagpal & Fukagawa, 2016; Perpelescu & Fukagawa, 2011). Because CENP-A determines where the chromosome itself is incorporated into the mitotic division machinery, it is vital for the centromere to be stable and organized (Fig. 1.6-2) (McAinsh & Meraldi, 2011; Musacchio & Desai, 2017; Nagpal & Fukagawa, 2016; Srivastava & Foltz, 2018). It is possible that the centromere can move and reinsert itself into the chromosome, although the cell has developed methods to stabilize the centromere through the cell cycle to prevent movement and duplication (Gambogi & Black, 2019; Moreno-Moreno, Torras-Llort, & Azorin, 2017; Morrison & Thakur, 2021). The cell stabilizes the functional centromere's location through post-translational modifications of CENP-A (Srivastava & Foltz, 2018). The cell also will inhibit the formation of a new functional centromere by degrading free, non-integrated CENP-A (Ranjitkar et al., 2010; Stellfox, Bailey, & Foltz, 2013). PTMs to chromatin surrounding the centromere, called pericentromeric heterochromatin, contains further modifications that help designate and anchor the centromere (Lawrimore & Bloom, 2019; Lawrimore et al., 2015; Stephens et al., 2013). As implied by the name, the pericentromeric chromatin is heterochromatic.

Another way the functional centromere is stabilized on the chromosome is by the recruitment of the CCAN (Cao, Zhou, Zhang, Luger, & Straight, 2018; Hori et al., 2017; Perpelescu & Fukagawa, 2011; Stellfox et al., 2013). This stabilization belies its purpose of associating with the centromere over the cell cycle, even when the kinetochore is not involved in chromosomal separation (Nagpal & Fukagawa, 2016). The human CCAN is made up of CENP-C/H/I/K/M/L/N/O/P/Q/R/S/T/U/W/X. Like the outer kinetochore, the sheer number of proteins is



**Figure 1.6-2. Diagram of the Constitutive Centromeric Associated Network (CCAN) in mitosis.**

(A) Cartoon schematic of the interactions between the interactions of the whole kinetochore. The histone H3 variant, CENP-A, is integrated with the other histones to form the CENP-A containing nucleosome, forming the basis for the centromere. Upon that, the CCAN is formed on top of the CENP-A nucleosomes. CENP-L and -N interact in a complex; CENP-H, I, K, and M form another, CENP-O,P,Q,U,R form another, CENP-T,W,S, and X form another, while CENP-C works independently. In the KMN network, recruited by the CCAN forms during mitosis to interact with the microtubules. KNL1 and Zwint form one complex, DSN1, MIS12, NSL1, PMF1 form the MIS12 complex, NDC80, NUF2, SPC24, and SPC25 form the NDC80 complex. Image repurposed from (Musacchio & Desai, 2017). (B) CCAN interactions with chromatin during mitosis and interphase. During interphase, CENP-N/L (Yellow) recruits CENP-C (orange) to the CENP-A (red) containing nucleosomes in the centromere. The CENP-N/L complex also recruits CENP-H, I, K, M complex (brown), which holds all the complexes together. CENP-T,W,S,X (green) forms a histone-like fold and will wrap around chromatin surrounding the CENP-A designated centromere. During mitosis, CENP-C can directly bind CENP-A nucleosomes instead of needing the CENP-N/L complex. In both situations, there will be surrounding H3-containing nucleosomes (orange spheres) instead of purely CENP-A nucleosomes. Image repurposed from (Nagpal & Fukagawa, 2016). (C) Simplified view of CENP-A's and the CCAN's interaction with chromatin. CENP-A, which directly interacts with CENP-C and N during mitosis, wraps into nucleosomes containing the other histones. The CENP-A nucleosomes then wrap DNA around it. The other CCAN members then create a link to the CENP-T,W,S,X complex, which wraps chromatin in an alternate direction to normal nucleosomes, further distinguishing the centromere. H3-containing nucleosomes will also be present, but not directly interact with elements of the CCAN. Image repurposed from (Srivastava & Foltz, 2018). (D) Detailed view of how the CCAN, KMN network, and microtubules interact during mitosis. The CCAN (light blue) interacts with the centromeric chromatin, including the CENP-A containing nucleosomes. CENP-N and CENP-C directly interact with CENP-A, while the TWSX complex interact with the surrounding chromatin. CENP-H,I,K,M bridge all the CCAN elements together. The KMN networks extrude in a rod-like manner from the CCAN elements and attach to the microtubules via the NDC80 complex. These attachments will be stabilized by post-translational modifications and other elements on top of the microtubules. Image repurposed from (McAinsh & Meraldi, 2011).

further complicated by the way these proteins interact to form networks and complexes to form the inner kinetochore. The complexes they form are CENP-H/I/K/M, CENP-N/L, CENP-O/P/Q/R/U, CENP-T/S/W/X, and CENP-C appears not to form a specific subcomplex separate from the CCAN (Hara & Fukagawa, 2017; McAinsh & Meraldi, 2011; Musacchio & Desai, 2017; Perpelescu & Fukagawa, 2011).

During mitosis, both CENP-C and CENP-N directly attach to CENP-A, thus are critical for localization and stabilization of the functional centromere (Cao et al., 2018; Carroll, Milks, & Straight, 2010; Carroll, Silva, Godek, Jansen, & Straight, 2009; Stellfox et al., 2013). CENP-C stabilizes CENP-A and interacts with the Mis12 complex as a key bridge between the centromere and the outer kinetochore (Perpelescu & Fukagawa, 2011; Stellfox et al., 2013). CENP-C also interacts with CENP-H, L, and N to stabilize the CCAN, although not in an exact linear manner. The CENP-H/I/K/M complex interacts with all other members of the CCAN, acting somewhat as a core for all the complexes to interact (Hara & Fukagawa, 2017). During interphase, the complex also targets CENP-A and acts as the initial interaction of the CCAN to the centromere (in mitosis, all members of the CCAN depend on CENP-C for proper centromeric localization). The CENP-L/N complex also acts as a critical junction for the assembly of a functional CCAN but relies on other proteins for proper targeting to the centromere and stabilization with the centromere. The CENP-T/W/S/X complex interacts directly with the DNA close to the centromere, but not CENP-A. The CENP-T/W/S/X complex contains a histone fold domain, which mimics histone structure, allowing it to bind DNA (Fig. 1.6-2B,C) (Nagpal & Fukagawa, 2016; Srivastava & Foltz, 2018). The CENP-T/W/S/X complex also binds to the Ndc80 complex, stabilizing the chromosome-outer kinetochore connection (Fig. 1.6-2D) (McAinsh & Meraldi, 2011). The function of the CENP-O/P/Q/R/U complex remains somewhat enigmatic, as

it does not substantially affect the stability of the other CCAN proteins or affect cell viability (Hara & Fukagawa, 2017). The CENP-O/P/Q/R/U complex sits on top of the H/I/K/M complex and interacts with microtubules, but its mitotic function still is somewhat unclear. CENP-U specifically may have roles in development, although the whole complex is still being researched (Hara & Fukagawa, 2017).

The centromere is also enriched in other proteins that may help its stability and reduce the likelihood it drifts from its designated spot. As mitosis progresses to metaphase, cohesin is removed from the chromosome arms, but is retained at the centromere (Carmena et al., 2012; van der Waal et al., 2012). The removal of cohesin is facilitated by Aurora B, which is paradoxically enriched in the centromere where cohesin is retained. Cohesin is retained at the centromere since it is enriched with a protein that antagonizes Aurora B's removal activity of cohesin (Verzijlbergen et al., 2014). Centromeric cohesin is maintained until the SAC is deactivated and cohesin is cleaved (van der Waal et al., 2012). The centromere is also enriched in condensin during mitosis, recruited by part of the CPC (Carmena et al., 2012; Stephens et al., 2013). This enrichment in condensin is thought to help biorient the spindle and make it easier for the spindle MTs to find the KTs. This function of condensin enrichment is thought to occur by stiffening the centromere and making the opposing KTs on the sister chromosomes preferentially point in opposite directions, where each of the centrosomes would be located. Due to the enrichment of condensin, it is also possible that it affects the stiffness of the centromere (Verzijlbergen et al., 2014). The final enriched element that may assist in the stability of the centromere is heterochromatin. The repeated DNA sequence in the pericentromere contains constitutive heterochromatin, which recruits histone readers of heterochromatin marks. This recruitment

could lead to a denser amount of chromatin flanking each side of the centromere and make CENP-A movement and drift difficult.

### 1.6.3 Centromere stretching and its stiffness

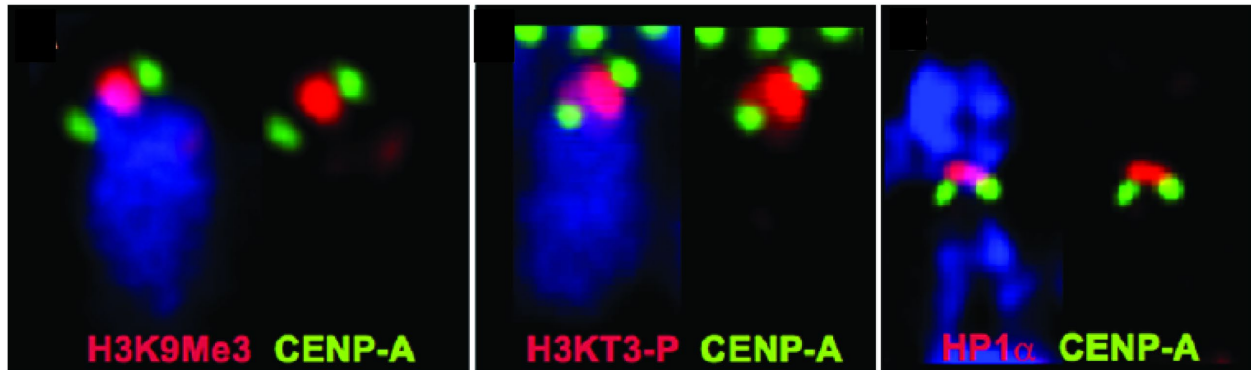
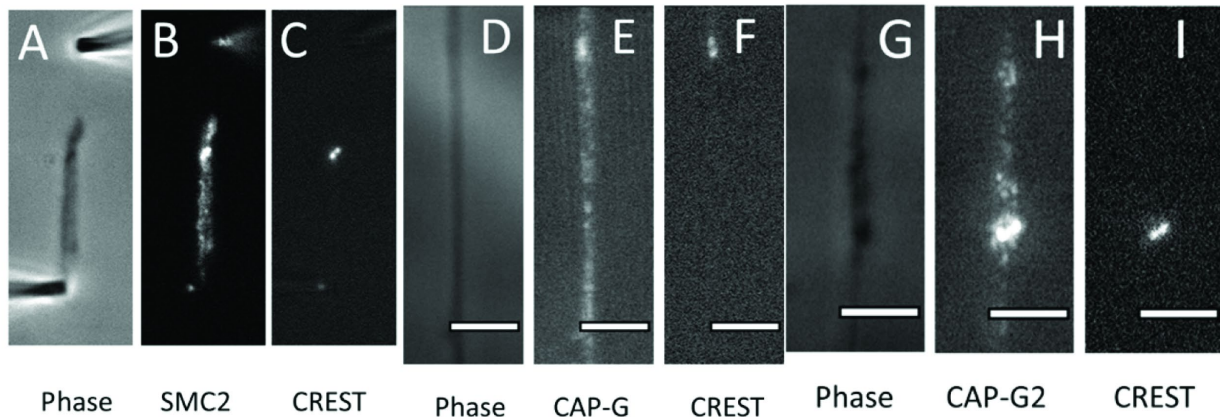
There have been several studies that seek to determine contributing factors of centromeric stiffness. Fig. 1.6-3 demonstrates the enrichment of heterochromatin factors (A) (Vagnarelli, Ribeiro, & Earnshaw, 2008) and condensin I and II (B) (M. Sun et al., 2018b) on centromeres during mitosis. One such study used yeast to observe the movement of the spindle pole bodies, a yeast analogue of the centrosomes, over mitosis and the effect of its movement by altering different chromatin organizational complexes (Stephens, Haase, Vicci, Taylor, & Bloom, 2011). By focusing on the length of the spindle pole bodies over time and its variation over time they could measure the stiffness of the centromere spring. Yeast KTs bundle together and form a singular spindle collection that surrounds all the KTs, allowing the researchers to track only one object in the experiments.

These experiments observed a difference in condensin's and cohesin's localization to the pericentromere (Lawrimore et al., 2015; Stephens et al., 2011; Stephens et al., 2013). Condensin localizes along the attachment line of the kinetochore, *i.e.*, proximal to the spindle axis. Cohesin localizes in a barrel-shape cloud surrounding the line of the kinetochore, *i.e.*, radially distal to the kinetochore. Mutations in condensin and cohesin both affected the spindle pole body length and its variation over time, suggesting that the stiffness of the centromeric spring and the underlying chromatin is affected by both complexes. This is in accord with the condensin data found in the axial-stretching experiments (perpendicular to the chromatin stretch in the spindle pole bodies) that use siRNA-based degradation of SMC2. This study also observed that reduced nucleosome occupancy in the pericentromeric chromatin, affected the spindle length, but not the variation

over time. This suggested that nucleosome occupancy and SMC complexes share some centromeric stabilizing functions but are not completely functionality identical.

This study also observed the localization of tagged DNA segments over mitosis. Alterations to nucleosome occupancy caused an increase in fluorescent smearing in one or both foci, which were greater in cohesin and condensin mutants (Lawrimore et al., 2015; Stephens et al., 2011; Stephens et al., 2013). Along the same line, the distance of the tagged DNA segments increased their distance from the spindle axis in all mutants with greater effects in the SMC complex mutants than the nucleosome occupancy mutant. This evidence suggests that the chromatin spring and enrichment of condensin, cohesin, and heterochromatin not only works to stiffen the mitotic spindle, but also to stabilize the surrounding chromatin around the centromere. This stabilization appears to be mostly facilitated by the SMC complexes, but heterochromatin also plays an important role. Additional studies also revealed chromosome movement coordination, which is dependent on condensin and cohesin, the dynamics of nucleosomes under spindle tension, and how chromatin tethers to the spindle (Stephens et al., 2013; Verdaasdonk & Bloom, 2011). The recruitment of condensin, cohesin, and heterochromatic enrichment at the centrosome probably have functional purposes in chromosome division coordination.

Experiments have also been done to observe centromeric stretching along the chromosome axis. The results of these experiments demonstrated that the centromere is exceptionally stiffer than the chromosome arms (Sun, 2014). The stiffness of the centromere is unsurprising, since the centromere is substantially enriched in chromatin-organizing proteins and chromatin compacting molecules, *i.e.*, condensin, cohesin, and heterochromatin. The centromere is at least 200-fold stiffer than the chromosome arms, and in some instances does not stretch when the length is increased to four-fold its starting length. This is more surprising when

**A****B**

(A) The centromere is enriched in heterochromatic elements. CENP-A (green), the molecule that designates chromatin at the centromere, can be found next to histones enriched in the heterochromatic elements, H3K9me<sup>3</sup>, and HP1 $\alpha$  (red) during mitosis. Blue designates the mitotic chromatin. The histone mark H3KT3-P (sic) is associated with the onset of mitosis, where H3T3 is phosphorylated to inhibit the binding of HP1 $\alpha$ , demonstrating that the increase in heterochromatic marks is still present during mitosis. Image repurposed from (Vagnarelli et al., 2008). (B) The centromere colocalizes with both forms of condensin. Isolated chromosomes stained with a fluorescent CREST antibody (pan-centromere binding) can be seen with an enrichment of SMC2 (all condensin), CAP-G (condensin I), and CAP-G2 (condensin II). Scale bar represents 5  $\mu$ m. Image repurposed from (M. Sun et al., 2018b).

comparing the spring constant of the centromere along the spindle axis, estimated at 0.345 pN/ $\mu$ m in yeast (Stephens et al., 2011), while the human chromosome arm was already about 75 pN/ $\mu$ m along the axis. There are many different aspects to consider though, such as the species of the centromere (yeast vs human), the size of the centromere, the direction of the force applied, the object stretching (the spindle poles vs the chromatin), and other considerations.

In addition to studying the spring constant of the unmodified centromere, centromere-stretching experiments were also performed in CENP-C depleted cells via siRNA depletion. These experiments used antibody-stained CENP-A or CREST to track the centromere. Even though the CCAN constructs a cage-like structure over the centromere, which also assists in its stability, limiting the amount it can drift, the depletion of CENP-C did not appear to greatly affect the stiffness of the centromere when stretched along the chromosome axis, in that it was still much stiffer than the chromosome arms. This presumes the axial force of stretching the chromosome will be transduced through the centromere in the same way as in the untreated experiments. CENP-C degradation experiments were unable to be performed in the yeast studies since they require a functional kinetochore for the assay.

In addition to the complexity involved in centromeric stiffness, there are several factors that determine the loading and stability of CENP-A on chromatin, *i.e.*, in the centromere. HJURP (Holiday Junction Recognition Protein), is the histone remodeling protein involved in depositing CENP-A containing nucleosomes into chromatin (French & Straight, 2013). The activity of HJURP and subsequent stability of the CENP-A nucleosome depends on many factors such as post-translational modifications of CENP-A (Bailey et al., 2013; Kunitoku et al., 2003), PTMs of surrounding histones (Shang et al., 2016), CCAN proteins (Carroll et al., 2009), and other associated proteins (Moree, Meyer, Fuller, & Straight, 2011), although the stability of CENP-A

does not appear to always depend on CCAN proteins. One specific study of interest demonstrated that both CENP-C and CENP-N can assist *in vitro*, CENP-A-containing nucleosomes from disassociating in high heat and high salt conditions, *i.e.*, the CCAN can help stabilize CENP-A nucleosomes (Cao et al., 2018). However, this study also demonstrated that degradation of these proteins using auxin-induced degradation did not affect the maintenance of CENP-A *in vitro* via fluorescence or affect their stability via salt extraction from living cells. An additional experiment using binding mutants of CENP-N and CENP-C also demonstrated their redundancy for the stability and maintenance of CENP-A in the centromere *in vitro*.

### **1.7 Introduction to the Chapters - questions asked and answered**

The structural and mechanical study of mitotic chromosomes through micromanipulation has been used through this thesis to understand all these fields relating to the construction of mitotic chromosomes. The first project in Chapter 2 demonstrated the morphological changes of rapid SMC complex degradation through AID-based treatments and degradation, but also showed a lack of mechanical change with their rapid degradation. The second project in Chapter 3 demonstrated how histone PTMs and complexes that interact with said PTMs affect the stiffness of mitotic chromosomes. Histone methylation and HP1 $\alpha$  stiffen mitotic chromosomes through non-redundant pathways, but histone acetylation did not affect the stiffness of mitotic chromosomes. The third project studied meiotic prophase I chromosome structure and the role of the SC in its stiffness in Chapter 4. In said project, we showed that meiotic prophase I chromosomes dissolved with nuclease treatment, but only weakened with protease treatments. The meiotic chromosome was much stiffer than mitotic chromosomes, but the wild-type chromosome was as stiff as a SYCP1 null mutant chromosome. The fourth project in Chapter 5

reveals that AID-based degradation of CENP-C and CENP-N does not affect the stiffness of the CENP-A containing region of the chromosomes. In Chapter 6, we consolidate the findings of these projects while proposing future experiments based on these projects and project suggestions not covered in this thesis. In the Appendix, we describe the methodology of chromosome isolation.

**Chapter 2. Rapid degradation of Structural Maintenance of Chromosome proteins using  
Auxin-Induced Degradation causes chromosomal morphological changes with no  
mechanical changes; Ki-67 degradation causes morphological changes and stiffens  
chromosomes**

*This chapter is a collection of unpublished experiments, related to each other by the rapid degradation of important structural proteins related to the mitotic chromosome, a future paper will be submitted upon completion of the future directions, using this chapter as the start. All experiments performed by myself. Cell lines received from the Kanemaki and Hirano/Imamoto labs at the National Institute of Genetics (Japan) and Riken (Japan), respectively as a collaborative project.*

SMC complexes are responsible for some of the most dramatic changes to chromosome structure during mitosis. Additional proteins that interact with chromatin, such as topoisomerases and Ki-67, assist in the formation of mitotic chromosomes. We carried out experiments to study the relationship between condensin, cohesin, and Ki-67 to mitotic chromosome structure, by measuring their mechanical properties. We utilized the Auxin-Induced Degradation system to rapidly degrade condensin, condensin I, condensin II, cohesin, and Ki-67, which resulted in morphological changes to the genome both in and out of the cell. However, despite the morphological changes, only Ki-67 degradation caused a mechanical change to the mitotic chromosome. This suggested that there are sources of organization contributing to mechanical stiffness that remain within the mitotic chromosome in the absence of SMC complexes.

## 2.1 Overview

The duplication and separation of the genome during mitosis is one of the most dramatic changes chromatin undergoes through the cell cycle. During mitosis the globular, relatively diffuse, transcriptionally active, and string-like interphase chromatin is transformed into the dense, compact, individualized, paired, and thick mitotic state. This transformation is facilitated by the action of large, chromatin-interacting molecules, including condensin, cohesin, topoisomerases, and Ki-67. Compacting and organizing the genome into thick bundles of chromatin causes the chromosomes to behave as individualized objects that can be manipulated by the cell. This individualization and organization allow the cell to ensure near-perfect, even distribution and separation into the two daughter cells. By compacting chromosomes into their rod-like shapes, they are easier for the cell to organize, manipulate, and separate. Compaction and individualization of mitotic chromosomes are intrinsically related to their folding, facilitated

by protein complexes. By removing entanglements between the chromosomes, they are less likely to break the underlying DNA strands in the chromatin and thus less likely to induce DNA damage and alter the genome. The even distribution of chromosomes also requires sister chromatid cohesion, which pairs the genetically identical sisters together until all chromosomes are attached to the separation machinery. This guarantees that each daughter cell will receive a complete copy of the genome.

The cell utilizes Structural Maintenance of Chromosomes (SMC) complexes in mitosis to facilitate both sister chromatid cohesion and chromatin compaction, which then leads to organization, individualization, and assists in removal of chromatin entanglements (Beseda et al., 2020; Boavida et al., 2021; Brahmachari & Marko, 2019; Klein et al., 1999; M. Sun et al., 2018b; Takagi et al., 2018). SMC complexes are formed by the association of two proteins containing coiled-coil arms and connected by a bridging kleisin unit, which may have further regulatory proteins attached to the kleisin (Fig. 1-3.2) (B. G. Lee et al., 2020; Palecek & Gruber, 2015). The formation of this basic structure creates a closed shape, adopting a line, triangle, or circular shape depending on the complex and purpose (Anderson et al., 2002). Cohesin is the SMC complex associated with mitotic sister chromatid cohesion (Henrikus & Costa, 2021; Peters & Nishiyama, 2012; Sonoda et al., 2001). Human cohesin is comprised of SMC1, SMC3 as the two SMC arms, Rad-21 as the mitotic kleisin, and either SA-1 or SA-2 as regulatory units (Losada et al., 2000). Condensin is the SMC complex associated with mitotic chromosome compaction, which also assists in individualization, organization, and topoisomerase recruitment for disentanglement (Bohn & Heermann, 2011; Brahmachari & Marko, 2019; Davidson & Peters, 2021; Houlard et al., 2015; M. Sun et al., 2018b; Takagi et al., 2018). In humans condensin has two isoforms, condensin I and condensin II (Gerlich et al., 2006; Green et al.,

2012; Matityahu & Onn, 2021; Ono et al., 2003). Both forms utilize SMC2 and SMC4 for their SMC arms. Condensin I utilizes CAP-H as its kleisin with the attached CAP-G and CAP-D2 accessory proteins, while condensin II utilizes CAP-H2, CAP-G2, and CAP-D3 for their respective purposes.

Condensin is thought to compact mitotic chromosomes through a process called loop extrusion. Loop extrusion describes how the ring-like structures of SMC complexes can actively push chromatin through their openings and how this activity shapes mitotic chromosomes (Murayama, 2018). The chromatin extruded through the rings of the SMC complexes could then be described as a loop of chromatin, which would be tethered to the SMC complex. Recent studies have supported the loop-extrusion hypothesis by biochemical, Hi-C, and modeling experiments (Eagen, 2018; Ganji et al., 2018; Golfier et al., 2020; Kim et al., 2019). Mitotic chromosomes are thought to form bottlebrush structures through loop extrusion clustering at the center of mitotic chromosomes through this activity (Davidson & Peters, 2021; Marko, 2008; Marko & Siggia, 1997). When clustered together at the middle of the chromosome, the loops are organized around the protein core, made up of stable SMC complexes. This organization around the core complexes also assists in the compaction of mitotic chromosomes and their individualization from other chromosomes. During interphase, cohesin and condensin II are also associated with chromatin to control its organization and are speculated to play a role in transcriptional regulation (Alpsoy et al., 2021; Beseda et al., 2020; Hocquet et al., 2018).

Condensin I depletion results in short, fat mitotic chromosomes, whereas condensin II depletion causes long, thin, kinked chromosomes (Elbatsh et al., 2019; Green et al., 2012; Ono et al., 2003; Walther et al., 2018). Condensin I and condensin II have different localizations over the cell cycle. Condensin II is nuclear during interphase and is the first isoform to interact with

and compact chromosomes, possibly as early as S-phase (Hocquet et al., 2018; Ono et al., 2013). Condensin I is cytoplasmic during interphase and only interacts with chromosomes after nuclear envelope breakdown in prometaphase. Subsequently, condensin II is found more centrally and stably on mitotic chromosomes than condensin I, which is more distal and dynamic on mitotic chromosomes (Walther et al., 2018). Condensin I outnumbers the molecules of condensin II by a factor of 4-6, which varies with the mitotic substage, allowing its relatively rapid dynamics to still greatly compact chromosomes (Gerlich et al., 2006). In normal mitotic chromosomes, it is hypothesized that condensin II forms initial large, stable loops of chromatin, while condensin I forms more, but smaller and more dynamic loops of chromatin off the condensin II loops (Davidson & Peters, 2021; Gerlich et al., 2006; Green et al., 2012; Walther et al., 2018).

Condensin depletion results in severe morphological changes to the entire mitotic chromosome. In multiple studies, degradation of condensin by removal of SMC2 caused the entire genome to become entangled and lack nearly all structure and individualization (M. Sun et al., 2018b; Takagi et al., 2018). One study utilized the morphology of the entire genome in mitotic cells when SMC2 was targeted for degradation via auxin treatment (Takagi et al., 2018) (See Fig. 2.1A for an example of auxin-induced degradation (AID) schematic). In these treatments, SMC2 depletion caused massive entanglements, but different from genomes lacking Ki-67 (discussed later). This phenotype became more deformed when both SMC2 and Ki-67 were degraded. The other study held mitotic chromosomes' genomes outside the cell in buffer for 2 hr. (Sun, 2014; M. Sun et al., 2018b). After condensin depletion using siRNA, the bundles became dramatically entangled and would continue expanding after two hours in buffer. These experiments also demonstrated that chromosomes lacking SMC2 were less stiff than those only

lacking condensin II via CAP-G2 siRNA, which were in turn less stiff than chromosomes only lacking condensin I via CAP-G siRNA.

Cohesin is also thought to extrude loops of chromatin, but its loop-extruding activity is relegated to interphase, where it is associated with establishing chromatin loops and facilitate interactions with promoters, but not compartments (Cremer et al., 2020; Hao et al., 2021). During mitosis, cohesin uses its SMC complex ring to bind sister chromatids together and establish sister chromatid cohesion (Diaz-Martinez & Clarke, 2009; Meadows & Millar, 2015; N. Zhang et al., 2008). The switch between cohesin's interphase, loop-extruding function and its mitotic, cohesive function is controlled changing its phosphorylation state over the cell cycle (Tedeschi et al., 2013). Although cohesin's loop extrusion is typically more associated with forming transcriptionally distinct chromatin domains, it can also compact interphase chromatin in a manner reminiscent of condensin if it is stabilized on interphase chromosomes.

While a substantial amount of morphological and mechanical studies of mitotic chromosomes studies the effects and roles of SMC complexes, there is evidence that the underlying chromatin can greatly affect their structure. Recent work on histones, histone PTMs, and HP1 $\alpha$  can all affect mitotic chromosome stiffness and structure when isolated from live cell culture cells (R. Biggs, Liu, Stephens, & Marko, 2019; Strom et al., 2021). Other work using this technique has also demonstrated that treatment with human topoisomerase II (TopoII) causes isolated newt mitotic chromosomes to become less stiff, and human chromosomes to stiffen demonstrating the stiffening effect of chromatin entanglements on mitotic chromosomes and TopoII's crosslinking capabilities (Kawamura et al., 2010; Sun, 2014). The removal of histone acetylation, which precedes mitosis, may affect chromosomal density to an even greater extent than condensin, where condensin's purpose is hypothesized to be used for chromatin

organization rather than compaction, although this is currently preliminary data (Schneider et al., 2021).

Chromatin entanglements are minimized in mitosis but can affect mitotic shape and function. Predominant methods of entanglement minimization during mitosis include their removal, the organization of chromosomes into rod-like structures, and the inhibition of chromosomal mixing. Chromatin entanglements are predominantly removed by TopoII, which is recruited in part to remaining entanglements through condensin's activity. Condensin's mechanism in organizing and compacting chromatin may assist with this reduction in entanglements, may affect chromatin structure to recruit TopoII, or may directly recruit TopoII (Baxter et al., 2011; Cuvier & Hirano, 2003; Dyson, Segura, Martinez-Garcia, Valdes, & Roca, 2021; Kimura & Hirano, 1997). The inhibition of mitotic chromosomal mixing is facilitated through the recruitment of Ki-67 to perichromosomal region of mitotic chromosomes (Endl & Gerdes, 2000; Gerdes, 1990). Once there, Ki-67 is thought to act as a surfactant barrier inhibiting the chromatin from escaping the barrier (Cuylen et al., 2016). This inhibition prevents the chromatin from other chromosomes from interacting, limiting interchromosomal entanglements. Ki-67 is mostly known as a cell proliferation marker, increasing greatly during mitosis, but its purpose on mitotic chromosomes is much less well understood (Gerdes et al., 1983).

We used isolated mitotic chromosomes with AID tags to investigate the structural, mechanical, and morphological purposes of SMC complexes and Ki-67. In this study, we used cell lines containing an AID tag on SMC2, CAP-H, CAP-H2, Rad-21, and Ki-67 for degradation of the tagged protein. We recapitulate the purported levels of condensin I and condensin II and stability of SMC2 on mitotic chromosomes by moving the chromosomes outside the cell (Takagi et al., 2018). We also show that in contrast to the previous studies on slow, siRNA-based

depletion of condensin proteins, the faster, AID-based degradation of these proteins did not affect the stiffness of mitotic chromosomes (M. Sun et al., 2018b). Additionally, we found that Rad-21 depletion did not affect the stiffness of mitotic chromosomes, while removing Ki-67 caused the mitotic chromosomes to become much stiffer. These data reinforce the concept that chromatin structure and DNA-based entanglements of mitotic chromosomes greatly affect their mechanical strength. These studies also show that there may be more chromosome isolation assays to help us understand mitotic chromosome structure. Since chromosome stiffness did not change from condensin degradation it demonstrates there is a difference between mechanical changes and morphological changes, which is not fully understood. This further demonstrates condensin placement on mitotic chromosomes is not the sole governor of mitotic chromosome stiffness and morphology.

## **2.2 Materials and Methods**

### **2.2.1 Cell culture and drug treatments**

Human cell culture cells, all of which were modified HCT116 or the baseline HCT116 line (see 2.2.5 for a detailed description of each cell line), were maintained in DMEM (Corning) with 10% fetal bovine serum (FBS) (HyClone) and 1% 100x penicillin/streptomycin (Corning). The cells were incubated at 37°C and 5% CO<sub>2</sub> for no more than 30 generations and were passaged every 2-4 days. Experiments on captured chromosomes used cells that recovered 1-3 days after plating and before chromosome capture. Cells were freely cycling and not treated with drugs designed to synchronize or otherwise affect the cell cycle. Auxin treatment was performed by aspirating the old untreated media and replacing it with the DMEM complete media with 0.5 mM Indole-3-Acetic Acid (IAA) 4 hours before performing the experiment. A schematic of

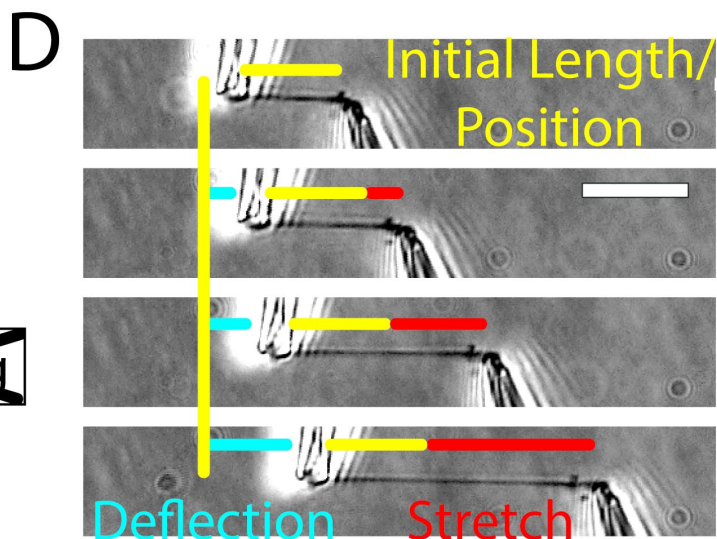
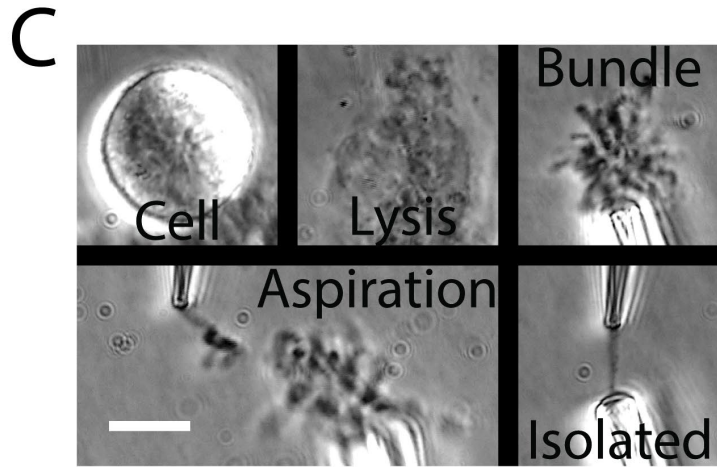
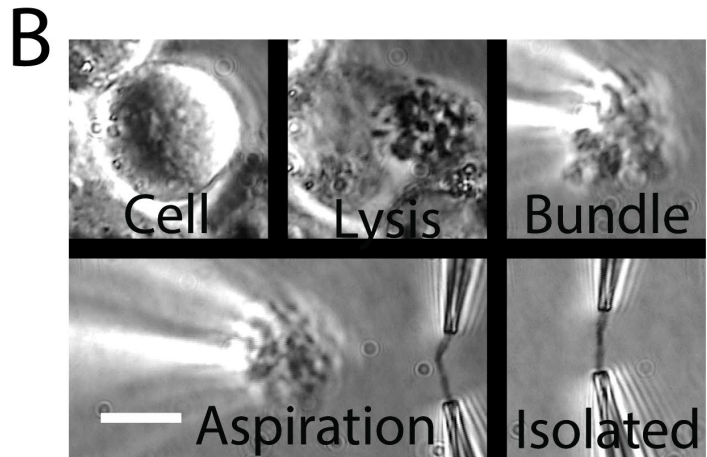
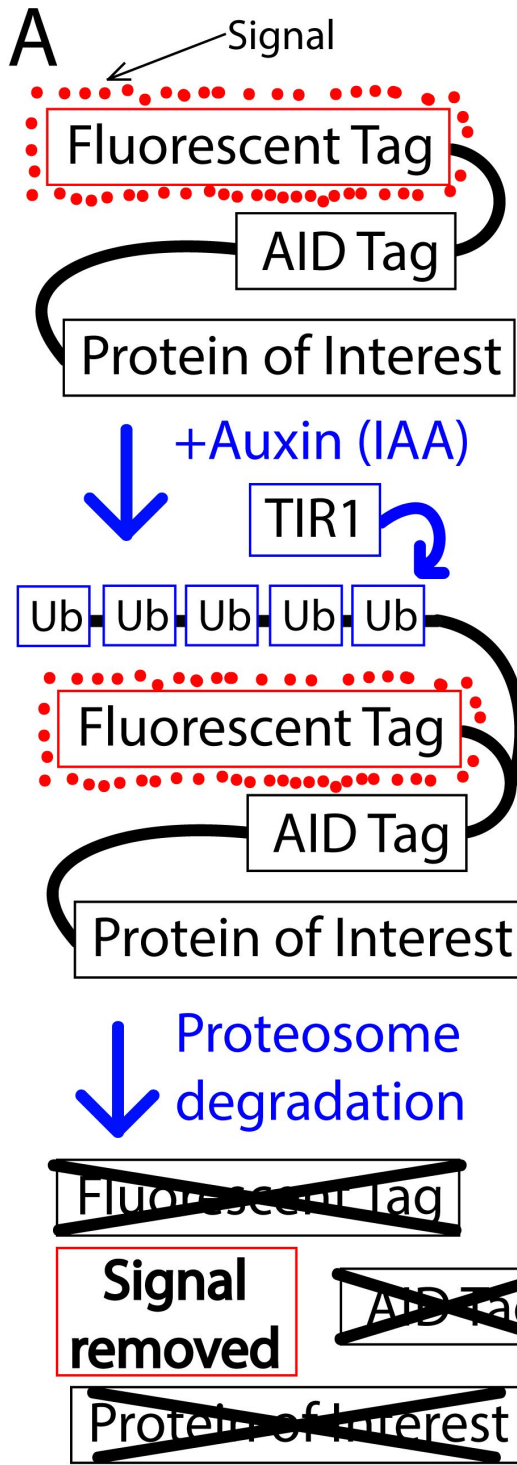


**Figure 2.1. Auxin treatment and single chromosome isolation.**

(A). Auxin treatment schematic. Auxin treatment will cause the TIR1 ubiquitin ligase to polyubiquitinate any protein with the AID tag. The poly-ubiquitinated protein will then be degraded by the proteasome, which will cause a decrease in the fluorescence if the AID-tagged protein also contains a fluorophore. (B). Single chromosome isolation by bundle removal. A mitotic cell is found in the free-cycling cell population. The cell is then sprayed with a 0.05% Triton solution in PBS to destabilize the cell membrane and lyse the cell. Once the cell is lysed, the bundle can be stabilized with a hold pipette. One free chromosome arm is then aspirated into the force pipette and the chromosome dragged away from the bundle, exposing the other arm. The other exposed arm of the chromosome is then aspirated into the stiff pipette, which was swapped with the Triton pipette. Once both ends of the chromosome is secured and aspirated into the pipettes, the bundle is aspirated into the hold pipette and removed from the well, leaving behind an isolated chromosome. Scale bar represents 10  $\mu\text{m}$ . (C). Chromosome isolation by bundle holding. The steps up until chromosome bundle capture are the same as in (B). The bundle is captured into a wide stiff pipette. A free chromosome arm is then aspirated into the force pipette. The rest of the bundle, not attached to the target chromosome is then aspirated into the stiff pipette, leaving only a single chromosome between the force pipette and the stiff pipette. Scale bar represents 10  $\mu\text{m}$ . (D). Example stretch of a chromosome for the force-extension experiment used in determining stiffness of mitotic chromosomes. The lower stiff pipette moves in a controlled and directed manner while the force pipette deflects from its original position. The stretch of the chromosome is measured as the stiff pipette movement minus the deflection of the force pipette. The force on the chromosome is measured as the deflection of the force pipette multiplied by its spring constant. A linear regression of the slope of the stretch vs force is used to calculate the spring constant of the chromosome. When the slope is multiplied by its initial length, we obtain the doubling force. Scale bar represents 10  $\mu\text{m}$ .

AID-based degradation can be found in Fig. 2.1A. Experiments on the SMC2 line were performed by treating the cells for 24 hours with 2  $\mu\text{g/ml}$  doxycycline as a control or an additional 4 hours with 2  $\mu\text{g/ml}$  doxycycline and 0.5 mM IAA for the auxin treatment. The SMC2 line had two populations of knockdowns: a population with significant remaining fluorescence and a population with no fluorescence. For chromosome isolation studies, the cells with no fluorescence were used.

### **2.2.2 Single chromosome capture: setup and microscopy**

Single chromosome capture experiments used an inverted microscope (IX-70; Olympus) with a 60x 1.42 NA oil immersion objective with a 1.5x magnification pullout at room temperature and atmospheric  $\text{CO}_2$  levels. Experiments were performed in less than 3 hours after removal from the incubator to ensure minimum damage to the cells being analyzed. Prometaphase cells were identified by eye and lysed with 0.05% Triton-X 100 in PBS. All other pipettes were filled with PBS. After lysis, the bundle of chromosomes was held with a pipette. One end of a random, loose chromosome was grabbed by the force pipette (WPI TW100F-6), moved from the bundle, and grabbed with the pulling pipette on the other end. The bundle was then removed to isolate the tracked and unbroken chromosome (Fig. 2.1B). In the bundle holding setup, the bundle would be aspirated into a wide-bore stiff pipette, leaving only a single chromosome between the stiff pipette and the force pipette (Fig. 2.1C).

### **2.2.3 Single chromosome capture: force measurement**

An easily bendable force pipette and stiff pulling pipette were used for stretching chromosomes. Once captured, the pipettes were moved perpendicular to the chromosome, stretching the chromosome to roughly its native length. The stiff pipette was then moved 6  $\mu\text{m}$  and returned to the starting position at a constant rate of 0.20  $\mu\text{m/sec}$  in 0.04  $\mu\text{m}$  steps using a

LabVIEW program, while tracking the stiff and force pipette. Fig. 2.1D shows an example stretch-deflection experiment. Deflection of the force pipette multiplied by its calibrated spring constant and divided by the distance between the pipettes (the stretch) was used to obtain the chromosome spring constant. Each chromosome was stretched at least 3 times to provide an accurate and reproducible measurement of the chromosome spring constant. The chromosome spring constant multiplied by its initial length gave the doubling force. The initial length was given by measuring the distance between the center of the pipettes in ImageJ and converting the pixels into microns while the chromosome was perpendicular to the pipettes. Chromosome cross sectional area was estimated as  $0.25\pi d^2$  with chromosome diameter  $d$  calculated as the full width at half maximum of an ImageJ line scan.

#### **2.2.4 Fluorescence of live cells, chromosome bundles, and isolated chromosomes**

Before isolating a chromosome from a cell, we would image the fluorescence intensity of the cell at a specified exposure time and at a specified power with a fluorescent LED light source. Analysis into a population of cells was also performed three independent times untreated, or with auxin treatment to obtain the expected distribution of cellular fluorescence of these cells, which were also treated with Hoechst (this was not done in experiments involving chromosome bundles or isolated chromosomes until after mechanical measurements and endogenous fluorescence were obtained, when performed). Experiments observing or tracking the fluorescence target molecules over time were done on chromosome bundles, isolated and stabilized as described in 3.2.2. Experiments isolating single chromosomes, used the fluorescence of the cell where the chromosome was extracted would be captured and reported.

### **2.2.5 Auxin Induced Degradation (AID) cell lines**

The cell lines used in this study were provided by Dr. Masato Kanemaki, a collaborator at the National Institute of Genetics in Japan, and by Dr. Masatoshi Takagi, Dr. Tatsuya Hirano and Dr. Naoko Imamoto, collaborators at RIKEN in Japan. HCT116 cells containing no ubiquitin ligase or AID tag were already in the lab. The Kanemaki lab provided the cell lines MK479, the constitutively expressed TIR1 gene with no AID target (the no tag line), and MK555, the mClover-mAID-Rad-21 cell line with the constitutive TIR1. The Imamoto and Hirano lab provided AID2, the mClover-mAID-Ki67 cell line with the constitutive TIR1, AID12, the mAID-mCherry-CAPH cell line with the constitutive TIR1, AID13, the mAID-mCherry-CAPH2 cell line with the constitutive TIR1, and AID30, the mAID-mCherry-SMC2 cell line with the doxycycline induced TIR1.

## **2.3 Results**

### **2.3.1 Fluorescence, localization, and removal of critical mitotic proteins**

Before starting the experiments, we needed to verify the proper signal and localization of the target proteins (Fig. 2.2A). Both control cell lines (HCT116 and MK479) showed no fluorescence in either interphase or mitosis and gave a baseline amount of the cellular and chromosomal fluorescence over background. Ki-67 (AID2) showed low fluorescence intensity in interphase cells with no clear localization pattern. Ki-67 was bright and localized to the perichromosomal surface (outside the surface of mitotic chromosomes) in mitotic cells, consistent with its role in mitosis and as a marker for proliferating cells (Gerdes et al., 1983). Rad-21 was bright and nuclear in interphase cells, as expected due to cohesin's importance in maintaining chromatin structure during interphase (Costantino et al., 2020). Rad-21 was bright and generally cellular (not well spatially defined) in mitosis, which is expected due to the

removal of cohesin from the chromosome arms and enrichment at the centromere during prometaphase (Peters & Nishiyama, 2012). CAP-H fluorescence was bright and cytoplasmic (found outside the nucleus) during interphase as expected for condensin I, which is cytoplasmic in interphase (Gerlich et al., 2006; Green et al., 2012; Walther et al., 2018). CAP-H was moderately bright and localized to chromosomes in mitosis as expected of condensin I, which interacts with chromosomes after nuclear envelope breakdown in prometaphase. CAP-H2 showed weak intensity and enriched in the nucleus in interphase as expected of condensin II, which is nuclear in interphase. CAP-H2 showed a weak signal concentrated on mitotic chromosomes in mitosis, as expected of condensin II due to its lower abundance on mitotic chromosomes to condensin I. SMC2 was bright and found in both the cytoplasm and nucleus in interphase as expected. SMC2 was very bright and enriched on mitotic chromosomes, as expected, being one of the condensin core particles (Davidson & Peters, 2021; Hirano, 2016).

The addition of 0.5mM auxin resulted in no change to either of the control cell lines, which demonstrated that auxin addition does not noticeably affect background fluorescence. The addition of 0.5 mM IAA over 4 hours of treatment resulted in a dramatic, statistically significant reduction in fluorescence, and thus target protein amount for Ki-67, Rad-21, CAP-H, and CAP-H2 (Fig. 2.2A, quantified in Fig. 2.2B,C). This demonstrated that the AID-based method of protein degradation was performing as expected. A 24-hour treatment with 2  $\mu\text{g}/\text{mL}$  doxycycline followed by a 4-hour incubation in media with 2  $\mu\text{g}/\text{mL}$  doxycycline and 0.5 mM IAA on the SMC2 line resulted in two populations, one that had very low fluorescence intensity and one that had fluorescence levels like the untreated cells. For chromosome bundle analysis and mechanics of chromosome isolation, we studied and specifically selected the cells with very low fluorescence.

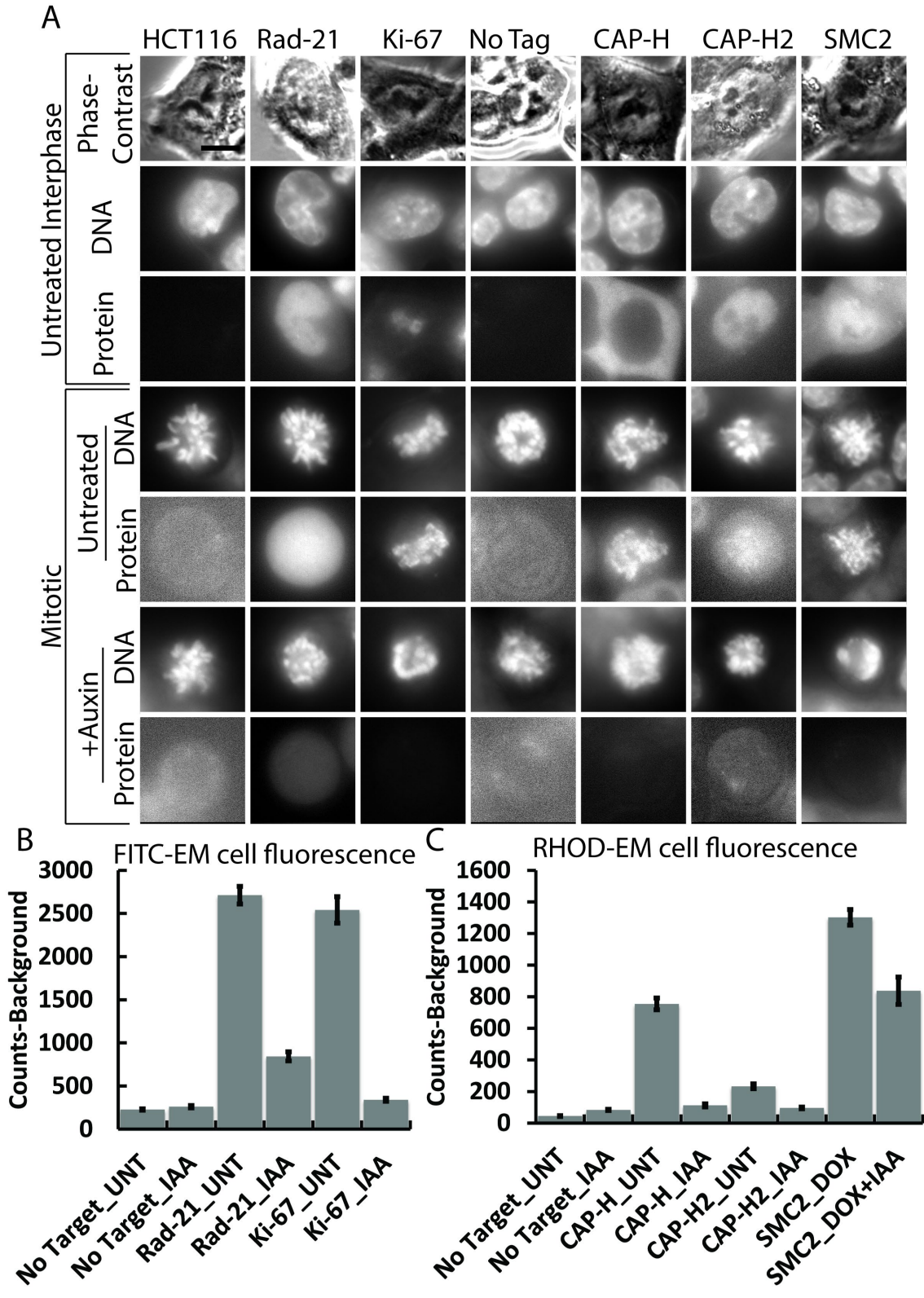


**Figure 2.2. The studied proteins localize to their correct locations and can be depleted with auxin treatment.**

(A). Example images of each of the studied cell lines and proteins in interphase and mitosis. The mitotic cells show their bundle morphology inside the cell with and without auxin treatment. The first three columns show their proteins in FITC-EM channel. The last four columns show their proteins in the RHOD-EM channel. Rad-21 localizes to the nucleus in interphase and is generally cellular localization in mitosis. The knockdown of Rad-21 leaves behind some noticeable signal, but the knockdown is still statistically significantly lower than the untreated Rad-21 line. Ki-67 is weak and localized to the nucleus in interphase, while it localizes to the peri-chromosomal region in mitosis. Its knockdown appears near complete. CAP-H localizes to the cytoplasm in interphase and localizes to the chromosomes in mitosis. The knockdown of CAP-H is near complete. CAP-H2 localizes to the nucleus in interphase and localizes to the chromosomes in mitosis. The knockdown of CAP-H2 is near complete. SMC2 is found throughout the cell and enriched in the nucleus in interphase, while it is strongly associated with the chromosomes in mitosis, somewhat enriched in the center of the cell, which is most likely due to its association with the centromere. SMC2 knockdown causes a moderate knockdown with a population of very low signal causing the signal to move the average down. In the chromosome isolation experiments, only the very low signal cells were selected. Scale bar represents 10  $\mu\text{m}$ . (B). Quantification of the FITC-EM signal in the FITC-EM expressing cell lines. The control cell line has a minimal signal above background with no change when auxin is added to the cells. The signal minus background is statistically significant between untreated and auxin treatments in both the Rad-21 and Ki-67 cell lines with Ki-67 knockdown resulting matching the level of control signal. (Control untreated  $n=75$ :  $225\pm 10$  counts above background; control auxin treated  $n=75$ :  $260\pm 15$  counts above background). (Rad-21 untreated  $n=75$ :  $2710\pm 105$  counts above background; Rad-21 auxin treated  $n=75$ :  $845\pm 55$  counts above background). (Ki-67 untreated  $n=75$ :  $2540\pm 155$  counts above background; Ki-67 auxin treated  $n=75$ :  $340\pm 15$  counts above background). All the DNA fluorescent images brightness and contrast thresholds have been adjusted to display the fluorescence of the bundles in the clearest possible manner. Scale bar represents 10  $\mu\text{m}$ . (C) Quantification of the RHOD-EM signal in the RHOD-EM expressing cell lines (all condensin subunits). The control cell line has a minimal signal over background, which does not change upon the addition of auxin. The signal minus background is statistically significant between untreated and auxin treatments in the CAP-H, CAP-H2, and SMC2 cell lines. CAP-H2 signal is weak, but statistically different from the control cell line. SMC2 depletion causes a moderate weakening but contains a very low fluorescence population. (Control untreated  $n=75$ :  $45\pm 5$  counts above background; control auxin treated  $n=75$ :  $85\pm 5$  counts above background). (CAP-H untreated  $n=75$ :  $755\pm 40$  counts above background; CAP-H auxin treated  $n=75$ :  $95\pm 5$  counts above background). (CAP-H2 untreated  $n=75$ :  $230\pm 15$  counts above background; CAP-H2 auxin treated  $n=75$ :  $85\pm 5$  counts above background). (SMC2 DOX treated  $n=50$ :  $1305\pm 15$  counts above background; SMC2 DOX+auxin treated  $n=50$ :  $835\pm 85$  counts above background).

### 2.3.2 Protein localization and their effects on mitotic chromosome bundles

While not indicative of every genome in the auxin treated cells, we have highlighted some interesting features of auxin-treated chromosome genomes inside the cell compared to their untreated counterparts (Fig. 2.2A). The example Rad-21 depletion genome had slightly more entangled chromosomes, slightly larger genome spread, and less rod-like chromosomes, instead forming a more punctate-like pattern. The example Ki-67 degradation genome had increased entanglements, loss of individualization of the mitotic chromosomes, appeared cloudier, but still maintained a rigid structure compared to degraded SMC2. The CAP-H depletion example genome was mildly entangled and slightly more spread out than the other examples. By contrast, the example CAP-H2 depletion bundle was small and tight in compared to most bundles, but also appeared to contain more entanglements than bundles from untreated cells. The SMC2 depletion example bundle (which had very low signal) showed stringy and entangled genomes that lacked rigidity and chromosome individualization, forming chromatin strings, which recapitulated the original paper (Takagi et al., 2018).

After we recapitulated the mitotic genome cellular shape results from the original paper, we sought to directly interact with the chromosomes to study their morphological properties outside the cell. We first isolated bundles to study and documented their shape outside of the cell (Fig. 2.3A). The bundles outside the cell had more freedom to expand, allowing us to potentially see the genome's structure and behavior in greater detail. While our results are not indicative of every bundle, some features seem to be observable. Rad-21 depleted bundles had more dispersed chromosomes from the center while maintaining their chromosomes' shape and individualization. Ki-67 depleted bundles were more entangled than untreated but had sharper edges and more rigid, better-outlined chromosomes compared to the SMC2 depleted bundles.

CAP-H depleted bundles tended to be slightly more entangled than untreated bundles. CAP-H2 depleted bundles tended to be somewhat entangled and have chromosome that were “bumpier” than usual, as if the chromatin itself was forming small punctae in phase-contrast imaging. Low intensity SMC2 depleted bundles typically adopted a round, ball-shaped bundle with some mitotic chromosomes forming their natural rod-shaped form.

We also visualized the fluorescent proteins on the mitotic bundles outside of the cell (Fig. 2.3A). This visualization allowed us to approximate the stability of the target proteins of interest in buffer outside the dynamic cellular environment. Unfortunately, most of the proteins were not photo-stable, especially outside of the cell, meaning that tracking their fluorescence over multiple exposures was unquantifiable. Once a single chromosome had been isolated, almost every protein studied had lost all its fluorescence, and thus their localization unable to be studied. Rad-21 fluorescence was very weak and occasionally found in the center of the chromosome bundle, possibly enriched on the centromere as that is their usual localization (see Chapter 5). Ki-67 fluorescence was comparatively bright and had a fuzzier outline on the bundle, demonstrating its perichromosomal binding. CAP-H bundles had moderate levels of fluorescence was found along the chromosome axis. CAP-H2 had a comparatively weaker signal to CAP-H was found along the chromosome axis, enriched in the presumed centromere. SMC2 fluorescence was very bright and stable on the chromosome, enriched on the presumed centromere.

### **2.3.3 Mechanical stiffness of isolated mitotic chromosomes**

Mitotic chromosome isolation and manipulation allowed us to study and compare their stiffness. We noticed that some untreated chromosomes from the cell lines had different doubling forces between them (Fig. 2.3B). The two control cell lines were not statistically significantly

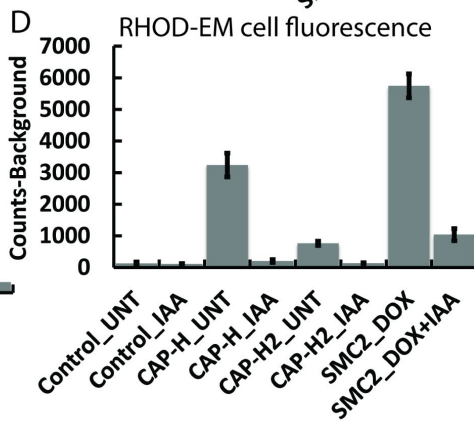
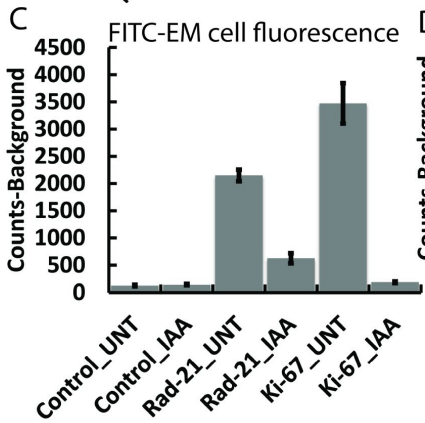
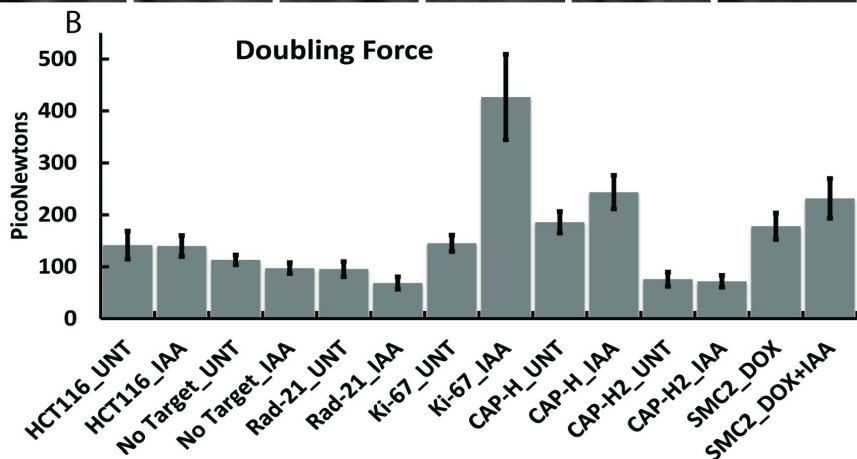
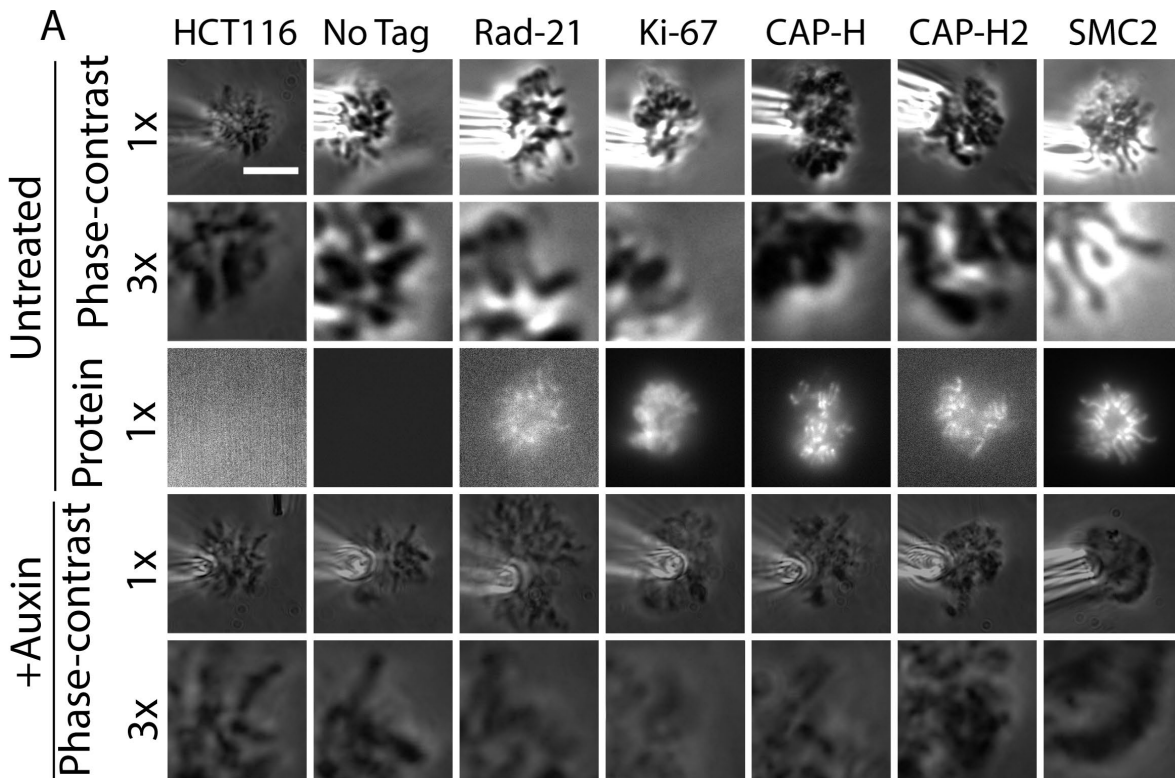


**Figure 2.3. Analysis of SMC2 fluorescence over time and bundles lacking SMC2.**

(A). Example chromosome bundles with their fluorescence and structure lacking key proteins. All the fluorescent images brightness and contrast thresholds have been adjusted to display the fluorescence of the bundles in the clearest possible manner. Scale bar represents 10  $\mu\text{m}$ . The images underneath the 1x bundles display a section of the bundle at 3-fold zoom to display higher detail of the chromosomes. (B). Doubling force for the isolated chromosomes for each cell line either with or without auxin. Untreated HCT116 (N=22) had a doubling force of  $140\pm 25$  pN and auxin treated HCT116 (N=19) had a doubling force of  $140\pm 25$  pN, which are not statistically significantly different. Untreated no-target (N=19) had a doubling force of  $115\pm 10$  pN and auxin treated no-target (N=19) had a doubling force of  $95\pm 10$  pN, which are not statistically significantly different. The untreated Rad-21 (N=15) line had a doubling force of  $95\pm 15$  pN and auxin treated Rad-21 (N=16) line had a doubling force of  $70\pm 10$  pN, which are not statistically significantly different. The untreated Ki-67 (N=25) line had a doubling force of  $145\pm 15$  pN and auxin treated Ki-67 (N=24) line had a doubling force of  $425\pm 80$  pN, which are not statistically significantly different. The untreated CAP-H (N=25) line had a doubling force of  $185\pm 20$  pN and auxin treated CAP-H (N=22) line had a doubling force of  $245\pm 30$  pN, which are not statistically significantly different. The untreated CAP-H2 (N=25) line had a doubling force of  $75\pm 15$  pN and auxin treated CAP-H2 (N=17) line had a doubling force of  $70\pm 10$  pN, which are not statistically significantly different. The doxycycline SMC2 (N=25) line had a doubling force of  $180\pm 25$  pN and doxycycline with auxin treated SMC2 (N=25) line had a doubling force of  $230\pm 40$  pN, which are not statistically significantly different. (C). Fluorescence of the FITC cell lines for the cells used in the chromosome isolation. All fluorescently tagged proteins were statistically significantly different from background and fluorescently tagged proteins in auxin treatment showed a statistically significant decrease with auxin treatment. Untreated control (N=9)  $130\pm 10$  counts above background. Auxin-treated control (N=9)  $140\pm 10$  counts above background. Untreated Rad-21 (N=11)  $2150\pm 105$  counts above background. Auxin-treated Rad-21 (N=11)  $625\pm 90$  counts above background. Ki-67 control (N=15)  $2475\pm 370$  counts above background. Auxin-treated Ki-67 (N=11)  $185\pm 10$  counts above background. (D). Fluorescence of the RHOD cell lines for the cells used in the chromosome isolation. Untreated control (N=9)  $130\pm 40$  counts above background. Auxin-treated control (N=11)  $110\pm 10$  counts above background. Untreated CAP-H (N=9)  $3240\pm 375$  counts above background. Auxin-treated CAP-H (N=10)  $200\pm 45$  counts above background. Untreated CAP-H2 (N=21)  $765\pm 65$  counts above background. Auxin-treated CAP-H2 (N=15)  $135\pm 15$  counts above background. Doxycycline SMC2 (N=10)  $5745\pm 380$  counts above background. Doxycycline-with-auxin-treated control (N=12)  $1040\pm 195$  counts above background.

different from each other without treatment. The untreated Rad-21's and Ki-67's untreated mitotic chromosome stiffnesses were not statistically significantly different from the two control cell lines. The untreated CAP-H's untreated mitotic chromosome stiffnesses were not statistically significantly different from the HCT116 but showed a statistically significant increase of 65% compared to the no tag cell lines. The untreated CAP-H2's untreated mitotic chromosome stiffness was statistically significantly weaker from the HCT116 (45% weaker) and the no tag (35% weaker) cell lines. The untreated SMC2's untreated mitotic chromosome stiffness was not statistically significantly different from the HCT116 but showed a statistically significant increase of 55% in stiffness compared to the untreated no tag cell lines.

While some cell lines changed their stiffness in comparison to the base cell lines, no depletion of any protein studied caused a decrease in stiffness in the mitotic chromosome (Fig. 2.3B). Auxin treatment of the HCT116 base cell line or the no tag cell line caused a statistically significant change in the mitotic chromosome stiffness. This demonstrates that auxin itself, even with an active TIR1 molecule does not affect stiffness. Only auxin treatment of the Ki67 line caused a statistically significant change from its untreated stiffness. Ki-67 depletion caused a near two-fold increase in mitotic chromosome stiffness. Despite previous experiments in condensin depletion via siRNA (M. Sun et al., 2018b), none demonstrated a stiffness change in a 4-hour treatment with IAA. This lack of change is additionally odd since SMC2, and to a potential lesser extent CAP-H and CAP-H2 depletion, caused mitotic bundle and genome shape defects. Rad-21 depletion had a minor, but statistically insignificant effect on mitotic stiffness.

#### **2.3.4 Studying the dynamics and effects specific to SMC2**

We found that SMC2 was very bright, stable, and resistant to photobleaching. This allowed us to track it over time, through multiple exposures. We tracked the fluorescence

intensity of the captured mitotic bundle by tracing the bundle in phase-contrast then measured the fluorescence of SMC2 in the fluorescent channel (reported values are counts above background) (Fig. 2.4A). We performed this either in rapid succession (15 seconds between exposures) of images (bleach) or every 15 minutes (hold) to determine the cell free dynamics of SMC2. We compared the intensity of the hold vs. the bleach exposure and saw a stable 65% population of SMC2 on mitotic chromosomes. Most of the mobile fluorescence was lost during the first hour. We also captured a bundle and exposed it to fluorescent light at time of capture and 2 hours later. This showed a near identical level of fluorescence loss as expected from a stable 65% population of SMC2. This information is quantified in Fig. 2.4B.

We could also study bundle behavior over time lacking SMC2 held in buffer. In previous experiments, SMC2 knockdown via AID and siRNA caused the chromosome bundle to become very entangled and lack chromosomal individualization inside the cell and held outside the cell, respectively (M. Sun et al., 2018b). The siRNA bundle-holding experiment also caused the chromosome bundle to swell in size while held in buffer. Our SMC2 depletion via AID-based degradation caused a similar rounded shape to the mitotic chromosome bundle in the cell and in buffer but did not swell when it was left in buffer for two hours (Fig. 2.4A).

We also studied SMC2's localization along mitotic chromosomes (Fig. 2.4C). When isolated from a chromosome bundle and cell, the fluorescence of SMC2 appeared both in a varied and semi-punctate pattern but could also be seen as a continuous line of fluorescence. When the chromosome was stretched, the SMC2 fluorescence pattern revealed punctate dots of SMC2 fluorescence at similar intensity as the unstretched chromosome, but with dark spots appearing in between the clusters of SMC2 fluorescent signals. This further suggested that SMC2 is not continuous on the chromosomal axis and there is no contiguous protein core.

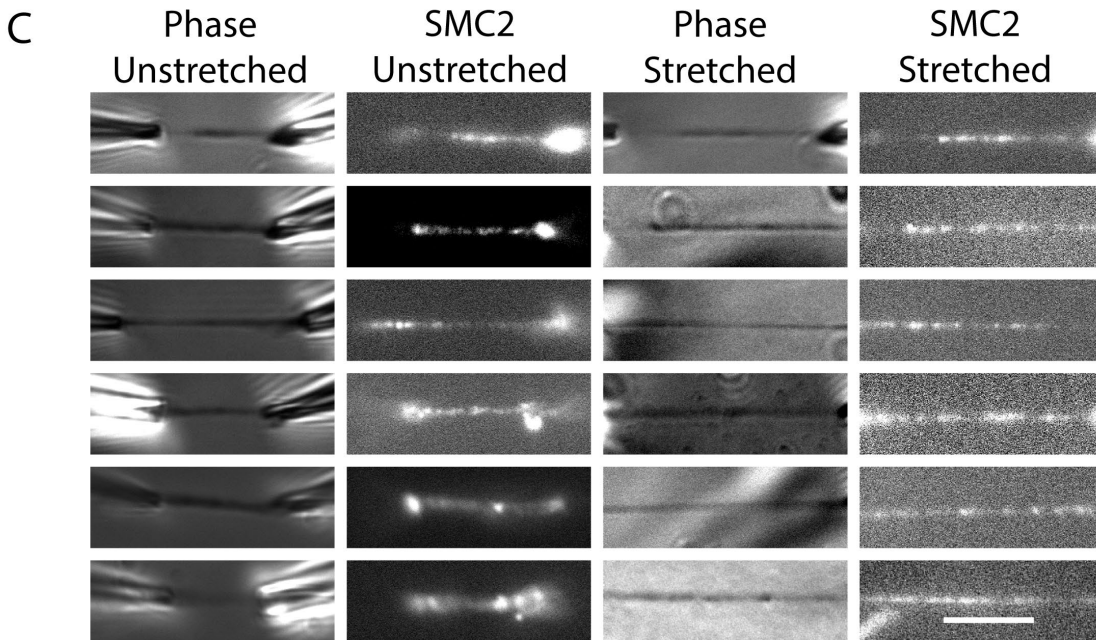
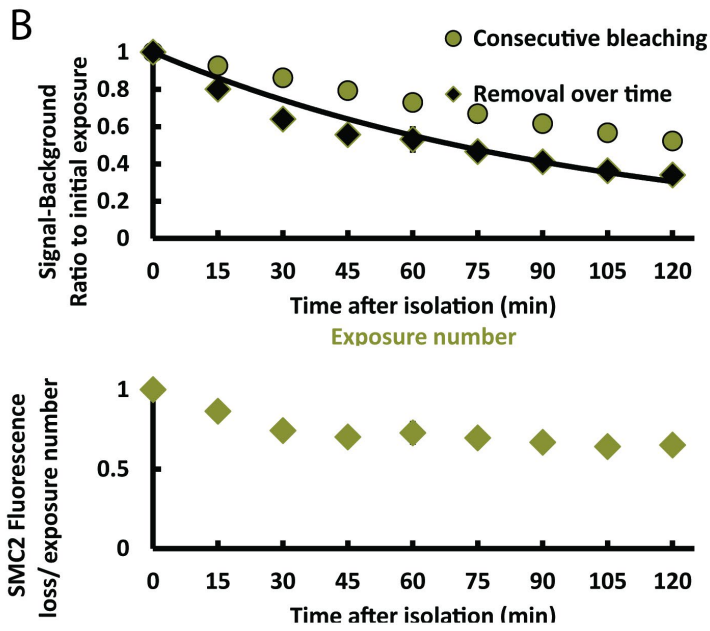
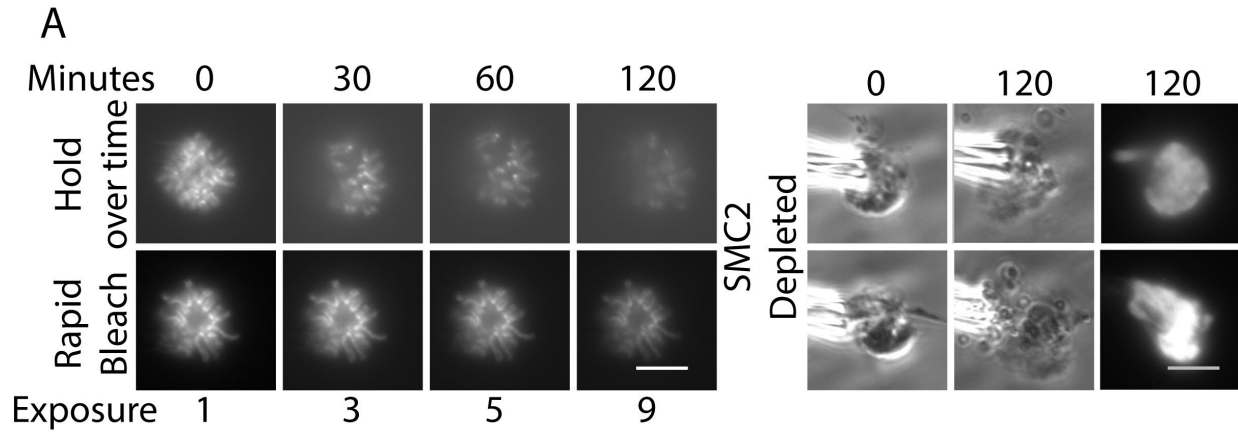


**Figure 2.4. Study of isolated mitotic bundles and chromosome mechanics.**

(A). Examples of the fluorescence of SMC2 of intensity over time held in media or over multiple fluorescent exposures. Scale bar represents 10  $\mu\text{m}$ . Example of the chromosome bundle lacking SMC2 at the beginning, and after being held in media for 2 hours in phase-contrast imaging and DNA staining. (B). The quantification of SMC2 fluorescence of the chromosome bundle after every exposure or after time held in media. The quantification of the held bundle fluorescence was then divided by the rapid exposure intensity with the same exposure number. (C). Example images of a single chromosome in brightfield and in the fluorescent channel tracking SMC2 both at roughly its innate length and stretched to different amounts. Scale bar represents 10  $\mu\text{m}$ .

## 2.4 Conclusions, discussion, and future directions

### 2.4.1 Results overview and recap

In this study, we sought to address how condensin I, condensin II, cohesin, and Ki-67 affect the mechanical stiffness of mitotic chromosomes using rapid, auxin-based degradation. In our hands, the molecules successfully localized to their expected locations and degraded with auxin treatment measured by fluorescence. We also detected these molecules on mitotic chromosome bundles, although most were acutely sensitive to photobleaching. SMC2 fluorescence was stable enough to measure its fluorescence over time. The stability of SMC2 on mitotic chromosomes held over a two-hour period, showed a 65% stable SMC2 population on mitotic chromosomes, even outside the cell. On isolated chromosomes, condensin could also be seen in punctate patterns, which showed greater spacing of the punctae while stretching the chromosome. These experiments showed a change in chromosome stiffness between cell lines, but only degradation of Ki-67 caused a difference in stiffness; rapid condensin or cohesin degradation did not affect mitotic chromosome stiffness.

Further experiments on mitotic chromosome bundle morphology can be performed in the future, which may be useful in understanding how these proteins shape mitotic chromosomes. The shape of the chromosome bundle became much more circular in SMC2 depleted cells, which demonstrated the importance of SMC2 to chromosome morphology. More systematic experiments that focus on imaging mitotic bundle morphology, could provide images that allow us to infer the role of the depleted protein to chromosomal structure. Some notable attributes include chromosomal individualization, bundle, compaction, chromosomal compaction, and interchromosomal connections. Tracking isolated *ex vivo* bundle morphology over time could also be developed into an additional assay for chromosome structure analysis. We may also be

able to track the stability of the target molecules by taking a single fluorescent image at set time points after initial bundle removal and cell lysis. This analysis could allow us to determine the stability of proteins outside of the cell. Differences found within this technique and other forms of protein dynamics, such as FRAP, would suggest different removal mechanisms in the cell as opposed to it passively diffusing off the mitotic chromosome (Gerlich et al., 2006).

#### **2.4.2 The change in mitotic stiffness between lines, but not missing proteins**

One of the strangest findings of this study is that rapid removal of condensin I, II, or both isoforms through CAP-H, CAP-H2, and SMC2 degradation, respectively, caused no change in chromosomal stiffness. This is puzzling because of how drastically the chromosome morphology changes in SMC2 depletion (Fig. 2.2, 2.3) (Takagi et al., 2018). These findings also contradict the original findings of condensin depletion using siRNA to remove condensin from the cell (M. Sun et al., 2018b). The differences between siRNA and AID-based degradations, suggest a difference in chromosome structure, despite depletion of the same protein. Identifying the differences between siRNA- and AID-based degradation may assist us in finding these structural changes.

Previous experiments have shown that SMC complexes that can affect chromosome stiffness. It has been shown that the underlying chromatin structure can affect mitotic chromosome stiffness, via histone PTMs, PTM readers, chromatin entanglements, and non-SMC complex crosslinks (R. Biggs et al., 2019; Kawamura et al., 2010; Strom et al., 2021; Sun, 2014). Investigations into chromosomal density through hyperacetylation of histones via HDAC inhibition suggested that chromatin structure, not SMC complexes, dominates chromosomal density (Schneider et al., 2021). Proteins other than condensin are also important for mitotic chromosome formation (Shintomi et al., 2015). Our AID-based depletion of condensin may

therefore be explained by a balancing of condensin removal with increased entanglements. The folding of chromatin performed by SMC complexes may remain in a stable state once its function has been performed meaning rapid depletion of condensin folds and stiffens mitotic chromosomes before rapid depletion. Another possibility is that the gel meshwork of mitotic chromosomes, when lacking their core structural proteins no longer form gels. The underlying fibers are immediately strained, appearing as a stiffer chromosome.

We may explain the different results between siRNA and AID-based degradation by comparing the rate of protein removal from the cell. In siRNA-based degradation, the depletion of the protein is based on the rate of protein turnover since it prevents additional protein translation from RNA (Caplen & Mousses, 2003). AID-based degradation of proteins by contrast utilizes the proteasome and results in rapid degradation of the target protein (Prozillo et al., 2020). Since condensin is a long-lived molecule, siRNA takes longer to deplete than the AID-based system. The lowered amount of condensin molecules occurs every cell cycle for siRNA-based depletion since it is allocated to each daughter cell. Chromatin may be reorganized and stiffened before rapid removal in the AID-based degradation experiments. siRNA-based depletion by contrast may have further effects by lacking condensin through the cell cycle, not just in mitosis. siRNA degradation could also leave enough condensin to recruit TopoII to disentangle the chromosome, where the near-complete removal of AID-based degradation immediately makes it so that TopoII is unable to localize to the chromosome for its disentangling effects.

A normal chromosome has a gel-like structure, crosslinked by condensin, which may assist with its ability to stretch very far before deforming. If a chromosome or other gel-like structure were depleted of its crosslinks, then it would immediately stretch the underlying fibers

rather than requiring the gel to tense the intervening fibers. Lacking the crosslinks could therefore lead to stretching the underlying, tensed fibers immediately, which would be more difficult to stretch than a normal, gel-like structure. The siRNA-based depletion was not performed at 100% depletion, therefore could have some remaining untensed fibers, which could be stretched once it was isolated instead of the near-complete depletion of SMC complexes of the AID-based technique. The inhomogeneous stretching of the chromosomes from siRNA-based, condensin-depleted cells also suggest this may be occurring (M. Sun et al., 2018b). This may also explain why the degradation of SMC2 via auxin-induced degradation did not cause the chromosome bundle to swell like in the siRNA-based degradation. The mitotic chromosomes still have some structure from the binding of Ki-67 (Takagi et al., 2018), which may help give the chromosome some structure, but this would exist in both siRNA- and AID-based degradation. Longer AID knockdowns could be studied and are discussed in depth in the future directions section.

### **2.4.3 Condensin studies based on fluorescence and dynamics**

Previous studies found that the ratio of condensin I to condensin II on mitotic chromosomes is about 1:4-6 (Walther et al., 2018). In our experiments we saw that the intensity over background of condensin I was about six times higher than condensin II, via CAP-H and H2 measurements (Fig. 2.2C, 2.3D). The study of condensin on mitotic chromosomes suggested that the limiting molecules of condensin on mitotic chromosomes are CAP-H and CAP-H2 (Walther et al., 2018). Thus, our results of the SMC2 fluorescence being higher than the sum of the CAP-H and CAP-H2 molecules is in accordance with these results. While one should not use these measurements of the ratio on mitotic chromosomes beforehand, since there could be differences in fluorophore behavior, it is interesting that our results recapitulate previous findings. An

interesting feature of these experiments is in the way it recapitulates some of the other experiments performed on condensin complexes. For instance, the relative intensity of CAP-H, CAP-H2, and SMC2 follow the same intensity on the isolated bundle as it does when the super resolution imaging when looking at the binding on the chromosome. This gives further credence that the isolation of mitotic chromosome bundles gives an accurate snapshot of proteins on the chromosome at time of isolation. This could be further developed as a method to study protein stability on mitotic chromosomes. Differences between FRAP studies could suggest the presence of an active removal process and exchange of the proteins in the live cell compared to passive diffusion in the chromosome bundle. Indeed, other studies have shown that the target protein itself can behave in facilitated dissociation when at high enough concentrations (Kamar et al., 2017). By holding the bundle outside the cell in buffer, we can see which proteins are inherently stable or labile on the chromosome. We have already seen this by tracking SMC2 on the mitotic chromosome, which showed about a 65% stable population on the mitotic chromosome with most of the unstable population unbinding within the first hour. Further experiments may answer if the dynamic nature of condensin I is due to intercellular exchange or innate weak binding of condensin I. We will also use this assay to study the innate stability of other proteins important in mitotic chromosome formation.

Since we can see location of important proteins on isolated mitotic chromosomes before and after stretching, we can infer their connectivity along mitotic chromosomes. This is most obvious with the location of SMC2, which organized into punctate patterns and remained as concentrated dots when the chromosome was stretched. This suggests that condensin molecules can form interconnected clusters, which are stable as seen in condensin multimer formation (Keenholtz et al., 2017). It also suggests that condensin does not remain as a stable, contiguous

core throughout the chromosome (Sun et al., 2011). Other proteins should be able to be studied by the colocalization of said proteins, provided photostability and intensity. One such proposed experiment is to find the localization of SMC2 with specific sequences on different chromosomes. If condensin and the labeled DNA sites tend to colocalize on mitotic chromosomes, it would suggest a sequence-specific loading site for condensin, which is still debated. Further studies on TopoII localization in conjunction with condensin I, II, or both isoforms and where it localizes in the absence of such proteins could also further our understanding of how condensin interacts and recruits TopoII.

With the ability to track fluorescent proteins, especially those like SMC2, we may also be able to track the formation of mitotic chromosomes through its different substages. From these different stages of mitosis, we may also be able to discern if there is a systematic change in the stiffness of mitotic chromosomes as it progresses. From that potential systematic change, we may further our understanding of how mitotic chromosomes are folded into mechanical structures. The tracking of fluorescence of condensin on mitotic chromosomes should also allow us to study the effects different proteins have on condensin binding and if those changes to condensin alone are able to change the stiffness.

#### **2.4.4 Analyzing the degradations of non-condensin molecules**

Although not fully understood, it is hypothesized that Ki-67 localizes to the outer boundary of mitotic chromosomes to act as a surfactant, inhibiting the amount mitotic chromosomes interact with each other (Cuylen et al., 2016). This is done to help organize, individualize, and disentangle the mitotic chromosomes for their separation (Takagi et al., 2018). Our experiments recapitulate the increase in entanglements of mitotic chromosomes inside mitotic cells when Ki-67 is degraded (Fig. 2.2A). Our experiments also showed that these

entanglements were stable even outside the cell (Fig. 2.3A). These results are both as expected, since we can presume that Ki-67 degradation caused an increase in entanglements. Depletion of Ki-67 also caused an increase in stiffness, which may be expected due to the relationship between chromatin entanglements and mitotic chromosome stiffness. Innate entanglements of chromosomes could be important for the formation of normally structured and stiff mitotic chromosomes, since TopoII treatment weakens mitotic chromosomes (Kawamura et al., 2010). The combination of TopoII treatment with the knockdown of Ki-67 may also be worthwhile in determining if there is an increase in TopoII-sensitive entanglements from Ki-67 knockdown, which could help in our understanding of how Ki-67 functions. Ki-67's function may also be more related to non-topological chromatin entanglements and instead merely stick to the surrounding chromosomes. If this sticking occurs like an increase in histones sticking to each other, as found in the increase of heterochromatin, then we may find that chromatin state is vital for properly folded and stiff mitotic chromosomes (R. Biggs et al., 2019; Strom et al., 2021).

The localization of cohesin is as expected in both interphase and mitosis, since it is responsible for interphase chromatin structure and its role in sister chromatid cohesion, enriched at the centromere (Lawrimore & Bloom, 2019). Another feature seen in these experiments is the spreading of mitotic chromosomes from each other in the mitotic bundle (Fig. 2.3A). This is somewhat expected, as sister chromatid cohesion is facilitated by cohesin. Additional experiments on the bundles may allow us to more precisely time the expanding phenotype and better characterize a quantifiable parameter of the Rad-21 depleted bundle outside of the cell.

Since cohesin is canonically most important for sister chromatid cohesion in mitosis, it is not entirely surprising that there is little to no change in the axial stiffness of whole mitotic chromosomes. While the predominant role of mitotic cohesin is thought to be sister chromatid

cohesion, there is also evidence that cohesin can influence the structure and mechanics of sections of mitotic chromosomes. This is mainly shown as an increase in the spread and value of the spindle body in yeast mitotic cells (Lawrimore, Doshi, Friedman, Yeh, & Bloom, 2018; Stephens et al., 2011; Stephens et al., 2013). Thus, the main point where cohesin depletion could affect the stiffness of mitotic chromosomes comes from their enrichment and stability at the centromere. However, since the centromere is one of the stiffest parts of the chromosome it may not greatly affect overall chromatin stiffness (Sun, 2014). If we imagine the mitotic chromosome as an object formed from springs connected in series, then reducing the stiffness in a small, but stiff area of the mitotic chromosome, like the centromere, then we may not see a large difference in stiffness on the entire object.

#### **2.4.5 Future directions of study**

The chromosome stiffness effects from Ki-67 and condensin degradation further suggest that chromatin entanglements play an important role in chromosome stiffness. Because chromatin entanglements are important in the mechanics, it is possible that chromosome compaction utilizes intra-chromatin entanglements and thus should be a focus of further study. One method of determining the level of crosslinks would be to treat the isolated chromosome with active TopoII. By documenting the change in stiffness of TopoII treatment, one could use this assay to estimate the amount of entanglement in the chromosome as well as determine how much those entanglements affect stiffness. Nuclease and protease treatments could also be used after protein degradation as an assay to identify chromosome entanglements. Any differences between degradations would further our understanding of how the underlying structures of mitotic chromosomes change with the depletion of the protein of interest.

The difference between the expected and actual stiffness results from condensin-depleted chromosome also demonstrates that we do not fully understand the full connection between chromosome mechanics, structure, and morphology. While the underlying structure of an object will determine its mechanics and morphology, there is no strict and specific relationship between them when the objects are complicated. The observation that the SMC2-depleted chromosome bundles lacked nearly all structure but were still as stiff as the untreated chromosomes challenges our assumptions that morphological changes to chromosomes, especially by changing their density (R. Biggs et al., 2019; Schneider et al., 2021), necessarily alters their stiffness. Thus, further investigations into methods of altering chromosome morphology, but still has the stiffness of a native chromosome could assist in our understanding of the structure-mechanics relationship, which our experiments have demonstrated to be not perfectly correlated.

A topic of future research could involve attempting to alter the timing and potential methods of knockdown. This could be accomplished by longer and multiple cell cycle lengths of removal. This may allow us to determine the point when the molecules were able to affect the mitotic chromosome mechanics through structure. If longer knockdowns show a change in chromosome mechanics, then it could suggest a mechanical use for condensins' actions before mitotic onset. However, it is possible that the cells remain stalled in mitosis because of chromosomal protein depletion, which would limit our ability to study chromosomes in mitosis lacking condensin. Additional experiments could also entail synchronizing cells and then adding auxin at specific points, such as in S-phase, G2 phase, or during substages of mitosis. This timing control may also be able to differentiate the different hypotheses of why there is such a dramatic difference between AID- and siRNA-based degradation. This is important because the timing of

these molecules and their actions during the different phases of the cell cycle could further our understanding as how these molecules are important outside of the late stages of mitosis.

These experiments also demonstrate that single chromosome isolation works with AID-based degradation. This means that many more targets can be analyzed in how they impact mitotic chromosome stiffness, bundle morphology, or other functions in other additional assays. Additionally, the use of labeled fluorescent proteins and their behavior outside the cell can also be informative to their localization on the mitotic chromosome. Their dynamics can also be studied outside the cell as a means in differentiating active and passive disassociation of the molecule on the mitotic chromosome.

**Chapter 3. Heterochromatin components HP1 $\alpha$  and histone hypermethylation stiffen mitotic chromosomes and change their structure; hyperacetylation on mitotic chromosomes does not result in chromosomal mechanical changes**

*This chapter was adapted from the manuscripts in Molecular Biology of the Cell and the mitotic section of the eLife paper (R. Biggs et al., 2019; Strom et al., 2021) for the histone PTMs and HP1 $\alpha$  experiments, respectively. All experiments and diagrams except Fig. 3.3C, 3.5C, 3.8F,G, and 3.9C,D were performed and created by myself, credit given in Figure legends.*

While the focus of most projects on mitotic chromosomes have been on major chromatin-organizing complexes and proteins responsible for large-scale, noticeable changes, the underlying chromatin is still a factor in folding mitotic chromosomes. In this chapter, we investigate how the underlying chromatin affects the form and stiffness of mitotic chromosomes. This is performed by analyzing chromosome stiffness following alterations to histone PTMs and histone PTM-interacting molecules. Although histone PTMs change between interphase and mitosis, this change and its effects on mitotic chromosomes remain poorly understood. By increasing histone marks associated with heterochromatin on mitotic chromosomes, we stiffen mitotic chromosomes. HP1 $\alpha$ , a mark that associates with heterochromatin, can bind to site-specific methyl marks on histones and DNA, which in turn can crosslink chromatin. In accordance with its crosslinking properties, we can also weaken mitotic chromosome stiffness by degrading HP1 $\alpha$ , although it is thought to be naturally removed from mitotic chromosomes. Although mitotic changes to histone PTMs involve a lowering of acetylation, their increase did not affect the stiffness of mitotic chromosomes. These results demonstrate that the underlying chromatin network can affect and stiffen the macroscopic object and it is not only affected by chromatin-interacting molecules.

### 3.1 Overview

Chromatin structure is important for many different cellular functions. A dramatic change in chromatin structure and organization occurs during the transition from interphase to mitosis as the open, diffuse, and transcriptionally accessible interphase chromatin becomes compact, rod-like, and transcriptionally repressed in mitosis (Doenecke, 2014; Oomen & Dekker, 2017; F. Wang & Higgins, 2013). While most work studying mitotic chromatin rearrangement focuses on

large chromatin-organizing complexes like cohesin, condensin, and topoisomerases (Vagnarelli, 2012), mitosis also is associated with characteristic changes to histone post-translational modifications (PTMs) (Oomen & Dekker, 2017; F. Wang & Higgins, 2013).

Histone PTMs are chemical changes to histones, typically to their tails, some of which are associated with different chromatin structures and densities (Rice & Allis, 2001; F. Wang & Higgins, 2013). Acetylation, notably of histone 3 lysine 9 (H3K9ac), is associated with euchromatin, which is loosely packed, gene rich, and actively transcribed (Doenecke, 2014). Methylation, notably H3K9me<sup>3</sup> and H3K27me<sup>3</sup>, is associated with heterochromatin, which is densely packed and poorly transcribed (Oomen & Dekker, 2017; Rice & Allis, 2001; F. Wang & Higgins, 2013). Histone PTMs may also intrinsically alter chromatin packing by changing the charge of histones (acetylation) and introducing hydrophobic moieties to histones (methylation) (Doenecke, 2014; Rice & Allis, 2001). Recent cryo-EM data has shown that histones are often positioned such that histone tails can physically interact with other nearby histone tails (Bilokapic et al., 2018), possibly enabling the alteration to chromatin structure.

Changes to histone PTMs are known to affect the structure and stiffness of cell nuclei during interphase. Increased euchromatin has been correlated with weaker nuclei, (Chalut et al., 2012; Haase et al., 2016; Krause, Te Riet, & Wolf, 2013) specifically decreasing the short-extension force response of nuclei, which is governed by chromatin stiffness, and contributes secondarily to long extensions (Stephens et al., 2017). Chromatin stiffness also contributes to nuclear shape (Banigan et al., 2017). Decreased chromatin-based nuclear rigidity caused by increased euchromatin has also been shown to cause abnormal nuclear morphology (Stephens et al., 2018), which is an indicator of different cellular diseases, including cancers (Chow, Factor, & Ullman, 2012). Increased heterochromatin has been shown to cause stiffer nuclei and

resistance to abnormal nuclear morphology (Stephens et al., 2017; Stephens et al., 2018). Thus, the correlations between chromatin state and histone PTMs with nuclear stiffness and shape indicate underlying connections between histone PTMs and chromatin stiffness.

Some histone PTM changes are associated specifically with mitosis. Bookmarking is the process where some histone PTMs are retained or stabilized during mitosis, which is thought to preserve the cell's transcriptional state through mitosis (Doenecke, 2014; Oomen & Dekker, 2017; F. Wang & Higgins, 2013). These marks are important for maintaining cellular identity and function. Several histone methyl marks, both euchromatic (*e.g.*, H3K4me<sup>3</sup>) and heterochromatic (*e.g.*, H3K9me<sup>3</sup> and H3K27me<sup>3</sup>) are possibly increased or maintained in mitosis (Park et al., 2011; Xu, Bai, Duan, Costa, & Dai, 2009; Zhiteneva et al., 2017). Increased H4K20me<sup>1</sup> has also been associated with the loading of condensin in mitosis, which organizes chromatin in mitosis (Beck, Oda, Shen, & Reinberg, 2012). Another hallmark of mitosis is the dramatic reduction in overall histone acetylation (Park et al., 2011; Zhiteneva et al., 2017), which may be important for mitotic compaction or related to the lower transcriptional activity during mitosis (F. Wang & Higgins, 2013).

Histone PTMs may also intrinsically affect mitotic chromosome organization (Vagnarelli, 2012; Zhiteneva et al., 2017). Recent experiments suggest that nucleosomes reconstituted using core histones from mitotic cells have a greater propensity to aggregate, compared to nucleosomes assembled using core histones from interphase cells (Zhiteneva et al., 2017). This suggests that histone PTMs and their changes in mitosis may intrinsically affect mitotic compaction through nucleosome-nucleosome interactions. Other experiments have shown that DNA forms the underlying connectivity of mitotic chromosomes (M. G. Poirier & Marko, 2002b; Sun et al., 2011) and condensin in the central axis of mitotic chromosomes is discontinuous (M. Sun, R.

Biggs, J. Hornick, & J. F. Marko, 2018a; Walther et al., 2018). It remains unclear how much chromatin-chromatin interactions could contribute to the stiffness of the mitotic chromosome, although previous studies have been performed on condensin and chromatin entanglements.

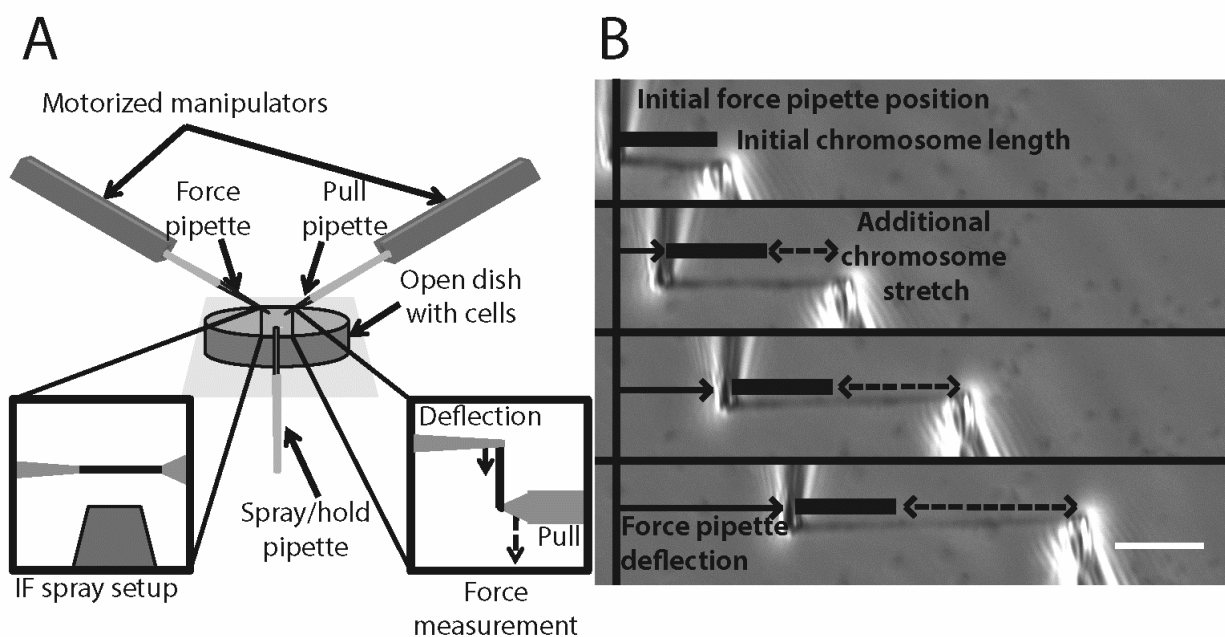
To study the effects of altering histone PTMs on mitotic chromosome structure, we measured the doubling forces of captured mitotic chromosomes (Fig. 3.1; the “doubling force” is the force required to double the length of a chromosome and quantifies chromosome elastic stiffness in a chromosome-length-independent way). In order to test the hypothesis that alterations to histone PTMs affect the compaction of mitotic chromosomes, we studied the effects of the histone deacetylase inhibitors (HDACis), valproic acid (VPA) (Marchion et al., 2005) and Trichostatin A (TSA) (Yoshida, Kijima, Akita, & Beppu, 1990), on the levels of H3K9ac in mitosis and how they affect the stiffness of human mitotic chromosomes. We also tested how the histone demethylase inhibitor (HDMi), methylstat (MS), which is a Jumonji C-specific inhibitor (Luo et al., 2011) (a key domain for several demethylases’ activity), alters the levels of H3K9me<sup>2,3</sup> and H3K27me<sup>3</sup> in mitosis, and affects the stiffness of human mitotic chromosomes. Our results show that HDACi treatments increase H3K9ac but cause no change to the stiffness of mitotic chromosomes, while MS treatment increased canonical heterochromatin marks and the mechanical stiffness of mitotic chromosomes.

Chromatin stiffness plays a key role during cell division, as mitotic chromosome mechanics are key to the proper segregation of the genome during mitosis (Batty & Gerlich, 2019; Ribeiro et al., 2009; Stephens et al., 2011; M. Sun et al., 2018b). We demonstrated that methylated histones/heterochromatin are a mechanical component of mitotic chromosomes (R. Biggs et al., 2019). However, in addition to methylated histones, protein ‘readers’ of epigenetic marks play a key role in defining heterochromatin (and euchromatin). A key histone methylation

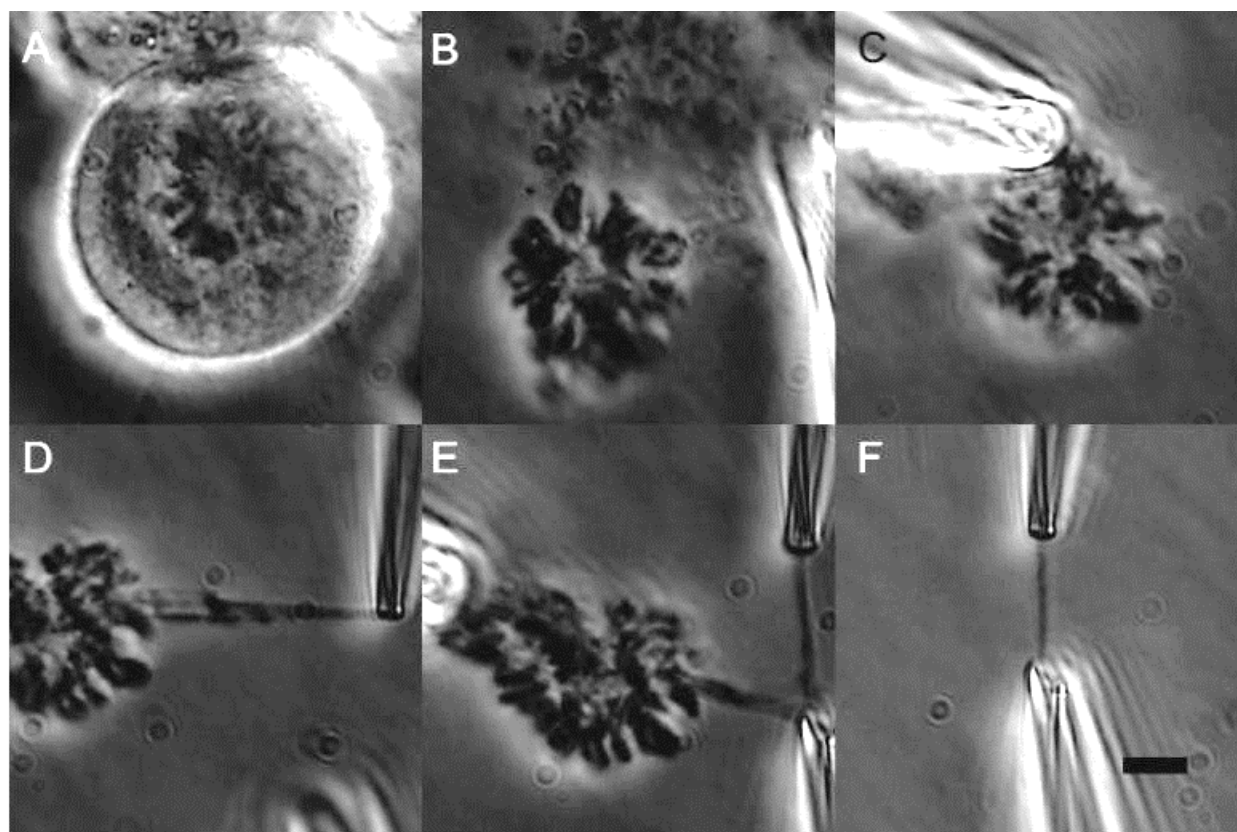
reader, Heterochromatin Protein 1 alpha (HP1 $\alpha$ ), remains poorly characterized as to its role in controlling the mechanical properties of heterochromatin. To what degree HP1 $\alpha$  contributes to the mechanical resistive capabilities of chromatin, how this contribution is intertwined with histone methylation, and how these result in proper nuclear and mitotic mechanics and function, are all open questions.

HP1 $\alpha$  is a major component of constitutive heterochromatin (James & Elgin, 1986; Singh et al., 1991; Wreggett et al., 1994). Functionally, HP1 $\alpha$  is a homodimer that binds to both DNA and to H3K9me<sup>2,3</sup> constitutive heterochromatin marks. The direct association of HP1 $\alpha$  with H3K9me<sup>2,3</sup> heterochromatin and its direct binding to Suv39h1/2, the histone methyltransferase that deposits H3K9me<sup>2,3</sup>, has led to reports that HP1 $\alpha$  is necessary for either maintenance or establishment of histone methylation in interphase (Bannister et al., 2001; Krouwels et al., 2005). Loss of HP1 $\alpha$  could therefore indirectly alter chromatin mechanics by modulating histone methylation levels. Alternatively, HP1 $\alpha$  homodimerization and/or higher-order oligomerization could directly impact mechanics through physical bridging of two chromatin fibers, resulting in crosslinking of DNA or H3K9me<sup>2,3</sup>-marked nucleosomes (Canzio et al., 2011; Cheutin et al., 2003; Machida et al., 2018). Consistent with this possibility, chromatin crosslinks have been suggested to be a key element of chromatin organization and mechanics (Banigan et al., 2017; Belaghzal et al., 2021; Lionetti et al., 2020; Stephens et al., 2017). The capacity of HP1 $\alpha$  to drive liquid-liquid phase separation (Larson et al., 2017; Strom et al., 2017) could also contribute to altered chromatin organization and mechanics, given the emerging evidence for links between phase separation and nuclear mechanics (Shin et al., 2018).

Recent experimental and modeling studies suggest chromatin proteins, like HP1 $\alpha$ , may contribute to mechanics by acting as physical linkers. Experimental data for nuclear mechanical



(A) Schematic of the single captured chromosome experimental setup. Single chromosomes were captured from mitotic HeLa cells in a custom-made well (Materials and Methods). Capture was performed after lysing the cell membranes with a PBS-Triton-X solution, where the chromosome was captured from the whole genome chromosome bundle (Fig. 3.2). Once captured, the chromosome could be stretched for measurements of the doubling force or sprayed with fluorescent antibodies for immunostaining experiments. (B) An example of an experiment to measure the doubling force of a mitotic chromosome. The force (thin pipette on the left) and pull (larger pipette on the right) pipettes were aligned to be roughly perpendicular to the captured chromosomes. The pull pipette then moved away from the force pipette, stretching the chromosome (dashed line). The stretching of the chromosome would cause the force pipette to deflect (thin, rightward arrow) from its original position (thin, vertical line), which was used to calculate the force on the chromosome for the amount of stretch at that point. Chromosome initial length (thick bar) (measured by the distance from the center of the pipettes) and diameter (not shown) measured using a still image in ImageJ. Scale bar represents 10  $\mu\text{m}$ .



(A) Morphology of a prometaphase mitotic HeLa cell: rounded morphology and clearly condensed chromosomes (B) The cell post Triton X-100 lysis (C) Chromosome bundle freed from the cell and after moving (D) The initial grab/aspiration of the chromosome into the force pipette (E) The second grab/aspiration of the other end of the chromosome into the stiff pipette (F) The chromosome after removal of the chromosome bundle. The chromosome is tracked as a single and unbroken object during the capture procedure. Scale bar represents 5  $\mu\text{m}$ .

response can only be reconciled with models that contain chromatin (an interior polymer), a lamina (a peripheral meshwork), and chromatin-chromatin and chromatin-lamina linkages (Banigan et al., 2017; Hobson & Stephens, 2020; Stephens et al., 2017). Further studies have suggested that these linkages may govern nuclear shape stability (Lionetti et al., 2020; K. Liu, Patteson, Banigan, & Schwarz, 2021; Schreiner, Koo, Zhao, Mochrie, & King, 2015). Experimental studies have shown chromatin linkages to the nuclear periphery aid shape stability and mechanics (Schreiner et al., 2015). Furthermore, recent chromosome conformation capture (Hi-C) and mechanics experiments suggest that chromatin is physically linked about once per 15 kb, since chromatin organization and mechanical response are perturbed only upon extreme chromatin fragmentation by restriction enzymes (Belaghzal et al., 2021). Whether chromatin-binding proteins like HP1 $\alpha$  provide mechanical and morphological stability to the nucleus and whether their function is to maintain histone modifications or act as physical linkers remains an open question.

Using these hypotheses, an AID-GFP-HP1 $\alpha$  line was created to test how its degradation affects the mechanical stiffness of nuclear mechanics (Strom et al., 2021). Without auxin treatment, HP1 $\alpha$  was shown to properly localize to its native position and did not perturb methylation levels. With auxin treatment, HP1 $\alpha$  could be rapidly degraded, shown by fluorescence and western blot. HP1 $\alpha$  could also recover when untreated for a day. Auxin degradation also weakened the nuclei in the chromatin regime and would recover to untreated stiffness when cotreated with methylstat. This suggests that the stiffness increase of methylstat functions in a parallel manner to HP1 $\alpha$ 's contribution to stiffness. The stiffness of nuclei also impacted the resistance of the nuclei against blebbing, morphology defects, and other such changes. Further experiments on morphology demonstrated that the crosslinking properties of

HP1 $\alpha$  is critical for maintaining the morphology of nuclei. Simulations of HP1 $\alpha$  also suggests that the ability of HP1 $\alpha$  to stiffen interphase nuclei relies on the crosslinking function of HP1 $\alpha$ .

These mechanisms could also affect mechanics in mitotic chromosomes, where HP1 $\alpha$  is also present (Akram et al., 2018; Serrano, Rodriguez-Corsino, & Losada, 2009). Most studies of epigenetic modification of chromatin and nuclear mechanics have focused on the interphase nucleus. However, it is conceivable that some of the epigenetic marks involved in heterochromatin formation during interphase might survive and have effects during cell division. Consistent with this, recent work indicates that hypermethylation of histones can persist into metaphase and is correlated with increased stiffness of mitotic chromosomes/metaphase chromatin (R. Biggs et al., 2019). However, it remains unknown whether the readers of those marks, such as HP1 $\alpha$ , contribute significantly to metaphase chromatin structure and mechanics and how important they are to ensuring the success of mitosis.

Here, we determine the mechanical role of the heterochromatin protein, HP1 $\alpha$ , and its independence from histone methylation. Using the novel CRISPR-derived HP1 $\alpha$ -AID-sfGFP cells, we observe increases in the incidence of mitotic errors, which are associated with disease in HP1 $\alpha$  depletion. Increasing histone methylation rescues mitotic chromosome mechanics associated with HP1 $\alpha$  depletion, indicating that these factors contribute to stiffness independently. These findings contribute to our understanding of the role of histone methylation and heterochromatin levels in controlling mitotic mechanics, and morphology in healthy and diseased cell states.

## 3.2 Methods

### 3.2.1 Cell culture and drug treatments

Human HeLa cells were maintained in DMEM (Corning) with 10% fetal bovine serum (FBS) (HyClone) and 1% 100x penicillin/streptomycin (Corning). The cells were incubated at 37°C and 5% CO<sub>2</sub> for no more than 30 generations and were passaged every 2-4 days. Experiments on captured chromosomes used cells that were allowed to recover 1-3 days before capture. Cells were freely cycling and not treated with drugs designed to affect or synchronize the cell cycle. For epigenetic drug treatments, the cells were plated as above in drug-free DMEM and allowed to recover for ~8 hr., then treated with 2 mM VPA (Sigma), 50 nM TSA (Sigma), or 2 μM MS (Cayman chemicals) all dissolved in DMEM. Chromosomes were then captured from the cells (see below) 16-24 hr. after treatment for VPA and TSA, or 40-48 hr. for MS treatments.

### 3.2.2 Fixed immunofluorescence (IF)

Cells were grown in small wells built on coverslips (Fisher) and treated as above. All solutions were diluted in PBS and wash steps performed with PBS (Lonza) at room temperature, unless noted otherwise. Slides were washed, fixed in 4% paraformaldehyde (EMS), washed, permeabilized with 0.10-0.20% Triton-X 100 (USBio), incubated in 0.06% Tween 20 (Fisher), washed, and blocked in 10% goat serum (Sigma). The slides incubated with primary overnight at 4°C. The slides were then washed, incubated in secondary, incubated in Hoechst (Life Tech), washed, and mounted. Primary and secondary solutions were diluted in 10% goat serum. HDACi treatments were assayed using a 1:400 rabbit anti-H3K9ac (Cell Signaling 9649) primary and a 1:500 488-nm anti-rabbit IgG (Invitrogen A11034) secondary. HDMi treatments used a 1:100 mouse anti-H3K9me<sup>2,3</sup> (Cell Signaling 5327) with a 1:1600 rabbit anti-H3K27me<sup>3</sup> (Cell Signaling 9733) primary and a 1:500 of 488-nm anti-mouse IgG (Invitrogen A11001) with a

1:500 of 594-nm anti-rabbit IgG (Invitrogen A11037) secondary. Mitotic cells were identified by finding cells that showed compact mitotic chromosomes in the Hoechst channel. The final IF values reported are given by the fluorescence signal to background ratio of the antibody of interest over the Hoechst signal to background ratio. Averages and standard errors are divided by the average untreated values in normalized graphs.

### **3.2.3 Single chromosome capture: setup and microscopy**

Single chromosome capture experiments used an inverted microscope (IX-70; Olympus) with a 60x 1.42 NA oil immersion objective with a 1.5x magnification pullout at room temperature and atmospheric CO<sub>2</sub> levels. Experiments were performed in less than 3 hours after removal from the incubator to ensure minimum damage to the cells being analyzed. Prometaphase cells were identified by eye and lysed with 0.05% Triton-X 100 in PBS. All other pipettes were filled with PBS. After lysis, the bundle of chromosomes was held with a pipette. One end of a random, loose chromosome was grabbed by the force pipette (WPI TW100F-6), moved from the bundle, and grabbed with the pulling pipette on the other end. The bundle was then removed to isolate the tracked and unbroken chromosome (Fig. 3.1A, 3.2).

### **3.2.4 Single chromosome capture: force measurement**

An easily bendable force pipette and stiff pulling pipette were used for stretching chromosomes. Once captured, the pipettes were moved perpendicular to the chromosome, stretching the chromosome to roughly its native length. The stiff pipette was then moved 6  $\mu\text{m}$  and returned to the starting position at a constant rate of 0.20  $\mu\text{m}/\text{sec}$  in 0.04  $\mu\text{m}$  steps using a LabVIEW program, while tracking the stiff and force pipette. Fig. 3.1B shows an example stretch-deflection experiment. Deflection of the force pipette multiplied by its calibrated spring constant and divided by the distance between the pipettes (the stretch) was used to obtain the

chromosome spring constant. Each chromosome was stretched at least 3 times to provide an accurate and reproducible measurement of the chromosome spring constant. The chromosome spring constant multiplied by its initial length gave the doubling force. The initial length was given by measuring the distance between the center of the pipettes in ImageJ and converting the pixels into microns while the chromosome was perpendicular to the pipettes. Chromosome cross sectional area was estimated as  $0.25\pi d^2$  with chromosome diameter  $d$  calculated as the full width at half maximum of an ImageJ line scan.

### **3.2.5 Single chromosome capture: immunofluorescence**

After force measurements, the chromosome was lifted above the glass surface and micro sprayed with a primary, secondary, and tertiary solution from a wide bore pipette, moving the chromosome between sprays. The solutions used 50  $\mu$ L PBS, 36-38  $\mu$ L H<sub>2</sub>O (Corning), 10  $\mu$ L 5% casein (Sigma), and 2  $\mu$ L each antibody. HDACi experiments used a rabbit anti-H3K9ac primary and a 488-nm anti-rabbit secondary. HDMi experiments used a mouse anti-H3K9me<sup>2,3</sup> and a rabbit anti-H3K27me<sup>3</sup> primary and a 488-nm anti-mouse IgG with a 594-nm anti-rabbit IgG secondary. The tertiary spray used Hoechst instead of an antibody. In experiments on mitotic chromosomes and bundles studying HP1 $\alpha$  the endogenous fluorescence of the AID-GFP tagged HP1 $\alpha$  was used on the same microscope. Images were taken of the unperturbed cell, the chromosomal/genome bundle periodically, and of the final isolated chromosome with no added fluorescent molecules.

### **3.2.6 Western blots**

Cells were grown in 100 mm dishes and treated as described in “cell culture and treatments”. TSA treatments were done at 200 nM. Cells were then harvested in PBS, centrifuged into a pellet, and lysed with RIPA buffer. The solution was then pelleted, and the supernatant saved.

The solution was then mixed with 2x Laemmli buffer, run on a 4-20% gradient SDS-PAGE gel, transferred to a nitrocellulose sheet, incubated in a primary solution, washed, and incubated in a secondary solution, then imaged.

### 3.2.7 Statistics

For fixed immunofluorescence, the reported *n* refers to the number of technical replicates, *i.e.*, the total number of cells analyzed. The *N* measurements are furthermore from a set of biological replicates, *i.e.*, separate cell colonies on separate slides. All interphase-staining results are from data taken from two biological replicates. Mitotic staining for H3K9ac and SMC2 were also obtained using 2 biological replicates. H3K9me<sup>2,3</sup> and H3K27me<sup>3</sup> data came from 4 biological replicates. For chromosomes, the reported *N* refers to each individual captured chromosome for both mechanical and immunofluorescence experiments; these experiments were from different slides (colonies) of cells and thus are independent biological replicates. Outliers were identified and discarded by using a generalized Studentized deviate test at  $\alpha = 0.05$ . All *p*-values calculated using a T test. All averaged values are reported as average  $\pm$  standard error.

## 3.3 Results

### 3.3.1 HDACis increases H3K9ac in mitosis but have no change in stiffness

To investigate the role of histone PTMs on mitotic chromosome compaction, we studied the effects of histone hyperacetylation. We induced histone hyperacetylation using the histone deacetylase inhibitors (HDACi), valproic acid (VPA) and Trichostatin A (TSA). Both VPA and TSA led to an increase in H3K9ac fluorescence intensity in fixed immunofluorescence (IF) (Fig. 3.3A,B) and Western blots in interphase cells (Fig. 3.3C). Having been able to induce hyperacetylation in interphase, we next tested whether the same treatment would cause histone

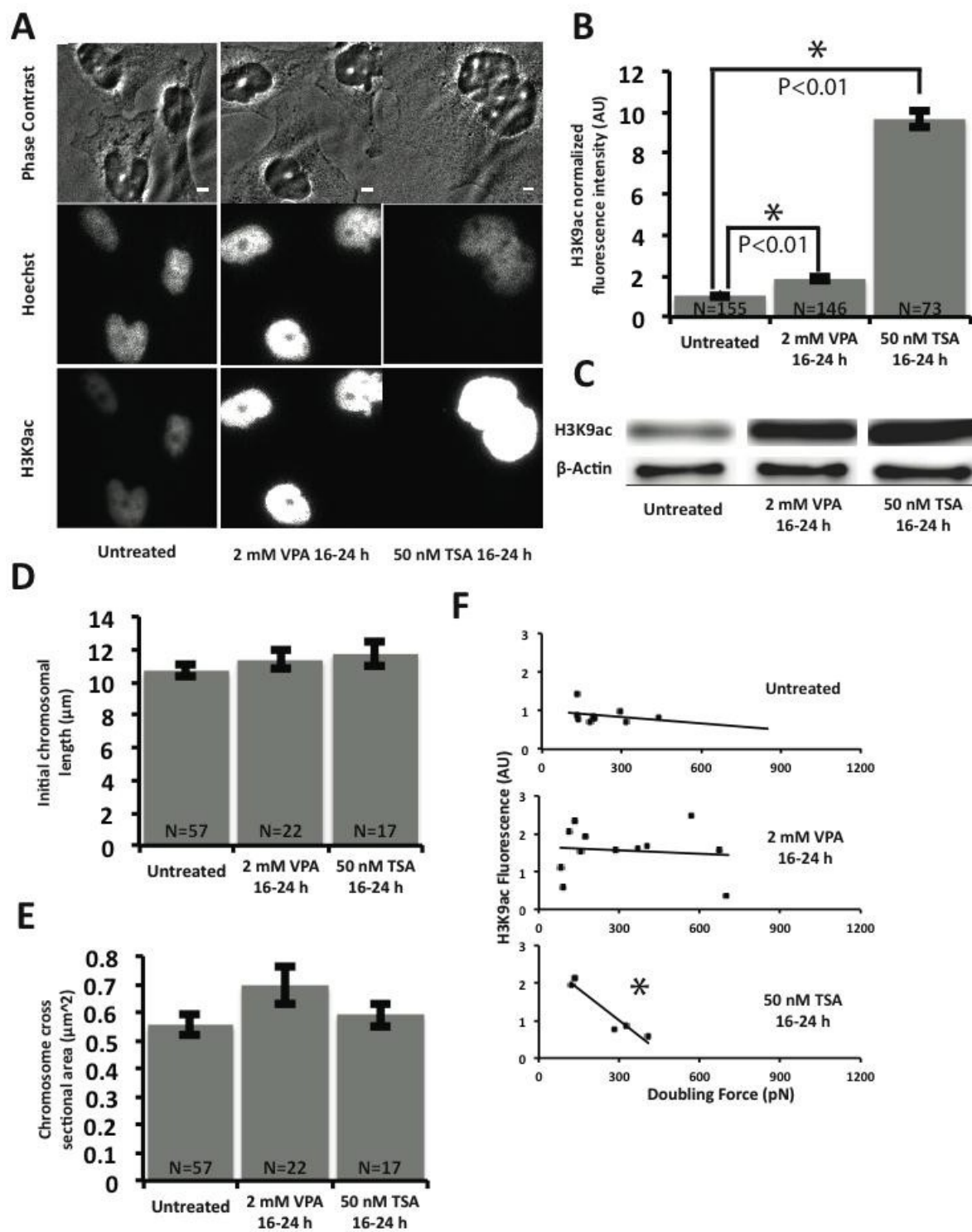


**Figure 3.3. Further fluorescent analysis of VPA and TSA treatments.**

Both treatments cause hyperacetylation in interphase cells, but do not affect chromosomal initial length or cross-sectional area. Only TSA displays a correlation between histone acetylation and doubling force. (A) Example representative images of levels of H3K9ac fluorescence measurement on fixed interphase cells. Scale bar represents 5  $\mu\text{m}$ . (B) Quantitative data of (A). The H3K9ac intensity ratio of untreated to 2 mM VPA 16-24 hr. treatment was  $1.9 \pm 0.1$  and is statistically significant. The H3K9ac intensity ratio of untreated to 50 nM TSA 16-24 hr. treatment was  $9.7 \pm 0.1$  and is statistically significant. (C) Western blot analysis of H3K9ac levels with  $\beta$ -Actin loading control in untreated, 2 mM VPA 16-24 hr., and 50 nM TSA 16-24 hr. treated cells. (D) Recorded initial length for mitotic chromosomes from untreated and HDACi treated cells. The average chromosome initial length was  $10.7 \pm 0.3 \mu\text{m}$  in untreated cells. The average chromosome initial length was  $11.4 \pm 0.6 \mu\text{m}$  in 2 mM VPA 16-24 hr. treated cells, statistically insignificant from untreated cells. The average chromosome initial length was  $11.7 \pm 0.7 \mu\text{m}$  in 50 nM TSA 16-24 hr. treated cells, statistically insignificant from untreated cells. (E) Recorded cross sectional area for mitotic chromosomes from untreated and HDACi treated cells. The average chromosome cross sectional area was  $0.56 \pm 0.04 \mu\text{m}^2$  in untreated cells. The average chromosome cross sectional area was  $0.69 \pm 0.07 \mu\text{m}^2$  in 2 mM VPA 16-24 hr. treated cells, statistically insignificant from untreated cells. The average chromosome cross sectional area was  $0.69 \pm 0.07 \mu\text{m}^2$  in 50 nM TSA 16-24 hr. treated cells, statistically insignificant from untreated cells. (F) Scatterplots of doubling force against H3K9ac fluorescence measurements. Using a linear fit the  $R^2$  were 0.06 for untreated, 0.01 2 mM VPA 16-24 hr. treatment, 0.91 for 50 nM TSA 16-24 hr. treatment. Error bars in SEM. All p values calculated via t test. All measurements recorded as statistically significant if  $p < 0.05$ . Asterisk in scatterplots represent a statistically significant correlation ( $p < 0.05$ ).

hyperacetylation in mitosis. In fixed IF experiments of mitotic cells the average ratios of HDACi-treated to untreated H3K9ac acetylation levels were  $1.4 \pm 0.1$  for VPA and  $2.3 \pm 0.3$  for TSA (Fig. 3.4A,B). In single captured chromosome experiments the average ratios of HDACi to untreated H3K9ac measurements were  $1.8 \pm 0.2$  for VPA and  $2.3 \pm 0.6$  TSA (Fig. 3.4C,D). These results indicated that we were able to create hyperacetylated chromatin in mitosis.

Next, we tested if this increase in acetylation would lead to a difference in stiffness for mitotic chromosomes, by measuring the doubling force of mitotic chromosomes extracted from untreated and HDACi-treated cells. Neither VPA nor TSA caused a statistically significant change in doubling force compared to untreated chromosomes (Fig. 3.4E). The average chromosome doubling forces were  $320 \pm 30$  pN in untreated cells,  $310 \pm 40$  pN in VPA treated cells, and  $330 \pm 30$  pN in TSA treated cells. The lack of change was not due to changes of initial length or cross-sectional area, as neither changed with HDACi treatments (Fig. 3.3D,E).

Plotting the averaged doubling force against H3K9ac fluorescence for untreated and HDAC inhibited chromosomes, we found that there was no statistically significant correlation between H3K9ac measurements and doubling force in either untreated chromosomes or VPA treatments (Fig. 3.4F). We do note that the TSA-treated chromosomes did show a statistically significant correlation between measured H3K9ac level and doubling force, with increasing acetylation leading to lower spring constant; however, when averaged over, there was no net effect of TSA treatment on chromosome spring constant. The correlation may be due to the specific mechanism of HDAC inhibition by TSA (no such correlation was observed for VPA), may reflect differences between specific chromosomes, or simply arise from the sample size being too small for this type of correlation analysis. Apart from this correlation, we concluded

that hyperacetylation of histones through HDACi treatment does not affect the overall stiffness of mitotic chromosomes.

### 3.3.2 Methylstat stiffens chromosomes and increases fixed cell histone methylation

Given that there was no overall effect of histone acetylation on chromosome doubling force, we wanted to test how altering histone methylation affects the stiffness of mitotic chromosomes. To induce hypermethylation, we used the histone demethylase inhibitor (HDMi) methylstat (MS), which increased both H3K9me<sup>2,3</sup> and H3K27me<sup>3</sup> as assayed via both Western blotting (Fig. 3.5A,B) and fixed-cell IF in interphase cells (Fig. 3.5C). Having been able to induce hypermethylation in interphase, we next tested whether the same treatment would cause histone hypermethylation in mitosis. In fixed IF experiments of mitotic cells the average ratio of MS to untreated H3K9me<sup>2,3</sup> measurement was  $1.6 \pm 0.1$  while the average ratio of MS to untreated H3K27me<sup>3</sup> measurement was  $3.9 \pm 0.5$  (Fig. 3.6A,B). In contrast to the fixed IF experiments, MS did not cause a statistically significant change in H3K9me<sup>2,3</sup> nor H3K27me<sup>3</sup> measurement using antibodies micro sprayed onto single captured chromosomes (Fig. 3.6C,D). While unexpected, this data is explainable due to a lack of antibody accessibility and penetration into the more compact hypermethylated chromosomes, and the short antibody incubation time for our micro spraying of captured chromosomes, relative to fixed IF staining (~10 min versus ~16 hr.).

To determine if increased methylation caused mitotic chromosomes to become stiffer, we measured the doubling force of MS treated chromosomes. MS treatment caused a statistically significant increase of about 80% in the doubling force of mitotic chromosomes, consistent with more compact chromatin (Fig. 3.6E). The average chromosome doubling forces were  $320 \pm 30$  pN in untreated cells and  $580 \pm 40$  pN in MS treated cells. This change was not due to a change in

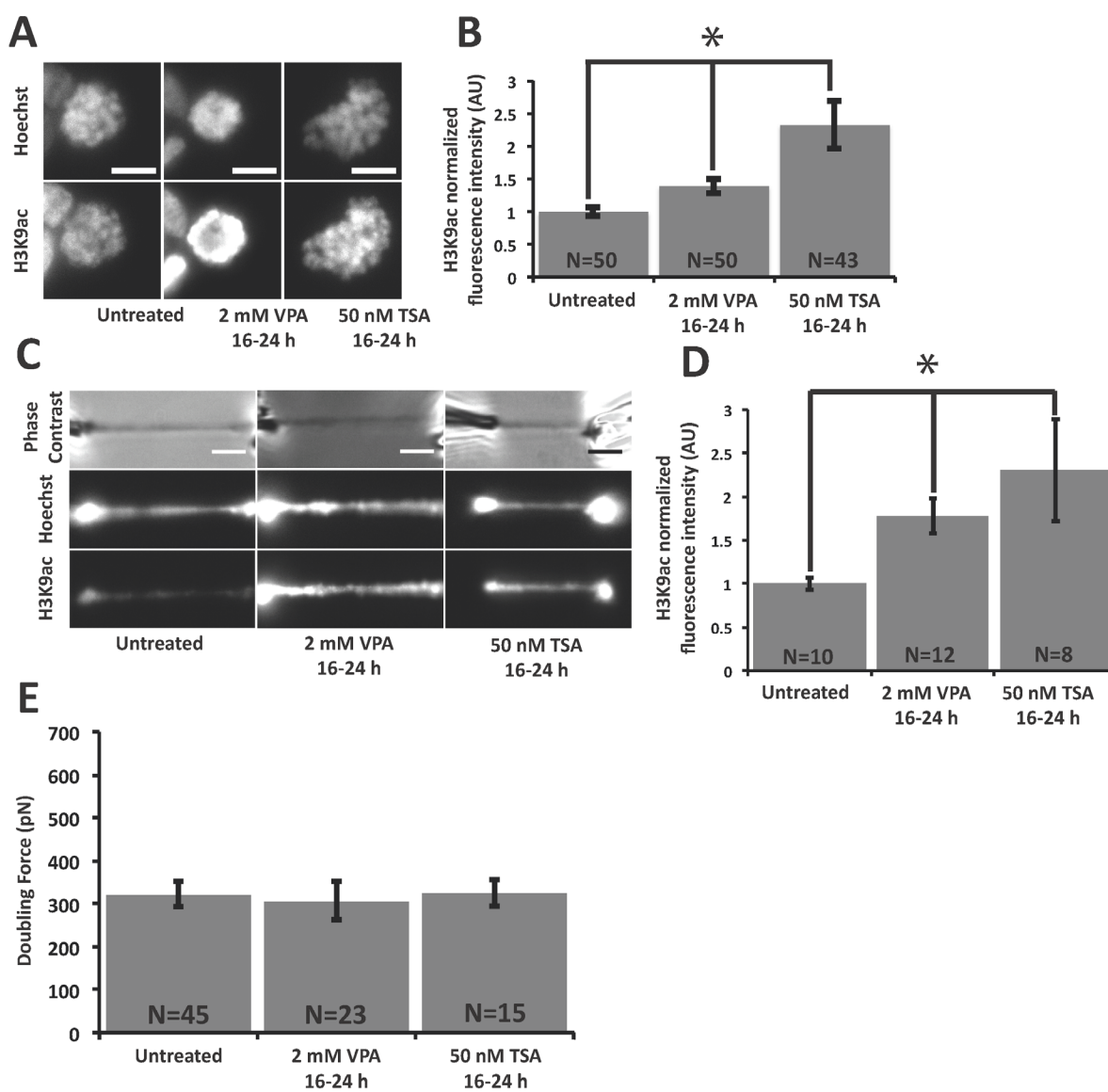


**Figure 3.4. HDACi cause increased H3K9ac fluorescence in mitotic fixed cells and captured chromosomes, but have little effect on the stiffness of mitotic chromosomes.**

(A) Example representative images of levels of H3K9ac fluorescence measurement on fixed mitotic cells. Scale bar represents 10  $\mu\text{m}$ . (B) Quantitative data of (A). The H3K9ac intensity ratio of untreated to 2 mM VPA 16-24 hr. treatment was  $1.4 \pm 0.1$  and is statistically significant. The H3K9ac intensity ratio of untreated to 50 nM TSA 16-24 hr. treatment was  $2.3 \pm 0.3$  and is statistically significant. (C) Example representative images of levels of H3K9ac fluorescence measurements on captured mitotic chromosomes. Scale bar represents 5  $\mu\text{m}$ . (D) Quantitative data of (C). The H3K9ac intensity ratio of untreated to 2 mM VPA 16-24 hr. treatment was  $1.8 \pm 0.2$  and is statistically significant. The H3K9ac intensity ratio of untreated to 50 nM TSA 16-24 hr. treatment was  $2.3 \pm 0.6$  and is statistically significant. (E) Recorded doubling force for mitotic chromosomes from untreated and HDACi treated cells. The average chromosome doubling forces were  $320 \pm 30$  pN in untreated cells. The average doubling force was  $310 \pm 40$  pN in 2 mM VPA 16-24 hr. treated cells, statistically insignificant from untreated cells. The average doubling force was  $330 \pm 30$  pN in 50 nM TSA 16-24 hr. treated cells, statistically insignificant from untreated cells. Error bars represent standard error. Asterisk in bar graphs represent a statistically significant difference ( $p < 0.05$ ). All p values calculated via t test.

either the initial chromosome length or cross-sectional area, as neither changed with MS treatment (Fig. 3.5D,E).

Plotting doubling force against H3K9me<sup>2,3</sup> measurements did not show any correlation in untreated, or MS treated cells (Fig. 3.5F left panels). Alternately, plotting doubling force against H3K27me<sup>3</sup> measurements (in MS treated cells, but not untreated) suggests a potential correlation between H3K27me<sup>3</sup> and chromosome stiffness (Fig. 3.5F right panels). However, there may be limitations of antibody accessibility on the chromosomes, so this correlation must be regarded as preliminary at best. Our results do indicate that hypermethylation, via MS treatment, leads to robustly higher H3K27me<sup>3</sup> levels, and causes chromosomes to become stiffer and possibly denser.

### **3.3.3 Methylstat treatment does not change SMC2 levels**

Since condensin is the most well-known contributor to chromosome strength, we sought to check whether levels of condensin on mitotic chromosomes increased when treated with MS. Previous work has shown that chromosome stiffness is approximately linearly proportional to the amount of condensin on the chromosome (M. Sun et al., 2018b). We used antibodies against SMC2, a core subunit of condensin, to determine if there was a difference in fluorescence intensities between untreated and MS treated cells and captured chromosomes. The experiments did not show a difference as measured using fixed cellular immunofluorescence (Fig. 3.7A,B) or for antibodies micro sprayed onto captured chromosomes (Fig. 3.7C,D), suggesting that the stiffening phenotype is independent of condensin loading.

### **3.3.4 HP1 $\alpha$ provides mechanical strength to mitotic chromosomes**

HP1 $\alpha$  is a protein associated with heterochromatin, which binds to the methylated histones, specifically H3K9me<sup>2,3</sup> and H3K27me<sup>3</sup>, which are both increased in methylstat treatment.

Previous experiments on the stiffness of nuclei showed that histone methylation, acetylation, and HP1 $\alpha$  showed that chromatin is very influential to the structure and mechanics of the nuclei (Stephens 2017; 2018, Strom 2021). Given HP1 $\alpha$ 's mechanical role in chromatin-based nuclear mechanics, we hypothesized that HP1 $\alpha$  could also contribute to mitotic chromosome mechanics. As in interphase nuclear mechanical response, heterochromatin has recently been shown to govern mitotic chromosome mechanics (R. Biggs et al., 2019). It has previously been reported that most HP1 $\alpha$  is removed from chromosomes during prophase by phosphorylation of H3S10, which is known to disrupt HP1 $\alpha$ -H3K9me<sub>2,3</sub> binding (Fischle et al., 2005; Hirota, Lipp, Toh, & Peters, 2005). However, some HP1 $\alpha$  binding is maintained throughout mitosis (Serrano et al., 2009), suggesting a possible role for HP1 $\alpha$  in mitotic chromosome mechanics.

We used fluorescence imaging and micropipette micromanipulation methods (R. Biggs et al., 2019; M. Sun et al., 2018b) to assay the presence of HP1 $\alpha$ -AID-sfGFP in prometaphase cells (identified by their round shape) and mitotic chromosomes without or with auxin treatment for 4 hr. to degrade HP1 $\alpha$  (Fig. 3.8B). Prometaphase cells show both chromosome-bound and diffuse, cytoplasmic HP1 $\alpha$ -AID-sfGFP signals. Both cytoplasmic and chromosomal HP1 $\alpha$ -AID-sfGFP signals nearly completely disappear upon auxin-induced degradation (Fig. 3.8B). To further verify the presence of HP1 $\alpha$  on mitotic chromosomes, we isolated mitotic chromosome bundles from cells via gentle lysis and capture. Fluorescence imaging of these isolated bundles without the high background fluorescence of the cytoplasm allowed us to observe that HP1 $\alpha$  is clearly present on mitotic chromosomes (Fig. 3.8A). In addition to concentrated foci, HP1 $\alpha$ -AID-sfGFP is also present on chromosome arms (Fig. 3.8C). Confocal imaging of live cells revealed that concentrated foci are located at the pericentromeric region, in agreement with

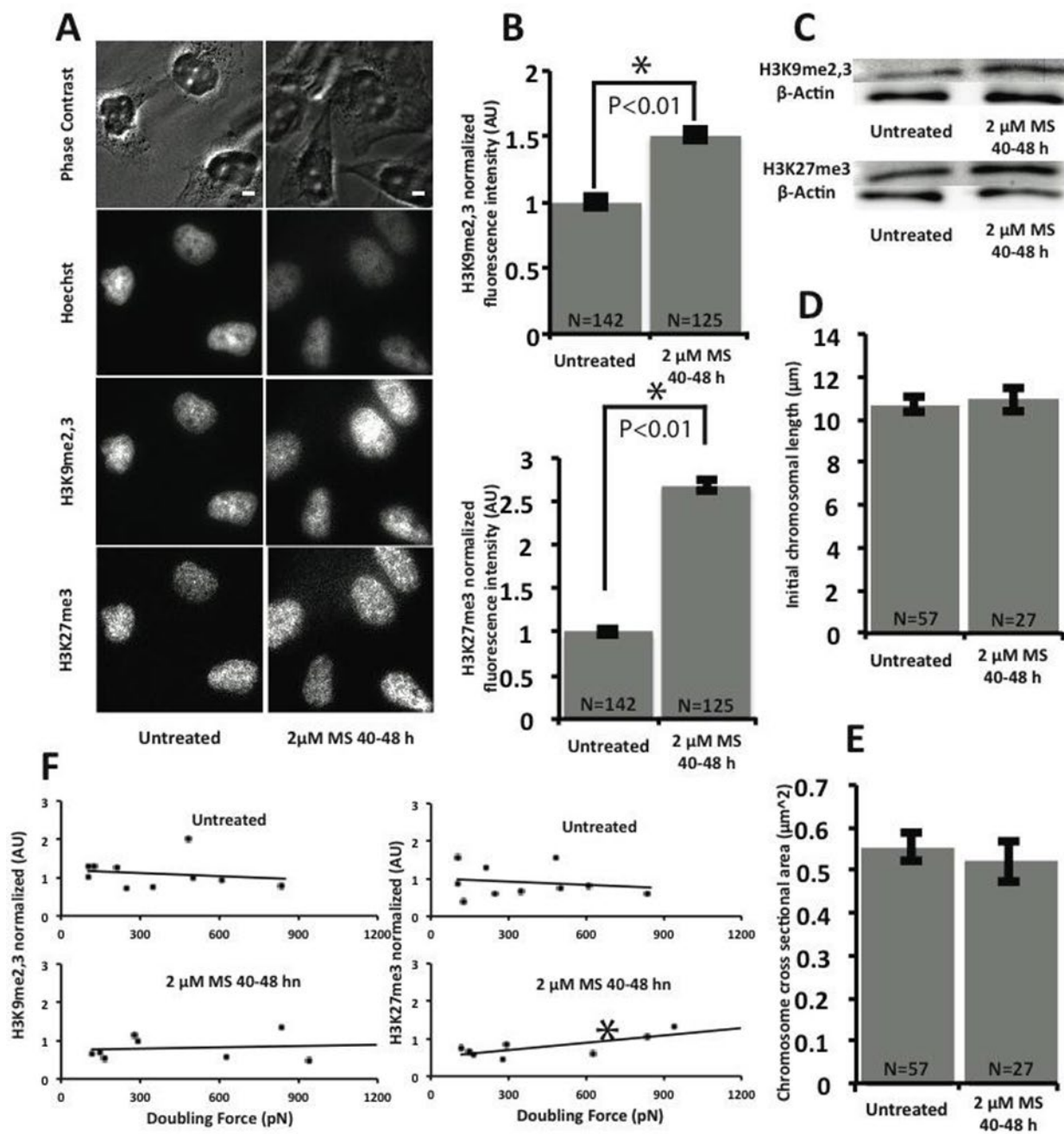


**Figure 3.5. Further fluorescent analysis of Methylstat treatments.**

Treatment causes hypermethylation in interphase cells, but do not affect chromosomal initial length or cross-sectional area. Only H3K27me3 fluorescence correlates with doubling force, only in methylstat treatment. (A) Example representative images of levels of H3K9me2,3 and H3K27me3 fluorescence measurement on fixed interphase cells. Scale bar represents 5  $\mu\text{m}$ . (B) Quantitative data of (A). The H3K9me2,3 intensity ratio of untreated to 2  $\mu\text{M}$  MS 40-48 hr. treatment was  $1.5 \pm 0.1$  and is statistically significant. The H3K27me3 intensity ratio of untreated to 2  $\mu\text{M}$  MS 40-48 hr. treatment was  $2.5 \pm 0.1$  and is statistically significant. (C) Western blot analysis of H3K9me2,3 (top) and H3K27me3 levels with  $\beta$ -Actin loading control in untreated and 2  $\mu\text{M}$  MS 40-48 hr. treated cells. (D) Recorded initial length for mitotic chromosomes from untreated and MS treated cells. The average chromosome initial length was  $10.7 \pm 0.3$   $\mu\text{m}$  in untreated cells. The average chromosome initial length was  $11.0 \pm 0.6$   $\mu\text{m}$  in 2  $\mu\text{M}$  MS 40-48 hr. treated cells, statistically insignificant from untreated cells. (E) Recorded cross sectional area for mitotic chromosomes from untreated and MS treated cells. The average chromosome cross sectional area was  $0.56 \pm 0.04$   $\mu\text{m}^2$  in untreated cells. The average chromosome cross sectional area was  $0.52 \pm 0.05$   $\mu\text{m}^2$  in 2  $\mu\text{M}$  MS 40-48 hr. treated cells, statistically insignificant from untreated cells. (F) Scatterplots of doubling force against H3K9me2,3 and H3K27me3 fluorescence measurements. Using a linear fit the  $R^2$  were 0.03 for untreated H3K9me2,3, 0.03 for untreated H3K27me3, 0.01 for 2  $\mu\text{M}$  MS 40-48 hr. treatment H3K9me2,3, 0.56 for 2  $\mu\text{M}$  MS 40-48 hr. treatment H3K27me3. Error bars in SEM. All p values calculated via t test. All measurements recorded as statistically significant if  $p < 0.05$ . Asterisk in scatterplots represent a statistically significant correlation ( $p < 0.05$ ).

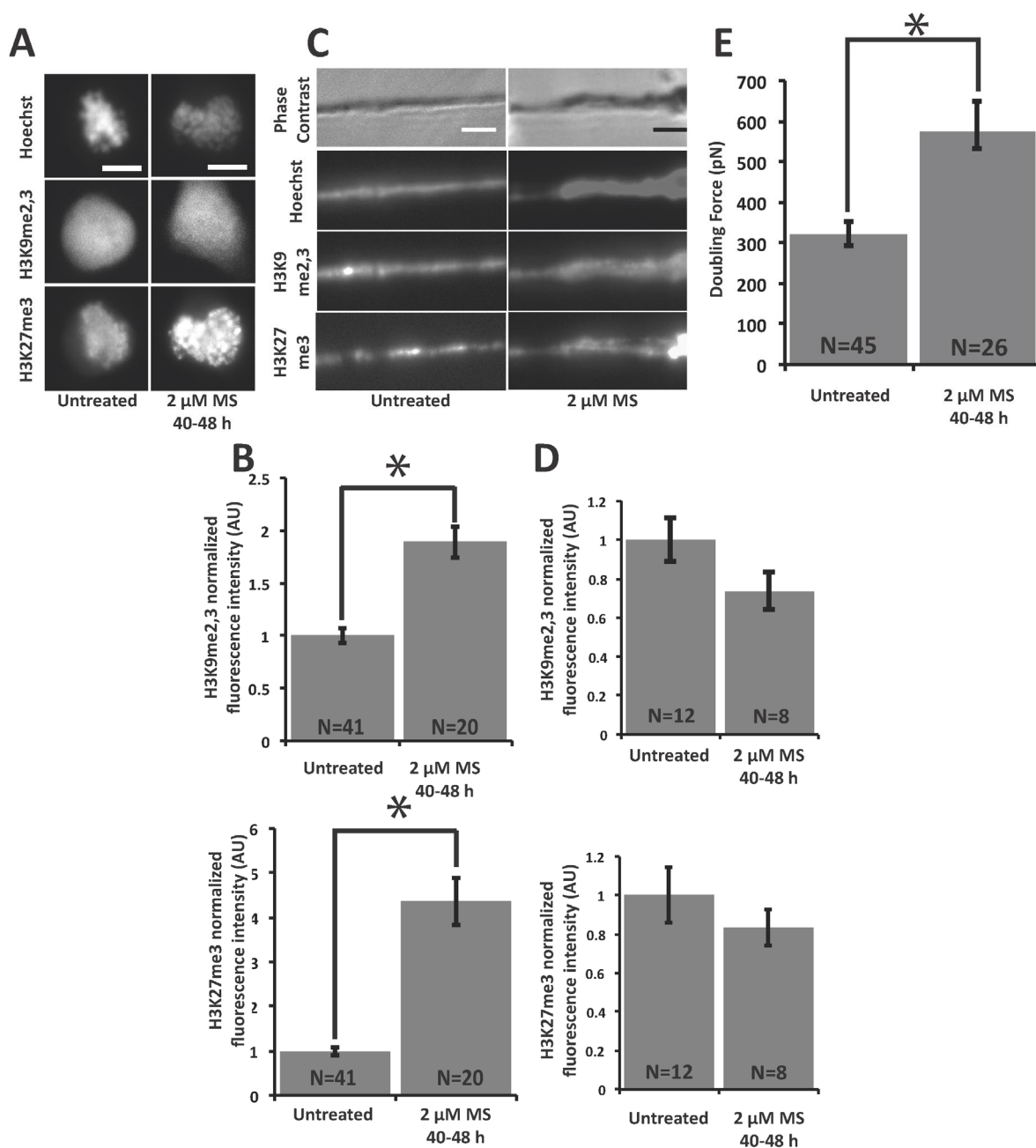


**Figure 3.6. Methylstat (HDMi) treatment causes an increase in methylation for mitotic fixed cells and stiffens mitotic chromosomes.**

(A) Example representative images of levels of H3K9me<sub>2,3</sub> and H3K27me<sub>3</sub> fluorescence intensity on fixed mitotic cells. Scale bar represents 10  $\mu\text{m}$ . (B) Quantitative data of (A). The H3K9me<sub>2,3</sub> intensity ratio of untreated to 2  $\mu\text{M}$  MS 40-48 hr. treatment was  $1.9 \pm 0.1$  and is statistically significant. The H3K27me<sub>3</sub> intensity ratio of untreated to 2  $\mu\text{M}$  MS 40-48 hr. treatment was  $4.4 \pm 0.5$  and is statistically significant. (C) Example representative images of levels of H3K9me<sub>2,3</sub> and H3K27me<sub>3</sub> fluorescence intensity on captured mitotic chromosomes. Scale bar represents 5  $\mu\text{m}$ . (D) Quantitative data of (C). The H3K9me<sub>2,3</sub> intensity ratio of untreated to 2  $\mu\text{M}$  MS 40-48 hr. treatment was  $0.73 \pm 0.10$ , statistically insignificant from untreated cells. The H3K27me<sub>3</sub> intensity ratio of untreated to 2  $\mu\text{M}$  MS 40-48 hr. treatment was  $0.81 \pm 0.09$ , statistically insignificant from untreated cells. (E) Recorded doubling force for mitotic chromosomes from untreated and MS treated cells. The average chromosome doubling forces were  $320 \pm 30$  pN in untreated cells. The average doubling force was  $580 \pm 40$  pN in 2  $\mu\text{M}$  MS 40-48 hr. treated cells, a statistically significant increase of  $\sim 80\%$  compared to untreated cells. Error bars represent standard error. Asterisk in bar graphs represent a statistically significant difference ( $p < 0.05$ ). All p values were calculated via t test.

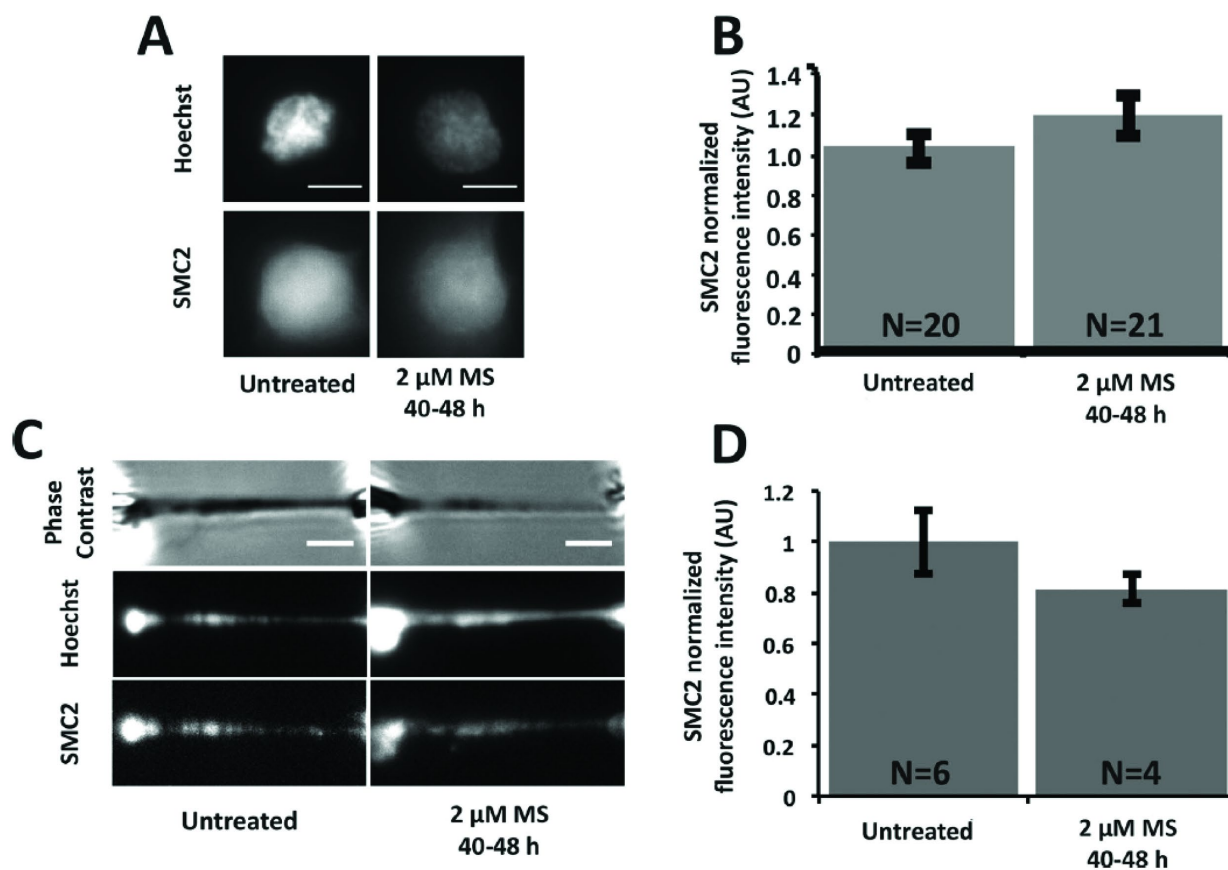


**Figure 3.7. Methylstat treatment does not cause a change in SMC2 fluorescent levels.** (A) Example representative images of levels of SMC2 fluorescence intensity on fixed mitotic cells. Scale bar is 10  $\mu$ m. (B) Quantitative data of (A). The SMC2 intensity ratio of untreated to 2  $\mu$ M MS 40-48 hr. treatment was  $1.1 \pm 0.1$ , statistically insignificant from untreated cells. (C) Example representative images of levels of SMC2 fluorescence on captured mitotic chromosomes. Scale bar is 5  $\mu$ m. (D) Quantitative data of (C). The SMC2 intensity ratio of untreated to 2  $\mu$ M MS 40-48 hr. treatment was  $0.82 \pm 0.05$ , statistically insignificant. All  $p$  values calculated via  $t$  test.

previously published reports (Akram et al., 2018; Fischle et al., 2005; Hirota et al., 2005; Serrano et al., 2009). By additional fluorescence imaging, we observed that HP1 $\alpha$ -AID-sfGFP is lost upon auxin-induced degradation (Fig. 3.8B,C). Thus, we confirmed that endogenous HP1 $\alpha$ -AID-sfGFP is associated with mitotic chromosome arms and pericentromeres, and it is degraded after 4 hr. of auxin treatment.

The mechanical role of HP1 $\alpha$  in mitotic chromosomes was investigated by micromanipulation force measurements. The isolated bundle of chromosomes was held by one micropipette while two additional micropipettes were used to capture and isolate a single chromosome (Fig. 3.8D). The single mitotic chromosome is then extended with the stiff pull pipette, while deflection of the other, much less stiff force pipette provides a force measurement, in the same manner as our other experiments (Fig. 3.8D). For each isolated chromosome, we calculated a force versus extension plot (Fig. 3.8D). Because each of the 23 human chromosomes is a unique length, we calculate a length-independent measurement by extrapolating the force-extension slope to determine the ‘doubling force’—the force at which the chromosome length would be doubled (i.e., force at 100% strain, Fig. 3.8E). Since the pipettes hold opposite ends of the chromosome, tension is distributed across the whole chromosome (Fig. 3.8D example images). Therefore, the resistive force measured includes contributions from chromatin, and thus HP1 $\alpha$ , in both the chromosome arms and the pericentromeric region.

We find that depletion of HP1 $\alpha$  reduced mitotic chromosome doubling force by approximately 40%, from  $262\pm 50$  pN in control cells (spring constant  $27$  pN/ $\mu$ m) to  $148\pm 12$  pN in auxin-treated cells ( $16$  pN/ $\mu$ m) ( $p=0.03$ , Fig. 3.8E), indicating that HP1 $\alpha$  significantly contributes to mitotic chromosome mechanics.

We next investigated whether histone methylation and the HP1 $\alpha$  protein separately govern chromosome mechanics during mitosis, as they do during interphase. Increasing histone methylation via methylstat treatment has previously been shown to play a critical role in mechanical stiffness of mitotic chromosomes (R. Biggs et al., 2019). Furthermore, evidence exists for direct biochemical interactions between epigenetic marks on nucleosomes, independent of mark-reading proteins such as HP1 $\alpha$  (Bilokapic et al., 2018; Zhiteneva et al., 2017). Thus, we aimed to determine whether histone methylation and HP1 $\alpha$  contribute independently to mitotic chromosome stiffness.

We treated cells with the histone demethylase inhibitor methylstat to increase levels of methylated histones in cells with or without HP1 $\alpha$ , controlled by the addition of auxin. Mitotic chromosomes isolated from cells treated with methylstat to increase methylated histone levels indeed show a significant, greater than 100% increase in doubling force from  $262\pm 50$  pN to  $745\pm 164$  pN ( $p=0.005$ , Fig. 3.8D,E), recapitulating previous results for HeLa cells (R. Biggs et al., 2019). Mitotic chromosomes isolated from cells treated with both methylstat to increase methylation and auxin to degrade HP1 $\alpha$  have a doubling force comparable to those treated with methylstat alone,  $452\pm 116$  pN ( $p=0.18$ , Fig. 3.8D,E). Oppositely, mitotic chromosomes from cells that were treated only with auxin compared to both auxin and methylstat had significantly different doubling forces ( $148$  vs.  $452$  pN,  $p=0.005$ ). The data suggest that histone methylation stiffens mitotic chromosomes independently of HP1 $\alpha$  and thus has a dominant role in determining mitotic chromosome mechanics. At the same time, we emphasize that HP1 $\alpha$  clearly plays a major role in mitotic chromosome mechanics in wild-type cells.

HP1 $\alpha$  depletion is known to lead to chromosomal instability, aberrant recombination, anaphase bridges, and lagging chromosomes (Chu et al., 2014). Therefore, HP1 $\alpha$ 's role in

metaphase chromosome mechanics may have functional importance during mitosis. To test this, we measured the percentage of mitotic cells with chromosome misalignment in metaphase or anaphase bridges during chromosome segregation in control, 4 hr., and 16 hr. auxin-treated HP1 $\alpha$ -degraded populations. HP1 $\alpha$  depletion resulted in significant increases in both metaphase misalignment, from 8% in control to 28% in auxin 4 hr. and 41% in auxin 16 hr. treatments, and mis-segregation as measured by ana/telophase bridges, from 15% to 28% in auxin 4 hr. and 50% in auxin 16 hr. treatments (all  $p < 0.05$ , Fig. 3.8F). Thus, loss of HP1 $\alpha$  disrupts chromosome mechanics and causes dysfunction in mitosis via chromosome misalignment and mis-segregation.

Abnormal mitosis has also been reported to disrupt nuclear morphology in the daughter cells (Gisselsson et al., 2001). Thus, we tracked cells treated without or with auxin for 24 hr. through mitosis to determine if abnormal mitosis resulted in abnormal nuclear morphology after mitosis. Abnormal mitosis in parental or untreated HP1 $\alpha$ -AID-sfGFP cells is rare, but it results in daughter cells with high nuclear curvatures (red dots, Fig. 3.8G). Cells with HP1 $\alpha$  degraded more frequently undergo abnormal mitosis (Fig. 3.8F,G). Interestingly, following both normal and abnormal mitosis, HP1 $\alpha$ -degraded daughter cells exhibit increased average nuclear curvature in G1, 4 hr. after mitosis (Fig. 3.8G). This data suggests abnormal mitosis upon HP1 $\alpha$  degradation may not be the primary cause of abnormal nuclear shape since normal mitosis under these conditions results in equally high curvature for daughter nuclei after mitosis (Fig. 3.8G). Taken together, HP1 $\alpha$  is necessary for proper mitotic chromosome mechanics and function, and its depletion results in abnormal mitosis and independently, abnormally shaped daughter interphase nuclei.

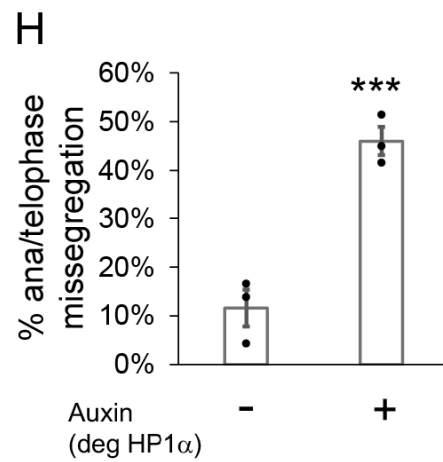
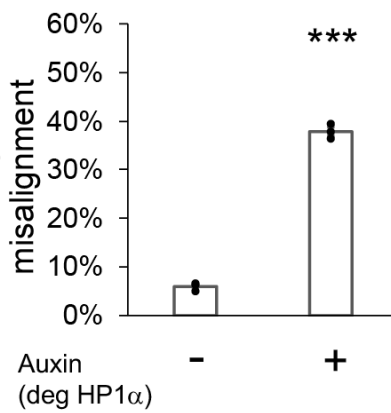
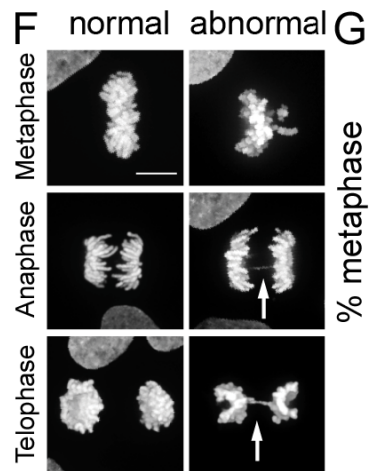
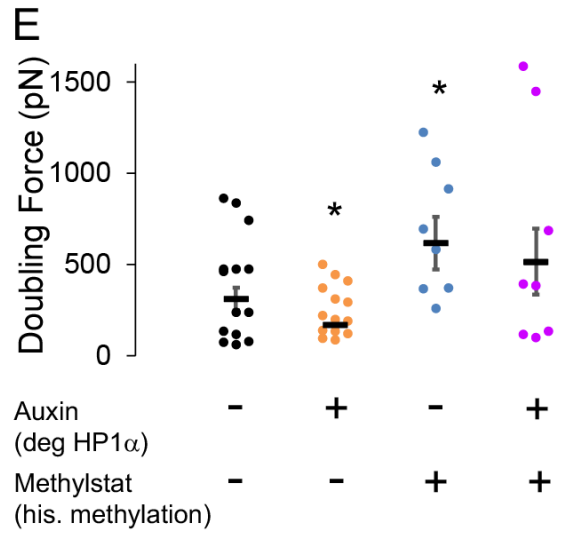
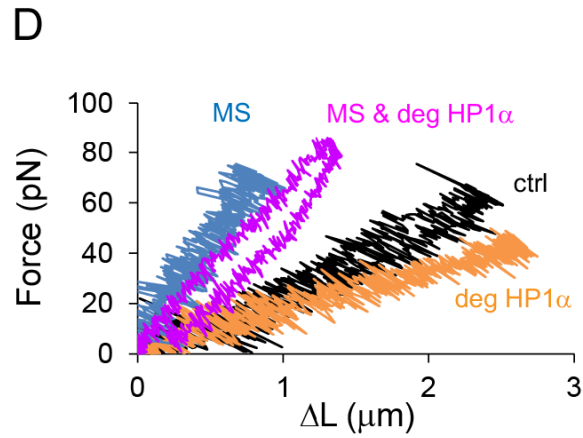
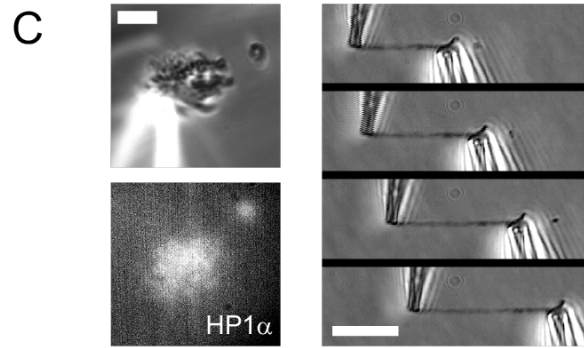
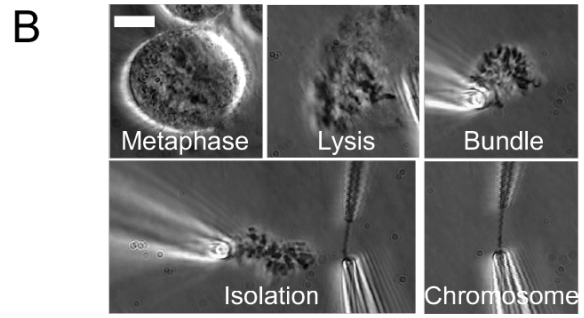
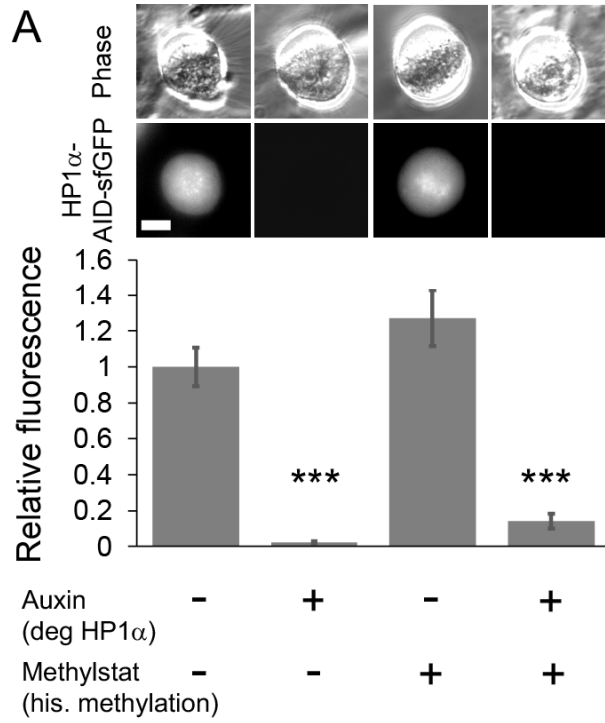


**Figure 3.7. HP1a is a mechanical component of the mitotic chromosome aiding proper segregation in mitosis.**

(A) Example image of the steps to isolating a mitotic chromosome from a live cell using micropipettes. Scale bar represents 10  $\mu\text{m}$ . (B) Representative live mitotic cells and isolated mitotic chromosome bundles imaged via phase contrast and HP1a-AID-sfGFP fluorescence intensity across treatments. Values calculated by measuring the cell's or chromosome bundle's fluorescence minus the background fluorescence, normalized to the average intensity of the untreated cellular HP1a fluorescent intensity. P Values reported as  $*** < 0.001$ , calculated by student's t-test. Scale bar represents 10  $\mu\text{m}$ . (C) Example images of the endogenous HP1a-AID-sfGFP fluorescence of an isolated mitotic bundle outside of the lysed cell. Yellow box denotes the area where the graphed line scan was drawn. The line scan reveals HP1a on chromosome arms. Scale bar represents 10  $\mu\text{m}$ . (D) Example images of a force-extension experiment. The right pipette pulls away from the left pipette, which stretches the chromosome and causes the left pipette to deflect. The left 'force' pipette has a premeasured bending constant (in pN/ $\mu\text{m}$ ) to calculate force. Left graph, example traces of force-extension experiments for the different conditions. Scale bar represents 10  $\mu\text{m}$ . (E) Graph of average doubling force (100% strain) in picoNewtons for each condition, which is determined by slope of the force extension traces and the initial chromosomes length. For B-E,  $n = 20$  for control and auxin treated,  $n = 16$  for methylstat, and  $n = 14$  auxin methylstat treated, p values calculated by student's t-test. (F) Example images of abnormal mitotic segregation via anaphase bridge or nondisjunction. Data in panels F and G not collected from personal data but included for its contribution and investigation in (Strom et al., 2021). Graphs of percentage of mitotic cells displaying abnormal metaphase misalignment (black bars) and anaphase/telophase missegregation (white bars) via presence of anaphase bridges or nondisjunction/aneuploidy in control untreated cells (-) or auxin-treated (+) cells for 4 or 16 hr. Metaphase misalignment three to four biological replicate experiments (black dots) consisting of  $n = 16, 15, 20, 37$ -aux,  $n = 33, 33, 24$  +aux 4 hr.,  $n = 22, 48, 58, 54$  +aux 16 hr. Anaphase and telophase missegregation 3–4 experiments (black dots) consisting of  $n = 29, 23, 30, 30$  -aux,  $n = 32, 29, 18$  +aux 4 hr.,  $n = 20, 35, 36, 45$  +aux 16 hr. p values reported as  $* < 0.05$ ,  $** < 0.01$ ,  $*** < 0.001$ ,  $**** < 0.0001$ , calculated by Student's t-test. Scale bar represents 20  $\mu\text{m}$ . (G) HP1a-AID-sfGFP cells - auxin or +auxin for 24 hr. were tracked through mitosis to determine if abnormal mitosis results in abnormally shaped daughter nuclei measured via nuclear curvature (parental 34 nuclei from 17 mitoses; -auxin 46 nuclei from 23 mitoses; +auxin 51 nuclei from 26 mitoses, p value from one-way ANOVA). Percentage of abnormal mitosis presented in Fig. 3.9. Error bars represent standard error. Scale bar represents 20  $\mu\text{m}$ .

### **3.4 Conclusions, discussion, and future directions**

#### **3.4.1 Histone PTM changes- original hypotheses and data analysis**

Our data show that increasing histone acetylation (specifically H3K9ac level) by HDACi treatment does not affect chromosome stiffness in mitosis (Fig. 3.4). Our original hypothesis had been that HDACi-induced histone hyperacetylation would weaken mitotic chromosomes. This hypothesis was based on the observations that histone acetylation is normally reduced in mitosis (Doenecke, 2014), and is thought to intrinsically affect nucleosome packing (Zhiteneva et al., 2017). Furthermore, we expected to see weaker mitotic chromosomes since interphase hyperacetylated chromatin is decompact (Doenecke, 2014) and hyperacetylating chromatin weakens the chromatin-dependent stiffness of interphase nuclei (Stephens et al., 2017; Stephens et al., 2018). However, our data indicate that mitotic chromosomes with hyperacetylated histones via HDACi treatment are overall just as stiff as mitotic chromosomes from untreated cells.

Unlike HDACi treatments, which do not change the doubling force of mitotic chromosomes, treatment by the HDMi MS causes increased histone methylation (assayed via H3K9 and H3K27 methylation) and a stiffer and likely denser mitotic chromosome without affecting SMC2 levels (Fig. 3.6, 3.7). These results support our original hypothesis that the increase of histone methylation and propensity of mitotic histones to condense would stiffen mitotic chromosome as observed for interphase nuclei (Stephens et al., 2017; Stephens et al., 2018), but contrast with our results involving mitotic hyperacetylated histones. Our data indicate that this stiffening is not due to overloading of condensin, which suggests other mechanisms/complexes may affect chromosomal stiffness.

### 3.4.2 Incorporating chromatin interactions into the model of mitotic chromosomes

To understand how chromatin may contribute to the overall stiffness of mitotic chromosomes, it is important to understand how mitotic chromosomes are organized. Early electron microscopy suggested that mitotic chromosomes are organized into loops of chromatin extending from a protein-rich core (Marsden & Laemmli, 1979). The currently heavily studied loop-extrusion model builds upon this classical bottlebrush model, describing how the bottlebrush is formed (Alipour & Marko, 2012; Gibcus et al., 2018; Goloborodko et al., 2016). In this model, chromatin loop-extruding complexes in the core of mitotic chromosomes create the bottlebrush structure. Non-histone chromatin-organizing complexes such as condensin and cohesin localize to the core of mitotic chromosomes and between sister chromatids, respectively (Ball & Yokomori, 2001; Piazza, Haering, & Rutkowska, 2013), which according to the model function as loop-extruding enzymes. A broadly similar model of extruded chromatin loops organized by the protein complexes condensin and cohesin has been used to describe the vertebrate and yeast centromere as a chromatin spring (Lawrimore et al., 2015; Ribeiro et al., 2009; Stephens et al., 2011).

We sought to incorporate the loop-extrusion model into the gel-network model of mitotic chromosomes. The gel-network model describes mitotic chromosomes as a gel of chromatin crosslinked by non-histone protein complexes, predominantly condensin (Fig. 3.10A) (M. G. Poirier & Marko, 2002b). There are two facets that govern the stiffness of a gel network: the density of crosslinks, and the pliability of the intervening cross-linked fibers (Gennes, 1979). Older work has shown that condensin is responsible for about half of the spring constant of the kinetochore (Ribeiro et al., 2009). Recent work has shown that condensin is approximately linearly correlated to the stiffness of mitotic chromosomes (M. Sun et al., 2018b), suggesting that

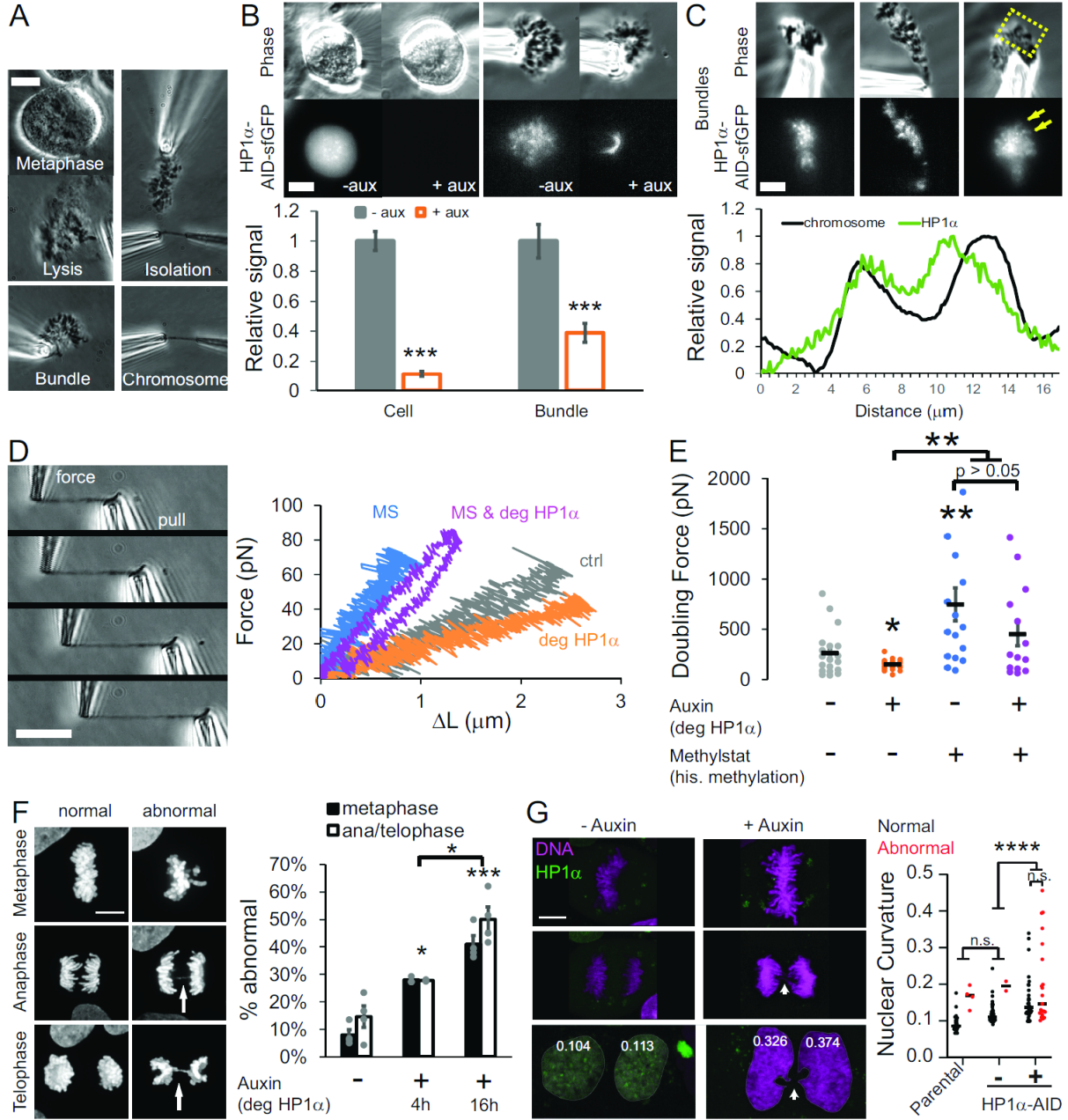


**Figure 3.8. HP1 $\alpha$ -AID-sfGFP displays cell and chromosome fluorescence and upon its degradation mitotic errors occur leading to higher curvature nuclei.**

(A) HP1 $\alpha$ -AID-sfGFP total fluorescence counts compared between mitotic cells and isolated mitotic chromosome bundles, which we imaged at 10-times the exposure time and same power, for untreated, auxin 4 hr., methylstat 2 days, and auxin +methylstat. Scale bar represents 10  $\mu$ m. (B) Example images of whole chromosomes decorated with HP1 $\alpha$ -AID-sfGFP in isolated chromosome bundles. Scale bar represents 10  $\mu$ m. (C) In vivo confocal imaging of HP1 $\alpha$ -AID-sfGFP relative to SiR-Hoechst labeling reveals pericentromeric foci concentration. Scale bar represents 10  $\mu$ m. (D) Tracking of the parental cell line, HP1 $\alpha$ -AID-sfGFP 24 hr. - auxin and +auxin-treated cells through mitosis for normal or abnormal behavior denoted by chromosome bridges (also reported in Fig. 3.8G). This data is analyzed from the same data as presented in main Fig. 3.8G, which shows nuclear curvature daughter nuclei. Data in panels C and D not collected from personal data but included for its contribution and investigation in (Strom et al., 2021).

most of the stiffness is governed by the chromatin loop-extruding elements, which are also apparently the primary crosslinking elements (Fig. 3.10A). Previous work has shown that DNA/chromatin constitutes the underlying connectivity of mitotic chromosomes, which makes up the underlying fiber (M. G. Poirier & Marko, 2002b; Sun et al., 2011). These data also show that the loop-extruding proteins cannot form a contiguous core. In considering mitotic chromosomes as a gel, condensins comprise the major crosslinks while chromatin forms the underlying fiber. Both the lack of change in stiffness when histones are hyperacetylated and the lack of increase in condensin levels on hypermethylated histones suggests that perturbing histone PTMs does not affect the number of primary, condensin-based crosslinks.

### **3.4.3 Understanding the implications of increased methylation stiffening mitotic chromosomes and lack of effect from hyperacetylation**

Since hyperacetylation of histones through HDACi treatments does not affect the stiffness of mitotic chromosomes, it cannot affect the number of crosslinks or the ability of the chromatin fiber to be stretched. This contrasts with interphase, where hyperacetylation weakens chromatin-based nuclear stiffness (Stephens et al., 2017; Stephens et al., 2018). This difference may be due to a lack of transcription in mitosis, acetyl-histone readers in mitosis, or other cell-cycle-dependent factors. These factors could actively decompact chromatin in interphase nuclei, but not in mitosis (Doenecke, 2014; F. Wang & Higgins, 2013). Furthermore, histone acetylation is drastically decreased in mitosis meaning that the effect of increased histone acetylation via HDACi may be negligible for metaphase chromosomes. While a decrease in acetylation in mitosis coincides with a higher degree of compaction (Zhiteneva et al., 2017), it appears that the increased acetylation of histones caused by our treatments with HDACis does not have an intrinsic effect on metaphase chromosome stiffness.

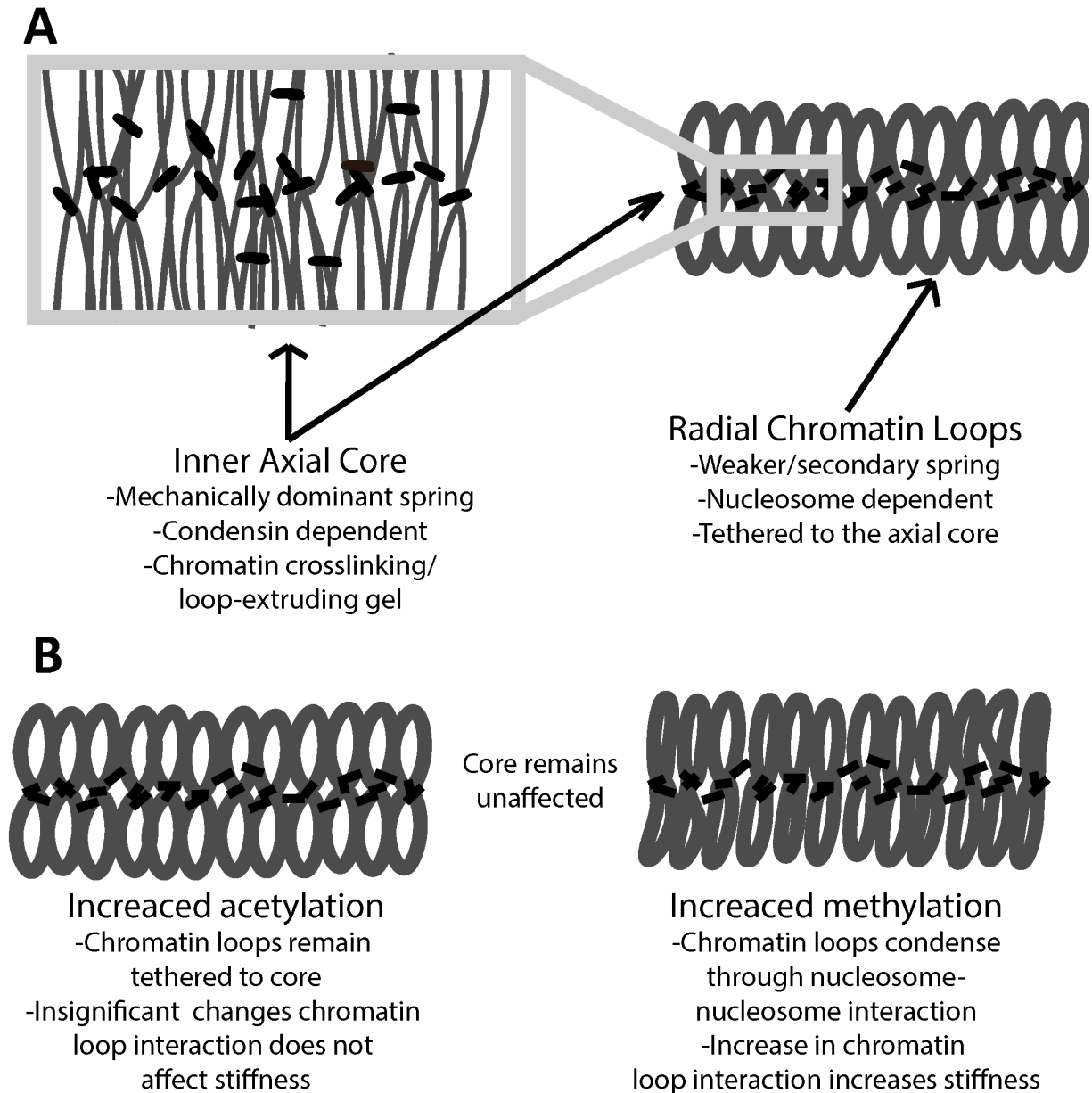
Our data suggest that hypermethylation of histones does affect mitotic chromosome structure, given the increased doubling force. Nucleosome-nucleosome interactions can stiffen mitotic chromosomes by either forming additional weaker crosslinks or the chromatin fibers themselves could become harder to stretch (Fig. 3.10B). Neither of these hypotheses necessarily affect the primary crosslinkers, condensins. These two hypotheses are not mutually exclusive, although future experiments may be able to determine which of them is predominantly true. Further chromosome-manipulation experiments of the sort presented in this paper should be able to determine precisely which PTMs are responsible for the structural changes, as well as elucidate if the changes in chromosome mechanics we have observed are achieved by histones alone or if they require other proteins for their mediation.

#### **3.4.4 Analysis of HP1 $\alpha$ affects mitotic chromosome stiffness**

Mechanical components of interphase chromatin may remain attached to mitotic chromosomes to maintain the mechanical strength of chromosomes during mitosis. Recent work has shown that heterochromatin-based histone modifications/methylation also control the mechanical strength of chromosomes, while euchromatin-based histone acetylation does not (R. Biggs et al., 2019). That paper hypothesized that increased histone methylation could be aided by ‘histone reader’ heterochromatin-associated proteins, specifically HP1 $\alpha$ . Our data reveal that, like HP1 $\alpha$  in interphase nuclei, HP1 $\alpha$  during mitosis is a significant mechanical component of the mitotic chromosome (Fig. 3.8). HP1 $\alpha$  degradation leads to more extensible mitotic chromosomes, but the stiffness can be recovered by hypermethylation via methylstat treatment. The fact that HP1 $\alpha$  still provides mechanical stiffness in mitotic chromosomes, a chromatin-only system without lamins, further supports that HP1 $\alpha$  mechanically functions as a chromatin crosslinker. Previous work has proposed that mitotic chromosomes are dense polymer gels based

on their elastic response, which relies on the continuity of the DNA backbone (M. G. Poirier & Marko, 2002b), topology (Kawamura et al., 2010), and the chromatin cross-bridging condensin protein complex (M. Sun et al., 2018b). Our experiments implicating HP1 $\alpha$  as a crosslinking element (in interphase) and measuring the mechanical contributions of HP1 $\alpha$  in mitotic chromosomes further support this picture. Methylation could serve as an additional compaction agent by providing further crosslinking, stiffening the chromatin fiber itself, or generating poor solvent conditions that further compact mitotic chromosomes (Batty & Gerlich, 2019; Gibcus et al., 2018; Maeshima et al., 2018). Together, these components generate the rigidity necessary for robust mitotic chromosomes.

Loss of HP1 $\alpha$  results in dysfunction, marked by improper chromosome alignment and segregation. Previous reports had noted that loss of HP1 $\alpha$  and HP1 $\gamma$ , specifically at the centromere, causes increased incidence of chromatin bridges (Y. H. Lee, Kuo, Stark, Shih, & Ann, 2013) and mitotic alignment errors (Yi et al., 2018), genetic deletion of HP1 $\alpha$  increases merotelic and syntelic attachments (Bosch-Presegue et al., 2017), and mitosis is dependent on HP1 $\alpha$  phosphorylation (Chakraborty, Prasanth, & Prasanth, 2014). Our findings with rapid degradation of HP1 $\alpha$  reveal a threefold increase in both misalignment and missegregation, which were mostly observed as anaphase bridges, which could be due, in part, to aberrant DNA damage repair (Chiolo et al., 2011; Peng & Karpen, 2007). Our results agree with HP1 $\alpha$  interacting with LRIF1 at the centromere, which when perturbed results in similar misalignment and missegregation (Akram et al., 2018). However, further work is required to determine if chromosome misalignment is due to a biochemical pathway or mechanical pathway where whole-chromosome mechanics controlled by HP1 $\alpha$  influences proper segregation.



(A) Gel based model of mitotic chromosomes, demonstrating the crosslinking elements as condensin and the intervening fibers as chromatin. This model is compatible with different models of mitotic chromosomes including the loop-extrusion model, in which condensin can act both as a crosslinking element and the loop-extruding element. (B) Methods on which changes to the chromatin fiber or interactions of the chromatin fiber can stiffen a gel network. These models are not mutually exclusive and can be used to describe how increased histone methylation introduces an increase in stiffness to mitotic chromosomes. Neither of these effects are changed when histones are hyperacetylated in mitosis.

### 3.4.5 Investigations into how chromatin could affect mitotic chromosome stiffness

Most of the work on the relation between histone PTMs and chromatin structure focuses on histone readers, but histone PTMs themselves may be intrinsically responsible for the stiffness change. It has been shown that chromatin reconstituted from mitotic histones aggregates more than chromatin reconstituted from interphase histones (Zhiteneva et al., 2017). This analysis indicates that histone methylation is coupled to the structure and mechanics of mitotic chromosomes, in that a 3.4-fold increase in methylation is associated with an 80% increase in chromosome stiffness. This change in intrinsic condensation tendency may be facilitated by direct nucleosome-nucleosome interactions due to histone tails in the manner observed by (Bilokapic et al., 2018). Our data suggest that the potential increase of histone methylation, rather than decreased acetylation, contributes to tighter packing of nucleosomes during mitosis.

One must keep in mind that the metaphase chromosome, while organized as a chromatin gel, likely has an underlying radial-loop architecture, with an excess of condensin crosslinkers near the central chromatin “axes” (sketched in Fig. 3.6A). It is conceivable that weak, multivalent attractions between nucleosomes, such as those that might be mediated by methylated histone tails, could drive compaction of the denser axial region of metaphase chromatids without generating adhesion between the outer, less dense radial loop “halos”. Uncontrolled adhesion between nucleosomes must be avoided: once individual nucleosomes adhere to one another, the whole genome will stick together and form a droplet, a situation incompatible with chromosome segregation (Marko & Siggia, 1997). Multivalency could be a key ingredient, as it can permit a rapid “turn-on” of inter-nucleosome attraction with local nucleosome concentration, allowing the relatively weak loop-extrusion-compaction by condensins to compact the axial region sufficiently so that attractions turn on there, but not in the

less dense loop halo. This scenario could explain how metaphase chromatids end up being dense in their axial interior while retaining mutually repulsive loop-halo exteriors, thus simultaneously achieving strong chromatin compaction while facilitating chromosome individualization, sister chromatid resolution, and making the overall mechanics of metaphase chromosomes sensitive to additional nucleosome attractions associated with specific PTMs.

In addition to the methylation of histones, the increase in stiffness of mitotic chromosomes and the stickiness of the underlying chromatin could be due to an increase in HP1 $\alpha$ 's binding. Previous analysis of histone PTM presumed a near complete release of HP1 $\alpha$  from chromosome arms, which would then have no influence on the chromatin structure. However, our newer results show that HP1 $\alpha$  remains on mitotic chromosomes and plays a significant role on mechanics. Since HP1 $\alpha$  is a chromatin crosslinker, since it can dimerize, bind methylated histones, and bind DNA, the crosslinking of chromatin makes it an obvious candidate of demonstrating the role chromatin crosslinking plays in stiffening the mitotic chromosome. It also emphasizes the similarity that chromatin stiffness changes through the cell cycle. These experiments also found that our technique could demonstrate differences in chromosome isolation compared to other techniques, which will further assist our understanding of mitotic chromatin and proteins associated with mitotic chromosome formation.

**Chapter 4. Micromanipulation of prophase I chromosomes from mouse spermatocytes  
reveals high stiffness and gel-like chromatin organization**

*This chapter has been adapted from my publication in Communications Biology (R. J. Biggs et al., 2020). All experiments and diagrams performed and created by myself except Fig. 4.1 and 4.6, credit given in Figure legends.*

Both mitotic and meiotic chromosome formation involves folding and organizing interphase chromatin into organized, compact, individualized, and paired chromosomes. Meiotic and mitotic chromosomes undergo similar phases of chromosomal reorganization, but the meiotic process goes through two cycles of division after one round of genomic duplication. Since meiotic chromosomes take the form of compact, thread-like objects, they can also be isolated and manipulated to probe their underlying structure and mechanics. In this chapter, we demonstrate the ability to isolate prophase I meiotic chromosomes from mouse spermatocytes. We find that meiotic chromosomes are substantially stiffer than the cell culture mitotic chromosomes but do behave like mitotic chromosomes when treated with nuclease and protease. This is surprising considering the presence of the protein-based synaptonemal complex which pairs replicated chromosomes together into a chromatid tetrad during meiotic prophase I. Furthermore, loss-of-function mutations of key synaptonemal complex proteins have little effect on meiotic chromosome mechanics.

#### **4.1 Overview**

Mitosis and meiosis are two forms of cell division that separate chromosomes, but whose purpose and mechanism of cell division are distinct. The underlying structures of mitotic and meiotic chromosomes are also distinct. One of the most obvious differences between mitosis and meiosis is the construction of the synaptonemal complex (SC) in meiotic prophase I (Fraune et al., 2012; Hassold & Hunt, 2001). The SC is a large, tripartite, protein-based lattice, which may act as a mechanically rigid structure to keep the homologous chromosomes close to pair them together (Ivanovska & Orr-Weaver, 2006; Schucker et al., 2015; Zickler & Kleckner, 1999). Through the substages of meiosis prophase I, the SC undergoes its initial formation in Leptotene,

an initial bridging (or synapsis) of homologous chromosomes in Zygotene, a completion of synapsis in Pachytene, and desynapsis in Diplotene, where the SC remains bridging the homologous chromosomes at the centromere and chiasma, the point of crossover (Bisig et al., 2012; Bolcun-Filas & Schimenti, 2012; Fraune et al., 2012; Garcia-Cruz et al., 2010; J. Lee & Hirano, 2011; Rong et al., 2016). The initial construction of the SC is facilitated by the lateral elements, SYnaptonemal Complex Protein 2 and 3 (SYCP2 and 3), while the bridging is facilitated by SYCP1 binding to itself and the lateral elements (Fraune et al., 2012; Gao & Colaiacovo, 2018; Schucker et al., 2015). The highly structured SC, its components, and the underlying chromatin have also been shown to be highly dynamic objects (Cobb & Handel, 1998; Enguita-Marruedo et al., 2018; Pattabiraman et al., 2017; Rog et al., 2017).

Another structural difference between mitosis and meiosis is the pairing of homologous chromosomes together in prophase I (Gray & Cohen, 2016; Liebe, Alsheimer, Hoog, Benavente, & Scherthan, 2004). Sister chromatids are paired before homologous chromosome pairing in prophase I and remain paired until they are separated during meiosis II. The four-chromatid structure (two sisters paired with two homologues) is called a bivalent (Berrios, 2017; Garcia-Cruz et al., 2010; Zickler & Kleckner, 1999). This pairing is done in part to separate the homologues, but also to facilitate genetic recombination (Kouznetsova et al., 2011; Pattabiraman et al., 2017). The SC may also assist in keeping the homologous chromosomes close and thus facilitate recombination (Kouznetsova et al., 2011; Rog et al., 2017). The exchange of genetic material in meiosis I is a prerequisite for the proper separation of homologous chromosomes in meiosis I (Cobb & Handel, 1998; Pattabiraman et al., 2017). Meiotic chromosomes also appear to limit the number of crossovers, typically at least once per chromosome, but usually at a set distance (Gray & Cohen, 2016; Kleckner et al., 2004; S. Wang et al., 2015; L. Zhang, Liang, et

al., 2014; L. Zhang, Wang, et al., 2014). This limitation is known as crossover interference (CI). While there is still much debate concerning how CI functions, one hypothesis suggests that the chromosome contains distinct “beam” and “film” domains, with chromatin dynamics along the beam causing stress fractures in the film allowing the homologous chromosomes to cross over (Kleckner et al., 2004; L. Zhang, Liang, et al., 2014). The fracture in the film also causes stress reduction in the beam, limiting where another stress fracture can occur (Kleckner et al., 2004; L. Zhang, Liang, et al., 2014).

The initial chromosome organizing complexes are also different between mitotic prometaphase and meiotic prophase I chromosomes. The Structural Maintenance of Chromosome (SMC) complex condensin is responsible for most of the morphology and stiffness of mitotic chromosomes (Bolcun-Filas & Schimenti, 2012; M. Sun et al., 2018b; Takagi et al., 2018). Meanwhile, condensin’s sister complex, cohesin, pairs sister chromosomes together, but is removed from the arms in mitotic prometaphase, remaining predominately at the centromere (Lawrimore et al., 2018; Mirkovic & Oliveira, 2017). Meiotic prophase I chromosomes on the other hand have much less condensin, which is utilized later (Ivanovska & Orr-Weaver, 2006; J. Lee, 2017; J. Lee & Hirano, 2011). Meiotic prophase I chromosomes construct their base organization using cohesin, which also participates in sister pairing, homologous pairing, the construction of the SC, and crossover formation (Garcia-Cruz et al., 2010; Kouznetsova et al., 2011; J. Lee, 2017; J. Lee & Hirano, 2011; Rong et al., 2016). This base structure is known as the cohesin core. The lateral elements of the SC will form on top of the cohesin core (Garcia-Cruz et al., 2010; Kouznetsova et al., 2011; Rong et al., 2016).

Since mitotic prometaphase and meiotic prophase I chromosomes have many structural differences, we developed a technique to physically capture and manipulate them to study their

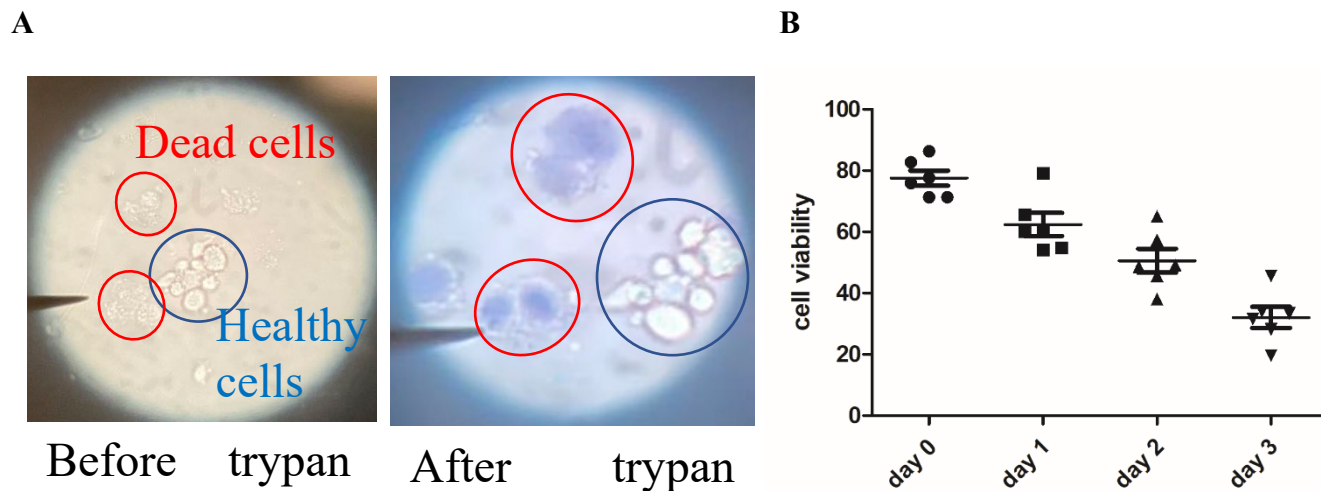


**Figure 4.1. Trypan cell viability assay.**

(A) Trypan invades dead cells without an intact cell membrane but is excluded from living cells. Brightfield image of the field of view is corresponding with the trypan imaging to demonstrate difference of living and dead cells. Data in panels A and B not collected from personal data but included for its contribution and investigation in Biggs et al 2019, experiments performed by Ning Liu. (B) Quantification of spermatocyte cell viability over time, start point of day testes extracted.

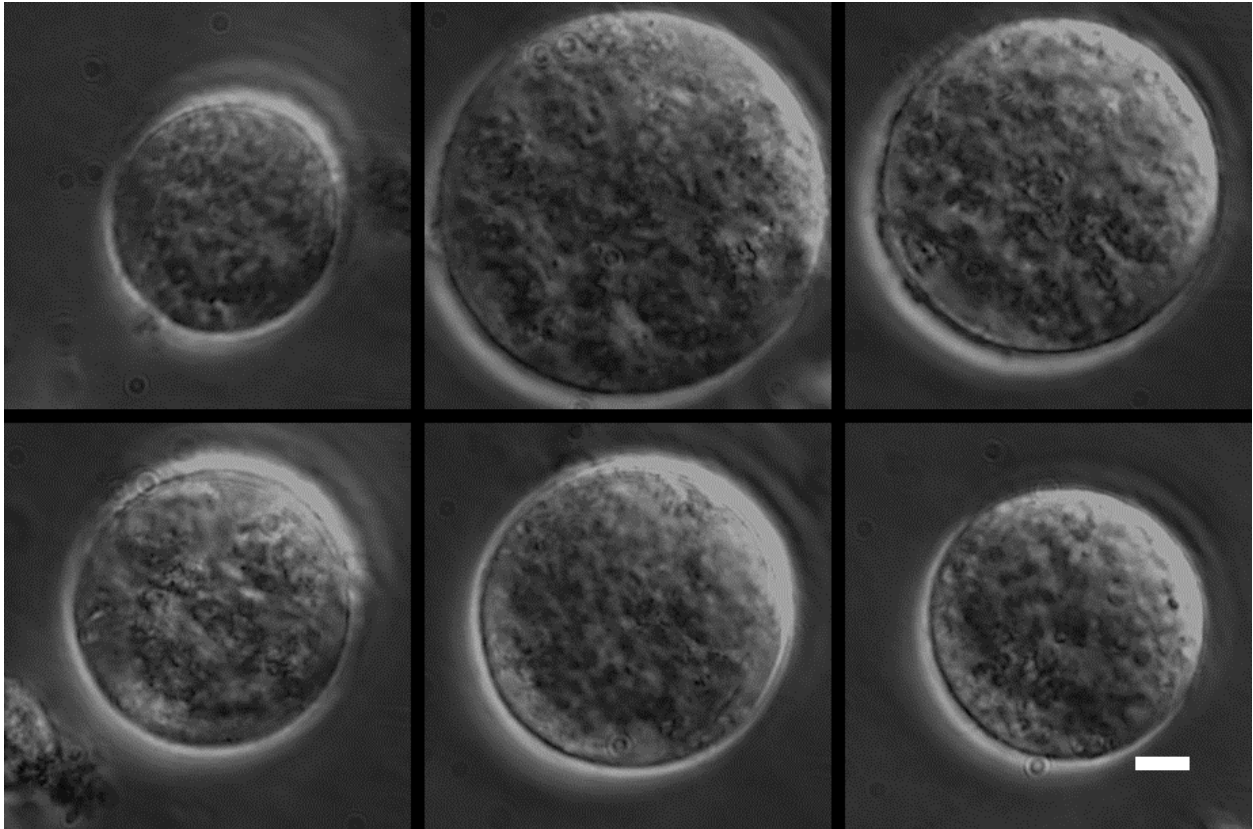


**Figure 4.2. Example images of wild-type (*Sycp1*<sup>+/+</sup>) meiotic cells before nuclei extraction.** Example of the *Sycp1*<sup>+/+</sup> meiotic cells with intact cell membrane before isolation where the chromosomes were extracted. Scale bar represents 5 $\mu$ m.

differences in connectivity and mechanical properties, relevant to their hypothesized dynamic nature and mechanobiological function. This approach has been used to investigate newt mitotic chromosomes, human mitotic chromosomes, and female mouse meiotic II chromosomes (Hornick et al., 2015; Kawamura et al., 2010; M. G. Poirier & Marko, 2002b; M. Sun et al., 2018b; Sun et al., 2011). Our research has found a way to capture and manipulate meiotic chromosomes from meiotic prophase I nuclei and perform similar tests on their structure and mechanics. Due to the fundamental role of SYCP1 in the maturation of the SC and its ability to bridge homologues with synapsis, we decided to test if there was a mechanical difference between WT and null mutant *Sycp1*<sup>-/-</sup> spermatocytes.

#### 4.2 Materials and methods

Mouse testes were extracted from adult mice with or without the SYCP1 null mutation and sent on ice to be dissected for extraction of spermatocytes containing meiotic prophase I cells for chromosome isolation. The testes would be kept in PBS or DMEM at 4°C for up to 3 days, after which the cells would appear damaged and the chromosomes not suitable for isolation. Spermatocyte samples were extracted from the testes by cutting at the surface of the testes (to maximize the number of meiosis I spermatocytes) in ~150 µL PBS and put into a well containing ~1.5 mL PBS for single chromosome isolation.

Viability tests were performed using Trypan Blue on cells kept for 0-4 days. While there is a marked decrease in cells that prohibit the entrance of Trypan Blue over time, indicating viable cells, there are still many cells that exhibit normal Trypan Blue exclusion (Fig. 4.1). In our experiments, we verified that the cell had a normal and intact cell membrane phenotype, a

rounded cell that dissolved when sprayed with the Triton-PBS solution. All the cells were imaged for documentation for this visualization, examples shown in Fig. 4.2.

Experiments on mitotic cell used mouse embryonic fibroblast (MEF) cells, which were maintained in DMEM (Corning) with 10% fetal bovine serum (FBS) (HyClone) and 1% 100x penicillin streptomycin (Corning). The cells were incubated at 37°C and 5% CO<sub>2</sub> for no more than 30 generations, passaged every 2-4 days. The cells were plated and allowed to recover 1-3 days before chromosome isolation (Fig. 4.3B). All mitotic cells performed in free-cycling cells and mitotic cells were identified by eye without drugs.

#### **4.2.2 Single chromosome isolation: Setup and microscopy.**

Single chromosome isolation experiments used an inverted microscope (IX-70; Olympus) with a 60x 1.42 NA oil immersion objective with a 1.5x magnification pullout at room temperature and atmospheric CO<sub>2</sub> levels. Experiments were performed in less than 3 hours after removal from the 4°C refrigerator (meiotic spermatocytes) or 37°C incubator (MEF cells) to ensure minimum damage to the cells and chromosomes being analyzed.

Meiotic prophase I (spermatocytes) and prometaphase (MEF) cells were identified by eye and lysed with 0.05% Triton-X 100 in PBS (Fig. 4.3A,B top left and middle panels). All other pipettes were filled with PBS. After lysis, the meiotic nuclei or mitotic bundle were held with a pipette (Fig. 4.3A,B top right panels). One end of a loose chromosome was grabbed by the force pipette, moved from the nuclei or bundle, and grabbed with the pulling pipette on the other end (Fig. 4.3A,B bottom left panels). The nuclei or bundle was then removed to isolate the chromosome (Fig. 4.3Avi; 4.3Bv).

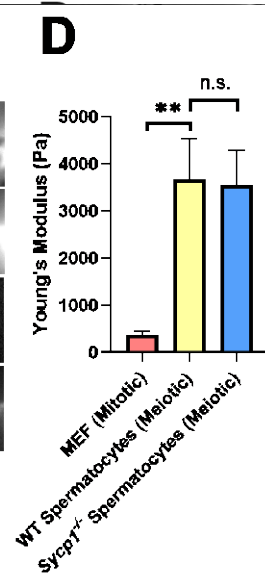
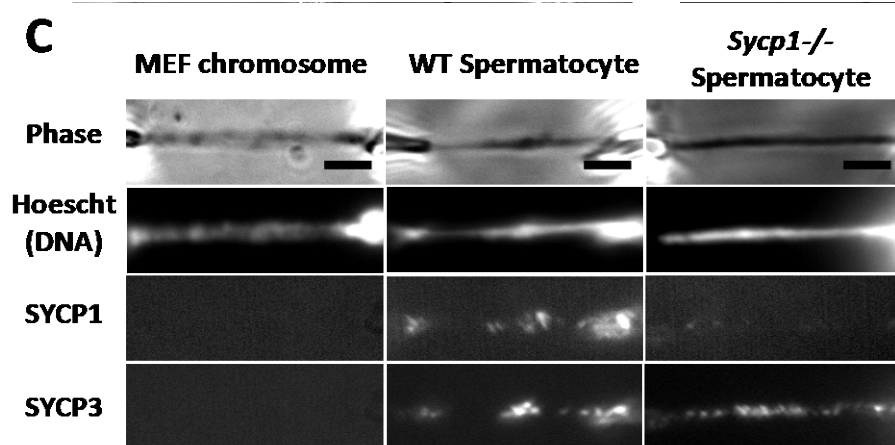
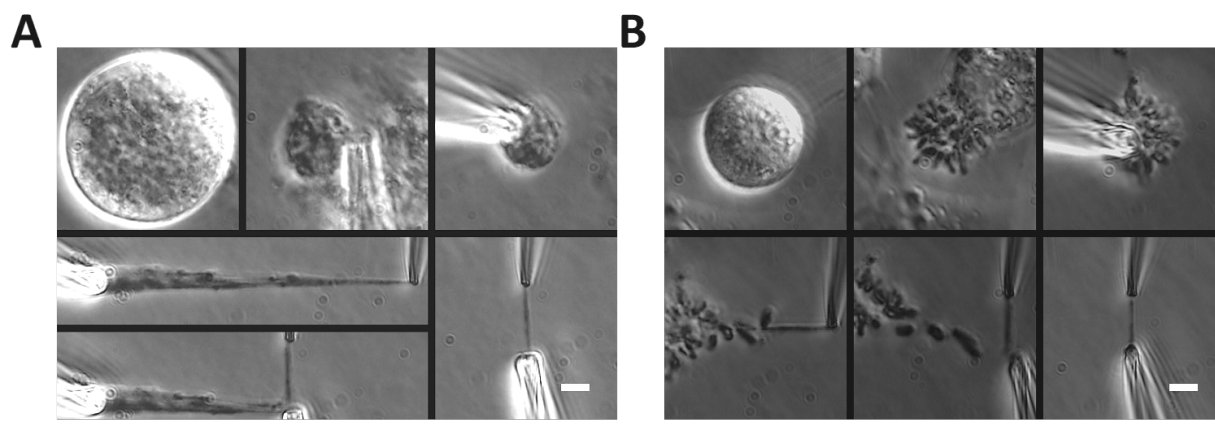
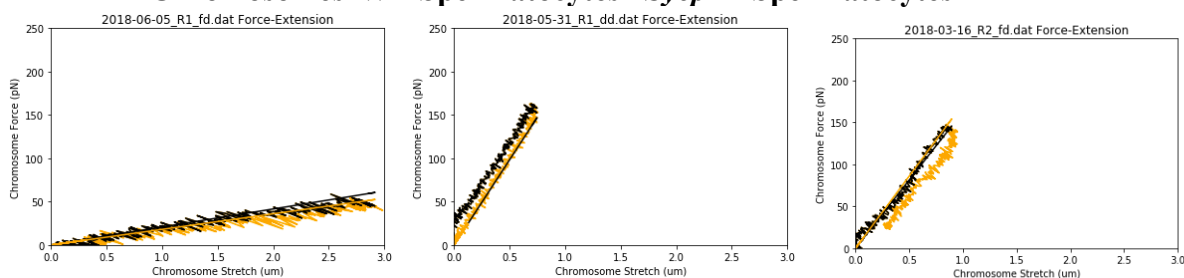


**Figure 4.3. Setup for micromanipulation experiments and chromosome isolation.**

(A) Representative images for isolating a meiotic chromosome. A large cell with thick lines (chromosomes) was identified (top left panel), lysed with Triton-100X in a pipette to release the prophase nucleus (top middle panel), upon which another pipette would grab and hold the prophase nucleus (top right panel). A chromosome end at the edge of the prophase nucleus would then be grabbed with a thin, force pipette (middle long panel), grabbed on the other end with a stiff pull pipette (bottom long panel), and then the prophase nucleus would be removed, leaving only the prophase chromosome isolated from the prophase nucleus (bottom right panel). Scale bar represents 5  $\mu\text{m}$ . (B) Representative images for isolating a mitotic chromosome. A rounded cell with defined lines (chromosomes), but not in a straight line (metaphase plate alignment) would be identified (top left panel), lysed with Triton-100X in a pipette to release the prometaphase mitotic bundle (top middle panel), upon which another pipette would grab and hold the bundle (top right panel). A chromosome end at the edge of the bundle would then be grabbed with a thin, force pipette and moved away from the bundle (bottom left panel), where the other end of the chromosome would be grabbed into a stiff, pull pipette (bottom middle panel), and the bundle would be removed to leave the chromosome isolated between the two pipettes (bottom right panel). Scale bar represents 5  $\mu\text{m}$ . (C) Staining of mitotic MEF chromosomes, WT and Sycp1 null mutant meiotic chromosomes with Hoechst (DNA), SYCP1, and SYCP3 (fluorescent by a secondary fluorophore) with a corresponding phase-contrast image. MEF chromosomes appear as rod-like structures in the phase-contrast channel that stain for DNA, but neither SYCP1 nor SYCP3. WT spermatocyte chromosomes appear as rod-like structures in the phase-contrast channel that stain for DNA, SYCP1, and SYCP3. Sycp1<sup>-/-</sup> spermatocyte chromosomes stain for DNA and SYCP3, but not SYCP1. Scale bar represents 5  $\mu\text{m}$ . (D) Stiffness of mitotic and meiotic chromosomes, reported as Young's Modulus. MEF chromosomes show a statistically significant difference between WT and Sycp1<sup>-/-</sup> spermatocyte chromosomes, while WT and Sycp1<sup>-/-</sup> mutant spermatocyte chromosomes do not show a statistically significant difference. MEF chromosomes had an average Young's modulus of  $370 \pm 70$  Pascals (Pa) over 10 chromosomes. Meiotic WT spermatocyte chromosomes had an average Young's modulus of  $3670 \pm 840$  Pa over 17 chromosomes. Meiotic Sycp1<sup>-/-</sup> mutant chromosomes had an average Young's modulus of  $3550 \pm 700$  Pa over 8 chromosomes. All averages reported as mean value  $\pm$  SEM. All p values calculated via t test.

### A MEF Chromosomes WT Spermatocytes *Sycp1*<sup>-/-</sup> Spermatocytes



### B

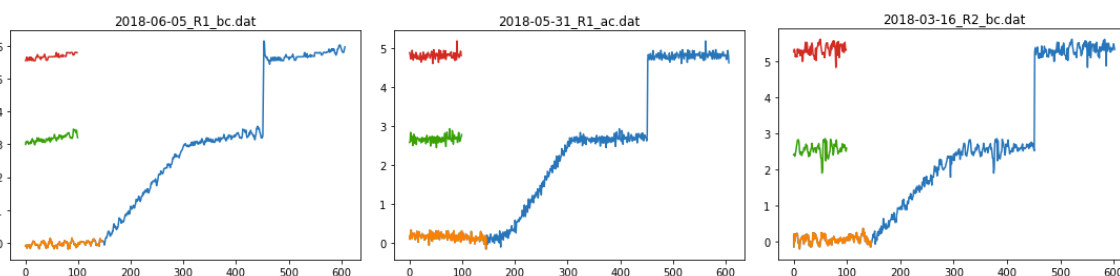


**Figure 4.4. Example Force-Extension plots and corresponding calibration plots.**

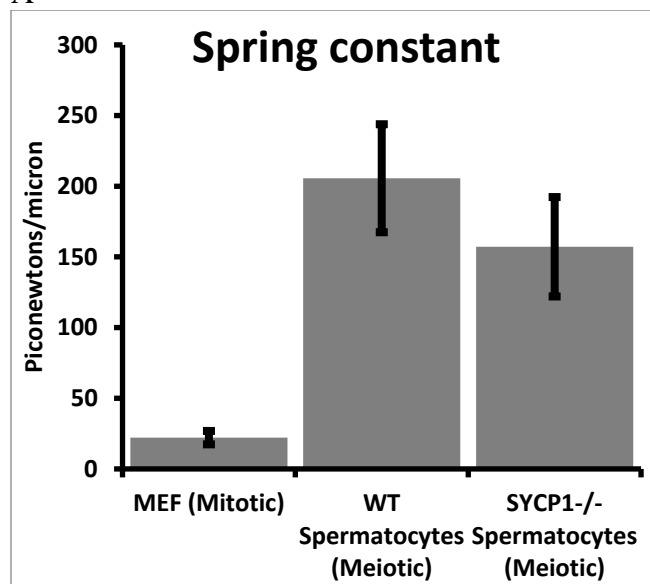
(A) Representative Force-Extension plot for mitotic MEF, meiotic wild-type, and *Sycp1*<sup>-/-</sup> mutant chromosomes, respectively (left to right). The black lines trace the outgoing trace and linear regression slope, while the orange lines track the return trace and return linear regression slope. (B) Example trace of a force pipette calibration against the same calibration standard pipette. The orange trace shows the original position of the pipette. The green trace shows the position when the calibration pipette was moved but held back by the unknown force pipette stiffness. The red trace shows the full deflection of the calibration pipette. The blue trace shows the position of the calibration pipette over the entire run.

### 4.2.3 Single chromosome isolation: Force measurement.

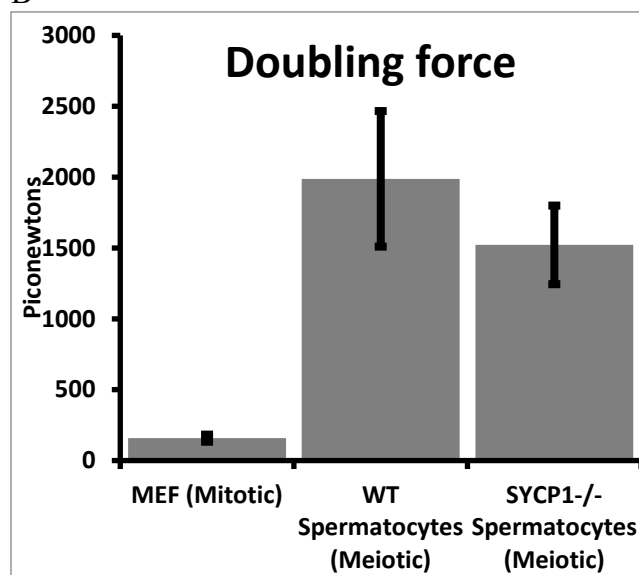
An easily bendable force pipette (WPI TW100F-6), and stiff pulling pipette (WPI TW100-6) were used for stretching chromosomes, forged using a micropipette puller (Sutter P-97) and a custom pipette cutting setup. Once isolated, the pipettes were moved perpendicular to the chromosome, stretching the chromosome to roughly its native length. The stiff pipette was then moved 6.0  $\mu\text{m}$  and returned to the starting position at a constant rate of 0.20  $\mu\text{m}/\text{sec}$  in 0.04  $\mu\text{m}$  steps in a LabVIEW protocol, while it tracked the stiff and force pipette. Refer to Fig. 4.4 for an example of force-extension trace. The deflection of the force pipette multiplied by its calibrated spring constant then divided by the distance between the pipettes (the stretch) was used to obtain the chromosome spring constant. The chromosome spring constant multiplied by its initial length gave the doubling force. Cross-sectional area was estimated as  $\pi r^2/2$ . The diameter was calculated as the full width at half maximum of an ImageJ scan. All other physical measurements taken (chromosomal doubling force, spring constant, initial length, and cross-sectional area) reported and shown in Fig. 4.5.

Young's/elastic moduli is defined as stress/strain and can be calculated with the formula  $E = (F/A) / (\Delta L/L_0)$ , where E is the Young's modulus, F is the force the object is under, A is the cross-sectional area,  $\Delta L$  is the change in length from  $L_0$ , which is the initial, unstretched length of the object. Rearranged, the Young's modulus can also be written as  $E = K * L_0 / A$ , where K is the spring constant of the object ( $F/\Delta L$ ). Our calculations in bulk are thus: the linear regression of the deflection-stretch line, multiplied by the force pipette spring constant, multiplied by the initial length, and divided by the cross-sectional area of the chromosome. See Fig. 4.4 for representative images for the linear regression line of the force-extension graph.

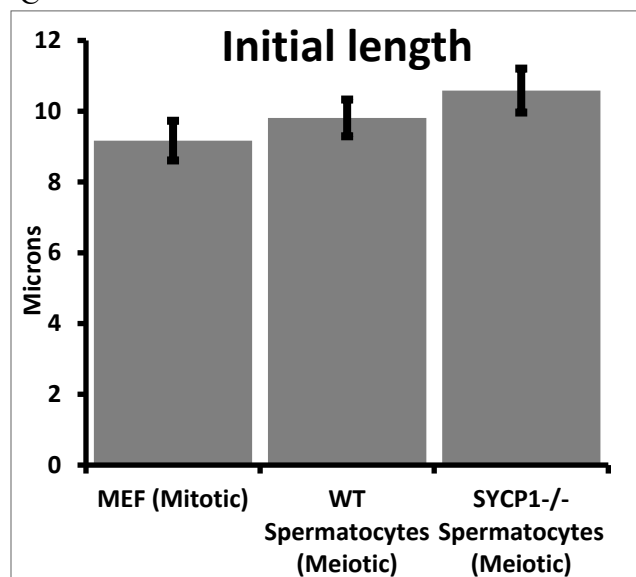
A



B



C



D

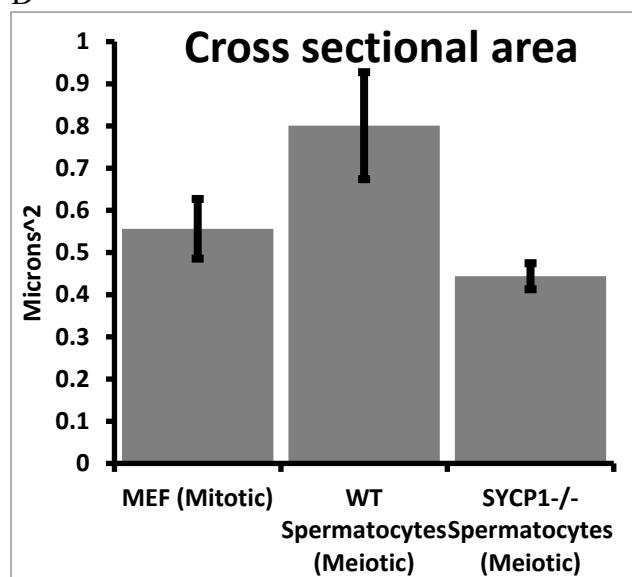


**Figure 4.5. Additional physical measurements of mitotic and meiotic chromosomes.**

(A) Spring constant distribution of chromosomes (the force it takes to stretch a chromosome a micron). Chromosomes from MEF culture cells have a Spring Constant of  $22 \pm 5$  pN/ $\mu$ m, WT Spermatocytes of  $206 \pm 38$  pN/ $\mu$ m, Sycp1<sup>-/-</sup> spermatocytes  $157 \pm 35$  pN/ $\mu$ m. MEF chromosomes were statistically significantly different from the spermatocytes, while the spermatocytes were not significantly different from each other. (B) Doubling force distribution of chromosomes (the force required to stretch the chromosome twice its initial length). Chromosomes from MEF culture cells have a Doubling Force of  $190 \pm 40$  pN, WT Spermatocytes of  $2130 \pm 440$  pN, Sycp1<sup>-/-</sup> spermatocytes  $1520 \pm 280$  pN. MEF chromosomes were statistically significantly different from the spermatocytes, while the spermatocytes were not significantly different from each other. (C). Initial length distribution of chromosomes (the length of the chromosome unstretched/at rest/isolated from the cell). Chromosomes from MEF culture cells have an Initial Length of  $9.2 \pm 0.5$   $\mu$ m, WT Spermatocytes of  $9.9 \pm 0.5$   $\mu$ m, Sycp1<sup>-/-</sup> spermatocytes  $10.6 \pm 0.6$   $\mu$ m. All groups were not significantly different from each other. (D) Cross sectional area distribution of chromosomes (the area of the chromosome thickness, estimated as the area of a cylinder using the full width at half maximum derived from a line scan in ImageJ). Chromosomes from MEF culture cells have an area of  $0.55 \pm 0.06$   $\mu$ m<sup>2</sup>, WT Spermatocytes of  $0.74 \pm 0.12$   $\mu$ m<sup>2</sup>, Sycp1<sup>-/-</sup> spermatocytes  $0.44 \pm 0.03$   $\mu$ m<sup>2</sup>. All groups were not significantly different from each other. All averages reported as mean value  $\pm$  SEM. All p values calculated via t test.

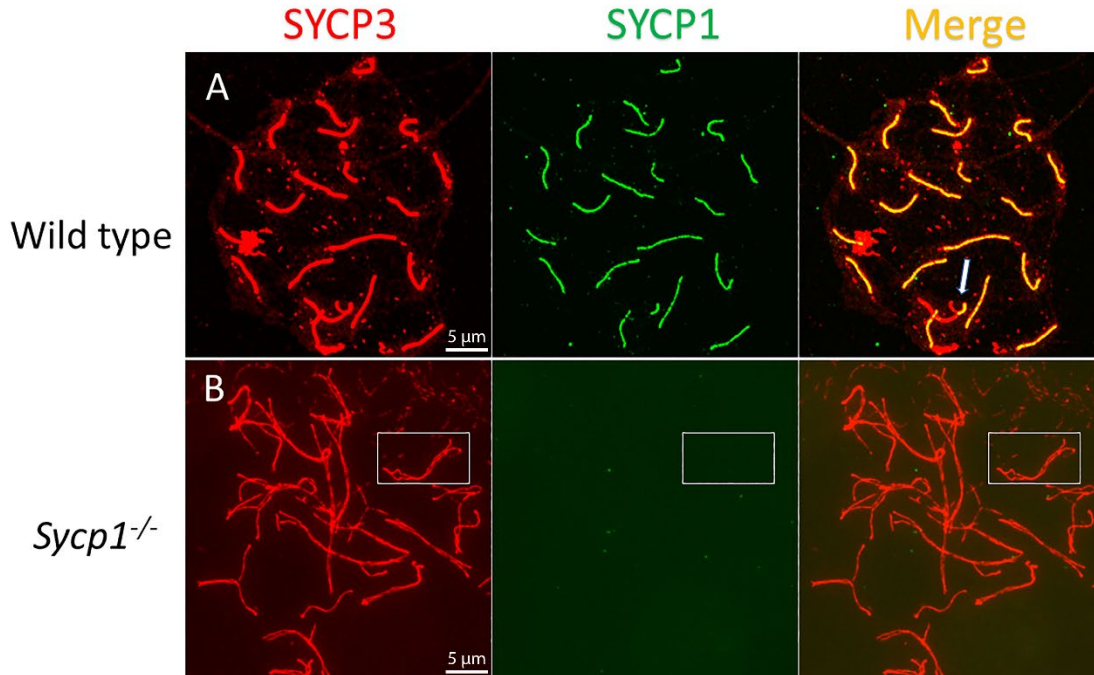
## 4.3 Results

### 4.3.1 Properties of meiotic prophase compared to mitotic chromosomes

Previous work on isolated prometaphase mitotic chromosomes revealed novel physical and structural properties, most notably that they are a gel meshwork of chromatin, whose stiffness is dependent on condensin (M. G. Poirier & Marko, 2002b; Mingxuan Sun, Ronald Biggs, Jessica Hornick, & John F. Marko, 2018; Sun et al., 2011). We utilized a similar approach to isolate meiotic prophase I chromosomes from mouse spermatocytes to study the mechanics of meiotic prophase I chromosomes and identify how the SYCP1 contributes to their stiffness. Isolating meiotic prophase I chromosomes was complicated by the presence of the nuclear envelope (Fig. 4.3A), which is absent during mitotic prometaphase (Fig. 4.3B). Since meiotic chromosomes' ends are attached to the nuclear envelope (Kouznetsova et al., 2011; Liebe et al., 2004), one end of a chromosome was easily identified and aspirated into a pipette then moved away from the nucleus. The location of the other chromosome end was estimated by looking for a change in chromosome morphology; that locus was then captured by a second pipette (Fig. 4.3A). This was followed by removal of the nucleus using a third pipette, which was stabilizing the nucleus (Fig. 4.3A). We verified that these chromosomes were in meiotic prophase I, by immunostaining against SYCP1 and SYCP3 (central and lateral SC components, respectively), which are present only during prophase I of meiosis (Fig. 4.3C center, Fig. 4.6) and absent on mitotic chromosomes (Fig. 4.3C left).

### 4.3.2 Nuclease treatments dissolve both chromosomes to a similar degree

To probe the underlying structure of the isolated meiotic chromosomes, we treated them with proteases and nucleases (M. G. Poirier & Marko, 2002b; Sun et al., 2011). Once a chromosome was isolated, a pipette filled with a restriction enzyme or nuclease with the proper buffer, and



Immunostaining for SYCP3 (red) and SYCP1 (green) in wild-type (A) and *Sycp1*<sup>-/-</sup> (B) spermatocytes. (A) In wild-type pachytene spermatocytes, all homologous chromosome pairs synapsed from one end to the other except sex chromosomes. Synapsis only occurs in the Pseudo Autosomal Regions (PAR) of the sex chromosome pairs (arrow). Data in panels F and G not collected from personal data but included for its contribution and investigation in Biggs et al 2019; experiments performed by Ning Liu. Scale bar represents 5 μm. (B) Synaptonemal complexes do not form between the paired homologous chromosomes in *Sycp1*<sup>-/-</sup>. One homolog pair is highlighted by a white frame. Note that there are no transverse filaments, SYCP1, between the two homologous chromosomes.

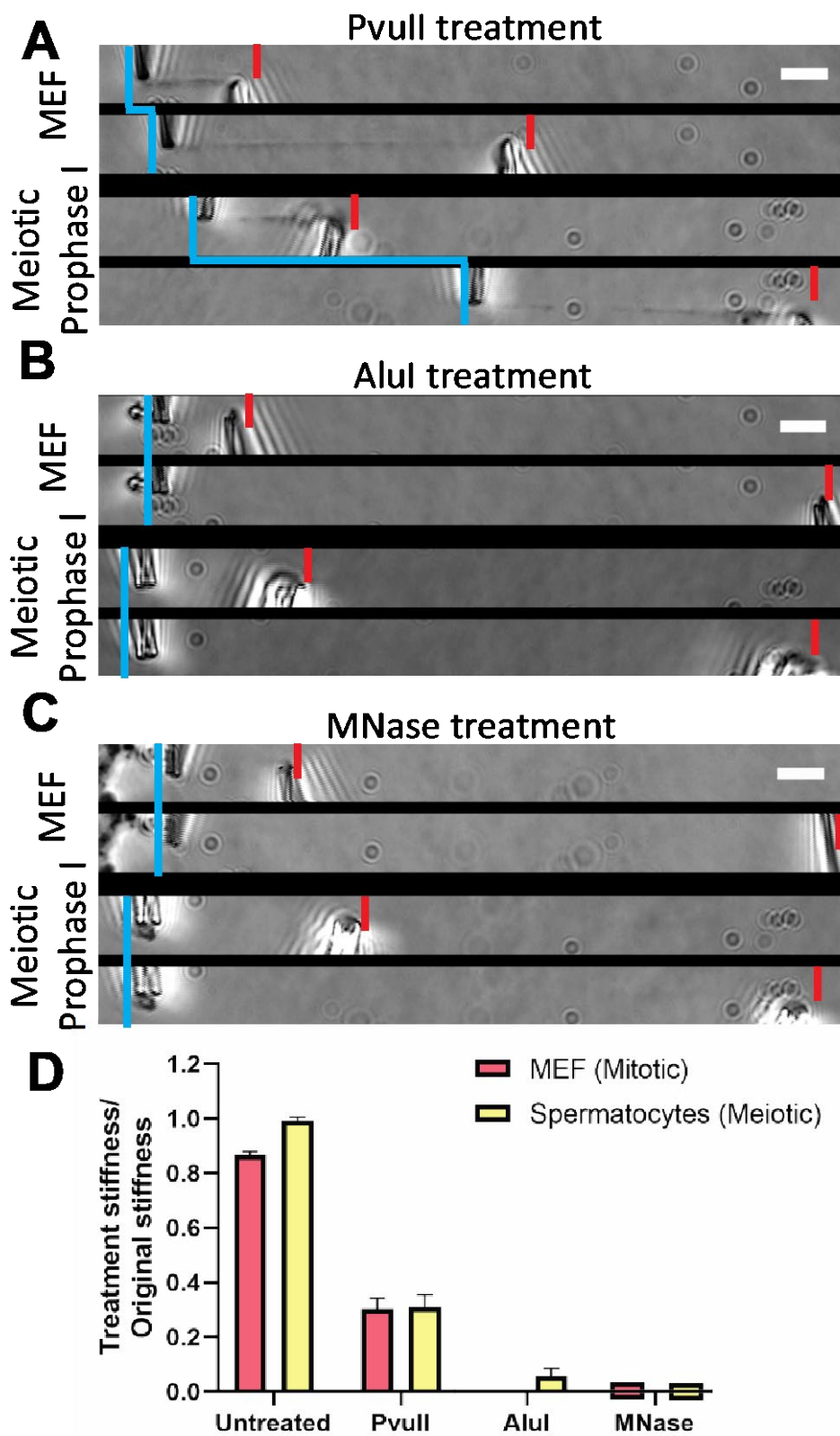


**Figure 4.7. Mitotic and meiotic chromosomes have a contiguous DNA connection, which is dissolved with 4bp restriction enzymes, but only weakens with 6bp restriction enzymes.**

(A-C) Blue lines mark positions of force pipettes. Force pipette movement means connection; no movement means no connection. Red notches mark positions of stiff pipettes. The first image is the initial position, while the lower image shows the pulled chromosome. (A) Both mitotic and meiotic chromosomes are weakened, but not fully digested when treated with PvuII (sequence = CAG<sup>^</sup>CTG). Scale bar represents 5  $\mu$ m. (B) Both mitotic and meiotic\* chromosomes lose connectivity when treated with AluI (sequence = AG<sup>^</sup>CT) \*- 1 in 4 trials of meiotic chromosomes did not fully digest the meiotic chromosome. Scale bar represents 5  $\mu$ m. (C) Both mitotic and meiotic chromosomes lose connectivity when treated with MNase (cleaves all DNA sequences). Scale bar represents 5  $\mu$ m. (D) Quantification of chromosome subsequent stretches after no treatment or after being treated with PvuII, AluI, and MNase. No treatment caused a 13 $\pm$ 4% weakening of mitotic chromosomes over 10 chromosomes and a 1 $\pm$ 4% weakening of meiotic chromosomes over 10 chromosomes. PvuII treatment caused a 70 $\pm$ 8% reduction in stiffness for MEF chromosomes over 4 chromosomes and 69 $\pm$ 9% reduction in stiffness for meiotic chromosomes over 4 chromosomes. One of four AluI treatments of meiotic chromosomes caused a 90% reduction in stiffness (rather than fully digesting), while AluI treatment digested 4 of 4 mitotic chromosomes. All MNase treatments caused full digestion of mitotic and meiotic chromosomes over 4 chromosomes each.

dispensed out of a wide-bore spray pipette close and perpendicular to the buffer, then dispensed out of a wide-bore spray pipette close and perpendicular to the chromosome for 10 minutes. Mitotic chromosomes were merely weakened when treated with a 6-base pair (bp)-sequence-specific restriction enzyme (PvuII), but completely dissolved when treated with 4-bp sequence-specific (AluI) and non-sequence-specific (MNase) (M. G. Poirier & Marko, 2002b; Sun et al., 2011) nucleases (Fig. 4.7). The chromosome is said to be completely dissolved if there is no visible material on the pipettes and there is no deflection of the force pipette when the stiff pipette was pulled away a great distance. If either chromosome type had a continuously stable connected protein core, one would be left behind when the DNA was dissolved in these treatments. Meiotic prophase I spermatocyte chromosomes behave nearly identical to mitotic chromosomes when treated with nucleases, in that they weakened when a 6-bp sequence specific restriction enzyme was sprayed onto the chromosomes but would completely digest away when treated with a 4-bp sequence specific restriction enzyme (Fig. 4.7). MNase treatment could also remove all connectivity between mitotic bundles and meiotic prophase nuclei (Fig. 4.8).

### **4.3.3 Protease treatments weaken but do not fully dissolve both chromosomes**

Treatment with the proteases trypsin and proteinase K only caused the chromosome to weaken, not disintegrate (Fig. 4.9). Meiotic prophase I chromosomes were also not fully disintegrated when treated with both proteases and were less affected by protease treatment compared to mitotic chromosomes (Fig. 4.9). This we found remarkable considering the amount of additional protein structures present on meiotic chromosomes, emphasizing the importance of chromatin to their organization. Since the chromosomes were still greatly weakened by these treatments, it shows that the proteins are still very important for maintaining the structure of the chromosome.

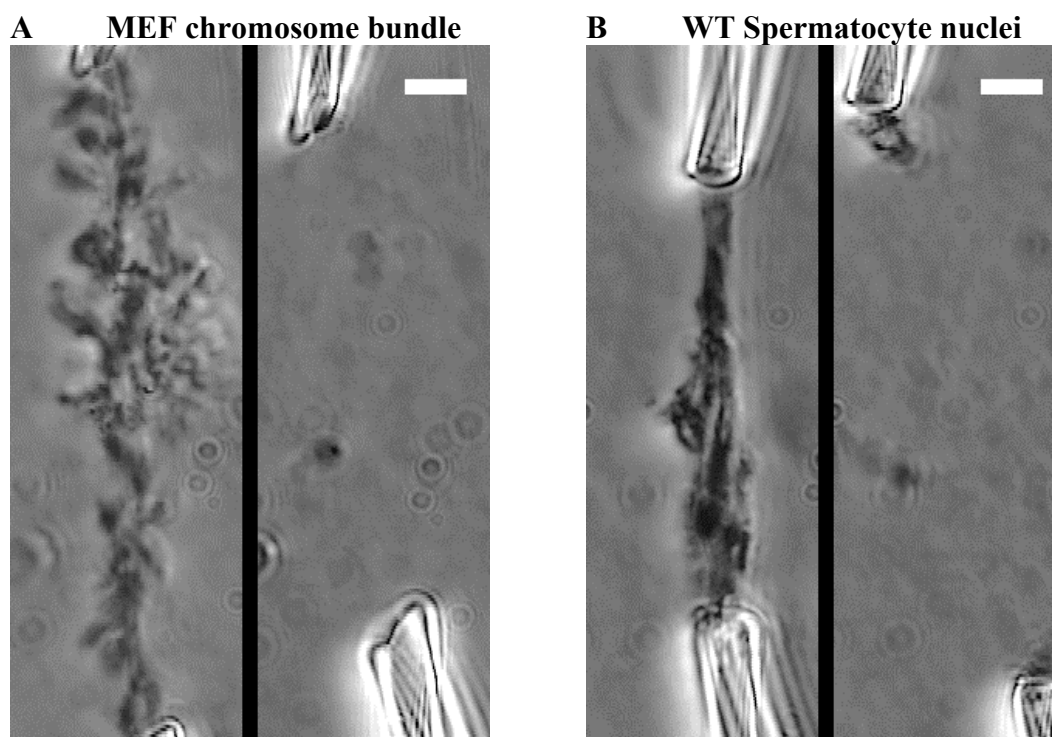


**Figure 4.8. Example MNase treatment of captured mitotic bundles and meiotic nuclei, both stretched between two pipettes.**

(A) MNase treatment of mitotic bundles causes loss of any chromosomes as seen in phase-contrast imaging. Scale bar represents 5  $\mu\text{m}$ . (B) MNase treatment of meiotic nuclei causes loss of any chromosomes as seen in phase-contrast imaging. Scale bar represents 5  $\mu\text{m}$ .

## **4.4 Conclusions, discussion, and future directions**

### **4.4.1 Meiotic chromosomes in the context of mitotic chromosomes**

By capturing and manipulating meiotic prophase I chromosomes and comparing them to mitotic chromosomes, several interesting similarities and differences in their structure are revealed. First, both meiotic prophase I and mitotic chromosomes show the same underlying structure, *i.e.*, a chromatin gel meshwork crosslinked by protein complexes (possibly predominantly SMC complexes (J. Lee, 2017; M. G. Poirier & Marko, 2002b; M. Sun et al., 2018b)). This general model is supported by experiments where both types of chromosomes are fully disintegrated when treated with nucleases but maintain their connectivity when treated with proteases while losing most of their stiffness. Meiotic cohesin is present between the arms of sister chromatids through meiotic prophase I (Garcia-Cruz et al., 2010). Likewise, condensin can be found compacting mitotic chromosomes along the chromosome arms (M. Sun et al., 2018b; Takagi et al., 2018). If these complexes formed a contiguous structure through self-attachment or other forms of protein bridging, then the contiguous protein structure would remain between the pipettes after nuclease treatment (M. G. Poirier & Marko, 2002b). This digestion occurs in the wild-type spermatocytes, indicating that the presence of SYCP1 is not sufficient to prevent this digestion.

### **4.4.2 Implications of meiotic chromosome digestion**

It is possible that the chromosomes we have studied are not fully synapsed, and that the fully synapsed SC forms a contiguous structure that is resistant to nuclease digestion (Schucker et al., 2015). Further experiments could be done to test this hypothesis: a result where meiotic chromosomes with intact SCs dissolved during nuclease treatment in pachytene (where the SC is fully synapsed) would support a highly dynamic picture of the SC structure (Rog et al., 2017). It

is also possible that isolation of the chromosomes to outside of the cell combined with the dynamic nature of the SC leads to the SC developing a non-contiguous structure when isolated. Gaps in the protein network, connected by chromatin, would therefore dissolve with nuclease treatment. These gaps would leave behind fragments of the SC, carried away by the flow of the spray liquid. This would eventually lead to the entire dissolution of the meiotic chromosome. These different scenarios are subjects for further study, but we emphasize that we have found that straightforward isolation of meiotic chromosomes led reproducibly and systematically to objects that were dissolved by nucleases, indicating a strong dependence on chromatin itself for their structural integrity.

#### **4.4.3 Hypothetical purpose of high meiotic chromosome stiffness**

By measuring their Young's moduli, derived from stretching experiments, we found meiotic prophase I chromosomes are 10-fold stiffer than mitotic prometaphase chromosomes, demonstrating their differences. The origin of this difference could be due to the SC, both in terms of its components and construction during meiotic prophase I (Kleckner et al., 2004; Zickler & Kleckner, 1999). Although meiotic prophase I chromosomes' stiffness is similar to the stiffness of meiotic II arrested chromosomes (Hornick et al., 2015). The underlying chromatin structure could also impact meiotic chromosome stiffness, as could meiotic bivalents, the resolution of chromatin entanglements, crossovers, and other such differences (Berrios, 2017; Broderick & Niedzwiedz, 2015; Kleckner et al., 2004; Kouznetsova et al., 2011; Pattabiraman et al., 2017; Zickler & Kleckner, 1999). Other factors could also include the difference between the resolution and compaction of chromosomes over time, leading to strong differences between mechanics of prophase and prometaphase chromosomes. Comparison of mitotic prophase and meiotic prophase chromosome mechanics would be of interest in this regard, but we have been

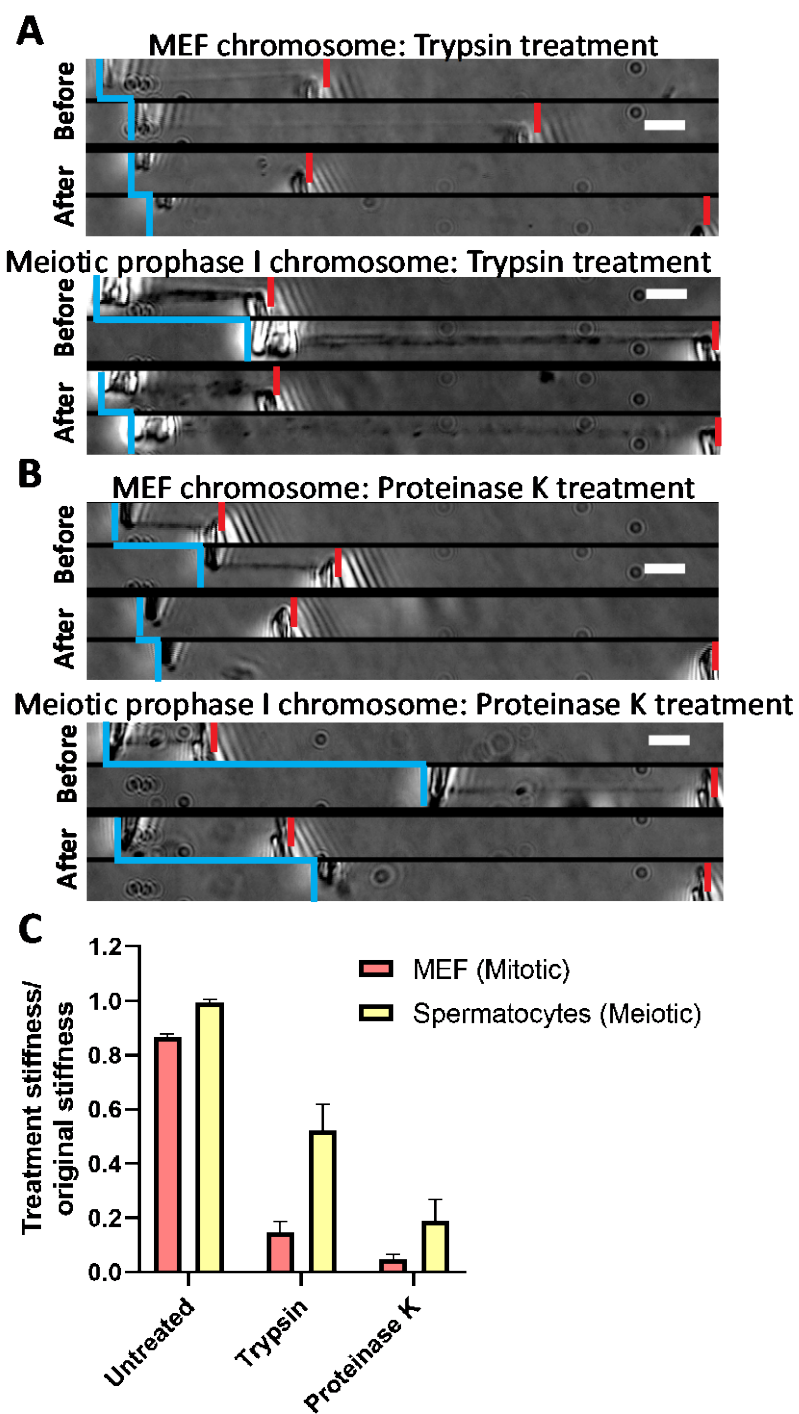


**Figure 4.9. Both meiotic and mitotic chromosomes are weakened, but do not dissolve when treated with Trypsin and Proteinase K.**

(A,B) Blue lines mark positions of force pipettes. Force pipette movement means connection; no movement means no connection. Red notches mark positions of stiff pipettes. The first pair shows the stretch deflection of the chromosome before treatment, while the next pair shows the stretch deflection after treatment. The first image is the initial position, while the lower image shows the pulled chromosome. (A) (Top.) MEF chromosomes lose all definition in the phase-contrast channel but can move force pipette after digestion when treated with Trypsin and are noticeably weaker than before treatment. (Bottom.) Meiotic chromosomes lose most definition in the phase-contrast channel but can move force pipette after digestion when treated with Trypsin and are noticeably weaker than before treatment. Scale bar represents 10  $\mu\text{m}$ . (B) (Top.) MEF chromosomes lose all definition in the phase-contrast channel but can move force pipette after digestion when treated with Proteinase K and are noticeably weaker than before treatment. (Bottom.) Meiotic chromosomes lose most definition in the phase-contrast channel but can move force pipette after digestion when treated with Proteinase K and are noticeably weaker than before treatment. Scale bar represents 10  $\mu\text{m}$ . (C) Quantification of untreated and protease-treatment weakening of mitotic and meiotic chromosomes. No treatment caused a  $13\pm 4\%$  weakening of mitotic chromosomes over 10 chromosomes and a  $1\pm 4\%$  weakening of meiotic chromosomes over 10 chromosomes. Trypsin treatment caused an  $85\pm 6\%$  weakening in mitotic chromosomes over 3 chromosomes and a  $48\pm 17\%$  weakening in meiotic chromosomes over 3 chromosomes. Proteinase K treatment caused a  $95\pm 3\%$  weakening in meiotic chromosomes over 3 chromosomes and an  $81\pm 13\%$  weakening in meiotic chromosomes over 3 chromosomes.

unable to isolate mitotic prophase chromosomes for mechanical study, due to the difficulty of extracting them from somatic cell nuclei.

Whatever the cause, there is an important consequence of the high Young's modulus in meiotic prophase I chromosomes. The bending of a beam can be thought of as differential stretching across its cross-section, indicating that the difference in stretching elasticity of meiotic prophase and mitotic chromosomes predicts a similar difference in their bending stiffnesses (Lifshitz, Kosevich, & Pitaevskii, 1986). Therefore, the function of a large stiffness of meiotic prophase chromosomes is consistent with the stress model of CI, which requires a large elastic stiffness to allow a single crossover event to affect a meiotic chromosome along its entire length (Kleckner et al., 2004; L. Zhang, Liang, et al., 2014). This higher stiffness, not required or observed for mitotic chromosomes, could follow from the underlying chromatin being more tightly packed and/or crosslinked in meiotic prophase I (*e.g.*, by meiotic cohesin and SC components) (Garcia-Cruz et al., 2010; J. Lee, 2017; Rog et al., 2017; Schucker et al., 2015). Determining the dependence between the quantitative degree of CI and meiotic chromosome stiffness, *e.g.*, in mutants or knockouts of specific proteins involved in CI could provide a strong test for the stress-release model of CI.

#### **4.4.4 Significance of the SYCP1 null mutant stiffness similarity to WT**

While the meiotic chromosome is much stiffer, its stiffness did not depend strongly on the presence of SYCP1, the central element of the SC. This was quite surprising, since the presence of a bridging element might be expected to act as a crosslinker of material across homologous chromosomes (Enguita-Marruedo et al., 2018; Kouznetsova et al., 2011; Schucker et al., 2015; Zickler & Kleckner, 1999). This crosslinking would bridge strands of chromatin together and presumably stiffen the whole structure. However, it is possible that this finding is

again consistent with the idea that the SC is very dynamic *in vivo* (Pattabiraman et al., 2017; Rog et al., 2017). This dynamic *in vivo* nature could lead to the SC being an insignificant contributor to the overall mechanical stiffness of the meiotic chromosome, possibly due to its isolation from the intracellular environment. Future investigations into the SC include the role of synapsis of SYCP1 across meiotic substages and the roles of SYCP2 and SYCP3 (Fraune et al., 2012; Gao & Colaiacovo, 2018; Rong et al., 2016). The underlying cohesin core of meiotic chromosomes promises to be an exciting topic for further investigation (Kouznetsova et al., 2011; J. Lee, 2017; Liebe et al., 2004; Pattabiraman et al., 2017; Schucker et al., 2015), since when mitotic chromosomes lack condensin, the main mitotic SMC complex, they completely lose their morphology and stiffness (Takagi et al., 2018).

#### **4.4.5 Future experiments on meiotic chromosomes**

The complex nature and dynamic structure of meiotic chromosomes are important to understand because of their essential role in sexual reproduction. Being physical objects, studying their mechanical properties furthers our understanding of how they function in the cell (*e.g.*, in determining the mechanism underlying CI) (Kleckner et al., 2004). Further experiments of the general type introduced here, comparing stiffness and nuclease sensitivity across substages of meiotic prophase may reveal the underlying mechanical function of the SC and its role in the connectivity of meiotic prophase I chromosomes. Mechanical experiments targeting the lateral elements of the SC could determine the difference in mechanical makeup of the SC by focusing on the elements loaded first onto the SC (Garcia-Cruz et al., 2010; J. Lee, 2017; J. Lee & Hirano, 2011). Isolation and manipulation of cohesin deficient mutants could facilitate discovery of the underlying crosslinkers of meiotic chromosomes, the impact of meiotic SMC complexes, and the contribution of sister chromatid cohesion in meiosis to the chromosomal structure (Kouznetsova

et al., 2011). Other functions such as the sensitivity of mechanics to alteration of topoisomerase presence or activity are also likely to uncover interesting relationships between chromatin entanglements and stiffness (Kleckner et al., 2004; Sun et al., 2011; L. Zhang, Wang, et al., 2014).

**Chapter 5. The innate high stiffness of the CENP-A labeled centromere is unaffected by the degradation of CENP-C and CENP-N by our detection methods**

*This chapter is a collection of unpublished experiments, related to each other by the rapid degradation of Constitutively Centromeric Associated Network proteins and tracking a CENP-A labeled centromere while stretching. A future paper will be submitted upon completion of the future directions, using this chapter as the start. All experiments performed by myself. Cell lines received from the Straight lab in Stanford as a collaborative project.*

The centromere is a part of the complicated interplay of the division machinery in chromosome separation that experiences a substantial amount of pulling force from the spindle microtubules. Previous unpublished studies have been performed that observed the amount of stretch the centromere undergoes. In these experiments, the centromere was incredibly stiff, barely stretching in comparison to the amount the chromosome arms stretched. CENP-C removal via siRNA did not change the stiffness of the centromere. In the experiments reported in this chapter, we continue to investigate the role of the Constitutively Centromeric Associated Network (CCAN) in centromeric stiffness. We find once again that degradation of CCAN has a minimal effect on the innate stiffness of the centromere, which is naturally very stiff, typically over 100-fold the stiffness of the chromosome arms. We propose further experiments on more CCAN elements as well as complexes enriched at the centromere, whose enrichment at the centromere may be responsible for its innate stiffness.

## 5.1 Overview

The centromere is a critical component of the chromosome that is important in coordinating the complex machinery involved in chromosome division during mitosis. In humans, the centromere is designated at a region of the chromosome containing series of repetitive DNA sequences (Morrison & Thakur, 2021). The centromere recruits the histone H3 variant, CENtromeric Protein-A (CENP-A) (Molina, Kouprina, Masumoto, Larionov, & Earnshaw, 2017; Moreno-Moreno et al., 2017; Srivastava & Foltz, 2018). Once integrated into the nucleosome CENP-A is further modified to designate the region as a functional centromere (Srivastava & Foltz, 2018). In between the sister centromeres, the cell recruits the chromosome passenger complex, which is important in the coordination and timing of chromosome separation

by stalling cohesin degradation until the mitotic spindle has completely formed (Carmena et al., 2012; van der Waal et al., 2012). The functional centromere recruits the kinetochore, a complex structure that bridges the chromosome to the microtubules, which provide the force generation needed to separate the sister chromosomes from one another (Musacchio & Desai, 2017). By studying the centromere and kinetochore, we can gain a greater understanding of the coordination involved in the events and biological machinery involved in mitosis.

The inner part of the kinetochore is called the Constitutively Centromeric Associated Network (CCAN). The CCAN is a network of several multi-protein complexes interacting together to directly interact with the centromere over the cell cycle (Hara & Fukagawa, 2017; McAinsh & Meraldi, 2011; Musacchio & Desai, 2017; Nagpal & Fukagawa, 2016; Perpelescu & Fukagawa, 2011). The human CCAN is composed of sixteen proteins interacting in four complexes plus a lone protein. The CENP-H/I/K/M complex acts as a core integrator of the CCAN, interacting with the CENP-L/N complex, the CENP-O/P/Q/R complex, the CENP-T/W/S/X complex, and CENP-C (Hara & Fukagawa, 2017). CENP-C acts as a crucial bridge between the centromere and the outer kinetochore by directly connecting to CENP-A and the KMN network, which binds microtubules (Carroll et al., 2010; Carroll et al., 2009). The CENP-L/N complex likewise interacts directly with CENP-A and is stabilized by its interactions with the CENP-H/I/K/M complex but does not interact with the KMN network. The CENP-T/W/S/X interacts directly with the KMN network and the CENP-H/I/K/M network and integrates into the chromatin surrounding CENP-A nucleosomes by forming a histone-like fold. The mitotic function of CENP-O/P/Q/R is poorly understood (Hara & Fukagawa, 2017; Musacchio & Desai, 2017).

As the name implies, the CCAN remains associated with the centromere through the cell cycle, in both interphase and mitosis. In both phases, the CCAN forms a close attachment around the centromere and directly anchors to the centromere through CENP-A, C, and N (Cao et al., 2018; Carroll et al., 2010; Carroll et al., 2009; McKinley et al., 2015). In interphase, the connection is responsible for limiting the amount of drift the centromere experiences, since additional centromeres on the chromosome can lead to adverse and uneven chromosomal division, leading to aneuploidy. Centromere drift inhibition is also achieved by degrading free CENP-A (Au et al., 2013; Ranjitkar et al., 2010; Srivastava & Foltz, 2018). During mitosis, the CCAN anchors the kinetochore to the centromere and transduces the force of the depolymerizing microtubules into a force that drives the separation of chromosomes (Cairo & Lacefield, 2020).

Other experiments have also investigated the stability of CENP-A in the centromere. Several post-translational modifications assist in the stability of CENP-A and the centromere (Gambogi & Black, 2019; Srivastava & Foltz, 2018). The CCAN has been shown to play an important role in the stability of CENP-A (Carroll et al., 2009; McKinley et al., 2015; Moree et al., 2011; Ranjitkar et al., 2010). Elements of the CCAN also help stabilize the CENP-A containing nucleosome itself (Cao et al., 2018). In this experiment, CENP-A nucleosomes were observed under electron microscopy and treated with destabilizing heat and salt. Nucleosomes containing CENP-A were less stable and less resistant to the destabilizing effects than the canonical H3. These CENP-A containing nucleosomes could be stabilized with the addition of CENP-C and CENP-N *in-vitro* on their own and further stabilized when both were added. The CENP-A nucleosomes were also stabilized when subjected to high salt and high temperature conditions when CENP-C and/or CENP-N were added. However, when cells expressing a fluorescent CENP-A and an Auxin-Induced Degron (AID) cell line (see Fig 5.1A) tagged to

CENP-C or CENP-N, the degradation of either CENP-C or CENP-N did not affect the fluorescent intensity of CENP-A or affect the amount of CENP-A purified from those cells. This suggests that the removal of CENP-C and CENP-N did not affect the stability of CENP-A *in vivo*, further suggesting that there may be other factors in a living cell that stabilize CENP-A in the centromere.

Recruitment of chromatin-organizing complexes are also thought to stabilize the functional centromere. The centromere is enriched in two Structural Maintenance of Chromosome (SMC) complexes, condensin and cohesin (Lawrimore & Bloom, 2019; Lawrimore et al., 2018). Cohesin is primarily responsible for sister chromatid cohesion until the metaphase spindle is properly formed, the chromosomes are all attached to their respective spindle, and anaphase onset begins (Henrikus & Costa, 2021; Peters & Nishiyama, 2012). Cohesin is lost from the chromosome arms in mitosis, remaining only at the centromere until anaphase onset (Peters & Nishiyama, 2012). Cohesin enrichment at the centromere and its protection from removal also is facilitated by its proximity to the CPC (C. Morales & Losada, 2018). Condensin on the other hand is known primarily for compacting and organizing chromatin into loops during mitosis while also imparting structural rigidity to the chromosome through this activity (Gerlich et al., 2006; Green et al., 2012; M. Sun et al., 2018b; Walther et al., 2018). Condensin's enrichment at the centromere is hypothesized to recruit topoisomerase II during anaphase and to stiffen the chromatin so that the sister chromosome kinetochores are preferentially pointed directly away from each other for spindle positioning (Dyson et al., 2021).

The centromere is further stabilized by its association with the centromeric heterochromatin. The chromatin surrounding the centromere is constitutively heterochromatic, called the pericentric heterochromatin (Morrison & Thakur, 2021; Musacchio & Desai, 2017).

This heterochromatic chromatin could function as a means of further stiffening the centromere, like condensin. This stiffness could help stabilize the centromere from drift through mechanical stabilization (Stephens et al., 2011; Stephens et al., 2013). However, the centromeric heterochromatin could be merely a byproduct of the repetitive DNA sequences associated with the centromere as repetitive regions are typically constitutively heterochromatic (Cao et al., 2018; Morrison & Thakur, 2021). The centromere is also associated with an increase in HP1 $\alpha$  during mitosis, which is another component of heterochromatin and imparts structural stiffness to chromosomes (Strom et al., 2021).

As an object important in transducing forces, there is interest in learning the physical properties of centromeres, including their spring constant and behavior as a spring-like object. One such study utilized the end-to-end distance of the spindle pole body in yeast, the microtubule-organizing center in yeast, analogous human centrosomes (Stephens et al., 2011; Stephens et al., 2013). This study demonstrated that perturbing the concentration and functionality of condensin, cohesin, and heterochromatin around the centromere caused the spindle pole body to drift to longer distances and have a larger variation in spindle length. This study also demonstrated that perturbing condensin, cohesin, and heterochromatin functionality also affected the amount of drift that the surrounding DNA sequences of the centromere would move, causing the surrounding DNA sequences to drift more.

An additional study observed the amount the centromere stretched while stretching the whole chromosome along its axis while tracking the centromere through fluorescent antibody labeling (Sun, 2014). The study demonstrated that the centromere stretches at least 200-fold less than the chromosome arms, demonstrating that it is about 200-fold stiffer than the chromosome arms. This result is unsurprising considering the amount of chromatin-organizing and chromatin-

compacting complexes enriched at and around the centromere, being especially enriched in molecules shown to stiffen mitotic chromosomes.

The previous study also utilized a siRNA-based degradation of CENP-C, an integral part of the CCAN, which is important for stabilizing the centromere from drift (Hori et al., 2017; Sun, 2014). This procedure could not be done in the yeast spindle-pole experiments, as those assays require a functional kinetochore to tether the centromere to the spindle pole, used to derive the stiffness of the centromere. A surprising result was that removal of CENP-C caused little to no change in the centromere's stiffness stretching along the chromosome axis. To follow up on those experiments, we utilized an AID-based system of degradation for rapid depletion of both CENP-C and CENP-N while tracking an intrinsically labeled CENP-A to study centromeric stretching along the chromosomal axis (Cao et al., 2018) (CENP-C/N stability, are additive). Our results show that we can degrade the punctate pattern of CENP-C and CENP-N with auxin, but the total cellular fluorescence reduction of both is much less. We also recapitulate the result that the intrinsic stiffness of the centromere is very high compared to the chromosome arms, assuming that the centromeric region is under the same stress being applied to the rest of the chromosome. By auxin degradation, we show that there is little effect of CENP-C or CENP-N effect on centromeric stiffness and that their degradation also does not reduce the stiffness of the entire chromosome.

## 5.2 Materials and Methods

Human cell culture cells, all of which were modified DLD1 cells, were maintained in DMEM (Corning) with 10% fetal bovine serum (FBS) (HyClone) and 1% 100x penicillin/streptomycin (Corning). The cells were incubated at 37°C and 5% CO<sub>2</sub> for no more

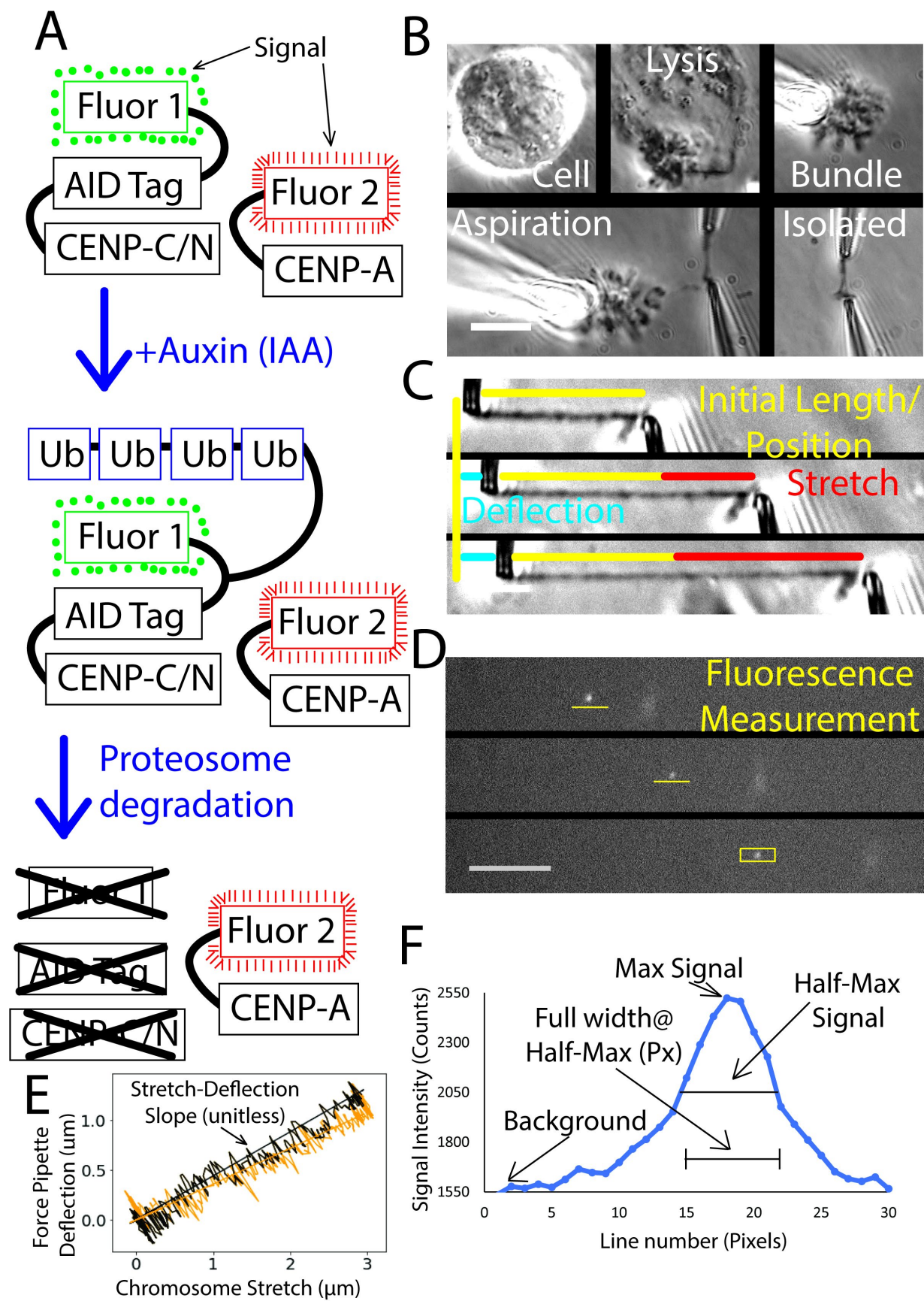


**Figure 5.1. Auxin treatment, chromosome isolation, and force measurements.**

(A). AID schematic. In the engineered cell lines, cells exposed to auxin will poly-ubiquitinate the AID tag, but not other proteins, which acts to signal the proteasome to degrade the marked protein. Since the fluorescence is connected to the protein of interest, it is used as readout of protein abundance. (B). Single chromosome isolation by bundle removal. A mitotic cell is found in the free-cycling cell population (Cell). The cell is then sprayed with a 0.05% Triton solution in PBS to destabilize the cell membrane and lyse the cell (Lysed). Once the cell is lysed, the bundle can be stabilized with a hold pipette (Bundle), then the Triton pipette is swapped with a stiff pipette. One free chromosome arm is then aspirated into the force pipette, dragged away from the bundle, to expose the other arm, which is then aspirated into the stiff pipette (Aspiration). Once both ends of the chromosome are secured and aspirated into the pipettes, the bundle is aspirated into the hold pipette and removed from the well, leaving behind an isolated chromosome. Scale bar represents 10  $\mu\text{m}$ . (C). Exaggerated example stretch of a chromosome in a stretch-deflection protocol. The lower, stiff pipette moves in a controlled and directed manner while the force pipette deflects from its original position while both pipettes are being tracked. The stretch of the chromosome is measured as the stiff pipette movement minus the deflection of the force pipette. The force on the chromosome is measured as the deflection of the force pipette multiplied by its spring constant. A linear regression of the slope of the stretch vs force is the spring constant of the chromosome, as shown in E. When the slope and the initial length are multiplied together, we obtain the doubling force. Scale bar represents 10  $\mu\text{m}$ . (D). Example centromere stretch. The same chromosome stretch is shown as in (C), but in the CENP-A fluorescent channel. The box-scan of the fluorescence in C works as the trace for panel F. (E). An example trace of the stretch-deflection measurement of a chromosome. The black zig-zag pattern represents the outgoing measurements, where the straight line represents the slope calculated as a least-squared fit of the linear regression of the line. The orange pattern and line represent the same measurements and slope, but in the return direction. The outgoing slope is multiplied by the spring constant of the force pipette to obtain the spring constant of the chromosome. Scale bar represents 10  $\mu\text{m}$ . (F). Calculation of the length of the centromere. A box scan of the fluorescence of the centromere is plotted by the average intensity of each line of the box. The intensity is measured in fluorescent counts and the length measured in pixels.

than 30 generations and were passaged every 2-4 days. Experiments on captured chromosomes used cells that recovered 1-3 days after plating. Cells were freely cycling and not treated with drugs designed to synchronize the cells or otherwise affect the cell cycle. Auxin treatment was performed by aspirating the untreated media, then replacing it with the DMEM complete media with 0.5 mM Indole-3-Acetic Acid (IAA) 4 hours before performing the experiment. An overview showing the molecular mechanism of auxin degradation can be seen in Fig. 5.1A.

### **5.2.2 Single chromosome capture: setup and microscopy**

Single chromosome capture experiments used an inverted microscope (IX-70; Olympus) with a 60x 1.42 NA oil immersion objective with a 1.5x magnification pullout at room temperature and atmospheric CO<sub>2</sub> levels. Experiments were performed in less than 3 hours after removal from the incubator to ensure minimum damage to the cells being analyzed. Prometaphase cells were identified by eye (Cell) and lysed with 0.05% Triton-X 100 in PBS (Lysed). (All other pipettes were filled with PBS). After lysis, the bundle of chromosomes was held with a pipette (Bundle). One end of a random, loose chromosome was grabbed by the force pipette (WPI TW100F-6), moved from the bundle, and grabbed with the pulling pipette on the other end (Aspirated). The bundle was then removed to isolate the tracked and unbroken chromosome (Isolated). All these steps are demonstrated and labeled in Fig. 5.1B.

### **5.2.3 Single chromosome capture: force measurement**

An easily bendable force pipette and stiff pulling pipette were used for stretching chromosomes. Once captured, the pipettes were moved perpendicular to the chromosome, stretching the chromosome to roughly its native length. The stiff pipette was then moved 6  $\mu\text{m}$  and returned to the starting position at a constant rate of 0.20  $\mu\text{m}/\text{sec}$  in 0.04  $\mu\text{m}$  steps using a LabVIEW program, while tracking the stiff and force pipette. Fig. 5.1C shows an example of

stretch-deflection but stretched further than 6  $\mu\text{m}$  for ease of observation. An example LabVIEW trace of deflection vs stretch and a slope of linear regression can be seen in Fig. 5.1E. Deflection of the force pipette multiplied by its calibrated spring constant and divided by the distance between the pipettes (the stretch) was used to obtain the chromosome spring constant. Each chromosome was stretched at least 3 times to provide an accurate and reproducible measurement of its spring constant. The chromosome spring constant multiplied by its initial length gave the doubling force. The initial length was given by measuring the distance between the centers of the pipettes and converting the pixels into microns while the chromosome was perpendicular to the pipettes. Centromere length was estimated as the full width at half maximum (FWHM) of an ImageJ line scan of the centromere's fluorescence. An example centromere stretch's fluorescence can be seen in Fig. 5.1D with the trace of a full width at half maximum trace seen in Fig. 5.1F.

#### **5.2.4 Fluorescent imaging of live cells, bundles, and isolated chromosomes**

Before isolating a chromosome from a cell, we would image the fluorescence intensity of the cell at a specified exposure time and at a specified power with a fluorescent LED light source. Analysis into a population of cells was also performed three independent times untreated, or with auxin treatment to obtain the expected distribution of cellular fluorescence of these cells, which were also treated with Hoechst Fig. 5.2A shows an example of this treatment. The fluorescence intensity of the centromere would be reported by drawing a circle around the centromere, using the CENP-A fluorescence as the basis for determining the location of the centromere in both the live cell and single isolated chromosome cases, Fig. 5.2B shows the method of fluorescent analysis. Hoechst was not used in experiments involving isolated chromosomes so that it would not affect the mechanics of the chromosome. On experiments

isolating single chromosomes, the fluorescence of the target cell where the chromosome was extracted would be captured and reported in addition to the fluorescence of the centromere on the isolated chromosome.

### **5.2.5 Measuring the centromere stretch on mitotic chromosomes**

For the analysis of centromeric stretch, we stretched the chromosome by pulling the chromosome 12  $\mu\text{m}$ , then taking an image in phase-contrast and in the CENP-A fluorescent channel. This was repeated 3-6 times from the chromosome's initial length. The length of the centromere after each pull was calculated as reported in 5.2.3 (using the FWHM) and demonstrated in Fig. 5.1F. We would also measure the length of the chromosome in the phase-contrast image from the middle of the stiff pipette to the middle of the force pipette. We would then plot the centromere length against the chromosome length at the same stretch and derive the slope of the curve using a least-square fit linear regression to obtain the centromere: chromosome stretch ratio. We would average the two centromere's ratio in instances where two centromeres could be analyzed into one data point. Periodically, the slope would be negative, due to the centromere appearing to shrink over the stretching protocol, possibly due to the centromere coming more into focus or into a single plane as it was stretched, but the centromere was always stretched much less than the entire chromosome by this method of analysis.

### **5.2.6 Auxin Induced Degradation (AID) cell lines**

The cell lines used in this study were provided by Dr. Aaron Straight, a collaborator at Stanford University. ASTC405 cells are Tir1 DLD1 cells with CENP-N AID sfGFP with homozygous CENP-A N-terminal Ruby 3xflag tag, while ASTC409 cells are Tir1 DLD1 cells with CENP-C AID YFP with heterozygous CENP-A C-terminal 3xFlag Ruby tag.

## 5.3 Results

### 5.3.1 CENP-C/N is removed in auxin treatment with no CENP-A intensity effects

We utilized a cell line that contained fluorescent-labeled CENP-A to track the centromere to analyze the amount of stretching the centromere underwent. We ensured that the CENP-A signal could be observed in isolated chromosomes and followed through a stretching experiment (Fig. 5.1D). We then tested the effectiveness of auxin treatment in ASTC 405 and 409 to degrade CENP-C and CENP-N respectively. We also showed that auxin treatment wouldn't affect CENP-A fluorescence. Fig. 5.2A shows an example image of a mitotic cell in phase-contrast, DNA stain (Hoechst), the CENP-C or CENP-N fluorescence, and the CENP-A fluorescence. In Fig. 5.2A, the chromosome arms are folded into the center of the cell as seen in the DNA signal. In the rough center of the DNA signal, the centromere can be observed where the CENP-A/centromere signal is located. In the untreated cells, the punctate signal of CENP-C or CENP-N can be seen co-localizing with the CENP-A signal. In the auxin treatment, the CENP-C and CENP-N signals cannot be seen above the cellular background. The methodology and examples of general background, cell background, cell fluorescence, and centromeric fluorescence is described in section 5.2.4 and demonstrated in Fig. 5.2B.

The cellular fluorescence over general background and centromeric fluorescence over cellular background is quantified in Fig. 5.2C,D respectively. A small, statistically significant decrease of CENP-C's cellular signal and a small, statistically significant increase of the CENP-A's cellular signal with auxin treatment in ASTC405 as seen in Fig. 5.2C's first, second, fifth, and sixth columns respectively. By contrast, there was no statistically significant difference in CENP-N's or CENP-A's cellular signal with auxin treatment as seen in Fig. 5.2C's third, fourth, seventh, and eighth columns. In Fig. 5.2D, auxin treatment shows a large decrease in both

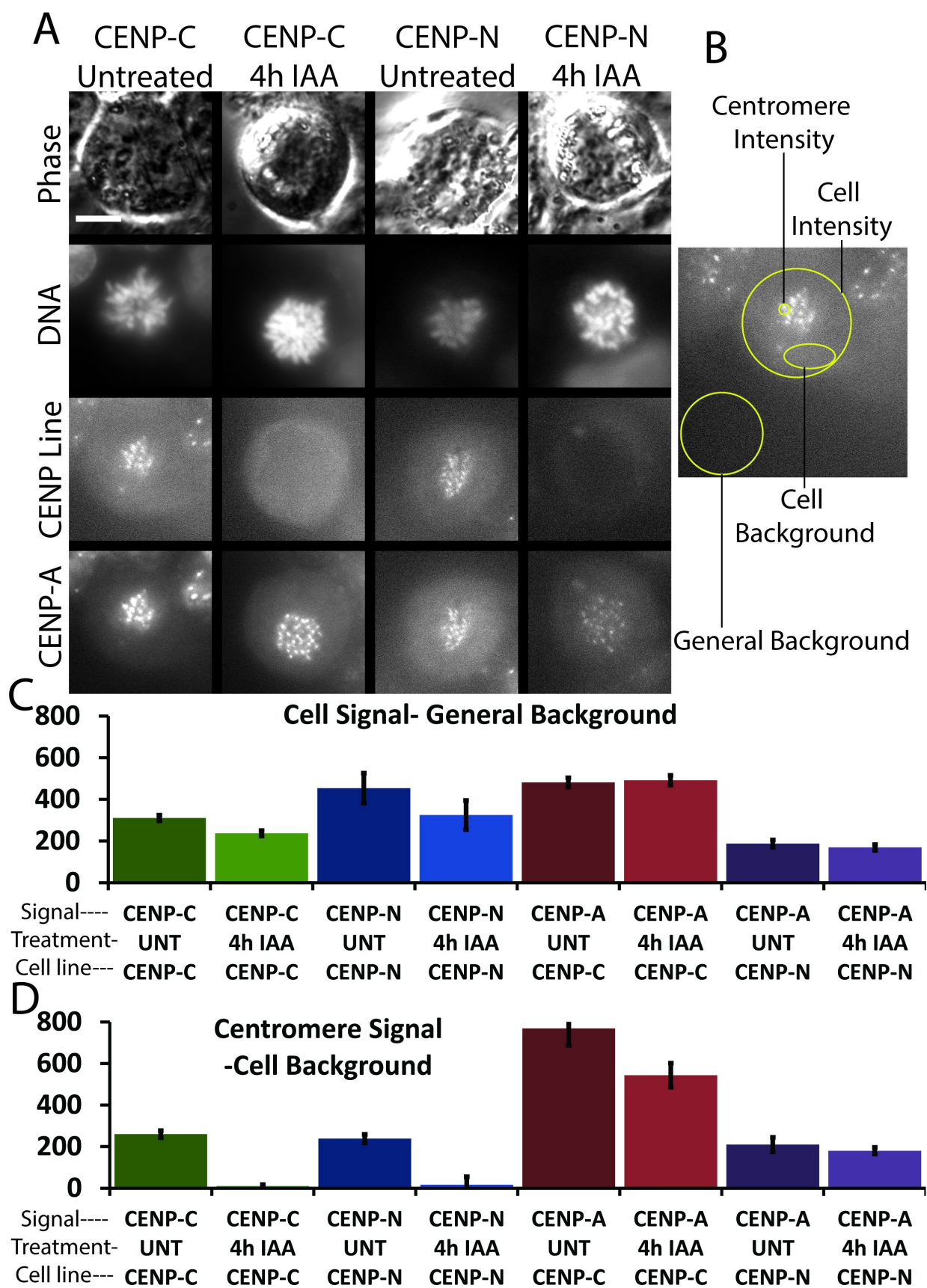


**Figure 5.2. Examples and measurements of the centromeric fluorescent measurements.**

(A) Cellular examples of fluorescent signals in mitotic cells and auxin treatment. Phase-contrast, DNA, CENP line, and CENP-A signal examples for the CENP-C and CENP-N cell lines with and without auxin treatments. Scale bar represents 10  $\mu\text{m}$ . (B). Methodology used in measuring fluorescent signals. The general background was taken from an average signal intensity of an area free from all cells. The cellular measurements were taken by obtaining the average fluorescent intensity from the whole cell. The cellular background was taken as the average signal intensity in the cell, but in an area free from any centromere punctae. The centromere intensity was taken as the average intensity of a small area containing the centromere punctate fluorescence. (C). Quantification of cellular centromeric fluorescence. The cellular fluorescence over general background of CENP-C and CENP-N with and without auxin treatment is slightly low, but statistically significant. The signal is not lowered for the CENP-A fluorescence in either cell lines. (Each bar has  $N=3$ ,  $n=75$ ; see below for more detail) (D). Quantification of centromeric fluorescence over cell background. There was a dramatic reduction in both CENP-C and CENP-N fluorescence when treated with auxin, but had no reduction in fluorescence for CENP-A. (Each bar has  $N=3$ ,  $n=75$ ; see below for more detail). Both C and D used over 3 wells with 25 cells each for a total of 75 cells.

CENP-C's, CENP-N's centromeric fluorescence with auxin treatment, but no statistically significant difference in CENP-A's centromeric fluorescence. The CENP-A and CENP-C/N signals were also always coincident with one another. These two panels in conjunction show that auxin treatment works on the punctate signal of the centromere on the target protein without affecting the tracking CENP-A signal for both cell lines. While the cellular fluorescence of each cell lines had some issues, our focus will be on centromeric fluorescence.

### **5.3.2 Short-term auxin treatments remove CENP-C/N with no stiffness effects**

To study centromeric stiffness, we isolated chromosomes with and without auxin treatment. Fig. 5.3A displays examples of isolated chromosomes and their respective CENP-C/N fluorescence and CENP-A fluorescence in ASTC-405/409 in their untreated and auxin treated cases respectively. An additional panel has been added to demonstrate that the two-centromere chromosome phenotype can occur in every condition. Like the centromeric fluorescence in cells, the single-chromosome-centromere fluorescence is also statistically significantly lower in auxin treatment for both CENP-C/N in ASTC405/409 without affecting the fluorescence of CENP-A with auxin treatment, which is quantified in Fig. 5.3D.

Since CENP-A was unaffected by auxin treatment, able to be tracked, and the degradation of CENP-C/N with auxin treatment was successful, we investigated the stiffness of chromosomes and centromeres. Before studying the mechanical effects of CENP-C/N degradation on the centromere, we analyzed the effect of whole-chromosome stiffness with and without auxin treatment, the results of which are consolidated in Fig. 5.3B. We found that degradation of CENP-C caused a statistically significant increase in doubling force from  $125 \pm 20$  pN in untreated cells to  $205 \pm 35$  pN in auxin treated cells. Degradation of CENP-N caused a

statistically insignificant increase in doubling force from  $135 \pm 15$  pN in untreated cells to  $175 \pm 30$  pN in auxin treated cells.

Moving to the centromere stretching experiments, we stretched the chromosome more than the amount for the whole-chromosome mechanics (5 consecutive  $12 \mu\text{m}$  stretches, instead of the 6 stretches at  $6 \mu\text{m}$ , returning to its original length), while observing the amount the CENP-A fluorescence stretches, as observed by its FWHM in the fluorescent channel. By eye, it appeared that the centromere didn't stretch at all in chromosomes from both the untreated and auxin treated cells, merely appearing to go in or out of focus. Because of this, we used a comparison between the chromosome arm stretch and centromere stretch as to not have infinitely stiff and negatively stiff centromere measurements. When quantifying the stretch of the centromere over the chromosome, as described in section 5.2.5, the centromeres of ASTC 405 and 409 were very stiff, either stretched 100-fold less than the chromosome arms or unable to be seen stretching. This quantification can be seen in Fig. 5.3C. In addition, we looked at centromere stretching in the cells with degraded CENP-C and CENP-N in ASTC 405 and 409, respectively. CENP-C/N degradation via auxin treatment did not statistically significantly change the amount the centromere stretched. We should note that the ability to detect the stretch of the centromere is based on our limitations in pixel size detection of the centromere, since we are dealing with a small object (about  $1 \mu\text{m}$ ) and our setup can only detect around  $90 \text{ nm}$  per pixel, we may be limited by our detection capabilities, the specific z-section imaging of the image, and any additional complications that arise from photobleaching. However, in our hands, both the untreated and CENP-C/N degradations show no obvious differences between them.

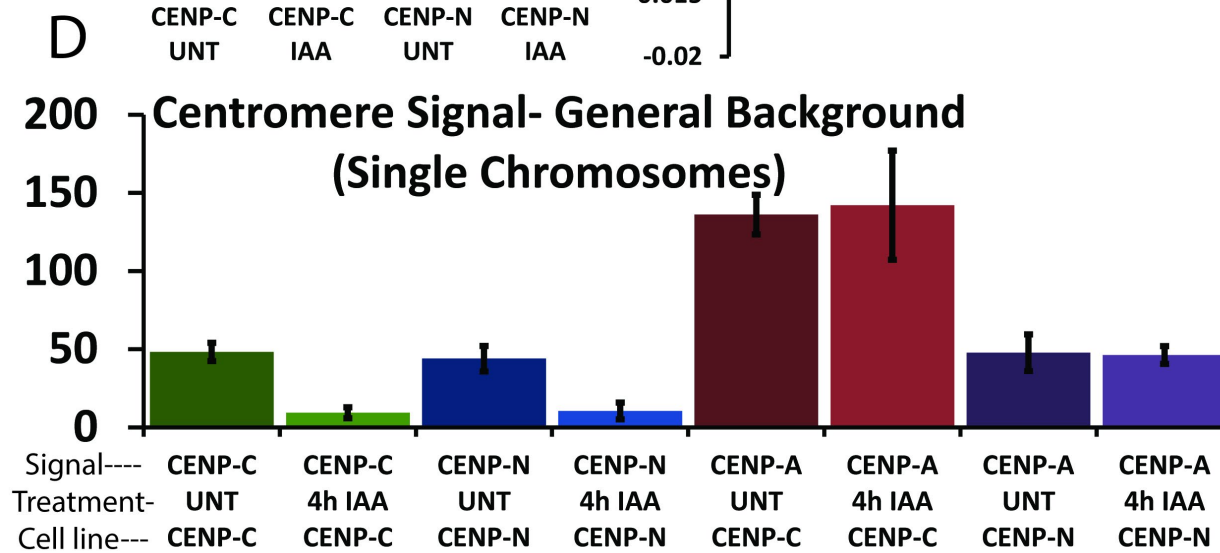
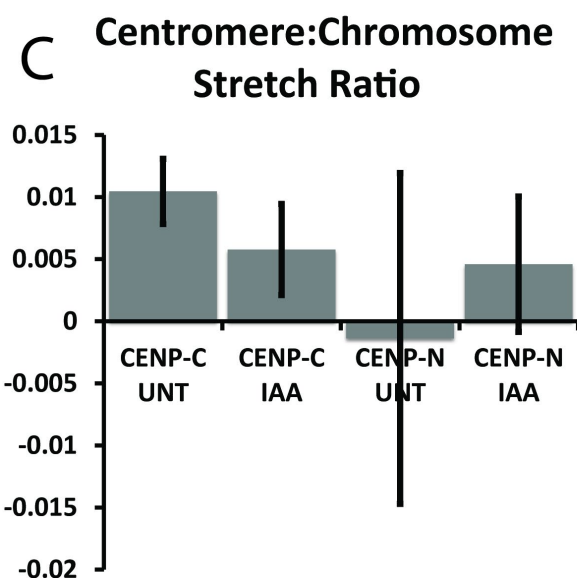
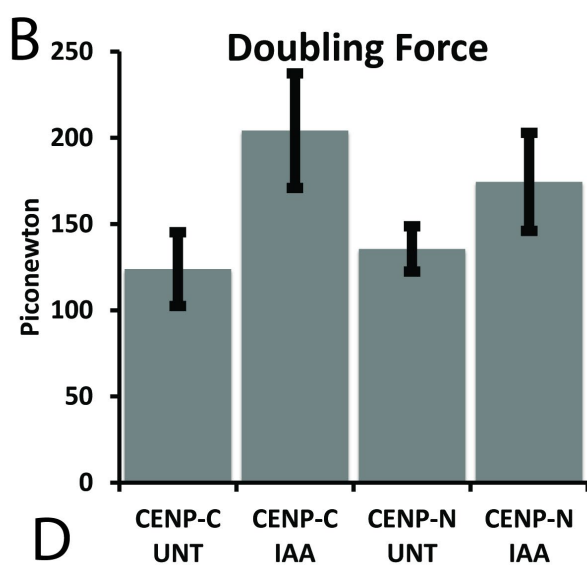
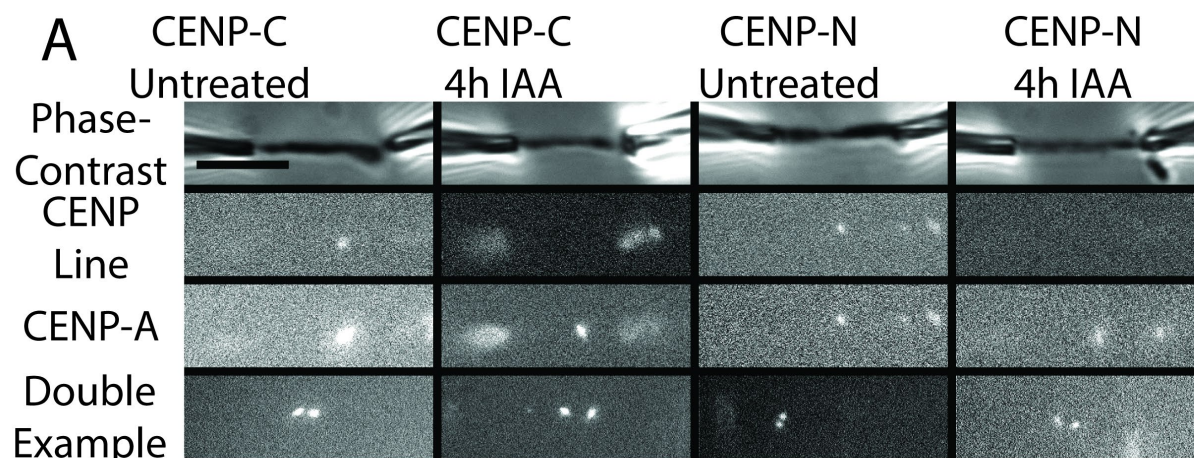


**Figure 5.3. Quantification of the mechanics and fluorescence of isolated chromosomes.**

(A) Example isolated chromosomes and centromere fluorescence. Here we show an example of an isolated chromosome in the CENP-C and CENP-N cell line, both with and without auxin treatment. The first row shows the phase-contrast imaging, while the lower two show the fluorescent imaging of the AID-tag-containing molecule (CENP-C or N) and CENP-A respectively. The examples show that the fluorescence of CENP-C and N are close to background but retain the fluorescence of the CENP-A signal, allowing us to measure its length over stretching. All conditions lead to instances that yield a doublet centromere, possibly from the association of the sister chromatids in mitosis. Scale bar represents 10  $\mu\text{m}$ . (B) Quantification of chromosomal stiffness. Here we show the quantification of the CENP-C and N cell lines chromosomal stiffness with and without auxin treatment. CENP-C degradation caused a statistically significant increase from  $125 \pm 20$  pN (N=11) to  $205 \pm 30$  pN (N=9) with auxin treatment. CENP-N degradation had no statistically significant change from  $135 \pm 15$  pN (N=11) to  $175 \pm 30$  pN (N=11) with auxin treatment. (C) Quantification of centromeric stretch over lines and conditions. The length of the centromere is calculated as the Full-Width at Half-Maximum, while the stretch of the chromosome as its entirety is calculated by analyzing the phase-contrast image of the chromosome and measuring the pipette-to-pipette distance. The CENP-A signal in the untreated CENP-C line stretched  $0.010 \pm 0.003$  (N=8) the length of the entire chromosome,  $0.006 \pm 0.004$  (N=7) in the auxin treated CENP-C line,  $-0.001 \pm 0.013$  (N=12) in the untreated CENP-N line, and  $0.005 \pm 0.005$  (N=8) in the CENP-N auxin treated line. The highest stretch (the untreated CENP-C line) indicates that the centromere is approximately 100-fold stiffer than the chromosome arms on average as the lowest estimate. (D) CENP intensity of the centromere in a single isolated chromosome on the single chromosome. The CENP-C signal was changed from  $50 \pm 5$  (N=11) counts above background to  $10 \pm 5$  (N=9) counts above background in auxin treatment. The CENP-N signal was changed from  $45 \pm 10$  (N=12) counts above background to  $10 \pm 5$  (N=10) counts above background in auxin treatment. The CENP-A signal was unchanged with auxin treatment in the CENP-C line from  $135 \pm 15$  counts above background to  $150 \pm 35$  counts above background in auxin treatment. The CENP-A signal was unchanged with auxin treatment in the CENP-N line from  $50 \pm 10$  counts above background to  $45 \pm 5$  counts above background in auxin treatment.

#### 5.4 Conclusions, discussion, and future directions

In this study, we sought to investigate if members of the CCAN would affect centromeric stiffness through tracking fluorescent CENP-A. We specifically performed experiments observing the degradation of CENP-C and CENP-N, which directly connect to CENP-A (Cao et al., 2018; Carroll et al., 2010; Carroll et al., 2009; McKinley et al., 2015). We found that we were able to degrade CENP-C and CENP-N without affecting the levels of CENP-A with auxin treatment. However, despite the critical roles played by CENP-C and CENP-N in CCAN function, (Musacchio & Desai, 2017; Perpelescu & Fukagawa, 2011), their degradation did not affect centromeric or chromosomal longitudinal stiffness to our detection capabilities. This suggests that the innate stiffness of the centromere may not be based on the CCAN, and its high stiffness is connected to other items. However, with higher detection capabilities or in repeated experiments and better focusing and z-scanning capabilities of the centromere, we may uncover some other ways the centromere is affected by CENP-C/N degradation. It should be noted that this hypothesis also assumes that the stretching stress is directly transduced along the centromere when the entire chromosome is stretched. Since these experiments did not affect centromeric stiffness, we are unable to comment on the ability of the centromere, which is innately very stiff, to affect overall chromosomal stiffness.

While the two centromeric proteins we chose to study were important for their direct connection to CENP-A and integral to the CCAN, the entirety of the CCAN is a complex and interdependent structure (Perpelescu & Fukagawa, 2011). Since both proteins chosen connect to CENP-A, it may be worthwhile to test a concurrent knockdown of CENP-C and CENP-N and study the effects on centromeric stretching if the presences of both are important for CCAN function (Cao et al., 2018). However, our preliminary results are still unexpected, as CENP-C is

the predominant factor in localizing the CCAN to the centromere during mitosis (Moree et al., 2011; Watanabe et al., 2019). Additional experiments could include depletion of proteins responsible for the CENP-H/I/K/M complex, which form the core integration structure for the CCAN (Musacchio & Desai, 2017). If both experiments show a lack of effect on the centromere's stiffness, we can be more certain that it is not only the CENP-C/N's role in centromeric stiffness, but that the CCAN is less important for imparting mechanical centromeric stiffness (providing further experiments also demonstrate we can stretch centromere and detect the amount of stretch the centromere undergoes). We can also look at the localization of the other CCAN proteins in CENP-C/N or both knockdowns to verify their effect on the CCAN formation. Once we verify the state of the CCAN in CENP-C/N knockdown, we can make further statements on the function of the CCAN in imparting stiffness to the centromere.

This chapter reports experiments where we attempt to longitudinally stretch the centromere via longitudinal stretching of the whole chromosome. It may be that the centromere (as judged by CENP-A fluorescence) does not have its size changed by CENP-C/N degradation, and that the centromere is somehow not connected to the part of the chromosome that is being longitudinally stretched. It may also be possible that the centromere retains its axial elastic response while losing its transverse (kinetochore-facing) elastic response when CENP-C/N is degraded. Given that we observe centromeric staining on and through the cross-section of the chromosome, and that the centromeric chromatin (CENP-A) appears to be very stiff, these hypotheses seem somewhat unlikely. Nevertheless, we can imagine that the CCAN might be substantially mechanically weaker following CENP-C/N degradation, yet our full-chromosome longitudinal-stretching assay may not be able to detect the change. An experiment that could test this possibility is attachment of a pipette/glass needle directly to the centromere itself (*e.g.*, by

using antibodies to centromeric proteins attached to the needle or pipette) and pull the chromosome along the transverse axis. An additional experiment could involve aspirating the chromosome in a manner that only leaves the centromere stuck between the two pipettes, allowing more force to be localized to the centromere. While more difficult to arrange than the present experiments, such experiments could be valuable as a more direct method to examine the structural roles played by centromeric proteins in CCAN integrity.

An additional way of testing the functionality of the CCAN in these experiments could be to perform these experiments with a longer knockdown of CCAN proteins. Since the CCAN is constantly associated with the centromere over the cell cycle (Cao et al., 2018; Gambogi & Black, 2019), there could be some limiting effects that do not occur during our 4-hour auxin treatment. The CCAN still imparts some remaining structural functionality through the cell cycle in interphase, which could be further abolished in longer-term knockdown experiments. A change in results would, however, be somewhat surprising, considering the experiments using siRNA-based degradation of CENP-C did not show any change in CENP-A stretching, which used a longer knockdown time (Sun, 2014). A change in results would also be somewhat perplexing, since localization of the CCAN in mitosis is dependent on CENP-C's presence, activity, and integration into the centromere. The dependence of the CCAN on CENP-C in mitosis also suggests that the CCAN may not be critical for creating the stiff centromere.

While there is a substantial lack of any effect on centromeric chromatin stretch with the depletion of CENP-C and CENP-N, investigations into CCAN and KMN stretch with auxin degradation of CENP-C/N may prove insightful. Further experiments could also investigate the innate stretch of the centromere while tracking CENP-C/N or other proteins to see if it matches the stiffness of the CENP-A-containing part of the chromosome. If the CCAN remains functional

and can still recruit parts of the KMN network in CENP-C and CENP-N degradation, we can further study CCAN stretch or KMN network stretch. This could be utilized to study how each of those underlying proteins affect the stability and stiffness of the inner kinetochore via studying the CCAN and the outer kinetochore via the KMN network. One would expect that there is a substantial reduction in both stiffness and stability of both networks, by their fluorescence smearing more in the CENP-C or CENP-N knockdown, or by breaking a solid fluorescent structure into many smaller structures.

If the CCAN truly does not affect the stiffness of the centromere at the chromatin level, it still leaves the question of what specifically and to what degree different objects stiffen the centromere. An obvious answer, which has been explored in the study of the centromere as a spring across the spindle are the SMC complexes, condensin and cohesin, and the enrichment in heterochromatin at the centromere (Lawrimore & Bloom, 2019; Stephens et al., 2011; Stephens et al., 2013). These would be an obvious choice to investigate as condensin, cohesin, and heterochromatin are enriched at the centromere. Condensin has been shown to affect the whole chromosome when their chromosomal levels are altered (M. Sun et al., 2018b). Cohesin has been shown to affect the spindle pole stiffness but may not affect centromeric stiffness along the chromosomal axis (Stephens et al., 2011; Stephens et al., 2013). To test the relationship between centromeric stiffness and these molecules, we could knock down condensin, cohesin, or alter histone PTM levels and repeat the centromere stretching via CENP-A tracking. Each molecule in part could allow us a glimpse into what specifically and to what extent each of the molecules affect the centromeric stiffness. The interplay of the CCAN and other parts of the chromosome, such as the chromosome passenger complex and other molecules that regulate integration of

chromatin-organizing molecules, could explain why degradation of CENP-C affects the mitotic chromosome as a whole, but not the underlying centromere.

Unfortunately for the experiment proposed above, condensin and heterochromatin, have been shown to affect whole-chromosome stiffness, meaning that the effects on centromeric stiffness could not give insight into how centromeric stiffness affects the stiffness of the whole mitotic chromosome. To probe this specific question, we would have to analyze the effect of perturbations to proteins, which regulate the recruitment of condensin, cohesin, and heterochromatin to the centromere, although this would also most likely affect the normal cell cycle function. If we could specifically alter centromeric stiffness and observe the overall chromosome stiffness, we would gain insights into chromosome structure. By investigating the relationship between the centromere's stiffness and the whole chromosome, we may be able to determine how the chromosome is folded, *i.e.*, whether it is a spring of chromatin in parallel or in series. By observing what molecules affect the centromere, we may also be able to understand why the centromere is very stiff. Some hypotheses include reducing the force the spindle imparts on the whole chromosome by stiffening its anchor point, an after effect from centromeric stabilization, orientation of the kinetochore, and needing to match the pulling force of the microtubule spindle.

The stiffness of the centromere may also relate to the stability of the centromere. When *in-vitro* CENP-A nucleosomes were analyzed for their stability, it was shown that the addition of CENP-C and CENP-N created more stable nucleosomes as well as creating very stable nucleosomes with the addition of both proteins (Cao et al., 2018). However, when inside the cell, it was shown that there was no loss of CENP-A from the centrosome when either CENP-C or CENP-N were depleted, as well as their simultaneous depletion, suggesting that there was no

change in stability when inside a living cell. Since we are studying the chromosome right out of a living cell, the stability may be correlated with the live cell instead of the *in-vitro* experiment. If this is the case, then it is possible that our results have a direct relationship with the stability of the nucleosomes in the centromere rather than testing the stretch of the centromere *de facto*. This hypothesis could be tested by observing other factors known to affect the stability of CENP-A in mitosis to see if there is a change in the perceived stretch of the centromere.

## Chapter 6. Conclusion – Achievements, findings, and future directions

*The following section details the published papers as achievements, the consolidation of all the projects into an overarching scientific finding on the stiffness of mitotic chromosomes, and future directions of the projects presented as follow-up experiments and projects based on the findings of the current state of all the presented projects.*

Several achievements associated with my Ph.D. thesis research will be discussed in this section including a retrospective on my thesis proposal from my qualifying exam. From these achievements, several general findings on the nature of mitotic chromosomes have been found. These general findings display some connected parts, which will also be covered in this section. These general findings also display some openings for the future directions in the study of mitotic chromosomes through micromanipulation, and some of these future projects will be explained. During my thesis research, there have also been several projects that have been discussed and hypothesized about, but which did not fit any overarching completed work. I will give a short rationale and motivation for these projects and the proposed experiments. This section will be written in first person as to emphasize the retrospective nature of the results as a whole.

### **6.1 Thesis proposal retrospective and achievements**

In my original thesis proposal, there was an emphasis on studying topoisomerase II (TopoII), which did not end up being explored. This would have been studied by observing its colocalization and interplay with condensin and cohesin (Aim1) and its effect on mitotic chromosome stiffness (Aim 2). While the colocalization of condensin and cohesin was not studied, the SMC-AID project (Chapter 2) allowed me to study the mechanical effect of their rapid removal on mitotic chromosomes. This project remains unpublished, but the work currently performed has laid a good groundwork for a future paper with further experiments. The project investigating the effects of altered histone PTMs on mitotic chromosome stiffness (Aim 3) was fully realized in a completed project/paper (R. Biggs et al., 2019). Investigating the role of HP1 $\alpha$

on mitotic chromosome stiffness further expanded upon this project, which has likewise been published (Strom et al., 2021).

The two remaining scientifically oriented projects were born of collaborations with those interested in exploring chromosomal stiffness. The properties of meiotic I prophase spermatocyte chromosomes by collaboration with Huanyu Qiao at UI Urbana, yielded a published paper demonstrating the structural similarities of meiotic I prophase and mitotic chromosomes (R. J. Biggs et al., 2020). The door also remains open for many future investigations into meiotic chromosomes through my efforts demonstrating the possibility of meiotic prophase chromosome isolation. The centromeric stiffness project was started by my predecessor, Mina Sun, in collaboration with Aaron Straight at Stanford. The work remains unpublished. However, the current results have laid the groundwork for a future paper, given some additional, straightforward experiments.

During my Ph.D. research time, I have published four papers, two of which I am the sole first author, one where I am a co-first author of three total first authors, and one where I am a second author. I provided necessary control mechanical experiments, centromere fluorescence colocalization experiments, and fluorescent structural experiments with fragmented antibodies in the paper investigating the role of condensin I, II, and both isoforms on mitotic chromosomes (M. Sun et al., 2018b). My first first-author paper investigated the mechanical role of histone PTMs on mitotic chromosomes (R. Biggs et al., 2019). This project was inspired by my experimental mentor, Andrew Stephens, who studied the role histone PTMs play in the stiffness of interphase nuclei. I was also able to collaborate with him in the follow-up paper observing the role in HP1 $\alpha$  on mitotic chromosome stiffness (Strom et al., 2021). My other first-author paper demonstrated that it is possible to isolate and study meiotic I chromosomes, which allowed us to

show that meiotic chromosomes are very stiff, but still dissolve with MNase treatment (R. J. Biggs et al., 2020). During my thesis research I have also created a new method of chromosome isolation, involving stabilizing the chromosome bundle after removal from the cell to grab a single chromosome from the bundle. With the help of my classmate, Daniel Shams, I also created a python script for analyzing the data of stretch-deflection curves and Microsoft Excel sheets for ease of comparison to further automating data analysis. These files will be incorporated into a methods paper and protocol manual for isolating chromosomes.

## **6.2 Scientific findings and themes**

While these achievements are notable, the purpose of a PhD thesis is to further the scientific understanding of the field, which my work has done. An underlying theme of my PhD work is that the underlying chromatin greatly affects the axial stiffness of mitotic and meiotic chromosomes. The projects on histone PTMs and HP1 $\alpha$  are the most direct form of these findings. I showed that histone hypermethylation treatment stiffens mitotic chromosomes without affecting condensin levels. It is interesting to note that histone hyperacetylation treatment causes no net change in stiffness as it does in interphase nuclei, despite being a mark actively downregulated during normal mitosis. Knockdown of HP1 $\alpha$ , which interacts with heterochromatic methyl marks, also demonstrates how the underlying chromatin influences the stiffness of mitotic chromosomes. Chromosomes weaken when HP1 $\alpha$  is removed from the cell, but chromosomes still stiffen when histones are hypermethylated while HP1 $\alpha$  is absent. This further shows that HP1 $\alpha$  stiffens mitotic chromosomes in an alternate pathway from the histone PTMs.

Our work in meiotic chromosomes also demonstrates the importance of chromatin in affecting chromosomal stiffness. We demonstrated that the underlying chromatin is responsible for the connectivity of meiotic chromosomes. While this work found a substantial difference in the stiffness of mitotic chromosomes and meiotic chromosomes, the underlying cause remains unknown. The cause may be due to chromatin differences in meiosis and mitosis. We also showed that meiotic prophase I chromosomes in mice possessing synaptonemal complex protein 1 (SYCP1)-null mutations had the same stiffness as wild-type chromosomes. This suggests that the large, chromatin-organizing synaptonemal complex appears to have little effect on meiotic chromosome stiffness. This further suggests an importance of other mechanisms, perhaps chromatin based, to stiffen mitotic chromosomes.

I have also demonstrated that the stiffness of the centromere does not rely on two critical constitutively centromeric associated network (CCAN) proteins, another chromatin-organizing complex. I demonstrated this by showing there was no difference in the amount CENP-A stretched in untreated and auxin-treated cells, which degraded CENP-C or CENP-N. This suggests that the CCAN is not responsible for the innately high stiffness of the centromere. Since the pericentromere is enriched of with heterochromatin, its enrichment could be partly responsible for the centromere's stiffness, again demonstrating the interplay of chromatin and chromosomal stiffness. However, since the centromere is also enriched in the SMC complexes, condensin and cohesin, their presence (and not the underlying chromatin) could be responsible for stiffening the centromere to provide it with mechanical rigidity.

My work on SMC complexes also reveals the important relationship between the underlying chromatin and mitotic chromosome stiffness by showing a lack of effect with rapid SMC degradation. The work on AID-based degradation of condensin demonstrated no change in

mechanical stiffness for any isoform, which is at odds with the siRNA-based removal of condensin. Perhaps these two projects demonstrate that the SMC complexes are important for shaping chromosomes into their mitotic shape, thus granting them their stiffness, but are not important as static objects in maintaining mitotic chromosome stiffness. The rapid depletion of SMC2 demonstrates that there is a difference between stiffness and morphology, as rapid depletion of SMC2 caused the chromosome bundle to lose its structure like siRNA-based depletion, but the rapid degradation of SMC2 maintained a similar stiffness to the untreated chromosomes. This conflict demonstrates the need for further research. The knockdown of cohesin did not affect chromosomal stiffness, which was expected, as its function on mitotic chromosomes does compact mitotic chromosomes. The knockdown of Ki-67 further suggests that chromatin entanglements stiffen mitotic chromosomes, further demonstrating the interplay of chromatin and mitotic chromosome stiffness.

### **6.3 Future directions from existing projects**

While my projects on mitotic chromosome stiffness have revealed some important structural information concerning mitotic chromosome structure, they have also raised further questions and revealed additional experiments, projects, and avenues of investigating chromosome structure through micromanipulation. I will give a quick summary of the findings of these projects, the questions they reveal, and describe the experiments that can be performed to address said questions. A general future direction we can take with micromanipulation as seen in multiple projects is AID-based degradation of proteins, which open many future experiments if an AID tag can be attached to a protein of interest. We have also been able to study fluorescent

molecules in the chromosome bundle and along mitotic chromosomes for further study of protein dynamics, which can be used in future projects.

### **6.3.1 SMC complex future directions**

When I used auxin treatment to degrade condensin, via CAP-H, CAP-H2, or SMC2 degradation, I found no change in the stiffness of isolated mitotic chromosomes. This finding is in direct contradiction to the findings that slow removal of CAP-G, CAP-G2, or SMC2 with siRNA-based treatments caused the mitotic chromosome to weaken. Future experiments using the AID-based system could potentially address this difference by varying the length of knockdown in the treatment to determine if the presence of condensin in interphase affects the mitotic chromosome and its stiffness. We could also vary the amount of auxin in the treatments to create a graph exploring the relationship between amount of said protein and the stiffness, not a mere binary of protein presence or absence. Our condensin degradation experiments did show a morphological phenotype with condensin removal, despite not affecting chromosome stiffness.

Since we can isolate and hold mitotic chromosome bundles, we may be able to further develop and analyze bundle morphology in relationship to protein knockdown as an additional assay for studying mitotic chromosome structure using chromosome micromanipulation. The bundle holding experiments could also be used to track fluorescence of a protein over time in untreated cells by imaging the bundles once after a set amount of time in buffer, which could further our understanding of protein dynamics on chromosomes.

These strains could be used further as a means of tracking the relative position, *i.e.*, colocalization of other proteins as well as fluorescently labeled DNA sequences through TALEN-transfected cells for specific DNA sequences. These experiments would allow us to better understand the relationship between proteins and their loading dynamics onto

chromosomes. Our TALEN-transfected cells can also be used and stretched to further determine their relationship with SMC molecules, stiffness relationship between a specific DNA sequence, and relationship to histone PTMs.

While the strain in our current possession has been useful in studying condensin's role on mitotic chromosomes, there may be other strains that perform better. The current AID-SMC2 strain has a less robust knockdown efficiency than other AID-tagged molecules and requires an additional treatment of doxycycline to activate the TIR1 complex and removing these problems may allow us to address the knockdown concerns in a more thorough manner.

Other condensin functions could also be further studied by comparing chromosome stiffnesses from SMC ATPase mutants (Elbatsh et al., 2019). Other cell lines with enzymatically degradable targets (TEV-cleavage sites) would definitively answer the question on condensin stiffness as well if engineered into a cell culture cell line (Houlard et al., 2015). Spraying purified condensin onto mitotic chromosomes or protein degraded chromosomes may yield interesting results, which could be related to its function (Keenholtz et al., 2017).

### **6.3.2 Histone PTM and chromatin state future directions**

In our studies of histone PTMs and associated histone PTM readers, we have shown that increased heterochromatin marks stiffen mitotic chromosomes, removal of heterochromatin-associated proteins weaken mitotic chromosomes, but altering histone acetylation does not affect mitotic chromosome stiffness (R. Biggs et al., 2019; Strom et al., 2021). This finding is surprising, considering interphase nuclei weaken with acetylation treatment and recent (although unpublished) experiments have shown that hyperacetylating histones in mitosis causes a decrease in density (Schneider et al., 2021; Stephens et al., 2018). However, these density experiments are performed with a substantially higher amount of HDACis over a shorter period. Recapitulating

our original findings (2 mM VPA or 50 nM TSA for 16-24 hr) and performing the treatment with the same HDACi treatment as in the density experiments (5  $\mu$ M TSA for 3-4 hr, typically with additional drugs that stall, synchronize, or otherwise affect the cell cycle) may be worthwhile.

Further avenues of investigation relating chromatin state to mitotic chromosome stiffness include altering DNA methylation and decreasing histone methylation or acetylation instead of increasing said marks to see if there is consistency with the marks or the direction of change (if the chromosome stiffens easily and weakens rarely). Alteration to other histone marks, especially phosphorylation, due to its role in the phospho-methyl switch, is another avenue worth pursuing. If hyperacetylation truly does not affect mitotic chromosome stiffness, the reason why it doesn't change could be an interesting avenue of further study.

### **6.3.3 Meiotic chromosome and synaptonemal complex future directions**

Our investigations into meiotic prophase I chromosomes demonstrated that they are much stiffer than mitotic chromosomes, which does not change when they lack SYCP1; they weaken with protease treatments and dissolve with nuclease treatments (R. J. Biggs et al., 2020). These findings have also opened the door to many future experiments. For instance, meiotic prophase I itself has many different substages, which could be detected by the presence of different antibodies to determine the substage of the cell/chromosome. These substages are also connected with several structural changes, which may relate to structure and stiffness. Comparing the stiffness of chromosomes isolated before or after SC formation, before or after crossover designation, or before and after the chiasmata may reveal some structural differences.

We could also study meiotic chromosomes by altering proteins in the cohesin core or the lateral elements (SYCP2/3), which precede the formation of the central element and the binding of SYCP1. Since my work has shown how to isolate and stretch meiotic prophase I

chromosomes and other experiments have shown methods of isolating meiotic II metaphase chromosomes (Hornick et al., 2015), additional comparisons may allow further comparisons in meiotic staging and stiffness. The mouse age between spermatocytes may also be an avenue of investigation, since there was a difference seen in female meiotic II chromosomes.

Other experiments could involve determining the relationship between fertility defects and meiotic chromosome stiffness. When the chromosomes are fully individualized in diplotene, it is possible that with very delicate control, we could also investigate stretching the chiasmata in diplotene. Finally, we may wish to use the bundle-hold method of stretching chromosomes to ensure that the force of removal from the prophase nuclei does not alter meiotic chromosome stiffness.

#### **6.3.4 Centromere and CCAN future projects**

Our investigations into centromeric stretching revealed the CENP-A region of the chromosome is very stiff compared to the chromosome arms, barely stretching with substantial force. This change is not affected by the removal of CENP-C or CENP-N. Studying the co-depletion of CENP-C and CENP-N may affect CENP-A stability, as previous experiments showed an additive effect of CENP-C and CENP-N to CENP-A stability. We could also use the cell lines to track CENP-C and CENP-N signal over a chromosome stretch in a similar manner CENP-A to see if the CCAN has a similar stiffness to the centromere.

Further experiments could also be used to investigate the stability of other complexes of the CCAN or the KMN network with CENP-C/N degradation; this could also be used to determine if my lack of results arise from degrading CENP-C/N not disrupting the whole CCAN, but merely the individual proteins. As in the chiasmata experiments, there may be a way to

stretch the centromere in a lateral manner either through grabbing a single chromatid arm per pipette or by using antibody-coated glass pipettes.

Another experiment could also involve tracking centromere stretching after degrading SMC2, CAP-H, CAP-H2, and Rad-21 with fluorescent-labeled anti-CREST antibody, since we have the strains for the AID-SMC complexes. Additionally, by using the previously studied histone PTM altering drugs and AID-based HP1 $\alpha$  degradation with the CREST antibodies, we can study the effects of heterochromatin on the stiffness of the centromere. It may also be useful to visualize the amount normal H3 stretches, so we can identify if there is a difference between centromeric and chromosome arm stretches.

#### **6.4 Future directions - other projects**

While there are many different follow-up projects described in this thesis, there are several other project ideas that use micromanipulation to explore different aspects of mitotic chromosome formation and structure. To start, we could study topoisomerase functions, as my original thesis proposal described. Topoisomerase II (TopoII) can disentangle mitotic chromosomes as well as bind, crosslink, and structurally interact with chromosomes. Some experiments have shown that TopoII's ability to change chromatin topology is separate from its ability to bind and hold chromatin (Lane et al., 2013). The Marko lab has access to the purified proteins from the experiments that use the different mutants of TopoII. Future experiments could also explore TopoII behavior by its removal or inhibition. The work on TopoII could be used in conjunction with our previously proposed colocalization experiments of condensin. Active TopoII spray onto mitotic chromosomes with high entanglements could also be used as an investigation into how Ki-67 and condensin removal affects chromatin entanglement.

Variation of mitotic chromosome stiffness between different cell types has already been seen in my investigations into SMC complexes but could be further studied and systematically studied to determine if there are constant properties between said cell types that demonstrate a fundamental change in chromosome structure that reveals itself in stiffness measurements. Since there are differences in the transcription profile and division protocols of different strains and tissue types, there may be a systematic difference between mitotic chromosomal stiffness between them that could be studied by a screen of chromosome stiffness over several tissue types. We could further study chromosomal stiffness by testing mitotic chromosome stiffness from tumor cells that display different levels of malignancy, drug resistance, metastasis, and so forth, which could assist in relating disease phenotype to mechanical properties. This could be performed in collaboration with a patient derived xenograft repository that we can access. Another screen could search for differences in developmental state and mitotic chromosomal stiffness. Since different cellular protocols, transcriptional state, and division protocols are different across cell stages in development, it may relate to differences in mitotic chromosomal stiffness. Thus, by performing this screen, we may be able to understand what specifically underlies the stiffness of mitotic chromosomes.

Another project that has been proposed is the relationship between DNA damage during mitosis and the stiffness of mitotic chromosomes. During mitosis, DNA damage is marked for repair by proteins that associate with the damaged site and would presumably stiffen the chromosome by attaching to the underlying chromatin. However, these sites are not repaired over mitosis and remain through mitosis until they are repaired in the following G1 phase of the cell cycle after cell division and chromosome decondensation. Since there are proteins physically binding to the underlying chromatin, studying the amount of DNA damage, relating it to the

lethality of the DNA damage, the type of DNA damage, and the repair-marking pathway of the damage, we may be able to relate a cellular process to the stiffness of mitotic chromosomes.

Mitotic arrests have been used to study chromosomal stiffness and the changes brought on by the arrests. This treatment caused an overloading of condensin on the proteins used a high amount of nocodazole. Future metaphase arrest experiments could be performed with a lower dose of nocodazole to verify that metaphase arrest and not the harsh treatment is responsible for the stiffening phenotype. These experiments could also be used in conjunction with our fluorescently labeled condensin subunits to easily observe condensin loading amount. We could also use metaphase arrest in conjunction with our centromere stretching experiments and histone tracking experiments to observe if there is a systematic change in the dynamics of histones or centromeres during metaphase. Further experiments could also investigate the role of SMC complexes in metaphase arrest (via SMC2, CAP-H, CAP-H2, Rad-21, Ki-67, or TopoII knockdown) by performing micromanipulation experiments. We could also use nuclease and protease treatments in conjunction with metaphase arrest treatments. In these treatments, we could see if there is a major structural difference in the movement to metaphase by comparing the relative weakening of nuclease or protease treatments to the typical prometaphase chromosomes. In addition to simply arresting cells in metaphase, we can also investigate the stiffness of the chromosome in different substages of mitosis by synchronizing cells in specific stages of mitosis, staining for specific markers of mitotic substages, or by synchronizing cells in at a specific time, then releasing them to isolate cells at a given point after their release (such as a thymidine block, which arrests cells in G2).

Future directions also include expanding this technique into other chromosome-containing systems. One recent example comes in the form of *Xenopus* cell-free chromosome

assembly. Previous work on an analogous method of capturing mitotic-like chromosomes demonstrated it was possible to isolate mitotic-folded chromosomes in egg extract (Almagro & Dimitrov, 2005; Shintomi et al., 2015). In this system, the biochemical reaction of adding sperm into egg extract caused the sperm chromatin to fold into dense strings of chromatin, mimicking the innate steps of folding mitotic chromosomes during development. A recent collaboration with Coral Zhou in the lab of Rebecca Heald at UC Berkeley has resulted in pilot experiments demonstrating that we can capture these egg-extract-based chromosomes, which can be further studied and optimized to allow more mitotic chromosome experiments to be performed. This is of note, since other experiments have shown that these chromosomes go through distinct phases of chromosome folding, which stop when lacking condensin or histone-remodeling enzymes and reach their end state with minimal factors (Shintomi et al., 2015).

While the experimental ideas for future projects are near-limitless, we will discuss an underlying concept of a future project. One question that has been revealed, but not answered in this thesis is the direct relationship between the mechanical features of chromosomes and their structure, indeed many of our future experiments attempt to address this underlying issue. Since the mitotic chromosome is a physical object, it should have several characteristic behaviors under tension and through repeated cycles of stretching. By performing a series of stretches, perhaps in rapid succession or in slightly overstretching the chromosome, we may be able to determine the specific types of connections the underlying chromatin makes when folded into a mitotic chromosome. By determining these connections, we may be able to make further judgements as to how the chromosome is folded. If we track different objects over a stretching experiment or track their displacement in relation to mechanical failure, we may be better equipped to guess the method that the cell folds mitotic chromosomes. This would help answer a

fundamental question of the relationship between the mechanical properties, stiffness, structure, and morphology of mitotic chromosomes.

## References

- Akram, S., Yang, F., Li, J., Adams, G., Liu, Y., Zhuang, X., . . . Liu, X. (2018). LRIF1 interacts with HP1alpha to coordinate accurate chromosome segregation during mitosis. *J Mol Cell Biol*, *10*(6), 527-538. doi:10.1093/jmcb/mjy040
- Alabert, C., Barth, T. K., Reveron-Gomez, N., Sidoli, S., Schmidt, A., Jensen, O. N., . . . Groth, A. (2015). Two distinct modes for propagation of histone PTMs across the cell cycle. *Genes Dev*, *29*(6), 585-590. doi:10.1101/gad.256354.114
- Alabert, C., Jasencakova, Z., & Groth, A. (2017). Chromatin Replication and Histone Dynamics. *Adv Exp Med Biol*, *1042*, 311-333. doi:10.1007/978-981-10-6955-0\_15
- Alipour, E., & Marko, J. F. (2012). Self-organization of domain structures by DNA-loop-extruding enzymes. *Nucleic Acids Res*, *40*(22), 11202-11212. doi:10.1093/nar/gks925
- Almagro, S., & Dimitrov, S. (2005). Assembly and micromanipulation of *Xenopus* in vitro-assembled mitotic chromosomes. *Curr Protoc Cell Biol*, Chapter 22, Unit 22 29. doi:10.1002/0471143030.cb2209s26
- Almagro, S., Riveline, D., Hirano, T., Houchmandzadeh, B., & Dimitrov, S. (2004). The mitotic chromosome is an assembly of rigid elastic axes organized by structural maintenance of chromosomes (SMC) proteins and surrounded by a soft chromatin envelope. *J Biol Chem*, *279*(7), 5118-5126. doi:10.1074/jbc.M307221200
- Alpsoy, A., Sood, S., & Dykhuizen, E. C. (2021). At the Crossroad of Gene Regulation and Genome Organization: Potential Roles for ATP-Dependent Chromatin Remodelers in the Regulation of CTCF-Mediated 3D Architecture. *Biology (Basel)*, *10*(4). doi:10.3390/biology10040272
- Anderson, D. E., Losada, A., Erickson, H. P., & Hirano, T. (2002). Condensin and cohesin display different arm conformations with characteristic hinge angles. *J Cell Biol*, *156*(3), 419-424. doi:10.1083/jcb.200111002
- Aragon, L. (2018). The Smc5/6 Complex: New and Old Functions of the Enigmatic Long-Distance Relative. *Annu Rev Genet*, *52*, 89-107. doi:10.1146/annurev-genet-120417-031353
- Au, W. C., Dawson, A. R., Rawson, D. W., Taylor, S. B., Baker, R. E., & Basrai, M. A. (2013). A novel role of the N terminus of budding yeast histone H3 variant Cse4 in ubiquitin-mediated proteolysis. *Genetics*, *194*(2), 513-518. doi:10.1534/genetics.113.149898
- Badrinarayanan, A., Reyes-Lamothe, R., Uphoff, S., Leake, M. C., & Sherratt, D. J. (2012). In vivo architecture and action of bacterial structural maintenance of chromosome proteins. *Science*, *338*(6106), 528-531. doi:10.1126/science.1227126
- Bailey, A. O., Panchenko, T., Sathyan, K. M., Petkowski, J. J., Pai, P. J., Bai, D. L., . . . Foltz, D. R. (2013). Posttranslational modification of CENP-A influences the conformation of centromeric chromatin. *Proc Natl Acad Sci U S A*, *110*(29), 11827-11832. doi:10.1073/pnas.1300325110
- Ball, A. R., Jr., & Yokomori, K. (2001). The structural maintenance of chromosomes (SMC) family of proteins in mammals. *Chromosome Res*, *9*(2), 85-96. doi:10.1023/a:1009287518015
- Banigan, E. J., & Mirny, L. A. (2020). The interplay between asymmetric and symmetric DNA loop extrusion. *Elife*, *9*. doi:10.7554/eLife.63528

- Banigan, E. J., Stephens, A. D., & Marko, J. F. (2017). Mechanics and Buckling of Biopolymeric Shells and Cell Nuclei. *Biophys J*, *113*(8), 1654-1663. doi:10.1016/j.bpj.2017.08.034
- Banigan, E. J., van den Berg, A. A., Brandao, H. B., Marko, J. F., & Mirny, L. A. (2020). Chromosome organization by one-sided and two-sided loop extrusion. *Elife*, *9*. doi:10.7554/eLife.53558
- Bannister, A. J., Schneider, R., & Kouzarides, T. (2002). Histone methylation: dynamic or static? *Cell*, *109*(7), 801-806. doi:10.1016/s0092-8674(02)00798-5
- Bannister, A. J., Zegerman, P., Partridge, J. F., Miska, E. A., Thomas, J. O., Allshire, R. C., & Kouzarides, T. (2001). Selective recognition of methylated lysine 9 on histone H3 by the HP1 chromo domain. *Nature*, *410*(6824), 120-124. doi:10.1038/35065138
- Barrington, C., Finn, R., & Hadjur, S. (2017). Cohesin biology meets the loop extrusion model. *Chromosome Res*, *25*(1), 51-60. doi:10.1007/s10577-017-9550-3
- Barysz, H., Kim, J. H., Chen, Z. A., Hudson, D. F., Rappsilber, J., Gerloff, D. L., & Earnshaw, W. C. (2015). Three-dimensional topology of the SMC2/SMC4 subcomplex from chicken condensin I revealed by cross-linking and molecular modelling. *Open Biol*, *5*(2), 150005. doi:10.1098/rsob.150005
- Batty, P., & Gerlich, D. W. (2019). Mitotic Chromosome Mechanics: How Cells Segregate Their Genome. *Trends Cell Biol*, *29*(9), 717-726. doi:10.1016/j.tcb.2019.05.007
- Baxter, J., Sen, N., Martinez, V. L., De Carandini, M. E., Schwartzman, J. B., Diffley, J. F., & Aragon, L. (2011). Positive supercoiling of mitotic DNA drives decatenation by topoisomerase II in eukaryotes. *Science*, *331*(6022), 1328-1332. doi:10.1126/science.1201538
- Bayani, J., & Squire, J. A. (2004). Traditional banding of chromosomes for cytogenetic analysis. *Curr Protoc Cell Biol*, Chapter 22, Unit 22 23. doi:10.1002/0471143030.cb2203s23
- Beck, D. B., Oda, H., Shen, S. S., & Reinberg, D. (2012). PR-Set7 and H4K20me1: at the crossroads of genome integrity, cell cycle, chromosome condensation, and transcription. *Genes Dev*, *26*(4), 325-337. doi:10.1101/gad.177444.111
- Belaghzal, H., Borrmann, T., Stephens, A. D., Lafontaine, D. L., Venev, S. V., Weng, Z., . . . Dekker, J. (2021). Liquid chromatin Hi-C characterizes compartment-dependent chromatin interaction dynamics. *Nat Genet*, *53*(3), 367-378. doi:10.1038/s41588-021-00784-4
- Bell, O., Tiwari, V. K., Thoma, N. H., & Schubeler, D. (2011). Determinants and dynamics of genome accessibility. *Nat Rev Genet*, *12*(8), 554-564. doi:10.1038/nrg3017
- Bennett, M. D. (1977). The time and duration of meiosis. *Philos Trans R Soc Lond B Biol Sci*, *277*(955), 201-226. doi:10.1098/rstb.1977.0012
- Berger, J. M., Gamblin, S. J., Harrison, S. C., & Wang, J. C. (1996). Structure and mechanism of DNA topoisomerase II. *Nature*, *379*(6562), 225-232. doi:10.1038/379225a0
- Berrios, S. (2017). Nuclear Architecture of Mouse Spermatocytes: Chromosome Topology, Heterochromatin, and Nucleolus. *Cytogenet Genome Res*, *151*(2), 61-71. doi:10.1159/000460811
- Beseda, T., Capal, P., Kubalova, I., Schubert, V., Dolezel, J., & Simkova, H. (2020). Mitotic chromosome organization: General rules meet species-specific variability. *Comput Struct Biotechnol J*, *18*, 1311-1319. doi:10.1016/j.csbj.2020.01.006

- Biggs, R., Liu, P. Z., Stephens, A. D., & Marko, J. F. (2019). Effects of altering histone posttranslational modifications on mitotic chromosome structure and mechanics. *Mol Biol Cell*, *30*(7), 820-827. doi:10.1091/mbc.E18-09-0592
- Biggs, R. J., Liu, N., Peng, Y., Marko, J. F., & Qiao, H. (2020). Micromanipulation of prophase I chromosomes from mouse spermatocytes reveals high stiffness and gel-like chromatin organization. *Commun Biol*, *3*(1), 542. doi:10.1038/s42003-020-01265-w
- Bilokapic, S., Strauss, M., & Halic, M. (2018). Cryo-EM of nucleosome core particle interactions in trans. *Sci Rep*, *8*(1), 7046. doi:10.1038/s41598-018-25429-1
- Bisig, C. G., Guiraldelli, M. F., Kouznetsova, A., Scherthan, H., Hoog, C., Dawson, D. S., & Pezza, R. J. (2012). Synaptonemal complex components persist at centromeres and are required for homologous centromere pairing in mouse spermatocytes. *PLoS Genet*, *8*(6), e1002701. doi:10.1371/journal.pgen.1002701
- Bloom, K. (2017). Liberating cohesin from cohesion. *Genes Dev*, *31*(21), 2113-2114. doi:10.1101/gad.309732.117
- Boavida, A., Santos, D., Mahtab, M., & Pisani, F. M. (2021). Functional Coupling between DNA Replication and Sister Chromatid Cohesion Establishment. *Int J Mol Sci*, *22*(6). doi:10.3390/ijms22062810
- Bohn, M., & Heermann, D. W. (2010). Topological interactions between ring polymers: Implications for chromatin loops. *J Chem Phys*, *132*(4), 044904. doi:10.1063/1.3302812
- Bohn, M., & Heermann, D. W. (2011). Repulsive forces between looping chromosomes induce entropy-driven segregation. *PLoS One*, *6*(1), e14428. doi:10.1371/journal.pone.0014428
- Bolcun-Filas, E., & Schimenti, J. C. (2012). Genetics of meiosis and recombination in mice. *Int Rev Cell Mol Biol*, *298*, 179-227. doi:10.1016/B978-0-12-394309-5.00005-5
- Bosch-Presegue, L., Raurell-Vila, H., Thackray, J. K., Gonzalez, J., Casal, C., Kane-Goldsmith, N., . . . Vaquero, A. (2017). Mammalian HP1 Isoforms Have Specific Roles in Heterochromatin Structure and Organization. *Cell Rep*, *21*(8), 2048-2057. doi:10.1016/j.celrep.2017.10.092
- Brackley, C. A., Johnson, J., Michieletto, D., Morozov, A. N., Nicodemi, M., Cook, P. R., & Marenduzzo, D. (2018). Extrusion without a motor: a new take on the loop extrusion model of genome organization. *Nucleus*, *9*(1), 95-103. doi:10.1080/19491034.2017.1421825
- Brahmachari, S., & Marko, J. F. (2018). DNA Mechanics and Topology. *Adv Exp Med Biol*, *1092*, 11-39. doi:10.1007/978-3-319-95294-9\_2
- Brahmachari, S., & Marko, J. F. (2019). Chromosome disentanglement driven via optimal compaction of loop-extruded brush structures. *Proc Natl Acad Sci U S A*, *116*(50), 24956-24965. doi:10.1073/pnas.1906355116
- Broderick, R., & Niedzwiedz, W. (2015). Sister chromatid decatenation: bridging the gaps in our knowledge. *Cell Cycle*, *14*(19), 3040-3044. doi:10.1080/15384101.2015.1078039
- Brooker, A. S., & Berkowitz, K. M. (2014). The roles of cohesins in mitosis, meiosis, and human health and disease. *Methods Mol Biol*, *1170*, 229-266. doi:10.1007/978-1-4939-0888-2\_11
- Buonomo, S. B., Clyne, R. K., Fuchs, J., Loidl, J., Uhlmann, F., & Nasmyth, K. (2000). Disjunction of homologous chromosomes in meiosis I depends on proteolytic cleavage of the meiotic cohesin Rec8 by separin. *Cell*, *103*(3), 387-398. doi:10.1016/S0092-8674(00)00131-8

- Burgess, A., Ruefli, A., Beamish, H., Warrener, R., Saunders, N., Johnstone, R., & Gabrielli, B. (2004). Histone deacetylase inhibitors specifically kill nonproliferating tumour cells. *Oncogene*, *23*(40), 6693-6701. doi:10.1038/sj.onc.1207893
- Burmann, F., Basfeld, A., Vazquez Nunez, R., Diebold-Durand, M. L., Wilhelm, L., & Gruber, S. (2017). Tuned SMC Arms Drive Chromosomal Loading of Prokaryotic Condensin. *Mol Cell*, *65*(5), 861-872 e869. doi:10.1016/j.molcel.2017.01.026
- Butin-Israeli, V., Adam, S. A., Goldman, A. E., & Goldman, R. D. (2012). Nuclear lamin functions and disease. *Trends Genet*, *28*(9), 464-471. doi:10.1016/j.tig.2012.06.001
- Cairo, G., & Lacefield, S. (2020). Establishing correct kinetochore-microtubule attachments in mitosis and meiosis. *Essays Biochem*, *64*(2), 277-287. doi:10.1042/EBC20190072
- Canzio, D., Chang, E. Y., Shankar, S., Kuchenbecker, K. M., Simon, M. D., Madhani, H. D., . . . Al-Sady, B. (2011). Chromodomain-mediated oligomerization of HP1 suggests a nucleosome-bridging mechanism for heterochromatin assembly. *Mol Cell*, *41*(1), 67-81. doi:10.1016/j.molcel.2010.12.016
- Cao, S., Zhou, K., Zhang, Z., Luger, K., & Straight, A. F. (2018). Constitutive centromere-associated network contacts confer differential stability on CENP-A nucleosomes in vitro and in the cell. *Mol Biol Cell*, *29*(6), 751-762. doi:10.1091/mbc.E17-10-0596
- Caplen, N. J., & Mousses, S. (2003). Short interfering RNA (siRNA)-mediated RNA interference (RNAi) in human cells. *Ann N Y Acad Sci*, *1002*, 56-62. doi:10.1196/annals.1281.007
- Carmena, M., Wheelock, M., Funabiki, H., & Earnshaw, W. C. (2012). The chromosomal passenger complex (CPC): from easy rider to the godfather of mitosis. *Nat Rev Mol Cell Biol*, *13*(12), 789-803. doi:10.1038/nrm3474
- Carroll, C. W., Milks, K. J., & Straight, A. F. (2010). Dual recognition of CENP-A nucleosomes is required for centromere assembly. *J Cell Biol*, *189*(7), 1143-1155. doi:10.1083/jcb.201001013
- Carroll, C. W., Silva, M. C., Godek, K. M., Jansen, L. E., & Straight, A. F. (2009). Centromere assembly requires the direct recognition of CENP-A nucleosomes by CENP-N. *Nat Cell Biol*, *11*(7), 896-902. doi:10.1038/ncb1899
- Casale, A. M., Cappucci, U., & Piacentini, L. (2021). Unravelling HP1 functions: post-transcriptional regulation of stem cell fate. *Chromosoma*. doi:10.1007/s00412-021-00760-1
- Chakraborty, A., Prasanth, K. V., & Prasanth, S. G. (2014). Dynamic phosphorylation of HP1alpha regulates mitotic progression in human cells. *Nat Commun*, *5*, 3445. doi:10.1038/ncomms4445
- Chalut, K. J., Hopfler, M., Lautenschlager, F., Boyde, L., Chan, C. J., Ekpenyong, A., . . . Guck, J. (2012). Chromatin decondensation and nuclear softening accompany Nanog downregulation in embryonic stem cells. *Biophys J*, *103*(10), 2060-2070. doi:10.1016/j.bpj.2012.10.015
- Cheutin, T., McNairn, A. J., Jenuwein, T., Gilbert, D. M., Singh, P. B., & Misteli, T. (2003). Maintenance of stable heterochromatin domains by dynamic HP1 binding. *Science*, *299*(5607), 721-725. doi:10.1126/science.1078572
- Chiang, T., Duncan, F. E., Schindler, K., Schultz, R. M., & Lampson, M. A. (2010). Evidence that weakened centromere cohesion is a leading cause of age-related aneuploidy in oocytes. *Curr Biol*, *20*(17), 1522-1528. doi:10.1016/j.cub.2010.06.069

- Chiolo, I., Minoda, A., Colmenares, S. U., Polyzos, A., Costes, S. V., & Karpen, G. H. (2011). Double-strand breaks in heterochromatin move outside of a dynamic HP1a domain to complete recombinational repair. *Cell*, *144*(5), 732-744. doi:10.1016/j.cell.2011.02.012
- Chow, K. H., Factor, R. E., & Ullman, K. S. (2012). The nuclear envelope environment and its cancer connections. *Nat Rev Cancer*, *12*(3), 196-209. doi:10.1038/nrc3219
- Chu, L., Huo, Y., Liu, X., Yao, P., Thomas, K., Jiang, H., . . . Yao, X. (2014). The spatiotemporal dynamics of chromatin protein HP1alpha is essential for accurate chromosome segregation during cell division. *J Biol Chem*, *289*(38), 26249-26262. doi:10.1074/jbc.M114.581504
- Cobb, J., & Handel, M. A. (1998). Dynamics of meiotic prophase I during spermatogenesis: from pairing to division. *Semin Cell Dev Biol*, *9*(4), 445-450. doi:10.1006/scdb.1998.0202
- Conduit, P. T., Wainman, A., & Raff, J. W. (2015). Centrosome function and assembly in animal cells. *Nat Rev Mol Cell Biol*, *16*(10), 611-624. doi:10.1038/nrm4062
- Costantino, L., Hsieh, T. S., Lamothe, R., Darzacq, X., & Koshland, D. (2020). Cohesin residency determines chromatin loop patterns. *Elife*, *9*. doi:10.7554/eLife.59889
- Cremer, M., Brandstetter, K., Maiser, A., Rao, S. S. P., Schmid, V. J., Guirao-Ortiz, M., . . . Cremer, T. (2020). Cohesin depleted cells rebuild functional nuclear compartments after endomitosis. *Nat Commun*, *11*(1), 6146. doi:10.1038/s41467-020-19876-6
- Cutts, E. E., & Vannini, A. (2020). Condensin complexes: understanding loop extrusion one conformational change at a time. *Biochem Soc Trans*, *48*(5), 2089-2100. doi:10.1042/BST20200241
- Cuvier, O., & Hirano, T. (2003). A role of topoisomerase II in linking DNA replication to chromosome condensation. *J Cell Biol*, *160*(5), 645-655. doi:10.1083/jcb.200209023
- Cuylen, S., Blaukopf, C., Politi, A. Z., Muller-Reichert, T., Neumann, B., Poser, I., . . . Gerlich, D. W. (2016). Ki-67 acts as a biological surfactant to disperse mitotic chromosomes. *Nature*, *535*(7611), 308-312. doi:10.1038/nature18610
- Davidson, I. F., Bauer, B., Goetz, D., Tang, W., Wutz, G., & Peters, J. M. (2019). DNA loop extrusion by human cohesin. *Science*, *366*(6471), 1338-1345. doi:10.1126/science.aaz3418
- Davidson, I. F., & Peters, J. M. (2021). Genome folding through loop extrusion by SMC complexes. *Nat Rev Mol Cell Biol*, *22*(7), 445-464. doi:10.1038/s41580-021-00349-7
- de Kretser, D. M., Loveland, K. L., Meinhardt, A., Simorangkir, D., & Wreford, N. (1998). Spermatogenesis. *Hum Reprod*, *13 Suppl 1*, 1-8. doi:10.1093/humrep/13.suppl\_1.1
- De Souza, C., & Chatterji, B. P. (2015). HDAC Inhibitors as Novel Anti-Cancer Therapeutics. *Recent Pat Anticancer Drug Discov*, *10*(2), 145-162. doi:10.2174/1574892810666150317144511
- Diaz-Martinez, L. A., & Clarke, D. J. (2009). Chromosome cohesion and the spindle checkpoint. *Cell Cycle*, *8*(17), 2733-2740. doi:10.4161/cc.8.17.9403
- Doenecke, D. (2014). Chromatin dynamics from S-phase to mitosis: contributions of histone modifications. *Cell Tissue Res*, *356*(3), 467-475. doi:10.1007/s00441-014-1873-1
- Dolan, M. (2011). The role of the Giemsa stain in cytogenetics. *Biotech Histochem*, *86*(2), 94-97. doi:10.3109/10520295.2010.515493

- Duncan, F. E., Hornick, J. E., Lampson, M. A., Schultz, R. M., Shea, L. D., & Woodruff, T. K. (2012). Chromosome cohesion decreases in human eggs with advanced maternal age. *Aging Cell*, *11*(6), 1121-1124. doi:10.1111/j.1474-9726.2012.00866.x
- Duygu, B., Poels, E. M., & da Costa Martins, P. A. (2013). Genetics and epigenetics of arrhythmia and heart failure. *Front Genet*, *4*, 219. doi:10.3389/fgene.2013.00219
- Dyson, S., Segura, J., Martinez-Garcia, B., Valdes, A., & Roca, J. (2021). Condensin minimizes topoisomerase II-mediated entanglements of DNA in vivo. *EMBO J*, *40*(1), e105393. doi:10.15252/embj.2020105393
- Eagen, K. P. (2018). Principles of Chromosome Architecture Revealed by Hi-C. *Trends Biochem Sci*, *43*(6), 469-478. doi:10.1016/j.tibs.2018.03.006
- Earnshaw, W. C., Halligan, B., Cooke, C. A., Heck, M. M., & Liu, L. F. (1985). Topoisomerase II is a structural component of mitotic chromosome scaffolds. *J Cell Biol*, *100*(5), 1706-1715. doi:10.1083/jcb.100.5.1706
- Eastland, A., Hornick, J., Kawamura, R., Nanavati, D., & Marko, J. F. (2016). Dependence of the structure and mechanics of metaphase chromosomes on oxidized cysteines. *Chromosome Res*, *24*(3), 339-353. doi:10.1007/s10577-016-9528-6
- Eijpe, M., Offenbergh, H., Jessberger, R., Revenkova, E., & Heyting, C. (2003). Meiotic cohesin REC8 marks the axial elements of rat synaptonemal complexes before cohesins SMC1beta and SMC3. *J Cell Biol*, *160*(5), 657-670. doi:10.1083/jcb.200212080
- Eissenberg, J. C., & Elgin, S. C. (2000). The HP1 protein family: getting a grip on chromatin. *Curr Opin Genet Dev*, *10*(2), 204-210. doi:10.1016/s0959-437x(00)00058-7
- Elbatsh, A. M. O., Kim, E., Eeftens, J. M., Raaijmakers, J. A., van der Weide, R. H., Garcia-Nieto, A., . . . Rowland, B. D. (2019). Distinct Roles for Condensin's Two ATPase Sites in Chromosome Condensation. *Mol Cell*, *76*(5), 724-737 e725. doi:10.1016/j.molcel.2019.09.020
- Endl, E., & Gerdes, J. (2000). The Ki-67 protein: fascinating forms and an unknown function. *Exp Cell Res*, *257*(2), 231-237. doi:10.1006/excr.2000.4888
- Enguita-Marruedo, A., Van Cappellen, W. A., Hoogerbrugge, J. W., Carofiglio, F., Wassenaar, E., Slotman, J. A., . . . Baarends, W. M. (2018). Live cell analyses of synaptonemal complex dynamics and chromosome movements in cultured mouse testis tubules and embryonic ovaries. *Chromosoma*, *127*(3), 341-359. doi:10.1007/s00412-018-0668-7
- Escalier, D. (2002). Genetic approach to male meiotic division deficiency: the human macronuclear spermatozoa. *Mol Hum Reprod*, *8*(1), 1-7. doi:10.1093/molehr/8.1.1
- Escobar, T. M., Loyola, A., & Reinberg, D. (2021). Parental nucleosome segregation and the inheritance of cellular identity. *Nat Rev Genet*, *22*(6), 379-392. doi:10.1038/s41576-020-00312-w
- Fenley, A. T., Anandkrishnan, R., Kidane, Y. H., & Onufriev, A. V. (2018). Modulation of nucleosomal DNA accessibility via charge-altering post-translational modifications in histone core. *Epigenetics Chromatin*, *11*(1), 11. doi:10.1186/s13072-018-0181-5
- Fischle, W., Tseng, B. S., Dormann, H. L., Ueberheide, B. M., Garcia, B. A., Shabanowitz, J., . . . Allis, C. D. (2005). Regulation of HP1-chromatin binding by histone H3 methylation and phosphorylation. *Nature*, *438*(7071), 1116-1122. doi:10.1038/nature04219
- Florian, S., & Mitchison, T. J. (2016). Anti-Microtubule Drugs. *Methods Mol Biol*, *1413*, 403-421. doi:10.1007/978-1-4939-3542-0\_25

- Fraune, J., Schramm, S., Alsheimer, M., & Benavente, R. (2012). The mammalian synaptonemal complex: protein components, assembly and role in meiotic recombination. *Exp Cell Res*, *318*(12), 1340-1346. doi:10.1016/j.yexcr.2012.02.018
- French, B. T., & Straight, A. F. (2013). Swapping CENP-A at the centromere. *Nat Cell Biol*, *15*(9), 1028-1030. doi:10.1038/ncb2833
- Gambogi, C. W., & Black, B. E. (2019). The nucleosomes that mark centromere location on chromosomes old and new. *Essays Biochem*, *63*(1), 15-27. doi:10.1042/EBC20180060
- Ganji, M., Shaltiel, I. A., Bisht, S., Kim, E., Kalichava, A., Haering, C. H., & Dekker, C. (2018). Real-time imaging of DNA loop extrusion by condensin. *Science*, *360*(6384), 102-105. doi:10.1126/science.aar7831
- Gao, J., & Colaiacovo, M. P. (2018). Zipping and Unzipping: Protein Modifications Regulating Synaptonemal Complex Dynamics. *Trends Genet*, *34*(3), 232-245. doi:10.1016/j.tig.2017.12.001
- Garcia-Cruz, R., Brieno, M. A., Roig, I., Grossmann, M., Velilla, E., Pujol, A., . . . Garcia Caldes, M. (2010). Dynamics of cohesin proteins REC8, STAG3, SMC1 beta and SMC3 are consistent with a role in sister chromatid cohesion during meiosis in human oocytes. *Hum Reprod*, *25*(9), 2316-2327. doi:10.1093/humrep/deq180
- Gasser, S. M., Laroche, T., Falquet, J., Boy de la Tour, E., & Laemmli, U. K. (1986). Metaphase chromosome structure. Involvement of topoisomerase II. *J Mol Biol*, *188*(4), 613-629. doi:10.1016/s0022-2836(86)80010-9
- Genes, P. G. d. (1979). *Scaling concepts in polymer physics*. Ithaca, N.Y.: Cornell University Press.
- Gerdes, J. (1990). Ki-67 and other proliferation markers useful for immunohistological diagnostic and prognostic evaluations in human malignancies. *Semin Cancer Biol*, *1*(3), 199-206. Retrieved from <https://www.ncbi.nlm.nih.gov/pubmed/2103495>
- Gerdes, J., Schwab, U., Lemke, H., & Stein, H. (1983). Production of a mouse monoclonal antibody reactive with a human nuclear antigen associated with cell proliferation. *Int J Cancer*, *31*(1), 13-20. doi:10.1002/ijc.2910310104
- Gerlich, D., Hirota, T., Koch, B., Peters, J. M., & Ellenberg, J. (2006). Condensin I stabilizes chromosomes mechanically through a dynamic interaction in live cells. *Curr Biol*, *16*(4), 333-344. doi:10.1016/j.cub.2005.12.040
- Gibcus, J. H., Samejima, K., Goloborodko, A., Samejima, I., Naumova, N., Nuebler, J., . . . Dekker, J. (2018). A pathway for mitotic chromosome formation. *Science*, *359*(6376). doi:10.1126/science.aao6135
- Gisselsson, D., Bjork, J., Hoglund, M., Mertens, F., Dal Cin, P., Akerman, M., & Mandahl, N. (2001). Abnormal nuclear shape in solid tumors reflects mitotic instability. *Am J Pathol*, *158*(1), 199-206. doi:10.1016/S0002-9440(10)63958-2
- Goel, V. Y., & Hansen, A. S. (2020). The macro and micro of chromosome conformation capture. *Wiley Interdiscip Rev Dev Biol*, e395. doi:10.1002/wdev.395
- Golfier, S., Quail, T., Kimura, H., & Bruges, J. (2020). Cohesin and condensin extrude DNA loops in a cell cycle-dependent manner. *Elife*, *9*. doi:10.7554/eLife.53885
- Goloborodko, A., Imakaev, M. V., Marko, J. F., & Mirny, L. (2016). Compaction and segregation of sister chromatids via active loop extrusion. *Elife*, *5*. doi:10.7554/eLife.14864

- Goodson, H. V., & Jonasson, E. M. (2018). Microtubules and Microtubule-Associated Proteins. *Cold Spring Harb Perspect Biol*, 10(6). doi:10.1101/cshperspect.a022608
- Goto, T., & Wang, J. C. (1982). Yeast DNA topoisomerase II. An ATP-dependent type II topoisomerase that catalyzes the catenation, decatenation, unknotting, and relaxation of double-stranded DNA rings. *J Biol Chem*, 257(10), 5866-5872. Retrieved from <https://www.ncbi.nlm.nih.gov/pubmed/6279616>
- Gottlicher, M. (2004). Valproic acid: an old drug newly discovered as inhibitor of histone deacetylases. *Ann Hematol*, 83 Suppl 1, S91-92. doi:10.1007/s00277-004-0850-2
- Gray, S., & Cohen, P. E. (2016). Control of Meiotic Crossovers: From Double-Strand Break Formation to Designation. *Annu Rev Genet*, 50, 175-210. doi:10.1146/annurev-genet-120215-035111
- Green, L. C., Kalitsis, P., Chang, T. M., Cipetic, M., Kim, J. H., Marshall, O., . . . Hudson, D. F. (2012). Contrasting roles of condensin I and condensin II in mitotic chromosome formation. *J Cell Sci*, 125(Pt 6), 1591-1604. doi:10.1242/jcs.097790
- Gruber, S., & Errington, J. (2009). Recruitment of condensin to replication origin regions by ParB/SpoOJ promotes chromosome segregation in *B. subtilis*. *Cell*, 137(4), 685-696. doi:10.1016/j.cell.2009.02.035
- Gulliya, K. S., Franck, B., Schneider, U., Sharma, R., Arnold, L., & Matthews, J. L. (1994). Topoisomerase II-dependent novel antitumor compounds merocil and merodantoin induce apoptosis in Daudi cells. *Anticancer Drugs*, 5(5), 557-566. doi:10.1097/00001813-199410000-00007
- Haase, K., Macadangang, J. K., Edrington, C. H., Cuerrier, C. M., Hadjiantoniou, S., Harden, J. L., . . . Pelling, A. E. (2016). Extracellular Forces Cause the Nucleus to Deform in a Highly Controlled Anisotropic Manner. *Sci Rep*, 6, 21300. doi:10.1038/srep21300
- Haering, C. H., & Jessberger, R. (2012). Cohesin in determining chromosome architecture. *Exp Cell Res*, 318(12), 1386-1393. doi:10.1016/j.yexcr.2012.03.016
- Hanke, A., Ziraldo, R., & Levene, S. D. (2021). DNA-Topology Simplification by Topoisomerases. *Molecules*, 26(11). doi:10.3390/molecules26113375
- Hao, X., Parmar, J. J., Lelandais, B., Aristov, A., Ouyang, W., Weber, C., & Zimmer, C. (2021). Super-resolution visualization and modeling of human chromosomal regions reveals cohesin-dependent loop structures. *Genome Biol*, 22(1), 150. doi:10.1186/s13059-021-02343-w
- Hara, M., & Fukagawa, T. (2017). Critical Foundation of the Kinetochore: The Constitutive Centromere-Associated Network (CCAN). *Prog Mol Subcell Biol*, 56, 29-57. doi:10.1007/978-3-319-58592-5\_2
- Hartl, T. A., Sweeney, S. J., Knepler, P. J., & Bosco, G. (2008). Condensin II resolves chromosomal associations to enable anaphase I segregation in *Drosophila* male meiosis. *PLoS Genet*, 4(10), e1000228. doi:10.1371/journal.pgen.1000228
- Hassold, T., & Hunt, P. (2001). To err (meiotically) is human: the genesis of human aneuploidy. *Nat Rev Genet*, 2(4), 280-291. doi:10.1038/35066065
- Hauf, S., Waizenegger, I. C., & Peters, J. M. (2001). Cohesin cleavage by separase required for anaphase and cytokinesis in human cells. *Science*, 293(5533), 1320-1323. doi:10.1126/science.1061376

- Henrikus, S. S., & Costa, A. (2021). Towards a Structural Mechanism for Sister Chromatid Cohesion Establishment at the Eukaryotic Replication Fork. *Biology (Basel)*, 10(6). doi:10.3390/biology10060466
- Henzel, J. V., Nabeshima, K., Schvarzstein, M., Turner, B. E., Villeneuve, A. M., & Hillers, K. J. (2011). An asymmetric chromosome pair undergoes synaptic adjustment and crossover redistribution during *Caenorhabditis elegans* meiosis: implications for sex chromosome evolution. *Genetics*, 187(3), 685-699. doi:10.1534/genetics.110.124958
- Hess, R. A., & Renato de Franca, L. (2008). Spermatogenesis and cycle of the seminiferous epithelium. *Adv Exp Med Biol*, 636, 1-15. doi:10.1007/978-0-387-09597-4\_1
- Hirano, T. (2004). Chromosome shaping by two condensins. *Cell Cycle*, 3(1), 26-28. Retrieved from <https://www.ncbi.nlm.nih.gov/pubmed/14657659>
- Hirano, T. (2016). Condensin-Based Chromosome Organization from Bacteria to Vertebrates. *Cell*, 164(5), 847-857. doi:10.1016/j.cell.2016.01.033
- Hirano, T., Kobayashi, R., & Hirano, M. (1997). Condensins, chromosome condensation protein complexes containing XCAP-C, XCAP-E and a *Xenopus* homolog of the *Drosophila* Barren protein. *Cell*, 89(4), 511-521. doi:10.1016/s0092-8674(00)80233-0
- Hirano, T., & Mitchison, T. J. (1994). A heterodimeric coiled-coil protein required for mitotic chromosome condensation in vitro. *Cell*, 79(3), 449-458. doi:10.1016/0092-8674(94)90254-2
- Hirota, T., Lipp, J. J., Toh, B. H., & Peters, J. M. (2005). Histone H3 serine 10 phosphorylation by Aurora B causes HP1 dissociation from heterochromatin. *Nature*, 438(7071), 1176-1180. doi:10.1038/nature04254
- Hobson, C. M., & Stephens, A. D. (2020). Modeling of Cell Nuclear Mechanics: Classes, Components, and Applications. *Cells*, 9(7). doi:10.3390/cells9071623
- Hocquet, C., Robellet, X., Modolo, L., Sun, X. M., Burny, C., Cuylen-Haering, S., . . . Bernard, P. (2018). Condensin controls cellular RNA levels through the accurate segregation of chromosomes instead of directly regulating transcription. *Elife*, 7. doi:10.7554/eLife.38517
- Hoencamp, C., Dudchenko, O., Elbatsh, A. M. O., Brahmachari, S., Raaijmakers, J. A., van Schaik, T., . . . Rowland, B. D. (2021). 3D genomics across the tree of life reveals condensin II as a determinant of architecture type. *Science*, 372(6545), 984-989. doi:10.1126/science.abe2218
- Holm, C., Stearns, T., & Botstein, D. (1989). DNA topoisomerase II must act at mitosis to prevent nondisjunction and chromosome breakage. *Mol Cell Biol*, 9(1), 159-168. doi:10.1128/mcb.9.1.159-168.1989
- Hori, T., Kagawa, N., Toyoda, A., Fujiyama, A., Misu, S., Monma, N., . . . Fukagawa, T. (2017). Constitutive centromere-associated network controls centromere drift in vertebrate cells. *J Cell Biol*, 216(1), 101-113. doi:10.1083/jcb.201605001
- Hornick, J. E., Duncan, F. E., Sun, M., Kawamura, R., Marko, J. F., & Woodruff, T. K. (2015). Age-associated alterations in the micromechanical properties of chromosomes in the mammalian egg. *J Assist Reprod Genet*, 32(5), 765-769. doi:10.1007/s10815-015-0453-y
- Houchmandzadeh, B., Marko, J. F., Chatenay, D., & Libchaber, A. (1997). Elasticity and structure of eukaryote chromosomes studied by micromanipulation and micropipette aspiration. *J Cell Biol*, 139(1), 1-12. doi:10.1083/jcb.139.1.1

- Houlard, M., Godwin, J., Metson, J., Lee, J., Hirano, T., & Nasmyth, K. (2015). Condensin confers the longitudinal rigidity of chromosomes. *Nat Cell Biol*, *17*(6), 771-781. doi:10.1038/ncb3167
- Howard-Till, R., & Loidl, J. (2018). Condensins promote chromosome individualization and segregation during mitosis, meiosis, and amitosis in *Tetrahymena thermophila*. *Mol Biol Cell*, *29*(4), 466-478. doi:10.1091/mbc.E17-07-0451
- Huynh, N. C., Everts, V., & Ampornaramveth, R. S. (2017). Histone deacetylases and their roles in mineralized tissue regeneration. *Bone Rep*, *7*, 33-40. doi:10.1016/j.bonr.2017.08.001
- Ivanovska, I., & Orr-Weaver, T. L. (2006). Histone modifications and the chromatin scaffold for meiotic chromosome architecture. *Cell Cycle*, *5*(18), 2064-2071. doi:10.4161/cc.5.18.3253
- James, T. C., & Elgin, S. C. (1986). Identification of a nonhistone chromosomal protein associated with heterochromatin in *Drosophila melanogaster* and its gene. *Mol Cell Biol*, *6*(11), 3862-3872. doi:10.1128/mcb.6.11.3862-3872.1986
- Janssen, A., Colmenares, S. U., & Karpen, G. H. (2018). Heterochromatin: Guardian of the Genome. *Annu Rev Cell Dev Biol*, *34*, 265-288. doi:10.1146/annurev-cellbio-100617-062653
- Jenuwein, T., & Allis, C. D. (2001). Translating the histone code. *Science*, *293*(5532), 1074-1080. doi:10.1126/science.1063127
- Jones, K. T., & Lane, S. I. (2013). Molecular causes of aneuploidy in mammalian eggs. *Development*, *140*(18), 3719-3730. doi:10.1242/dev.090589
- Joti, Y., Hikima, T., Nishino, Y., Kamada, F., Hihara, S., Takata, H., . . . Maeshima, K. (2012). Chromosomes without a 30-nm chromatin fiber. *Nucleus*, *3*(5), 404-410. doi:10.4161/nucl.21222
- Kadauke, S., & Blobel, G. A. (2013). Mitotic bookmarking by transcription factors. *Epigenetics Chromatin*, *6*(1), 6. doi:10.1186/1756-8935-6-6
- Kamar, R. I., Banigan, E. J., Erbas, A., Giuntoli, R. D., Olvera de la Cruz, M., Johnson, R. C., & Marko, J. F. (2017). Facilitated dissociation of transcription factors from single DNA binding sites. *Proc Natl Acad Sci U S A*, *114*(16), E3251-E3257. doi:10.1073/pnas.1701884114
- Kawamura, R., Pope, L. H., Christensen, M. O., Sun, M., Terekhova, K., Boege, F., . . . Marko, J. F. (2010). Mitotic chromosomes are constrained by topoisomerase II-sensitive DNA entanglements. *J Cell Biol*, *188*(5), 653-663. doi:10.1083/jcb.200910085
- Keeney, S. (2008). Spo11 and the Formation of DNA Double-Strand Breaks in Meiosis. *Genome Dyn Stab*, *2*, 81-123. doi:10.1007/7050\_2007\_026
- Keeney, S., Giroux, C. N., & Kleckner, N. (1997). Meiosis-specific DNA double-strand breaks are catalyzed by Spo11, a member of a widely conserved protein family. *Cell*, *88*(3), 375-384. doi:10.1016/s0092-8674(00)81876-0
- Keenholtz, R. A., Dhanaraman, T., Palou, R., Yu, J., D'Amours, D., & Marko, J. F. (2017). Oligomerization and ATP stimulate condensin-mediated DNA compaction. *Sci Rep*, *7*(1), 14279. doi:10.1038/s41598-017-14701-5
- Kim, Y., Shi, Z., Zhang, H., Finkelstein, I. J., & Yu, H. (2019). Human cohesin compacts DNA by loop extrusion. *Science*, *366*(6471), 1345-1349. doi:10.1126/science.aaz4475

- Kimura, K., Cuvier, O., & Hirano, T. (2001). Chromosome condensation by a human condensin complex in *Xenopus* egg extracts. *J Biol Chem*, 276(8), 5417-5420. doi:10.1074/jbc.C000873200
- Kimura, K., & Hirano, T. (1997). ATP-dependent positive supercoiling of DNA by 13S condensin: a biochemical implication for chromosome condensation. *Cell*, 90(4), 625-634. doi:10.1016/s0092-8674(00)80524-3
- Kixmoeller, K., Allu, P. K., & Black, B. E. (2020). The centromere comes into focus: from CENP-A nucleosomes to kinetochore connections with the spindle. *Open Biol*, 10(6), 200051. doi:10.1098/rsob.200051
- Kleckner, N., Zickler, D., Jones, G. H., Dekker, J., Padmore, R., Henle, J., & Hutchinson, J. (2004). A mechanical basis for chromosome function. *Proc Natl Acad Sci U S A*, 101(34), 12592-12597. doi:10.1073/pnas.0402724101
- Klein, F., Mahr, P., Galova, M., Buonomo, S. B., Michaelis, C., Nairz, K., & Nasmyth, K. (1999). A central role for cohesins in sister chromatid cohesion, formation of axial elements, and recombination during yeast meiosis. *Cell*, 98(1), 91-103. doi:10.1016/S0092-8674(00)80609-1
- Kouzarides, T. (2007). Chromatin modifications and their function. *Cell*, 128(4), 693-705. doi:10.1016/j.cell.2007.02.005
- Kouznetsova, A., Benavente, R., Pastink, A., & Hoog, C. (2011). Meiosis in mice without a synaptonemal complex. *PLoS One*, 6(12), e28255. doi:10.1371/journal.pone.0028255
- Kouznetsova, A., Novak, I., Jessberger, R., & Hoog, C. (2005). SYCP2 and SYCP3 are required for cohesin core integrity at diplotene but not for centromere cohesion at the first meiotic division. *J Cell Sci*, 118(Pt 10), 2271-2278. doi:10.1242/jcs.02362
- Krause, M., Te Riet, J., & Wolf, K. (2013). Probing the compressibility of tumor cell nuclei by combined atomic force-confocal microscopy. *Phys Biol*, 10(6), 065002. doi:10.1088/1478-3975/10/6/065002
- Krenn, V., & Musacchio, A. (2015). The Aurora B Kinase in Chromosome Bi-Orientation and Spindle Checkpoint Signaling. *Front Oncol*, 5, 225. doi:10.3389/fonc.2015.00225
- Krouwels, I. M., Wiesmeijer, K., Abraham, T. E., Molenaar, C., Verwoerd, N. P., Tanke, H. J., & Dirks, R. W. (2005). A glue for heterochromatin maintenance: stable SUV39H1 binding to heterochromatin is reinforced by the SET domain. *J Cell Biol*, 170(4), 537-549. doi:10.1083/jcb.200502154
- Kschonsak, M., Merkel, F., Bisht, S., Metz, J., Rybin, V., Hassler, M., & Haering, C. H. (2017). Structural Basis for a Safety-Belt Mechanism That Anchors Condensin to Chromosomes. *Cell*, 171(3), 588-600 e524. doi:10.1016/j.cell.2017.09.008
- Kueng, S., Hegemann, B., Peters, B. H., Lipp, J. J., Schleiffer, A., Mechtler, K., & Peters, J. M. (2006). Wapl controls the dynamic association of cohesin with chromatin. *Cell*, 127(5), 955-967. doi:10.1016/j.cell.2006.09.040
- Kuga, T., Nakayama, Y., Iwamatsu, A., Fukumoto, Y., Yokomori, K., & Yamaguchi, N. (2007). Separation of a disulfide-linked phosphoprotein by diagonal SDS-PAGE with optimized gel crosslinking. *Anal Biochem*, 370(2), 252-254. doi:10.1016/j.ab.2007.07.019
- Kumada, K., Yao, R., Kawaguchi, T., Karasawa, M., Hoshikawa, Y., Ichikawa, K., . . . Noda, T. (2006). The selective continued linkage of centromeres from mitosis to interphase in the absence of mammalian separase. *J Cell Biol*, 172(6), 835-846. doi:10.1083/jcb.200511126

- Kunitoku, N., Sasayama, T., Marumoto, T., Zhang, D., Honda, S., Kobayashi, O., . . . Hirota, T. (2003). CENP-A phosphorylation by Aurora-A in prophase is required for enrichment of Aurora-B at inner centromeres and for kinetochore function. *Dev Cell*, 5(6), 853-864. doi:10.1016/s1534-5807(03)00364-2
- Lane, A. B., Gimenez-Abian, J. F., & Clarke, D. J. (2013). A novel chromatin tether domain controls topoisomerase IIalpha dynamics and mitotic chromosome formation. *J Cell Biol*, 203(3), 471-486. doi:10.1083/jcb.201303045
- Larson, A. G., Elnatan, D., Keenen, M. M., Trnka, M. J., Johnston, J. B., Burlingame, A. L., . . . Narlikar, G. J. (2017). Liquid droplet formation by HP1alpha suggests a role for phase separation in heterochromatin. *Nature*, 547(7662), 236-240. doi:10.1038/nature22822
- Lawrimore, J., & Bloom, K. (2019). The regulation of chromosome segregation via centromere loops. *Crit Rev Biochem Mol Biol*, 54(4), 352-370. doi:10.1080/10409238.2019.1670130
- Lawrimore, J., Doshi, A., Friedman, B., Yeh, E., & Bloom, K. (2018). Geometric partitioning of cohesin and condensin is a consequence of chromatin loops. *Mol Biol Cell*, 29(22), 2737-2750. doi:10.1091/mbc.E18-02-0131
- Lawrimore, J., Vasquez, P. A., Falvo, M. R., Taylor, R. M., 2nd, Vicci, L., Yeh, E., . . . Bloom, K. (2015). DNA loops generate intracentromere tension in mitosis. *J Cell Biol*, 210(4), 553-564. doi:10.1083/jcb.201502046
- Lee, B. G., Merkel, F., Allegretti, M., Hassler, M., Cawood, C., Lecomte, L., . . . Haering, C. H. (2020). Cryo-EM structures of holo condensin reveal a subunit flip-flop mechanism. *Nat Struct Mol Biol*, 27(8), 743-751. doi:10.1038/s41594-020-0457-x
- Lee, J. (2017). The Regulation and Function of Cohesin and Condensin in Mammalian Oocytes and Spermatocytes. *Results Probl Cell Differ*, 63, 355-372. doi:10.1007/978-3-319-60855-6\_15
- Lee, J., & Hirano, T. (2011). RAD21L, a novel cohesin subunit implicated in linking homologous chromosomes in mammalian meiosis. *J Cell Biol*, 192(2), 263-276. doi:10.1083/jcb.201008005
- Lee, Y. H., Kuo, C. Y., Stark, J. M., Shih, H. M., & Ann, D. K. (2013). HP1 promotes tumor suppressor BRCA1 functions during the DNA damage response. *Nucleic Acids Res*, 41(11), 5784-5798. doi:10.1093/nar/gkt231
- Lesecque, Y., Glemin, S., Lartillot, N., Mouchiroud, D., & Duret, L. (2014). The red queen model of recombination hotspots evolution in the light of archaic and modern human genomes. *PLoS Genet*, 10(11), e1004790. doi:10.1371/journal.pgen.1004790
- Liebe, B., Alsheimer, M., Hoog, C., Benavente, R., & Scherthan, H. (2004). Telomere attachment, meiotic chromosome condensation, pairing, and bouquet stage duration are modified in spermatocytes lacking axial elements. *Mol Biol Cell*, 15(2), 827-837. doi:10.1091/mbc.e03-07-0524
- Lifshitz, E. M., Kosevich, A. M., & Pitaevskii, L. P. (1986). Chapter II. In E. M. Lifshitz, A. M. Kosevich, & L. P. Pitaevskii (Eds.), *Theory of Elasticity (Third Edition)* (pp. 38-86). Oxford: Butterworth-Heinemann.
- Lionetti, M. C., Bonfanti, S., Fumagalli, M. R., Budrikis, Z., Font-Clos, F., Costantini, G., . . . La Porta, C. A. M. (2020). Chromatin and Cytoskeletal Tethering Determine Nuclear Morphology in Progerin-Expressing Cells. *Biophys J*, 118(9), 2319-2332. doi:10.1016/j.bpj.2020.04.001

- Liow, L. H., Van Valen, L., & Stenseth, N. C. (2011). Red Queen: from populations to taxa and communities. *Trends Ecol Evol*, *26*(7), 349-358. doi:10.1016/j.tree.2011.03.016
- Liu, K., Patteson, A. E., Banigan, E. J., & Schwarz, J. M. (2021). Dynamic Nuclear Structure Emerges from Chromatin Cross-Links and Motors. *Phys Rev Lett*, *126*(15), 158101. doi:10.1103/PhysRevLett.126.158101
- Liu, L. F., Liu, C. C., & Alberts, B. M. (1980). Type II DNA topoisomerases: enzymes that can unknot a topologically knotted DNA molecule via a reversible double-strand break. *Cell*, *19*(3), 697-707. doi:10.1016/s0092-8674(80)80046-8
- Losada, A., Hirano, M., & Hirano, T. (1998). Identification of *Xenopus* SMC protein complexes required for sister chromatid cohesion. *Genes Dev*, *12*(13), 1986-1997. doi:10.1101/gad.12.13.1986
- Losada, A., Yokochi, T., Kobayashi, R., & Hirano, T. (2000). Identification and characterization of SA/Scp3 subunits in the *Xenopus* and human cohesin complexes. *J Cell Biol*, *150*(3), 405-416. doi:10.1083/jcb.150.3.405
- Luo, X., Liu, Y., Kubicek, S., Myllyharju, J., Tumber, A., Ng, S., . . . Wang, X. (2011). A selective inhibitor and probe of the cellular functions of Jumonji C domain-containing histone demethylases. *J Am Chem Soc*, *133*(24), 9451-9456. doi:10.1021/ja201597b
- Lyons, N. A., & Morgan, D. O. (2011). Cdk1-dependent destruction of Ecol1 prevents cohesion establishment after S phase. *Mol Cell*, *42*(3), 378-389. doi:10.1016/j.molcel.2011.03.023
- Machida, S., Takizawa, Y., Ishimaru, M., Sugita, Y., Sekine, S., Nakayama, J. I., . . . Kurumizaka, H. (2018). Structural Basis of Heterochromatin Formation by Human HP1. *Mol Cell*, *69*(3), 385-397 e388. doi:10.1016/j.molcel.2017.12.011
- Maeshima, K., Eltsov, M., & Laemmli, U. K. (2005). Chromosome structure: improved immunolabeling for electron microscopy. *Chromosoma*, *114*(5), 365-375. doi:10.1007/s00412-005-0023-7
- Maeshima, K., Ide, S., & Babokhov, M. (2019). Dynamic chromatin organization without the 30-nm fiber. *Curr Opin Cell Biol*, *58*, 95-104. doi:10.1016/j.ceb.2019.02.003
- Maeshima, K., Imai, R., Hikima, T., & Joti, Y. (2014). Chromatin structure revealed by X-ray scattering analysis and computational modeling. *Methods*, *70*(2-3), 154-161. doi:10.1016/j.ymeth.2014.08.008
- Maeshima, K., Matsuda, T., Shindo, Y., Imamura, H., Tamura, S., Imai, R., . . . Nagai, T. (2018). A Transient Rise in Free Mg(2+) Ions Released from ATP-Mg Hydrolysis Contributes to Mitotic Chromosome Condensation. *Curr Biol*, *28*(3), 444-451 e446. doi:10.1016/j.cub.2017.12.035
- Makrantonis, V., & Marston, A. L. (2018). Cohesin and chromosome segregation. *Curr Biol*, *28*(12), R688-R693. doi:10.1016/j.cub.2018.05.019
- Marchion, D. C., Bicaku, E., Daud, A. I., Sullivan, D. M., & Munster, P. N. (2005). Valproic acid alters chromatin structure by regulation of chromatin modulation proteins. *Cancer Res*, *65*(9), 3815-3822. doi:10.1158/0008-5472.CAN-04-2478
- Marko, J. F. (2008). Micromechanical studies of mitotic chromosomes. *Chromosome Res*, *16*(3), 469-497. doi:10.1007/s10577-008-1233-7
- Marko, J. F., De Los Rios, P., Barducci, A., & Gruber, S. (2019). DNA-segment-capture model for loop extrusion by structural maintenance of chromosome (SMC) protein complexes. *Nucleic Acids Res*, *47*(13), 6956-6972. doi:10.1093/nar/gkz497

- Marko, J. F., & Siggia, E. D. (1997). Polymer models of meiotic and mitotic chromosomes. *Mol Biol Cell*, 8(11), 2217-2231. doi:10.1091/mbc.8.11.2217
- Marsden, M. P., & Laemmli, U. K. (1979). Metaphase chromosome structure: evidence for a radial loop model. *Cell*, 17(4), 849-858. doi:10.1016/0092-8674(79)90325-8
- Martin, C. A., Murray, J. E., Carroll, P., Leitch, A., Mackenzie, K. J., Halachev, M., . . . Jackson, A. P. (2016). Mutations in genes encoding condensin complex proteins cause microcephaly through decatenation failure at mitosis. *Genes Dev*, 30(19), 2158-2172. doi:10.1101/gad.286351.116
- Matityahu, A., & Onn, I. (2021). Hit the brakes - a new perspective on the loop extrusion mechanism of cohesin and other SMC complexes. *J Cell Sci*, 134(1). doi:10.1242/jcs.247577
- Matoba, K., Yamazoe, M., Mayanagi, K., Morikawa, K., & Hiraga, S. (2005). Comparison of MukB homodimer versus MukBEF complex molecular architectures by electron microscopy reveals a higher-order multimerization. *Biochem Biophys Res Commun*, 333(3), 694-702. doi:10.1016/j.bbrc.2005.05.163
- McAinsh, A. D., & Meraldi, P. (2011). The CCAN complex: linking centromere specification to control of kinetochore-microtubule dynamics. *Semin Cell Dev Biol*, 22(9), 946-952. doi:10.1016/j.semcdb.2011.09.016
- McIntosh, J. R. (2016). Mitosis. *Cold Spring Harb Perspect Biol*, 8(9). doi:10.1101/cshperspect.a023218
- McKinley, K. L., Sekulic, N., Guo, L. Y., Tsinman, T., Black, B. E., & Cheeseman, I. M. (2015). The CENP-L-N Complex Forms a Critical Node in an Integrated Meshwork of Interactions at the Centromere-Kinetochore Interface. *Mol Cell*, 60(6), 886-898. doi:10.1016/j.molcel.2015.10.027
- Meadows, J. C., & Millar, J. B. (2015). Sharpening the anaphase switch. *Biochem Soc Trans*, 43(1), 19-22. doi:10.1042/BST20140250
- Meikrantz, W., Supryniewicz, F. A., Halleck, M. S., & Schlegel, R. A. (1990). Identification of mitosis-specific p65 dimer as a component of human M phase-promoting factor. *Proc Natl Acad Sci U S A*, 87(24), 9600-9604. doi:10.1073/pnas.87.24.9600
- Mirkovic, M., & Oliveira, R. A. (2017). Centromeric Cohesin: Molecular Glue and Much More. *Prog Mol Subcell Biol*, 56, 485-513. doi:10.1007/978-3-319-58592-5\_20
- Molina, O., Kouprina, N., Masumoto, H., Larionov, V., & Earnshaw, W. C. (2017). Using human artificial chromosomes to study centromere assembly and function. *Chromosoma*, 126(5), 559-575. doi:10.1007/s00412-017-0633-x
- Morales, C., & Losada, A. (2018). Establishing and dissolving cohesion during the vertebrate cell cycle. *Curr Opin Cell Biol*, 52, 51-57. doi:10.1016/j.ceb.2018.01.010
- Morales, V., Giamarchi, C., Chailleux, C., Moro, F., Marsaud, V., Le Ricousse, S., & Richard-Foy, H. (2001). Chromatin structure and dynamics: functional implications. *Biochimie*, 83(11-12), 1029-1039. doi:10.1016/s0300-9084(01)01347-5
- Moree, B., Meyer, C. B., Fuller, C. J., & Straight, A. F. (2011). CENP-C recruits M18BP1 to centromeres to promote CENP-A chromatin assembly. *J Cell Biol*, 194(6), 855-871. doi:10.1083/jcb.201106079
- Moreno-Moreno, O., Torras-Llort, M., & Azorin, F. (2017). Variations on a nucleosome theme: The structural basis of centromere function. *Bioessays*, 39(4). doi:10.1002/bies.201600241

- Morrison, O., & Thakur, J. (2021). Molecular Complexes at Euchromatin, Heterochromatin and Centromeric Chromatin. *Int J Mol Sci*, 22(13). doi:10.3390/ijms22136922
- Murayama, Y. (2018). DNA entry, exit and second DNA capture by cohesin: insights from biochemical experiments. *Nucleus*, 9(1), 492-502. doi:10.1080/19491034.2018.1516486
- Musacchio, A., & Desai, A. (2017). A Molecular View of Kinetochore Assembly and Function. *Biology (Basel)*, 6(1). doi:10.3390/biology6010005
- Nagasaka, K., & Hirota, T. (2015). Clarifying the role of condensin in shaping chromosomes. *Nat Cell Biol*, 17(6), 711-713. doi:10.1038/ncb3183
- Nagpal, H., & Fukagawa, T. (2016). Kinetochore assembly and function through the cell cycle. *Chromosoma*, 125(4), 645-659. doi:10.1007/s00412-016-0608-3
- Nasmyth, K. (2001). Disseminating the genome: joining, resolving, and separating sister chromatids during mitosis and meiosis. *Annu Rev Genet*, 35, 673-745. doi:10.1146/annurev.genet.35.102401.091334
- Nasmyth, K. (2002). Segregating sister genomes: the molecular biology of chromosome separation. *Science*, 297(5581), 559-565. doi:10.1126/science.1074757
- Negri, C., Bernardi, R., Donzelli, M., & Scovassi, A. I. (1995). Induction of apoptotic cell death by DNA topoisomerase II inhibitors. *Biochimie*, 77(11), 893-899. doi:10.1016/0300-9084(95)90009-8
- Neto, F. T., Bach, P. V., Najari, B. B., Li, P. S., & Goldstein, M. (2016). Spermatogenesis in humans and its affecting factors. *Semin Cell Dev Biol*, 59, 10-26. doi:10.1016/j.semcdb.2016.04.009
- Nicklas, R. B. (1983). Measurements of the force produced by the mitotic spindle in anaphase. *J Cell Biol*, 97(2), 542-548. doi:10.1083/jcb.97.2.542
- Nicklas, R. B., & Koch, C. A. (1969). Chromosome micromanipulation. 3. Spindle fiber tension and the reorientation of mal-oriented chromosomes. *J Cell Biol*, 43(1), 40-50. doi:10.1083/jcb.43.1.40
- Onn, I., Heidinger-Pauli, J. M., Guacci, V., Unal, E., & Koshland, D. E. (2008). Sister chromatid cohesion: a simple concept with a complex reality. *Annu Rev Cell Dev Biol*, 24, 105-129. doi:10.1146/annurev.cellbio.24.110707.175350
- Ono, T., Losada, A., Hirano, M., Myers, M. P., Neuwald, A. F., & Hirano, T. (2003). Differential contributions of condensin I and condensin II to mitotic chromosome architecture in vertebrate cells. *Cell*, 115(1), 109-121. doi:10.1016/s0092-8674(03)00724-4
- Ono, T., Yamashita, D., & Hirano, T. (2013). Condensin II initiates sister chromatid resolution during S phase. *J Cell Biol*, 200(4), 429-441. doi:10.1083/jcb.201208008
- Oomen, M. E., & Dekker, J. (2017). Epigenetic characteristics of the mitotic chromosome in 1D and 3D. *Crit Rev Biochem Mol Biol*, 52(2), 185-204. doi:10.1080/10409238.2017.1287160
- Page, S. L., & Hawley, R. S. (2004). The genetics and molecular biology of the synaptonemal complex. *Annu Rev Cell Dev Biol*, 20, 525-558. doi:10.1146/annurev.cellbio.19.111301.155141
- Palecek, J. J. (2018). SMC5/6: Multifunctional Player in Replication. *Genes (Basel)*, 10(1). doi:10.3390/genes10010007
- Palecek, J. J., & Gruber, S. (2015). Kite Proteins: a Superfamily of SMC/Kleisin Partners Conserved Across Bacteria, Archaea, and Eukaryotes. *Structure*, 23(12), 2183-2190. doi:10.1016/j.str.2015.10.004

- Park, J. A., Kim, A. J., Kang, Y., Jung, Y. J., Kim, H. K., & Kim, K. C. (2011). Deacetylation and methylation at histone H3 lysine 9 (H3K9) coordinate chromosome condensation during cell cycle progression. *Mol Cells*, *31*(4), 343-349. doi:10.1007/s10059-011-0044-4
- Pattabiraman, D., Roelens, B., Woglar, A., & Villeneuve, A. M. (2017). Meiotic recombination modulates the structure and dynamics of the synaptonemal complex during *C. elegans* meiosis. *PLoS Genet*, *13*(3), e1006670. doi:10.1371/journal.pgen.1006670
- Pauli, A., Althoff, F., Oliveira, R. A., Heidmann, S., Schuldiner, O., Lehner, C. F., . . . Nasmyth, K. (2008). Cell-type-specific TEV protease cleavage reveals cohesin functions in *Drosophila* neurons. *Dev Cell*, *14*(2), 239-251. doi:10.1016/j.devcel.2007.12.009
- Paulson, J. R., Hudson, D. F., Cisneros-Soberanis, F., & Earnshaw, W. C. (2021). Mitotic chromosomes. *Semin Cell Dev Biol*, *117*, 7-29. doi:10.1016/j.semcd.2021.03.014
- Paulson, J. R., & Laemmli, U. K. (1977). The structure of histone-depleted metaphase chromosomes. *Cell*, *12*(3), 817-828. doi:10.1016/0092-8674(77)90280-x
- Peng, J. C., & Karpen, G. H. (2007). H3K9 methylation and RNA interference regulate nucleolar organization and repeated DNA stability. *Nat Cell Biol*, *9*(1), 25-35. doi:10.1038/ncb1514
- Perpelescu, M., & Fukagawa, T. (2011). The ABCs of CENPs. *Chromosoma*, *120*(5), 425-446. doi:10.1007/s00412-011-0330-0
- Peters, J. M., & Nishiyama, T. (2012). Sister chromatid cohesion. *Cold Spring Harb Perspect Biol*, *4*(11). doi:10.1101/cshperspect.a011130
- Petry, S. (2016). Mechanisms of Mitotic Spindle Assembly. *Annu Rev Biochem*, *85*, 659-683. doi:10.1146/annurev-biochem-060815-014528
- Pfeifer, C. R., Xia, Y., Zhu, K., Liu, D., Irianto, J., Garcia, V. M. M., . . . Discher, D. E. (2018). Constricted migration increases DNA damage and independently represses cell cycle. *Mol Biol Cell*, *29*(16), 1948-1962. doi:10.1091/mbc.E18-02-0079
- Piazza, I., Haering, C. H., & Rutkowska, A. (2013). Condensin: crafting the chromosome landscape. *Chromosoma*, *122*(3), 175-190. doi:10.1007/s00412-013-0405-1
- Piazza, I., Rutkowska, A., Ori, A., Walczak, M., Metz, J., Pelechano, V., . . . Haering, C. H. (2014). Association of condensin with chromosomes depends on DNA binding by its HEAT-repeat subunits. *Nat Struct Mol Biol*, *21*(6), 560-568. doi:10.1038/nsmb.2831
- Plohl, M., Luchetti, A., Mestrovic, N., & Mantovani, B. (2008). Satellite DNAs between selfishness and functionality: structure, genomics and evolution of tandem repeats in centromeric (hetero)chromatin. *Gene*, *409*(1-2), 72-82. doi:10.1016/j.gene.2007.11.013
- Poirier, M., Eroglu, S., Chatenay, D., & Marko, J. F. (2000). Reversible and irreversible unfolding of mitotic newt chromosomes by applied force. *Mol Biol Cell*, *11*(1), 269-276. doi:10.1091/mbc.11.1.269
- Poirier, M. G., Eroglu, S., & Marko, J. F. (2002). The bending rigidity of mitotic chromosomes. *Mol Biol Cell*, *13*(6), 2170-2179. doi:10.1091/mbc.01-08-0401
- Poirier, M. G., & Marko, J. F. (2002a). Micromechanical studies of mitotic chromosomes. *J Muscle Res Cell Motil*, *23*(5-6), 409-431. Retrieved from <https://www.ncbi.nlm.nih.gov/pubmed/12785094>
- Poirier, M. G., & Marko, J. F. (2002b). Mitotic chromosomes are chromatin networks without a mechanically contiguous protein scaffold. *Proc Natl Acad Sci U S A*, *99*(24), 15393-15397. doi:10.1073/pnas.232442599

- Poirier, M. G., Monhait, T., & Marko, J. F. (2002). Reversible hypercondensation and decondensation of mitotic chromosomes studied using combined chemical-micromechanical techniques. *J Cell Biochem*, *85*(2), 422-434. doi:10.1002/jcb.10132
- Poonperm, R., Takata, H., Hamano, T., Matsuda, A., Uchiyama, S., Hiraoka, Y., & Fukui, K. (2015). Chromosome Scaffold is a Double-Stranded Assembly of Scaffold Proteins. *Sci Rep*, *5*, 11916. doi:10.1038/srep11916
- Pope, L. H., Xiong, C., & Marko, J. F. (2006). Proteolysis of mitotic chromosomes induces gradual and anisotropic decondensation correlated with a reduction of elastic modulus and structural sensitivity to rarely cutting restriction enzymes. *Mol Biol Cell*, *17*(1), 104-113. doi:10.1091/mbc.e05-04-0321
- Prakash, K., & Fournier, D. (2018). Evidence for the implication of the histone code in building the genome structure. *Biosystems*, *164*, 49-59. doi:10.1016/j.biosystems.2017.11.005
- Prieto, E. I., & Maeshima, K. (2019). Dynamic chromatin organization in the cell. *Essays Biochem*, *63*(1), 133-145. doi:10.1042/EBC20180054
- Prozillo, Y., Fattorini, G., Santopietro, M. V., Suglia, L., Ruggiero, A., Ferreri, D., & Messina, G. (2020). Targeted Protein Degradation Tools: Overview and Future Perspectives. *Biology (Basel)*, *9*(12). doi:10.3390/biology9120421
- Qiao, H., Chen, J. K., Reynolds, A., Hoog, C., Paddy, M., & Hunter, N. (2012). Interplay between synaptonemal complex, homologous recombination, and centromeres during mammalian meiosis. *PLoS Genet*, *8*(6), e1002790. doi:10.1371/journal.pgen.1002790
- Ranjitkar, P., Press, M. O., Yi, X., Baker, R., MacCoss, M. J., & Biggins, S. (2010). An E3 ubiquitin ligase prevents ectopic localization of the centromeric histone H3 variant via the centromere targeting domain. *Mol Cell*, *40*(3), 455-464. doi:10.1016/j.molcel.2010.09.025
- Rao, S. S. P., Huang, S. C., Glenn St Hilaire, B., Engreitz, J. M., Perez, E. M., Kieffer-Kwon, K. R., . . . Aiden, E. L. (2017). Cohesin Loss Eliminates All Loop Domains. *Cell*, *171*(2), 305-320 e324. doi:10.1016/j.cell.2017.09.026
- Remeseiro, S., Cuadrado, A., Carretero, M., Martinez, P., Drosopoulos, W. C., Canamero, M., . . . Losada, A. (2012). Cohesin-SA1 deficiency drives aneuploidy and tumorigenesis in mice due to impaired replication of telomeres. *EMBO J*, *31*(9), 2076-2089. doi:10.1038/emboj.2012.11
- Ribeiro, S. A., Gatlin, J. C., Dong, Y., Joglekar, A., Cameron, L., Hudson, D. F., . . . Vagnarelli, P. (2009). Condensin regulates the stiffness of vertebrate centromeres. *Mol Biol Cell*, *20*(9), 2371-2380. doi:10.1091/mbc.E08-11-1127
- Rice, J. C., & Allis, C. D. (2001). Histone methylation versus histone acetylation: new insights into epigenetic regulation. *Curr Opin Cell Biol*, *13*(3), 263-273. doi:10.1016/s0955-0674(00)00208-8
- Riggs, A. D. (1990). DNA methylation and late replication probably aid cell memory, and type I DNA reeling could aid chromosome folding and enhancer function. *Philos Trans R Soc Lond B Biol Sci*, *326*(1235), 285-297. doi:10.1098/rstb.1990.0012
- Rodriguez-Paredes, M., & Esteller, M. (2011). Cancer epigenetics reaches mainstream oncology. *Nat Med*, *17*(3), 330-339. doi:10.1038/nm.2305
- Rog, O., Kohler, S., & Dernburg, A. F. (2017). The synaptonemal complex has liquid crystalline properties and spatially regulates meiotic recombination factors. *Elife*, *6*. doi:10.7554/eLife.21455

- Rong, M., Matsuda, A., Hiraoka, Y., & Lee, J. (2016). Meiotic cohesin subunits RAD21L and REC8 are positioned at distinct regions between lateral elements and transverse filaments in the synaptonemal complex of mouse spermatocytes. *J Reprod Dev*, 62(6), 623-630. doi:10.1262/jrd.2016-127
- Saksouk, N., Simboeck, E., & Dejardin, J. (2015). Constitutive heterochromatin formation and transcription in mammals. *Epigenetics Chromatin*, 8, 3. doi:10.1186/1756-8935-8-3
- Sales-Gil, R., & Vagnarelli, P. (2020). How HP1 Post-Translational Modifications Regulate Heterochromatin Formation and Maintenance. *Cells*, 9(6). doi:10.3390/cells9061460
- Schneider, M. W. G., Gibson, B. A., Otsuka, S., Spicer, M. F. D., Petrovic, M., Blaukopf, C., . . . Gerlich, D. W. (2021). A chromatin phase transition protects mitotic chromosomes against microtubule perforation. *bioRxiv*, 2021.2007.2005.450834. doi:10.1101/2021.07.05.450834
- Schreiner, S. M., Koo, P. K., Zhao, Y., Mochrie, S. G., & King, M. C. (2015). The tethering of chromatin to the nuclear envelope supports nuclear mechanics. *Nat Commun*, 6, 7159. doi:10.1038/ncomms8159
- Schucker, K., Holm, T., Franke, C., Sauer, M., & Benavente, R. (2015). Elucidation of synaptonemal complex organization by super-resolution imaging with isotropic resolution. *Proc Natl Acad Sci U S A*, 112(7), 2029-2033. doi:10.1073/pnas.1414814112
- Schwabish, M. A., & Struhl, K. (2004). Evidence for eviction and rapid deposition of histones upon transcriptional elongation by RNA polymerase II. *Mol Cell Biol*, 24(23), 10111-10117. doi:10.1128/MCB.24.23.10111-10117.2004
- Sedeno Cacciatore, A., & Rowland, B. D. (2019). Loop formation by SMC complexes: turning heads, bending elbows, and fixed anchors. *Curr Opin Genet Dev*, 55, 11-18. doi:10.1016/j.gde.2019.04.010
- Sen, A., & Caiazza, F. (2013). Oocyte maturation: a story of arrest and release. *Front Biosci (Schol Ed)*, 5, 451-477. doi:10.2741/s383
- Serrano, A., Rodriguez-Corsino, M., & Losada, A. (2009). Heterochromatin protein 1 (HP1) proteins do not drive pericentromeric cohesin enrichment in human cells. *PLoS One*, 4(4), e5118. doi:10.1371/journal.pone.0005118
- Shang, W. H., Hori, T., Westhorpe, F. G., Godek, K. M., Toyoda, A., Misu, S., . . . Fukagawa, T. (2016). Acetylation of histone H4 lysine 5 and 12 is required for CENP-A deposition into centromeres. *Nat Commun*, 7, 13465. doi:10.1038/ncomms13465
- Shetty, M. G., Pai, P., Deaver, R. E., Satyamoorthy, K., & Babitha, K. S. (2021). Histone deacetylase 2 selective inhibitors: A versatile therapeutic strategy as next generation drug target in cancer therapy. *Pharmacol Res*, 170, 105695. doi:10.1016/j.phrs.2021.105695
- Shin, Y., Chang, Y. C., Lee, D. S. W., Berry, J., Sanders, D. W., Ronceray, P., . . . Brangwynne, C. P. (2018). Liquid Nuclear Condensates Mechanically Sense and Restructure the Genome. *Cell*, 175(6), 1481-1491 e1413. doi:10.1016/j.cell.2018.10.057
- Shintomi, K., & Hirano, T. (2011). The relative ratio of condensin I to II determines chromosome shapes. *Genes Dev*, 25(14), 1464-1469. doi:10.1101/gad.2060311
- Shintomi, K., Inoue, F., Watanabe, H., Ohsumi, K., Ohsugi, M., & Hirano, T. (2017). Mitotic chromosome assembly despite nucleosome depletion in *Xenopus* egg extracts. *Science*, 356(6344), 1284-1287. doi:10.1126/science.aam9702
- Shintomi, K., Takahashi, T. S., & Hirano, T. (2015). Reconstitution of mitotic chromatids with a minimum set of purified factors. *Nat Cell Biol*, 17(8), 1014-1023. doi:10.1038/ncb3187

- Singh, P. B., Miller, J. R., Pearce, J., Kothary, R., Burton, R. D., Paro, R., . . . Gaunt, S. J. (1991). A sequence motif found in a *Drosophila* heterochromatin protein is conserved in animals and plants. *Nucleic Acids Res*, *19*(4), 789-794. doi:10.1093/nar/19.4.789
- Sobecki, M., Mrouj, K., Camasses, A., Parisis, N., Nicolas, E., Lleres, D., . . . Fisher, D. (2016). The cell proliferation antigen Ki-67 organises heterochromatin. *Elife*, *5*, e13722. doi:10.7554/eLife.13722
- Sonoda, E., Matsusaka, T., Morrison, C., Vagnarelli, P., Hoshi, O., Ushiki, T., . . . Takeda, S. (2001). Scc1/Rad21/Mcd1 is required for sister chromatid cohesion and kinetochore function in vertebrate cells. *Dev Cell*, *1*(6), 759-770. doi:10.1016/s1534-5807(01)00088-0
- Srinivasan, M., Fumasoni, M., Petela, N. J., Murray, A., & Nasmyth, K. A. (2020). Cohesion is established during DNA replication utilising chromosome associated cohesin rings as well as those loaded de novo onto nascent DNAs. *Elife*, *9*. doi:10.7554/eLife.56611
- Srinivasan, M., Scheinost, J. C., Petela, N. J., Gligoris, T. G., Wissler, M., Ogushi, S., . . . Nasmyth, K. A. (2018). The Cohesin Ring Uses Its Hinge to Organize DNA Using Non-topological as well as Topological Mechanisms. *Cell*, *173*(6), 1508-1519 e1518. doi:10.1016/j.cell.2018.04.015
- Srivastava, S., & Foltz, D. R. (2018). Posttranslational modifications of CENP-A: marks of distinction. *Chromosoma*, *127*(3), 279-290. doi:10.1007/s00412-018-0665-x
- Stellfox, M. E., Bailey, A. O., & Foltz, D. R. (2013). Putting CENP-A in its place. *Cell Mol Life Sci*, *70*(3), 387-406. doi:10.1007/s00018-012-1048-8
- Stephens, A. D., Banigan, E. J., Adam, S. A., Goldman, R. D., & Marko, J. F. (2017). Chromatin and lamin A determine two different mechanical response regimes of the cell nucleus. *Mol Biol Cell*, *28*(14), 1984-1996. doi:10.1091/mbc.E16-09-0653
- Stephens, A. D., Haase, J., Vicci, L., Taylor, R. M., 2nd, & Bloom, K. (2011). Cohesin, condensin, and the intramolecular centromere loop together generate the mitotic chromatin spring. *J Cell Biol*, *193*(7), 1167-1180. doi:10.1083/jcb.201103138
- Stephens, A. D., Haggerty, R. A., Vasquez, P. A., Vicci, L., Snider, C. E., Shi, F., . . . Bloom, K. (2013). Pericentric chromatin loops function as a nonlinear spring in mitotic force balance. *J Cell Biol*, *200*(6), 757-772. doi:10.1083/jcb.201208163
- Stephens, A. D., Liu, P. Z., Banigan, E. J., Almassalha, L. M., Backman, V., Adam, S. A., . . . Marko, J. F. (2018). Chromatin histone modifications and rigidity affect nuclear morphology independent of lamins. *Mol Biol Cell*, *29*(2), 220-233. doi:10.1091/mbc.E17-06-0410
- Stephens, A. D., Liu, P. Z., Kandula, V., Chen, H., Almassalha, L. M., Herman, C., . . . Marko, J. F. (2019). Physicochemical mechanotransduction alters nuclear shape and mechanics via heterochromatin formation. *Mol Biol Cell*, mbcE19050286T. doi:10.1091/mbc.E19-05-0286-T
- Stevens, D., Gassmann, R., Oegema, K., & Desai, A. (2011). Uncoordinated loss of chromatid cohesion is a common outcome of extended metaphase arrest. *PLoS One*, *6*(8), e22969. doi:10.1371/journal.pone.0022969
- Stevens, F. E., Beamish, H., Warrenner, R., & Gabrielli, B. (2008). Histone deacetylase inhibitors induce mitotic slippage. *Oncogene*, *27*(10), 1345-1354. doi:10.1038/sj.onc.1210779
- Stewart-Morgan, K. R., Petryk, N., & Groth, A. (2020). Chromatin replication and epigenetic cell memory. *Nat Cell Biol*, *22*(4), 361-371. doi:10.1038/s41556-020-0487-y

- Strom, A. R., Biggs, R. J., Banigan, E. J., Wang, X., Chiu, K., Herman, C., . . . Stephens, A. D. (2021). HP1alpha is a chromatin crosslinker that controls nuclear and mitotic chromosome mechanics. *Elife*, *10*. doi:10.7554/eLife.63972
- Strom, A. R., Emelyanov, A. V., Mir, M., Fyodorov, D. V., Darzacq, X., & Karpen, G. H. (2017). Phase separation drives heterochromatin domain formation. *Nature*, *547*(7662), 241-245. doi:10.1038/nature22989
- Strunnikov, A. V., Hogan, E., & Koshland, D. (1995). SMC2, a *Saccharomyces cerevisiae* gene essential for chromosome segregation and condensation, defines a subgroup within the SMC family. *Genes Dev*, *9*(5), 587-599. doi:10.1101/gad.9.5.587
- Strunnikov, A. V., Larionov, V. L., & Koshland, D. (1993). SMC1: an essential yeast gene encoding a putative head-rod-tail protein is required for nuclear division and defines a new ubiquitous protein family. *J Cell Biol*, *123*(6 Pt 2), 1635-1648. doi:10.1083/jcb.123.6.1635
- Sun, M. (2014). *Functions of DNA-Associating Proteins in Large-Scale Chromosome Organization*. (Molecular Biology). Northwestern university, Northwestern University.
- Sun, M., Biggs, R., Hornick, J., & Marko, J. F. (2018a). Condensin controls mitotic chromosome stiffness and stability without forming a structurally contiguous scaffold. *Chromosome Res*. doi:10.1007/s10577-018-9584-1
- Sun, M., Biggs, R., Hornick, J., & Marko, J. F. (2018). Condensin controls mitotic chromosome stiffness and stability without forming a structurally contiguous scaffold. *Chromosome Research*. doi:10.1007/s10577-018-9584-1
- Sun, M., Biggs, R., Hornick, J., & Marko, J. F. (2018b). Condensin controls mitotic chromosome stiffness and stability without forming a structurally contiguous scaffold. *Chromosome Res*, *26*(4), 277-295. doi:10.1007/s10577-018-9584-1
- Sun, M., Kawamura, R., & Marko, J. F. (2011). Micromechanics of human mitotic chromosomes. *Phys Biol*, *8*(1), 015003. doi:10.1088/1478-3975/8/1/015003
- Takagi, M., Ono, T., Natsume, T., Sakamoto, C., Nakao, M., Saitoh, N., . . . Imamoto, N. (2018). Ki-67 and condensins support the integrity of mitotic chromosomes through distinct mechanisms. *J Cell Sci*, *131*(6). doi:10.1242/jcs.212092
- Tedeschi, A., Wutz, G., Huet, S., Jaritz, M., Wuensche, A., Schirghuber, E., . . . Peters, J. M. (2013). Wapl is an essential regulator of chromatin structure and chromosome segregation. *Nature*, *501*(7468), 564-568. doi:10.1038/nature12471
- Toselli-Mollereau, E., Robellet, X., Fauque, L., Lemaire, S., Schiklenk, C., Klein, C., . . . Bernard, P. (2016). Nucleosome eviction in mitosis assists condensin loading and chromosome condensation. *EMBO J*, *35*(14), 1565-1581. doi:10.15252/embj.201592849
- Toth, A., Ciosk, R., Uhlmann, F., Galova, M., Schleiffer, A., & Nasmyth, K. (1999). Yeast cohesin complex requires a conserved protein, Eco1p(Ctf7), to establish cohesion between sister chromatids during DNA replication. *Genes Dev*, *13*(3), 320-333. doi:10.1101/gad.13.3.320
- Uhlmann, F., & Nasmyth, K. (1998). Cohesion between sister chromatids must be established during DNA replication. *Curr Biol*, *8*(20), 1095-1101. doi:10.1016/s0960-9822(98)70463-4
- Uhlmann, F., Wernic, D., Poupart, M. A., Koonin, E. V., & Nasmyth, K. (2000). Cleavage of cohesin by the CD clan protease separin triggers anaphase in yeast. *Cell*, *103*(3), 375-386. doi:10.1016/s0092-8674(00)00130-6

- Upton, A. L., & Sherratt, D. J. (2013). Breaking symmetry in SMCs. *Nat Struct Mol Biol*, 20(3), 246-249. doi:10.1038/nsmb.2525
- Vagnarelli, P. (2012). Mitotic chromosome condensation in vertebrates. *Exp Cell Res*, 318(12), 1435-1441. doi:10.1016/j.yexcr.2012.03.017
- Vagnarelli, P., Ribeiro, S. A., & Earnshaw, W. C. (2008). Centromeres: old tales and new tools. *FEBS Lett*, 582(14), 1950-1959. doi:10.1016/j.febslet.2008.04.014
- van der Waal, M. S., Hengeveld, R. C., van der Horst, A., & Lens, S. M. (2012). Cell division control by the Chromosomal Passenger Complex. *Exp Cell Res*, 318(12), 1407-1420. doi:10.1016/j.yexcr.2012.03.015
- van Nuland, R., & Gozani, O. (2016). Histone H4 Lysine 20 (H4K20) Methylation, Expanding the Signaling Potential of the Proteome One Methyl Moiety at a Time. *Mol Cell Proteomics*, 15(3), 755-764. doi:10.1074/mcp.R115.054742
- Varier, R. A., Outchkourov, N. S., de Graaf, P., van Schaik, F. M., Ensing, H. J., Wang, F., . . . Timmers, H. T. (2010). A phospho/methyl switch at histone H3 regulates TFIID association with mitotic chromosomes. *EMBO J*, 29(23), 3967-3978. doi:10.1038/emboj.2010.261
- Verdaasdonk, J. S., & Bloom, K. (2011). Centromeres: unique chromatin structures that drive chromosome segregation. *Nat Rev Mol Cell Biol*, 12(5), 320-332. doi:10.1038/nrm3107
- Verzijlbergen, K. F., Nerusheva, O. O., Kelly, D., Kerr, A., Clift, D., de Lima Alves, F., . . . Marston, A. L. (2014). Shugoshin biases chromosomes for biorientation through condensin recruitment to the pericentromere. *Elife*, 3, e01374. doi:10.7554/eLife.01374
- Villasenor, R., & Baubec, T. (2021). Regulatory mechanisms governing chromatin organization and function. *Curr Opin Cell Biol*, 70, 10-17. doi:10.1016/j.ceb.2020.10.015
- Voelkel-Meiman, K., Moustafa, S. S., Lefrancois, P., Villeneuve, A. M., & MacQueen, A. J. (2012). Full-length synaptonemal complex grows continuously during meiotic prophase in budding yeast. *PLoS Genet*, 8(10), e1002993. doi:10.1371/journal.pgen.1002993
- Walther, N., Hossain, M. J., Politi, A. Z., Koch, B., Kueblbeck, M., Odegard-Fougner, O., . . . Ellenberg, J. (2018). A quantitative map of human Condensins provides new insights into mitotic chromosome architecture. *J Cell Biol*, 217(7), 2309-2328. doi:10.1083/jcb.201801048
- Wang, F., & Higgins, J. M. (2013). Histone modifications and mitosis: countermarks, landmarks, and bookmarks. *Trends Cell Biol*, 23(4), 175-184. doi:10.1016/j.tcb.2012.11.005
- Wang, L., Xu, Z., Khawar, M. B., Liu, C., & Li, W. (2017). The histone codes for meiosis. *Reproduction*, 154(3), R65-R79. doi:10.1530/REP-17-0153
- Wang, R. S., Yeh, S., Tzeng, C. R., & Chang, C. (2009). Androgen receptor roles in spermatogenesis and fertility: lessons from testicular cell-specific androgen receptor knockout mice. *Endocr Rev*, 30(2), 119-132. doi:10.1210/er.2008-0025
- Wang, S., Zickler, D., Kleckner, N., & Zhang, L. (2015). Meiotic crossover patterns: obligatory crossover, interference and homeostasis in a single process. *Cell Cycle*, 14(3), 305-314. doi:10.4161/15384101.2014.991185
- Warrener, R., Beamish, H., Burgess, A., Waterhouse, N. J., Giles, N., Fairlie, D., & Gabrielli, B. (2003). Tumor cell-selective cytotoxicity by targeting cell cycle checkpoints. *FASEB J*, 17(11), 1550-1552. doi:10.1096/fj.02-1003fje
- Warrener, R., Chia, K., Warren, W. D., Brooks, K., & Gabrielli, B. (2010). Inhibition of histone deacetylase 3 produces mitotic defects independent of alterations in histone H3 lysine 9

- acetylation and methylation. *Mol Pharmacol*, 78(3), 384-393. doi:10.1124/mol.109.062976
- Wassmann, K. (2013). Sister chromatid segregation in meiosis II: deprotection through phosphorylation. *Cell Cycle*, 12(9), 1352-1359. doi:10.4161/cc.24600
- Watanabe, R., Hara, M., Okumura, E. I., Herve, S., Fachinetti, D., Ariyoshi, M., & Fukagawa, T. (2019). CDK1-mediated CENP-C phosphorylation modulates CENP-A binding and mitotic kinetochore localization. *J Cell Biol*, 218(12), 4042-4062. doi:10.1083/jcb.201907006
- Wreggett, K. A., Hill, F., James, P. S., Hutchings, A., Butcher, G. W., & Singh, P. B. (1994). A mammalian homologue of *Drosophila* heterochromatin protein 1 (HP1) is a component of constitutive heterochromatin. *Cytogenet Cell Genet*, 66(2), 99-103. doi:10.1159/000133676
- Wutz, G., Varnai, C., Nagasaka, K., Cisneros, D. A., Stocsits, R. R., Tang, W., . . . Peters, J. M. (2017). Topologically associating domains and chromatin loops depend on cohesin and are regulated by CTCF, WAPL, and PDS5 proteins. *EMBO J*, 36(24), 3573-3599. doi:10.15252/embj.201798004
- Xia, Y., Ivanovska, I. L., Zhu, K., Smith, L., Irianto, J., Pfeifer, C. R., . . . Discher, D. E. (2018). Nuclear rupture at sites of high curvature compromises retention of DNA repair factors. *J Cell Biol*, 217(11), 3796-3808. doi:10.1083/jcb.201711161
- Xie, G., Walker, R. R., 3rd, & Irianto, J. (2020). Nuclear mechanosensing: mechanism and consequences of a nuclear rupture. *Mutat Res*, 821, 111717. doi:10.1016/j.mrfmmm.2020.111717
- Xu, D., Bai, J., Duan, Q., Costa, M., & Dai, W. (2009). Covalent modifications of histones during mitosis and meiosis. *Cell Cycle*, 8(22), 3688-3694. doi:10.4161/cc.8.22.9908
- Yandim, C., Natisvili, T., & Festenstein, R. (2013). Gene regulation and epigenetics in Friedreich's ataxia. *J Neurochem*, 126 Suppl 1, 21-42. doi:10.1111/jnc.12254
- Yang, F., De La Fuente, R., Leu, N. A., Baumann, C., McLaughlin, K. J., & Wang, P. J. (2006). Mouse SYCP2 is required for synaptonemal complex assembly and chromosomal synapsis during male meiosis. *J Cell Biol*, 173(4), 497-507. doi:10.1083/jcb.200603063
- Yi, Q., Chen, Q., Liang, C., Yan, H., Zhang, Z., Xiang, X., . . . Wang, F. (2018). HP1 links centromeric heterochromatin to centromere cohesion in mammals. *EMBO Rep*, 19(4). doi:10.15252/embr.201745484
- Yoshida, M., Kijima, M., Akita, M., & Beppu, T. (1990). Potent and specific inhibition of mammalian histone deacetylase both in vivo and in vitro by trichostatin A. *J Biol Chem*, 265(28), 17174-17179. Retrieved from <https://www.ncbi.nlm.nih.gov/pubmed/2211619>
- Yuan, L., Liu, J. G., Zhao, J., Brundell, E., Daneholt, B., & Hoog, C. (2000). The murine SCP3 gene is required for synaptonemal complex assembly, chromosome synapsis, and male fertility. *Mol Cell*, 5(1), 73-83. doi:10.1016/s1097-2765(00)80404-9
- Yusuf, M., Kaneyoshi, K., Fukui, K., & Robinson, I. (2019). Use of 3D imaging for providing insights into high-order structure of mitotic chromosomes. *Chromosoma*, 128(1), 7-13. doi:10.1007/s00412-018-0678-5
- Zaidi, S. K., Nickerson, J. A., Imbalzano, A. N., Lian, J. B., Stein, J. L., & Stein, G. S. (2018). Mitotic Gene Bookmarking: An Epigenetic Program to Maintain Normal and Cancer Phenotypes. *Mol Cancer Res*, 16(11), 1617-1624. doi:10.1158/1541-7786.MCR-18-0415

- Zhang, L., Liang, Z., Hutchinson, J., & Kleckner, N. (2014). Crossover patterning by the beam-film model: analysis and implications. *PLoS Genet*, *10*(1), e1004042. doi:10.1371/journal.pgen.1004042
- Zhang, L., Wang, S., Yin, S., Hong, S., Kim, K. P., & Kleckner, N. (2014). Topoisomerase II mediates meiotic crossover interference. *Nature*, *511*(7511), 551-556. doi:10.1038/nature13442
- Zhang, N., Kuznetsov, S. G., Sharan, S. K., Li, K., Rao, P. H., & Pati, D. (2008). A handcuff model for the cohesin complex. *J Cell Biol*, *183*(6), 1019-1031. doi:10.1083/jcb.200801157
- Zhao, P. A., Rivera-Mulia, J. C., & Gilbert, D. M. (2017). Replication Domains: Genome Compartmentalization into Functional Replication Units. *Adv Exp Med Biol*, *1042*, 229-257. doi:10.1007/978-981-10-6955-0\_11
- Zhiteneva, A., Bonfiglio, J. J., Makarov, A., Colby, T., Vagnarelli, P., Schirmer, E. C., . . . Earnshaw, W. C. (2017). Mitotic post-translational modifications of histones promote chromatin compaction in vitro. *Open Biol*, *7*(9). doi:10.1098/rsob.170076
- Zickler, D., & Kleckner, N. (1999). Meiotic chromosomes: integrating structure and function. *Annu Rev Genet*, *33*, 603-754. doi:10.1146/annurev.genet.33.1.603

## Appendix

### **Methods for isolating human mitotic chromosomes using micromanipulation**

#### **A1 Background, previous findings, and theory of chromosome isolation**

Mechanical properties of materials are important aspects in understanding how the material functions. Studying how perturbing the underlying components affects the overall structure and mechanical properties of the initial material can further our understanding of the relationship between the two. This is especially useful for studying materials that are complex, both in terms of underlying components, and in arrangement of those components. One such system is biological components, like mitotic chromosomes, which uses many different proteins to organize the thread-like DNA and chromatin into stiffer rods. A method of studying the mechanical properties of materials is to physically isolate and manipulate it. In the case of mitotic chromosomes, despite the difficulty in isolating them from the cell, experiments have been performed by physical isolation and manipulation to study their physical properties and the effects perturbing underlying components have on the overall structure.

By studying single chromosome isolation, several facets of mitotic chromosome structure have already been uncovered and investigated. Several basic physical behaviors of mitotic chromosomes have been discovered by mechanically stretching an untreated chromosome at different rates, revealing they possess viscoelastic properties that are very resistant to deformations and breakages (Houchmandzadeh et al., 1997; M. Poirier et al., 2000; M. G. Poirier, Eroglu, et al., 2002). The underlying DNA-based connectivity of mitotic chromosome has been discovered in newt, human, and mice chromosomes using DNase treatments on isolated mitotic chromosomes (R. Biggs et al., 2019; R. J. Biggs et al., 2020; Pope et al., 2006;

Sun et al., 2011). The structural and mechanical significance of proteins have likewise been examined by treatment with proteases, which cause the chromosome to weaken greatly while not completely disassociating. Investigations into large, structural, chromatin-organizing complexes like condensin, cohesin, and topoisomerases have also been studied (Kawamura et al., 2010; M. Sun et al., 2018b). Investigations into histone PTMs and global phosphorylation on mitotic chromosomes have also been studied to demonstrate how the underlying chromatin or the state changes of proteins affects the mitotic chromosome structure (R. Biggs et al., 2019; Eastland et al., 2016). All these experiments rely on being able to manipulate and obtain data from physically isolated chromosomes, which can be manipulated.

We will describe the type of experiments that can be performed on isolated mitotic chromosomes and how to isolate a chromosome for such a purpose. The experiments covered will detail microscope setup to perform these experiments, the creation of micropipettes for physically interacting with mitotic cells, the use of motorized micromanipulators, the micropipettes used in physically interacting and isolating the mitotic chromosome, spray-based direct treatment of isolated mitotic chromosomes, the method and physics behind force-extension experiments and how to physically derive its spring constant, and fluorescent experiments on an isolated mitotic chromosome.

## **A2 Equipment considerations for performing chromosome isolation**

The difficulty in isolating, studying, and manipulating sub-cellular materials involve overcoming three different categories of difficulty: the size, force scale, and entanglements of the objects. The first two difficulties are addressed using specialized equipment, while the last is addressed with chemicals and physical manipulation. The difficulty in isolation is also assuaged by practice in performing these experiments. While there are many variants that can work for this

procedure, the current setup can be seen in Section A6, while the overall considerations will be discussed in the following paragraphs. In general, the length and force difficulties are handled at the microscope/sample-holding levels and at the micropipette/ manipulator levels.

At the microscope or sample-holding levels, working with very small objects requires high-magnification objective (60x-90x) and a microscope to visualize the micron-sized objects of interest. At this magnification, high-quality imaging typically requires the use of an oil-immersion objective for an inverted microscope. An inverted microscope is used so that micropipettes can enter from above and interact with the mounted sample. The size of the objects also tends to them have low contrast in white light. Phase-contrast, DIC, or other high-contrast imaging light sources are required to increase the contrast at these lower levels of light and contrast. A lower-magnification (10x) air objective is also useful so a wider field of view can be seen when searching for objects, such as in centering micropipettes (Section A3.1).

For these experiments, vibrations need to be minimized so that the surrounding environment does not disturb the pico- to nano-newton-sensitive devices. This is done partly through using a high-quality, smooth stage movement system. To further reduce vibrations, a large, sturdy microscope air table should be employed and pressurized to minimize fluctuations and vibrations. The microscope should then be mounted to this table. Preventing airflow in the room from disrupting the stability of the sample is also important. This can be achieved by placing the microscope in a small microscope room and by placing a plastic-wrapped cage around the microscope, mounted to the air table.

On the manipulation side, the use of micropipettes allows the gentle and controlled interaction with sub-cellular molecules for their isolation. Pulling and cutting small capillary tubes is used to create micropipettes with micron-sized inner diameters at their tips (see Section

A4.3 for details on how to make micropipettes). The use of a pulling machine allows for consistency in creating micropipettes. After pulling, breaking the micropipette tips on a heated wire assisted with a microscope allows the creation of the desired, micron-sized opening (with practice). Breaking the micropipette tips can also be facilitated using a micropipette forge. These micropipettes are then placed in micropipette holders, designed to minimize drift when sitting in their mounts. The micropipette holders are further secured in micropipette mounts, which are further stabilized as described in the next paragraph.

Mounting the micropipette mounts to the previously described air table allows for the micropipette to possess greater stability and protection from vibrations in the surrounding environment. The mounts likewise should be very sturdy and utilize a stabilizing bridge between mounts where required. The use of motorized manipulators is also recommended so very small movements can be performed stably and reliably. These machines also allow the speed to be controlled in a consistent manner and the micropipette movement can be repeated reliably with computer-assisted consistency in the force-extension experiments. The reliability is useful as large changes on the isolated object can damage it through overstretching.

Flow control of the micropipette is achieved by attaching the micropipette holder to a pressure system. This pressure system should be able to apply pressure and vacuum for dispensing liquid and aspirating the object(s) of interest in a very controlled manner. This can also be achieved using small tubing attached to a water-containing syringe to generate the hydrostatic and hydraulic control. The tubing can be sealed watertight using Parafilm once connections are made.

The use of fluorescent-based analysis and imaging of proteins in cells and sub-cellular objects is useful in their study, with additional features that can be visualized through

manipulating the larger object. The considerations of these experiments include fluorescent intensity to background fluorescence. Other sources can detail these considerations in detail, but in short, the use of a fluorescent light source, emitter filters between the light source and sample, a dichroic mirror to create a directionality between the excitation light source and detector, collection filters between the sample and the detector can all be utilized and adjusted to maximize the fluorescence of the detected sample. Fluorescent labeling of proteins and DNA can be performed using endogenous labeling, fluorescent antibody labeling, and fluorescent small molecules.

### **A3 Stepwise descriptions for performing chromosome isolation**

#### **A3.1 Experimental setup and pipette centering**

Centering the pipettes and familiarization with the setup of the experiment is crucial to any further experiments in chromosome isolation, although there are several steps that require practice to perform quickly. Several of these steps require mastery and familiarization with other protocols, detailed in Section A4, before proceeding. The steps to setup are detailed here. The general strategy for setup and centering of each pipette is to pull, cut, and fill the pipettes, then anchor them in a pipette holder in the pipette mount, then move the pipette roughly to the center of the microscope, increasing in magnification in each step as best as possible. The magnifications are by eye, at low magnification (here described as 10x) and at high magnification (here described as 60x) for the final centering.

#### **Centering protocol**

1. Remove sample well from incubator and petri dish and place it on a slide holder
2. Secure sample on slide holder with adhesive cellophane (Scotch) tape
3. Move objective turret to 60x objective and place drop of microscope oil on it

4. Place slide holder into microscope holder slot
5. Raise objective until oil touches bottom of the glass slide on the sample
6. Find an identifiable marker at 60x to center all the pipettes around
7. Lower objective, switch the objective to 10x, raise at 10x to find marker
8. Pull, cut, vacuum aspirate, backfill, and remove bubbles from a force pipette
9. Lower force pipette holder until water fills entire tubing
10. Secure force pipette into pipette holder and secure pipette holder in left pipette mount
11. Move force pipette tip into center of well by eye, using the light to estimate center
12. Move force pipette until its shadow is found, try not to drive pipette into glass bottom
13. If tip of force pipette is not seen, pull back until tip is found and focus on tip
14. Move force pipette tip to identifiable marker, switching focus between tip and marker
15. Repeat steps 8-14 for the Triton (right-hand mount) and hold pipette (center mount)
16. Lower turret and change objective to 60x, raise to focus again on marker
17. Change the speed of all motorized manipulators to their slow speed
18. Move all pipettes into frame at 60x towards marker, using higher pullout tab if using
19. Check all pipettes respond to applied forces, are unclogged, and correct in size
20. Raise pipettes above glass surface until barely visible

### **A3.2A Cell lysis and isolation of the chromosome through bundle removal**

The process of mitotic chromosome isolation is conceptually very simple: lyse the cell, stabilize the mitotic chromosome bundle, grab each arm of the target mitotic chromosome, and gently remove the bundle. However, the isolation of mitotic chromosomes and other sub-cellular items is difficult and requires a substantial amount of practice, even with the assistance of motorized manipulators, small-opening pipettes, and the stability of the equipment used. The

difficulty arises from the complexity in isolating objects from something as inhomogeneous and complicated as a living cell, as its complexity results in many objects cluttering, sticking to, or otherwise attaching to the desired object of interest. There is also remaining difficulty in isolating objects at such a small scale and working at such a small force scale. Despite the difficulty, the following steps will attempt to simplify the process as much as possible for easy and repeatable isolation attempts.

1. Pull, cut, vacuum aspirate stiff pipette in preparation for future use in isolation
2. Move around sample well until a prometaphase cell with loose bundle is found
3. Capture image of cell and all fluorescence desired for documentation
4. Move Triton pipette to edge of cell facing hold pipette, gently spray onto cell
5. Document the lysed cell by capturing an image of it in its lysed state
6. If bundle falls easily out of cell, proceed to step 9, or continue until bundle out of cell
7. Maneuver bundle out of cell with Triton or hold pipette, if it works, proceed to step 9
8. Attempt to create larger opening and move hold pipette into cell
9. Gently aspirate bundle into hold pipette with minimal, but secure attachments
10. Remove any cell debris on bundle using Triton pipette without getting bundle stuck
11. Raise hold pipette above surface, move to an empty area of sample well, lower pipette
12. Document the image of the isolated mitotic chromosome bundle with a picture
13. Raise Triton pipette and remove it from its mount and holder
14. Backfill, remove bubbles from stiff pipette, center as before in Triton pipette place
15. Move force and stiff pipettes close to bundle, verify they do not have innate suction
16. Find a target, loose mitotic chromosome arm, and gently aspirate it into force pipette
17. Document the initial capture of the chromosome arm

18. Move pipette away from bundle to expose other chromosome arm, do not overstretch
19. Gently aspirate other chromosome arm into stiff pipette
20. Move stiff pipette to make chromosome parallel between pipettes and in same plane
21. Document the attachment of both chromosome arms in force and stiff pipette
22. Aspirate chromosome bundle into hold pipette but do not aspirate target chromosome
23. Quickly, but gently move chromosome bundle away from target chromosome
24. Verify that target chromosome is good quality and undamaged, otherwise try again
25. Document the final isolated chromosome and any desired fluorescent images

### **A3.2B Alternative forms and methods of chromosome isolation**

While the bundle-removal method has been the most reliable method in isolating a single chromosome from a mitotic cell per time and attempts of isolation, there are other techniques that may be necessary in certain situations to isolate a mitotic chromosome. To this end, alternative forms of isolation are presented here as brief descriptions of alternate steps.

#### **A3.2B1 Bundle-hold chromosome isolation method**

The bundle-hold method is used in cells that cannot cleanly grab and separate a chromosome from its bundle without severely damaging the chromosome. This can occur in situations where the chromosome is too heavily entangled with the other chromosomes in the bundle, or in situations where there are additional barriers to bundle removal, such as in meiotic prophase I cells. In short, the bundle-hold method switches the position of the hold and Triton pipette and utilizes the hold pipette as a stiff pipette. First, lyse the cell as normal and maneuver the bundle out of the cell as normal, using the center Triton pipette, grabbing the bundle with the hold pipette opposite the force pipette. Then use the force pipette to grab a chromosome arm and drag it away from the hold/stiff pipette. Aspirate the chromosome bundle gently into the

hold/stiff pipette until the only connection between the force and stiff pipette is a single chromosome. Stabilizing the chromosome bundle in the hold pipette may require some constant aspiration, which may affect the results. This method also may not reliably isolate a single chromosome as the other methods but is the gentlest and least damaging of all removal methods.

### **A3.2B2 Cell-removal method**

Periodically, the chromosomes in the bundle are attached loosely enough or the cell holds onto the bundle strongly enough that both chromosome arms can be aspirated into both the stiff and force pipette without needing to stabilize the bundle. In this method, lyse the cell with a very small opening, so only a chromosome arm drifts out of the cell. Switch the Triton pipette with a stiff pipette if the Triton pipette is opposite the force pipette or move onto the next step with no pipette swapping. Aspirate the chromosome arm into the force pipette, drag it away from the cell and expose the other chromosome arm. Aspirate the other arm into the stiff pipette. Gently move the pipettes and or the stage such that the pipettes also move away from the cell until the interchromosomal tethers are snapped. This method was the original isolation protocol but would typically leave the chromosome bundle attached to the stiff pipette when moving in human cells, such that it would have a higher rate of failure in human cells.

### **A3.2B3 Free capture method**

Periodically, chromosomes will not be attached to the mitotic chromosome bundle and drift out of the cell already unattached to the chromosome bundle. In this situation, the speed of capturing the chromosome and the force of perturbing the surrounding liquid are all the considerations needed, as it may drift away quickly from view and moving the pipettes in the liquid will have a greater effect on the isolated chromosome than a chromosome bundle. Move

the force pipette to gently aspirate one chromosome arm of the single chromosome, then anchor the stiff pipette opposite the force pipette and gently aspirate the other end into the stiff pipette.

### **A3.3 Force-extension experiments of chromosome isolation**

Measuring the physical properties of objects by physical manipulation is one of the ultimate goals in mitotic chromosome isolation with micropipettes. While the most difficult part of this technique is the isolation of the chromosome, there are still considerations that must be observed in stretching the chromosome, although they mainly consist of stretching the chromosome in a way that leaves it undamaged. Tracking software that is analyzed in real time is recommended for this protocol, but analysis of the stretch-deflection of the chromosome, stiff pipette, and force pipette can be analyzed later if the video of the experiment is recorded. In the method where video is recorded and the experiment analyzed later, analysis and tracking of the pipettes still require an image tracking software. Analysis of the tracking positions is further covered in Section A5.

1. Change motorized pipettes' step sizes to match the step size in the pulling program
2. Move pipettes to be in same focal plane and keep them in the same focal plane
3. Move pipettes so chromosome is perpendicular to stiff and force pipettes
4. Move the chromosome so it is approximately its native length or slightly stretched
5. If using video capture, move to step 9
6. Start tracking software, move tracking windows to pipettes' tips, set reference image
7. Ensure tracking windows can capture pipette movement in direction of pull
8. Press "reset data array" button to reset tracking time to 0
9. Let the pipettes rest for 10 seconds to determine if there is substantial drift, redo if so
10. Press the "run" button that causes the stiff pipette to pull away from the pipette

11. Let program run, watching the pull-deflection graphs, note any oddities
12. If using the tracking software, end run and save file
13. Repeat steps 6 to 12 for desired pull number, move pipettes or chromosome as needed
14. All images of the chromosome before pull and pull parameters should be documented

### **A3.4 Calibration of force pipettes using a calibration pipette**

This technique of measuring the spring constant of an isolated object requires the ability to have a reliable force readout while measuring the stretch of the object. Our protocol using two micropipettes relies on the deflection of the force pipette as a force readout. To convert the deflection of the force pipette ( $\mu\text{m}$ ) into a force sensor (pN), we must know the spring constant ( $\text{pN}/\mu\text{m}$ ) of the force pipette. The conversion of deflection to force then becomes simple multiplication ( $(\text{pN}/\mu\text{m}) * \mu\text{m} = \text{pN}$ ). We calibrate most pipettes using a calibration pipette of a known spring constant ( $k_k$ ), where the ratio of the pipettes pushing against one another is used to calculate the spring constant of the unknown force pipette ( $k_f$ ). When initially lined up, the pipettes have no force acting on them. When the calibration pipette moves into the force pipette, it tries to move its full movement, but is held back by the force of the force pipette. Once the force pipette is removed, the calibration pipette moves its full distance. This method gives us three plateaus,  $x_0$  where there is no force on the pipettes and no force acting on any pipette,  $x_a$  where there is a force balance of the calibration pipette trying to fully move to its position held back by the force of the unknown force pipette, and  $x_b$  where the calibration pipette moves its full position without the interference of the force pipette. The ratio of the two pipette's spring constant is  $k_k * (x_b - x_a) = k_f * (x_a)$ , meaning that the force pipette's spring constant is  $k_f = k_k * ((x_b - x_a) / (x_a))$ . To remove any effect of the initial drift at the start of the calibration, we can use the equation  $k_f = k_k * (((x_b - x_0) - (x_a - x_0)) / (x_a - x_0))$ .

1. Change pipettes' step sizes to match the step size in push program (no return)
2. Center pipettes in DI water-filled well (A3.1), calibration in move position
3. Move pipettes to be in same focal plane and keep them in the same focal plane
4. Move pipettes so calibration and force pipettes overlap slightly at tips
5. If using video capture, move to step 10
6. Start tracking software, move tracking windows to calibration pipettes' tip, do not overlap with force pipette, set reference image
7. Ensure tracking windows can capture pipette movement in direction of push
8. Push force pipette into calibration pipette, pull back until pipette not deflecting ( $x=0$ )
9. Press "reset data array" button to reset tracking time to 0
10. Let the pipettes rest for 10 seconds ( $x_0$ ), determine if has substantial drift, redo if so
11. Press the "run" button that causes the calibration pipette to push into force pipette
12. Let program run, watching the calibration movement graph, note any oddities
13. Once first plateau reached, let rest for 10 seconds ( $x_a$ )
14. After rest, quickly move force pipette away in opposite direction of calibration pipette
15. Let rest another 10 seconds to obtain final plateau ( $x_b$ )
16. If using the tracking software, end run and save file
17. Repeat steps 4 to 16 for desired pull number, move pipettes and windows as needed
18. If consistent with movement and plateau times, quick analysis program can be used
19.  $k_f = k_k * (((\bar{x}_b - \bar{x}_0) - (\bar{x}_a - \bar{x}_0)) / (\bar{x}_a - \bar{x}_0))$ , where  $\bar{x}$  is the average of  $x$

### **A3.5 Measuring initial chromosomal length and cross-sectional area**

In addition to the spring constant, by measuring the initial length and cross-sectional area allows us to control for differences in initial length and cross-sectional area across to compare

different chromosomes. This can be easily performed by a documented image of the captured chromosome, analyzing it in an imaging processing software (ImageJ used here), and approximating the chromosome as a uniform cylinder.

1. Open the isolated chromosome image in ImageJ or another image software
2. Measure the length in pixels from stiff pipette center to force pipette center
3. Multiply pixel length by micron/pixel (mpp) (objective/magnification dependent)
4. For cross sectional area, create a box around chromosome; no pipettes in box
5. Scan box where maximum starts to dip back down or stabilizes on each side
6. Measure where each side is half maximum intensity (full width at half maximum)
7. Document this distance as the pixel diameter ( $d_p$ ); convert to micron by mpp ( $d_i$ )
8. Use area formula that  $A=\pi*r^2$ ;  $A=0.25*\pi*d^2$ ; use  $d_i$  for unit consistency

### **A3.6 Spray experiment procedure for enzyme and antibody treatment**

One of the benefits of directly isolating a mitotic chromosome is the ability to directly treat it with different molecules. This can be done with enzymatic molecules for studying its morphology or mechanical change when treated with the enzyme without the interference of other molecules in the cell. This can also be done with fluorescent antibodies to track the location or colocalization of different molecules along the mitotic chromosome. This tracking also allows us to stretch the chromosome and see better spatial resolution of where those molecules are located or how they behave under stress. The main concern with these experiments is the control and balance of the spray solution, spraying with enough pressure that the liquid is dispensed, and the molecule reaches the chromosome, but controlled so the spray does not damage the isolated chromosome and change its structure unintentionally.

1. Center an isolated chromosome (A1.3.2B), raise above glass surface

2. Move perpendicular to spray pipette with pipettes in the same focal plane
3. Make spray solution and centrifuge at 20,000 rcf for 10 min, keep on ice if needed
4. Cut a 200  $\mu$ l tube at the bottom, place in holder, aliquot 50  $\mu$ l solution into tube
5. Pull and cut a wide-bore spray pipette, mark a back line  $\sim$ 10 mm from back
6. Mark a fill line  $\sim$ 3 cm from wide part of tip; each linear mm contains 0.44  $\mu$ l
7. Vacuum fill spray pipette to fill line, note approximate fill time, aim for  $\sim$ 10 sec
8. Back fill pipette from back line to back of pipette
9. Set spray pipette liquid to neutral pressure, no flow or vacuum
10. Mount and center spray pipette near chromosome at 10x, then 60x
11. Slowly raise water/pressure level on spray pipette until desired flow rate achieved
12. Monitor the chromosome and flow rate over dispensing the liquid
13. If performing additional sprays, move chromosome to new area of well
14. Document spray volume and time of spray per sprayed item
15. Always be careful flow rate is balanced between dispensing and overstretching

### **A3.7 Fluorescent experiments and considerations**

The ability to fluorescently detect molecules on mitotic chromosomes and follow them over time, stretching, treatment, etc. is a benefit to chromosome isolation and a useful metric to compare against chromosomal stiffness. There are several considerations and troubleshooting steps one should take when performing fluorescent experiments, which we will detail.

1. Document the fluorescent channel, exposure time, and intensity per picture
2. Initial test of a fluorophore should document photobleaching tendency
3. Fluorescence is usually brighter and more resilient in the cell than once lysed
4. Fluorescence is usually brighter and more resilient in the bundle than isolated

5. Fluorescence of high energy and intensity may damage chromatin
6. Focus image to the best of your ability before exposing item to fluorescence
7. Any additional antibody or molecule on chromosome may affect stiffness
8. Perform mechanical measures before spray and antibody experiments
9. Capture innate fluorescence of cell before lysis, bundle before isolation, and isolated chromosome before mechanical experiments (so time is not a factor)
10. Document the time in between lysis and bundle or chromosome fluorescence

#### **A4. Stepwise support protocols for single mitotic chromosome isolation**

##### **A4.1A O-Ring well handling: Creation**

The experiments in chromosome isolation from cell culture cells and other contained cells require the cells to be placed in a contained vessel. This vessel must be open to the micropipettes and have a wide enough opening that the pipettes can access the bottom of the well at an angle, since that is how they are mounted on the microscope. The easiest way for this to be made is through a pair of rubber O-Rings sealed with wax on top of a glass coverslip. The rubber O-Rings can be cleaned and reused in experiments once the wax is removed with simple mechanical removal and cleaning with soap and water, then set in an ethanol tube.

1. Melt paraffin wax on top of hotplate, place clean Kimwipe on top
2. Place pair of O-Rings in EtOH onto heated Kimwipe to evaporate
3. Spray glass coverslip with glass cleaner, fully wipe off with Kimwipe
4. Spray coverslip with EtOH, tap excess on heated Kimwipe, lay coverslip flat
5. Move O-Ring pair into melted wax with tweezers, dip once in wax, let rest in wax
6. Repeat steps 2 to 4
7. Using tweezers, place wax O-Ring pair quickly and delicately onto dry coverslip

8. Ensure seal between glass and rings are suitable, store in unheated petri dish
9. Repeat until desired amount of wells made, sterilize under UV for 30 min, store

#### **A4.1B O-Ring well handling: Cleaning rings and recovery**

1. Let old wells sit at room temperature and CO<sub>2</sub> for at least 24 hr
2. Fill wells with DI water and let sit for at least 10 min
3. Pour off water into collection beaker, fill and pour into beaker 3 times rapidly
4. Thoroughly remove wax from rings, rub through hands, fingers, rings, and nails
5. Place wax-removed rings in soapy water beaker, let sit while cleaning other rings
6. Replace gloves with clean gloves, scrub all rings with soap and water 3 times
7. As a pair, twist rings between fingers to further scrub remaining wax off rings
8. Once all rings scrubbed clean, rinse soap off rings, place in DI water beaker
9. Rinse DI water beaker with DI water 3 times, dumping water in between rinses
10. Dry rings off by placing on 2mL pipette, place in EtOH containing 50mL beaker

#### **A4.2A Making micropipettes- Pulling micropipettes**

The method of interacting with the cell, bundle, and chromosomes in a stable manner that can perform their functions at a low force and length scale of the chromosomes is through pipettes. Due to many different uses and requirements of making micropipettes, their creation and treatment is a critical step in micromanipulation. Because of its importance, but difficulty in making well-performing pipettes, it is a skill that should be invested in perfecting. The entire process of making a pipette in general is pulling a pipette to make a hollow, needle-like object out of glass capillary tubes, cutting an opening in the needle that will affect its functionality, and filling the micropipette with liquid to transduce the force of the hydrostatic pressure from the syringes. We will describe in detail all the steps in this process for ease of learning the technique.

1. Turn on micropipette pulling machine and open pulling shield
2. Place uncut micropipette into the groove of the micropipette-pulling machine
3. Slide micropipette into slot placing where notch is located and secure screw tight
4. Slide knobs together by pressing down on metal tabs and pushing screws together
5. While pressed together, tighten other side with screw, close pulling shield
6. Set machine to pull the desired program, press enter, then pull button
7. Let machine pull pipette, then remove from machine and place in cutting holder
8. Turn on heating element and cutting light source, find cutting wire and pipette
9. Line up desired cut position with cutting wire, quickly pass wire through pipette

#### **A4.3B Making micropipettes- Filling the micropipette and bubble removal**

1. Place cut pipette into vacuum pipette holder, leaving a finger's worth of space
2. Secure pipette in holder, lower pipette into liquid, start vacuum, wait 1-15 min
3. Stop vacuum, raise pipette, loosen holder, remove from holder
4. Place filling syringe tip into pipette, lower to bottom of pipette, fill from bottom
5. Remove bubbles from tip by gently flicking pipette body, close to tip

#### **A4.3C Making micropipettes- Size considerations**

Several considerations should be made when cutting micropipette openings, such as the purpose of the pipette, the required control of the opening, the effect of innate vacuum, etc. Force and stiff pipettes, which directly interact with a single chromosome for isolation, should be made using capillary tubes with a filament as the filament limits the amount of innate vacuum of the final micropipette. Both the force and stiff pipettes should be cut with a 1  $\mu\text{m}$  opening, matching the width of the chromosome arm attempting to be isolated. The force pipette should be made with a very long taper using Program 30 (See Section A6). Cutting the 1  $\mu\text{m}$  opening will usually

be done at an area that vibrates and will require repositioning when turning on the heat as it changes position when the heat is turned on. All other pipettes can be pulled with a relatively short taper using Program 27 (See Section A6). The 1  $\mu\text{m}$  opening for the stiff pipette is found close to the tip of the pulled pipette. The Triton and hold openings should be cut to the same approximate size, with the hold pipette slightly larger. These pipette openings should be made 3-5  $\mu\text{m}$ , which occurs around a zone where the amber colored region of the pipette tip turns dark although this can vary with different pipettes. This size is selected as it creates a good balance between the Triton pipette needs for spray control of the Triton solution onto cell membranes and the hold pipette needs to aspirate whole chromosome bundles with enough control that the target chromosome isn't accidentally aspirated when removing the bundle. Spray pipettes use very large openings of about 40-50  $\mu\text{m}$ , which occur relatively high on the pipette. A challenge in cutting spray pipette openings is the tendency for the opening to snap higher than the target area aligned under the cutting wire and the tendency for uneven openings to occur when cutting the opening. Due to the amount of deformation caused to the cutting wire when making a spray pipette, it is recommended that they are cut with no heat, as the wider opening, thus stiffer area, can break the pipette with no heat.

#### **A4.4 Hydrostatic controls- Handling the pressure and aspiration of micropipettes**

To control liquid flow, spray Triton solution, spray enzymatic molecules, interact with and anchor chromosome bundles and individual chromosomes, a method of transmitting vacuum and pressure along the tubing is required. This can be done by several methods including the use of a pressure and vacuum pump connected to the tubes. However, the method currently used involves the use of simple hydrostatics and bulbs connected to syringes. The pressure in the tube can be increased by squeezing a rubber bulb at the top of the syringe or a vacuum created by

squeezing the bulb and attaching it to the top of the syringe. Pressure and vacuum can also be controlled by connecting a plastic Pasteur pipette to the bottom of the syringe and pushing or aspirating air out of the pipette. For spray control, the level of resting water is adjusted by lowering or raising the syringe or the water in the syringe for a steady stream of hydrostatic pressure to dispense the liquid in the spray pipette in the well.

#### **A4.5 Creation of a calibration pipette using a force-sensing transducer**

The creation of a calibration pipette with a known spring constant is required for the methodology used in calibrating pipettes for the techniques and methodology described in Section A3.4. To obtain this pipette and create it with a known spring constant, use of a force-sensing transducer is recommended as a master calibration pipette, with a spring constant around 1 nN/ $\mu\text{m}$ , as this is the lowest value that gives consistent readings on a very sensitive force-sensing transducer (see Section A6 for the currently used force transducer). The master calibration pipette can be used to measure weaker calibration pipettes that can serve as the main calibration pipette. It is recommended for consistency to use a single calibration pipette of approximately the same stiffness of the force pipettes per project. For other setups, the program should be setup that the calibration pipette is moved a set distance repeatedly and the computer records the voltage on the voltmeter for each instance of the calibration pipette movement. The purpose of the sensor is to translate the force of the calibration pipette into a voltage; the voltage can then be converted back into a force given the volt per force of the sensor. By pressing the calibration pipette into the sensor at specific and repeatable amounts, the spring constant of the calibration pipette can be derived as force (given by the sensor) divided by distance (given by the preprogrammed distance for the pipette to move).

1. Place and anchor force transducer (sensor) onto microscope slide holder

2. Ensure probe on sensor is perpendicular to pipette
3. Plug sensor into voltmeter connected to computer, power on voltmeter
4. Find and center sensor probe at 10x, find and center calibration pipette
5. Press new calibration pipette against sensor, lining up perpendicularly
6. Place the calibration pipette along the entire flat width of the sensor
7. Run movement/voltage software (see Section A6)
8. Watch that movements do not slip on the sensor and record stiffness
9. Repeat enough times for a satisfactory agreement for stiffness
10. Remove all items opposite the way they were added

#### **A5. Explicit physics and derivation of chromosomal stiffness using stretch-deflection**

All the experiments involved in this thesis heavily rely on physics and basic mechanics for the results. As such, it is important to go into further detail in how to derive the spring constants for both the chromosome and force pipette. When stretching the chromosome, the pulling of the chromosome is done slow enough that each of the images captured in the tracking can be approximated as a static image where the forces are balanced. This force balance means that if the movement were stopped, no directed movement would occur and thus the chromosome pulling force is balanced by the deflecting force pipette as is the stiff pipette, but this side of the force extension balance is ignored for simplicity.

The initial length and cross-sectional area are taken when there are no forces on the chromosome, *i.e.*, no compression or tension forces by stretching. The start of a tracking force-extension experiment likewise starts under no compression or tension, but since our stretches remain in the linear regime of the stretch, the curves of the stretch-deflection tracking should maintain the same value. Over each image of the stretch deflection pull, the forces are balanced

between the chromosome tension from the stretch and deflection of the force pipette. Thus, the force on the force pipette is the same force that the chromosome is experiencing for the amount of stretch it is undergoing. The force on the pipette is known by multiplying the spring constant of the force pipette by its deflection from its starting point. Since the initial length, cross sectional area, and spring constant of the force pipette are all constants, they can be factored into the equation of deriving the spring constant of the chromosome after creating the stretch-deflection curve. The stretch of the chromosome can be derived as the pull of the stiff pipette minus the deflection of the force pipette, as it is anchored between them and the only object affecting the relationship between the two.

In finding the spring constant of the force pipette by pressing it into a calibration pipette, there are also balanced forces involved in their derivation. At the beginning of the run, there are no forces on the objects, but are positioned directly next to each other. After the calibration pipette is pushed into the force pipette, there is a waiting period to ensure the forces are balanced and no movement is occurring for either pipette. When the forces are balanced in the first plateau, the pushing force of the calibration pipette is balanced by the deflection of the force pipette, attempting to move back to its original position. In mathematical terms, the distance to the original position from the original position multiplied by the spring constant of the force pipette is equal to deflection to the final distance once the force pipette is removed from the plateau distance. This then allows us to derive the force pipette's spring constant as the calibration pipette's spring constant multiplied by the plateau to final position divided by the initial to plateau position.

#### **A6. Current setup**

-Microscope body: Olympus IX70

- Air table: Newport VH 3660-OPT air table at 90PSI
- Low-magnification objective: Olympus UPlanFl 10x/0.30 Ph1
- High-magnification: 60x Olympus PlanApoN 1.42 NA Oil Ph3  $\infty$ /0.17/FN26.5 UIS2
- Phase-contrast illuminator: Olympus IX-ILL100 100W
- Fluorescent light source: Lumen Dynamics X-Cite XT600-T
- Fluorescent cube: Semrock Brightline DA/FI/TR 3x-A OMF
- Shutter controller: Sutter Lambda 10-3 (also under Metamorph/computer control)
- Motorized stage controller: Prior H128V3
- Camera 1: Pelco MC3651H-2 CCD
- Camera 2: Andor iXon3 TI/CCD-TX285 SPD-31
- Motorized manipulators (x2): Sutter MP285
- Manual manipulator: WPI KiteR
- Micropipette puller: Sutter P-97
- Micropipette pulling program 27: P=500; H=564; pull = 110; vel =110; time = 100
- Micropipette pulling program 30: P=500; H=561; pull = 220; vel =200; time = 20
- Capillary tubes: WPI TW100-6 (non-filament); TW100F-6 (filament)
- Micropipette filling tip: WPI Microfil MF28G-5; 28-gauge 97 mm long
- Micropipette cutting: Custom machined pieces, platinum wire, direct current device
- Pressure setup: 10 mL syringe with Tygon S3 E-3603 ACF00001 tubing
- Tubing dimentions: 3/32 in OD, 1/32 in ID, 1/32 in wall
- Pressure control: rubber bulbs and plastic Pasteur pipettes
- Vacuum: PV830 pneumatic PicoPump connected to a wall-mounted vacuum system
- LabView scripts in:

my computer/system (C:)/documents and setting/labuser/desktop/ronllb/

- Image-capture software: Custom LabView script “view & save image.vi”
- Image-tracking software: Custom LabView script “time-series-position4-live.vi”
- Movement software: Custom LabView script “slow-mp285\_John\_update\_feb05.vi”
- Analysis software: Custom Python script “1ProjectFullAnalysis\_v1.0.py”
- Voltage sensor: Keithley 2000 series electrometer
- Force transducer: FemtoTools FT-S100
- Voltage-based calibration software: Custom LabView script “femptoolstepcal.vi”